AGE, PROVENANCE, AND STRUCTURE OF THE WEATHERBY FORMATION, EASTERN IZEE SUB-BASIN, BLUE MOUNTAINS PROVINCE, OREGON AND IDAHO

by

Bryant Douglas Ware

A thesis

submitted in partial fulfillment

of the requirements for the degree of

Master of Science in Geology

Boise State University

May 2013

BOISE STATE UNIVERSITY GRADUATE COLLEGE

DEFENSE COMMITTEE AND FINAL READING APPROVALS

of the thesis submitted by

Bryant Douglas Ware

Thesis Title: Age, Provenance, and Structure of the Weatherby Formation, Eastern Izee Sub-Basin, Blue Mountains Province, Oregon and Idaho

Date of Final Oral Examination: 14 November 2012

The following individuals read and discussed the thesis submitted by student Bryant Douglas Ware, and they evaluated his presentation and response to questions during the final oral examination. They found that the student passed the final oral examination.

Mark D. Schmitz, Ph.D.	Chair, Supervisory Committee
Clyde J. Northrup, Ph.D.	Member, Supervisory Committee
Craig M. White, Ph.D.	Member, Supervisory Committee

The final reading approval of the thesis was granted by Mark D. Schmitz, Ph.D., Chair of the Supervisory Committee. The thesis was approved for the Graduate College by John R. Pelton, Ph.D., Dean of the Graduate College.

ACKNOWLEDGEMENTS

First off, I would like to extend many thanks Dr. Mark Schmitz for advising and helping me throughout this thesis, teaching and assistance in lab procedures, the great opportunity to work with him in the Boise State University Isotope Geology Laboratory, and finally reading, rereading, rereading the rereads, and critiquing this thesis many times over. I would also like to thank Dr. C.J. Northrup for all his help throughout the thesis and helpful discussions on the tectonic and structural story of this area. I would like to thank Dr. Craig White for being on my committee and providing much assistance on studying and interpreting thin sections of these rocks as well as helpful critiques of this thesis. I would like to thank Dr. Jim Crowley for all his assistance in lab procedures and analyses on the TIMS, friendship, and always being around to help and pass the many hours spent in the clean lab. I would like to thank Dr. Paul Olin for his assistance in the ICPMS lab, geologic conversations, and most of all, invaluable comments and critiques during the preparation of my defense. I thank Dr. Karen Viskupic for all of her help and support throughout my years here at Boise State, enthusiasm and concern for my endeavors after Boise State, as well as the priceless GK-12 opportunity. I would like to thank Debbie Pierce for help in rock sample processing and Dr. Walt Snyder for advisement and geologic discussions over the years. I would like to thank all of my friends who talked geology with me and helped edit posters and finally, I would like to

thank my family for all of their love and support throughout this processes; I could not have done without it.

ABSTRACT

The terranes of the Blue Mountains province of eastern Oregon and west-central Idaho provide an important link between the geology of the North American Cordillera exposed in Canada and Alaska in the north and Nevada and California in the south. The Izee basin is a volcanic-rich sedimentary sequence onlapping the volcanic arc and accretionary mélange terranes of the Blue Mountains, and comprises the marine flysch Weatherby Formation at its eastern extent. This study sought to establish the stratigraphic and structural relationships between the Weatherby Formation and the proximal Baker and Olds Ferry terranes. Small-scale mapping, structural measurements, and geochronological data have been used to interpret the Weatherby Formation as the synformal remnant of a larger forearc basin deposited onto both the Olds Ferry and Baker terranes, and deformed by movement along the Connor Creek fault during amalgamation of the Wallowa and Olds Ferry terranes.

New high precision U-Pb zircon ages of volcanic-rich turbidite horizons found within the marine flysch of the Weatherby Formation provide new constraints on activity in the Olds Ferry volcanic arc. The youngest primary volcaniclastic horizons within the Weatherby Formation are early Middle Jurassic (*Aalenian*), ca.173 Ma. Detrital zircon analysis of sediments stratigraphically above the youngest primary volcaniclastic horizon indicate reworking of Middle Jurassic zircons and no input of new volcanic material into

the basin after about 170 Ma, implying Olds Ferry volcanism continued into, but no later than, the *Aalenian*.

Field observations coupled with new volcanic ages provide new constraints on the deformation of the Weatherby Formation and confirm the synformal structural model developed from mapping of bedding and cleavage orientations. The southern flanks of the basin at the unconformity between the upper Huntington and Weatherby Formations conform to an upright, open folded stratigraphic section of sediments, whereas the northern flanks of the basin in the vicinity of the Connor Creek fault display tight folding and overturning. High precision U-Pb geochronology of primary volcaniclastic rocks corroborates the structural measurements, and demonstrates that the Weatherby Formation has been folded into a synformal structure via movement along the Connor Creek fault. A 192 Ma volcanic exposed near the Connor Creek fault is interpreted as a fault-bounded slice of the underlying Huntington Formation riding along a splay of the Connor Creek fault system. The Connor Creek fault is interpreted as a significant contractional structure related to the internal amalgamation of the terranes.

U-Pb zircon dating of granitoids in the southern Blue Mountains province demonstrates that a belt of southwest-northeast trending plutons consistently youngs from 129.4 Ma in the southwest to 123.8 Ma in the northeast. Of these the Lookout Mountain pluton stitches the Connor Creek fault, indicating the movement along the fault occurred after the deposition of ca.170 Ma volcanics, and before ca.129 Ma intrusions of these Early Cretaceous plutons. Compared with the western Izee sub-basin, however, the Weatherby Formation lacks *Oxfordian* sediments, suggesting the propagation of the

Connor Creek fault occurred as early as the *Callovian*, leading to termination of basin development.

Detrital zircon geochronology of sandstones from the Weatherby Formation strengthens provenance correlations between the eastern and western Izee sub-basin sediments. Similar to Early to Middle Jurassic sediments in the western Izee sub-basin (LaMaskin et al., 2011b), the Weatherby Formation contains Neoproterozoic and Mesoproterozoic zircons in all samples. These Precambrian zircons indicate a Laurentian influence, suggesting the basin was proximal to the western North American margin throughout its Jurassic depositional history. At the same time, over 65% of the zircons from each sample indicate a Mesozoic influence primarily from the late Early Jurassic to Middle Jurassic, suggesting a local influx of Jurassic volcanism from the Olds Ferry volcanic arc. This provenance confirms the model of the Weatherby as a forearc basin to the Olds Ferry fringing arc along the North American plate margin. Tighter constraints on the depositional histories of the Huntington Formation and the Weatherby Formation provide better temporal correlations with other Late Triassic to Middle Jurassic forearc systems in the Canadian Cordillera, including the Ashcroft basin in southern British Columbia, the Bowser basin in central British Columbia, and the Whitehorse Trough in northern British Columbia and southern Yukon.

TABLE OF CONTENTS

LIST OF TABLES

LIST OF FIGURES

CHAPTER ONE: BACKGROUND AND PREVIOUS STUDIES OF THE NORTH AMERICAN CORDILLERA AND THE BLUE MOUNTAINS PROVINCE

North American Cordilleran Tectonics

The North American Cordillera is a well-studied orogenic region that has evolved through many different tectonic environments throughout its geologic history. Over the past 600 Ma, the Cordillera has experienced large-scale rifting, passive margin tectonics with large amounts of deposition, and convergent margin subduction and subsequent collision of island arcs to form the western margin of the United States, Canada, and northern parts of western Mexico. The Blue Mountains province is the only exposed portion of the northern U.S. Cordillera in a gap of over 600 km of Cenozoic flood basalt cover and sediments (Figure 1.1). The following abridged geologic history of the western North American margin will help to better understand the insights further study of the Blue Mountains province will provide to the North American Cordillera's evolutional history.

The North American Cordilleran mountain chain stretches from northern Mexico to Alaska and forms a significant portion of the Circum-Pacific orogenic belt that extends nearly continuously for about 25,000 Km around the Pacific Ocean (Dickinson, 2004). The belt of mountains is due to the subduction of oceanic lithosphere along a great circle of the globe due to the breakup of the super continent Pangaea in the early Mesozoic (Dickinson, 2004). A large foreland basin developed to the east and evolved along with contractional evolution of the Cordilleran margin from the Jurassic to the Cenozoic

(DeCelles, 2004). Although the majority of the allochthons composing the Cordillera accreted in the Paleozoic and Mesozoic, the breakup of Rodinia in the mid-Neoproterozoic must be discussed to understand the complex history of the Cordilleran margin of North America.

The Cordilleran margin framework first began to develop in the Neoproterozoic during the breakup of the super continent Rodinia. Rodinia formed in the early to mid-Mesoproterozoic (Dickinson, 2004). Rifting of Rodinia first began in the mid-Neoproterozoic but was diachronous. Geologic evidence suggests that the northern part of the Cordillera began to separate first between 770-735 Ma, forming an Atlantic-type passive margin in the Cordilleran region by about 600 Ma (Burchfiel et al., 1992; Dickinson, 2004). The marine and nonmarine igneous clastic rocks with interbedded carbonates that first began to accumulate in the developing ocean basin and subsequent passive margin have been named the Windermere Supergroup (Burchfiel et al., 1992; Dickinson, 2004). The Windermere sediments were deposited along the newly developed passive margin and formed the basal sediments of the Cordilleran miogeocline (Burchfiel et al., 1992). Red bed deposits in the southern part of the Cordillera suggest that while the northern Cordillera was beginning to rift the southern Cordillera only formed intercontinental basins; actual separation of continental masses beginning around 600 Ma (Dickinson, 2004). The Laurentian passive margin, which formed on the eastern edge of the newly rifted ocean basin breaking up the supercontinent of Rodinia, forms the underlying structure of the North American Cordillera.

After the break-up of Rodinia, the newly developed passive margin and oceanic basin experienced thermotectonic subsidence and deposition. This process continued

forming the miogeocline of the Cordillera on the edge of the North American Craton into the upper Devonian (Burchfiel et al., 1992; Dickinson, 2004). The Windermere sequence forms westward thickening strata that are overlain by strata influenced by major sea level fluctuations. There is no break in the stratigraphy from the Middle Cambrian to the upper Devonian (Burchfiel et al., 1992). The miogeocline is important to the evolutionary history of the Cordillera because it is the intact pre-Mesozoic margin of North America onto which the exotic elements of the Cordillera were accreted (Saleeby, 1983) (Figure 1.1). Stable miogeoclinal sedimentation continued until the Late Devonian, when intra-oceanic subduction to the west of the Laurentian continental block caused intra-oceanic island arc allochthons within the mature ocean basin to be thrust eastward as accretionary prisms across the miogeoclinal belt (Saleeby, 1983; Dickinson, 2004). The overthrust of these allochthonous bodies onto the Cordilleran margin is interpreted to have occurred during two discrete episodes, the Antler and Sonoma orogenies (Dickinson, 2004).

The Antler orogenic event can be confidently recognized along the Robert Mountains thrust in the Great Basin of Nevada (Burchfiel et al., 1992; Dickinson, 2004) (Figure 1.2). Here the allochthon has been thrust at least 200 km eastward over same age autochthonous miogeoclinal facies that have accumulated along the Cordilleran margin (DeCelles, 2004; Dickinson, 2004). The movement along the Robert Mountains thrust was constrained by overlapping upper Mississippian-Pennsylvanian shallow marine sediments (DeCelles, 2004). The Idaho Batholith obscures the trace of the Antler allochthon through the region east of the Blue Mountains, but Antler allochthon affinity deposits have been interpreted to reappear in northeastern Washington and southern Canada (Burchfiel et al., 1992; Dickinson, 2004). The Kootenay structural arc across the

USA-Canada border, and the Yukon-Tanana terrane farther to the north, have been affected by post-Triassic deformation and tectonic transport of the Antler and Sonoma allochthons during Mesozoic arc continent collision. This deformation has complicated the interpretations of the original character of the two events in Canada and Alaska (Dickinson, 2004).

The Sonoma orogeny began about 110 million years after the end of the Antler orogeny, with the thrusting of the Golconda allochthon onto the North American continental margin during Permian-Triassic time (Burchfiel et al., 1992; Dickinson, 2004). The Cordilleran evolution during this time period is marked by continental fringing arc magmatism and the incremental accretion of subduction complexes along a trench on the continental slope (Dickinson, 2004). The Sonoma orogenic event may be correlated with initial emplacement of the Blue Mountains terranes onto the North American continental margin. In the Klamath-Sierran region of North America, volcanic and volcaniclastic deposits of island arc affinity are as old as late Middle Devonian. These arcs went through phases of increased volcanism throughout the Late Paleozoic (Burchfiel et al., 1992). The increase of material accreted by the Antler and Sonoma orogenies on to the continental margin caused down flexing of the Laurentian margin in the early Mesozoic; forming a system of back arc basins (Burchfiel et al., 1992) and peripheral foreland sedimentary basins (Dickinson, 2004) across the miogeoclinal sediments along the fringe of the interior craton.

A continuous magmatic arc was established along the margin of North America during the Middle-Triassic to Middle-Jurassic, locally producing forearc basins. The arc trench system is evidence for seafloor subduction to the east under the Laurentian margin

(Dickinson, 2004). West of the Triassic-Jurassic arc, highly deformed mélange sediments, ranging in age from Devonian to Early Jurassic, and containing blocks of sandstones, limestones, mafic volcanic rocks, and other ophiolite lithologies, can be correlated in the Canadian Cordillera, the Blue Mountains province, the Klamath-Sierran region, and central Mexico (Burchfiel et al., 1992; Dickinson, 2004). This variably deformed belt of oceanic strata thrust panels has been referred to as the Cache Creek assemblage from its type location in southern Canada. The assemblage is characterized by the lithologies mentioned above and the presence of late Paleozoic Tethyan fauna within carbonate blocks (Burchfiel et al., 1992; Dickinson, 2004). The upper Paleozoic Tethyan fauna within the Cache Creek assemblages, first recognized by Monger and Ross (1971), underpin the interpretation that some terranes of the Cordillera have a significant amount of longitudinal displacement (Saleeby, 1983). Localized Late Triassic to Jurassic (?) blueschist facies rocks of both exotic and intact metamorphic terranes are present within this assemblage, indicating that, in the late Paleozoic to early Mesozoic, a subduction related accretionary prism was present west of the North American margin (Burchfiel et al., 1992). The nearly continuous Cache Creek assemblage forms a suture zone between the fringing volcanic arc rocks along the Triassic-Jurassic continental margin and another belt of accreted island arc assemblages lying further to the west (Dickinson, 2004) (Figure 1.2).

In Jurassic-Cretaceous time, intraoceanic island arcs that subducted sea floor to the west, produced arc-continent collisions along the Cordilleran margin, closing the Cache Creek suture zone, and stepping the subduction zone and magmatic arc along the continental margin outward from the continental interior (Dickinson, 2004). Crustal

shortening beginning in the Late Jurassic lead to backarc thrusting and subsequent downflexing of a retro-foreland basin due to tectonic loading forming a belt that stretched from the Canadian Cordillera to the Sevier thrust belt (Dickinson, 2004). Magmatism continued throughout the region emplacing Late Triassic to Cretaceous calc-alkaline granitoid plutons along a > 4000 km long belt within the terranes of the accreted Cordilleran margin (DeCelles, 2004). The Late Cretaceous plutons were derived primarily from the underthrust continental crust rather than being directly related to arc magmatism of the subduction zone to the west (Dickinson, 2004). The sub-horizontal subduction of the Farallon plate in the Late Cretaceous through the Eocene produced the Laramide orogeny and caused igneous activity to move more inland, promoting the basement-involved crustal shortening of the Rocky Mountains (Dickinson, 2004).

Following the Laramide orogeny, the subduction angle began to steepen causing mid-Cenozoic magmatism to step back outward toward the coast (Dickinson, 2002; Dickinson, 2004). The development of the San Andreas transform fault in the Early Miocene initiated crustal extension within the Basin and Range province disrupting rocks of the Cordilleran orogen (Dickinson, 2004). The Pacific Northwest experienced extensive volcanic flood basalts covering a wide area of Mesozoic rocks behind the Cascade volcanic arc in the early Miocene (Dickinson, 2004).

The Canadian Cordillera

Four super terranes have been recognized within the Canadian Cordillera, the most inboard of which is the Quesnel terrane (Quesnellia) (Figure 1.1). A terrane is a group of related rocks identified primarily by the stratigraphy that is separated from other packages of sediments by discontinuities that cannot be interpreted by simple facies

changes or unconformities (Coney et al., 1980). A superterrane is the amalgamation of two or more terranes of different origin together prior to accretion to a continent. Quesnellia is composed of Triassic to Early Jurassic sedimentary, volcaniclastic, and volcanic rocks that have under gone low-grade metamorphism (Monger, 1977, 1985; Mortimer, 1986, 1987; Gabrielse et al., 1991; Monger et al., 1982, 1991; Souther, 1991; Dostal et al., 2001; Untershutz et al., 2002). Devonian to Permian age arc and oceanic affinity deposits form the basement rocks to Quesnellia (Untershutz et al., 2002). Early interpretations of Quesnellia refer to the terrane as an intraoceanic arc that accreted to the North American margin in the Middle Jurassic (Ghosh, 1995; Monger et al., 1982, 1991). Evolved Nd isotopic and geochemical features of volcanic rocks within Quesnellia show inconsistencies with Nd isotopic and geochemical features expected from a typical intraoceanic arc (Unterschutz et al., 2002). Instead, the Nd isotopic and trace element geochemical compositions from Quesnellia suggest a mixed source of a primitive arc and evolved continental crust (Unterschutz et al. 2002), indicating Quesnellia was most likely a proximal fringing arc to the North American continent.

The Cache Creek terrane is centrally located in the Canadian Cordillera, making up an apparent suture zone between the terranes to the east and west. The Cache Creek terrane is composed of Mississippian to Early Jurassic, subduction-related accretionary material, and a dismembered oceanic basement with slices of chert, argillite, volcaniclastic rocks, gabbros, basalts, and blueschist rocks (Terry, 1977; Monger et al., 1982; Ash, 1994; Mihalynuk, 1999; Mihalynuk et al., 1994; English et al., 2010). Fossils found within limestone horizons throughout the Cache Creek terrane suggest a more exotic affinity than the rest of the Canadian Cordillera (English et al., 2010). Fossils

found in Quesnellia and Stikinia indicate a relation to ancestral North America, whereas fossils found within the Cache Creek terrane include an equatorial assemblage from the Tethyan realm (Monger and Ross, 1971; Orchard et al., 2001; English et al., 2010). The Cache Creek terrane is interpreted as a stable oceanic platform that was subducted before and during the amalgamation of Stikinia to the North American continent (Mihalynuk et al., 1994).

Two accreted tectonic elements have been recognized along the Canadian Cordillera west of the Cache Creek suture belt, the Stikinia arc terrane and the Insular superterrane. The Stikinia arc is a sequence of late Middle Triassic to Middle Jurassic volcanic and volcaniclastic rocks with forearc basin deposits to the northeast of the primary volcanic deposits (Dickinson, 2004). The presence of a forearc basin between the volcanic and volcaniclastic deposits in the west, and the Cache Creek mélange assemblage to the east, suggest that the arc complex subducted oceanic seafloor downward to the west (Dickinson, 2004). Geologic evidence of the stratigraphy within the forearc basin, the island arc deposits, and the western margin of the Cache Creek assemblage suggest that the northern extent of the Stikinia arc accreted to the continental margin first, with a progressive southward closure along the Cache Creek suture zone (Mihalynuk et al., 1994; Dickinson, 2004).

The Insular superterrane lies most outboard along the Canadian Cordillera and consists of pre-Devonian to Permian strata of the Alexander terrane, Permian arc volcanics and Triassic basalt and limestones of the Wrangellia terrane, and Jurassic-Cretaceous cross-cutting plutons and overlap sequences (Saleeby, 1983; Dickinson, 2004). Evidence of a pluton intruding both the Alexander terrane and the Wrangellia

terrane suggest that they were joined together by the Carboniferous, before they accreted to the Cordilleran margin (Gardner et al., 1988; Dickinson, 2004). Reconstructing the collision of the Stikinia arc and the Insular superterrane to the Cordilleran margin has been problematic. Dickinson (2004) suggested that seafloor was subducted downward to the west, bringing the Insular superterrane to the vicinity of the east-facing Stikinia arc with the two groups accreting to the Cordilleran margin together sometime in the Mesozoic.

Initial models by Tempelman-Kuilt (1979) explaining the distribution of terranes suggested that the terranes are slices of North America that were rifted away from the continental margin forming an intervening ocean and later accreting back to the western margin. The variations in rock types are explained in this model by arc volcanic rocks forming as subduction began to bring the two landmasses back together and obduction of the oceanic material during the final stages of closure. This model, however, does not explain how the Cache Creek terrane, hosting fossils with a distinct Tethyan fauna, is enclosed by arc terranes with North American faunas (Mihalynuk et al., 1994). A new model allowing for juxtaposition of equatorial Tethyan faunas and North American faunas as a result of great northward translation of the terranes was proposed by Coney et al. (1980) and Monger and Irving (1980). Paleomagnetic data was used as the basis for transcurrent movement of the terranes; however, in the mid 1980's, a revision of the geologic timescale and reference poles for North America caused latitudinal translations of terranes 100's and 1000's of kilometers to be incompatible with paleomagnetic data. Mega thrusts have also been suggested as a means to explain the distribution; however, this does not account for the similarities found between Stikinia and Quesnellia.

Mihalynuk et al. (1994)'s model proposed an oroclinal development of the Canadian Cordilleran terranes to explain the similarities between the rocks of Stikinia and Quesnellia (Figure 1.3). The Stikine arc and Quesnel arc were part of the same arc chain, much like that of the Aleutian arc and Kurile arc of the northern pacific, with at least a 120° angle between the two limbs to allow sufficient emplacement of Cache Creek platform carbonates. Rifting to the west of the Stikine arc initiated closure of the Cache Creek Ocean causing counterclockwise rotation of the Stikine arc, resulting in final collision of the Stikine and Quesnel arcs in the Middle Jurassic (Mihalynuk et al., 1994).

The Blue Mountains Province

The Blue Mountains province comprises the Paleozoic and Mesozoic crustal basement rocks of eastern Oregon, west-central Idaho, and southeastern Washington (Figure 1.4). First, a discussion of the province as a whole will be presented, followed by a more detailed presentation of each terrane.

These Paleozoic and Mesozoic rocks of the Blue Mountains province are exposed in an erosional window through extensive overlying Cenozoic volcanic and sedimentary deposits and thus are the only exposed rocks linking the Canadian Cordillera with the western U.S. Cordillera in the eastern California and Nevada regions. Initial studies of the Blue Mountains region were conducted in the 1960's and 70's, spearheaded by Howard Brooks and Tracy Vallier. The rocks of the Blue Mountains province were split into terranes interpreted to have accreted to the North American margin between the late Permian and Middle Jurassic.

The pre-Cenozoic rocks of the Blue Mountains province have previously been divided into four distinct accreted tectonic terranes. The northwestern most volcanic arc

terrane has previously been referred to as the Wallowa Mountains - Seven Devils Mountains volcanic arc terrane (Brooks and Vallier, 1978), the northern Mesozoic terrane or Seven Devils terrane (Dickinson and Thayer, 1978, Dickinson, 1979), or simply the Wallowa-Seven Devils volcanic arc terrane (Brooks, 1979). The zone of highly deformed oceanic crust has previously been referred to as the dismembered ocean crust terrane (Vallier et al., 1977), central mélange terrane (Dickinson and Thayer, 1978), or the ocean crust terrane (Brooks, 1979). To the south of the oceanic mélange, a terrane of primarily Jurassic sediments referred to as the forearc basin terrane (Brooks, 1979), the Mesozoic clastic terrane (Dickinson, 1979), or the Jurassic flysch terrane (Brooks and Vallier, 1978), rests on the southernmost volcanic rocks. In the southern extent of the Blue Mountains province, another volcanic arc is present and has been previously referred to as the Juniper Mountains-Cuddy Mountains volcanic arc terrane (Brooks and Vallier, 1978), the Huntington volcanic arc terrane (Brooks, 1979), or the Huntington arc terrane (Dickinson, 1979). Dickinson and Thayer (1978) initially grouped the Jurassic flysch sediments and the southern volcanic rocks into one terrane they termed the Mesozoic terrane. These names were later abandoned because of the references to processes implied by each terranes name (Vallier, 1995). Silberling et al. (1984) named the terranes of the Blue Mountains province based on their locality instead of interpreted origins: from north to south, the Wallowa terrane, the Baker terrane, the Olds Ferry terrane, and an overlying sedimentary onlap sequence, the Izee terrane. Dickinson and Thayer (1978) grouped the Izee sediments as part of the Olds Ferry terrane based primarily on the lithology of the Izee sediments. Recent work on the Izee sediments by Dorsey and LaMaskin (2007) request the Izee terrane no longer be referred to as a

distinct terrane, arguing that sediments of the same type and age can be found deposited within all three terranes, indicating that formation of the Jurassic marine sediments occurred after the amalgamation of the Blue Mountains province terranes. Due to the previous data and new results from the eastern Izee sediments, this study will refer to the Izee "terrane" as the Izee basin.

The deposits of the Wallowa terrane are dominated by intra-oceanic island arc igneous rocks of Late Permian to Early Triassic age, overlain by extensive Late Triassic sedimentary and volcaniclastic rocks (Brooks and Vallier, 1978; Dickinson and Thayer, 1978; Brooks, 1979). The Baker terrane is the most structurally complex of the Blue Mountains. It is composed of an assemblage of mafic and felsic igneous and marine sedimentary rocks that have undergone polyphase deformation and pervasive metamorphism in the greenschist facies, with locally developed blueschist facies (Brooks and Vallier, 1978; Dickinson and Thayer, 1978; Brooks, 1979; Vallier, 1995). The Baker terrane contains late Devonian to Late Triassic fusulinids, conodonts, corals, and crinoids found locally in limestone lenses, as well as Permian to Early Jurassic radiolarian found in cherts (Vallier et al., 1977; Wardlaw et al., 1982; Coward, 1983; Nestell, 1983; Blome et al., 1986; Ferns et al., 1987; Nestell et al., 1995; Nestell and Nestell, 1998; Nestell and Orchard, 2000; Schwartz et al., 2011b). The Olds Ferry terrane comprises mafic to felsic volcanic and plutonic arc rocks and associated volcaniclastic sediments of Middle Triassic to Early Jurassic age (Brooks and Vallier, 1978; Dickinson and Thayer, 1978; Brooks, 1979). The Olds Ferry terrane has been interpreted as a North American fringing arc, based upon its inboard position (Dickinson, 2004) and more recently on the basis of isotope geochemistry and the presence of xenocrystic North American zircons in its

constituent volcanic rocks (Kurz, 2010; Tumpane, 2010). Forearc flysch deposits that overlap the Olds Ferry terrane in the east and the Baker terrane in the west dominate the Izee basin.

Many models have been proposed to piece together the complex tectonic history of the Blue Mountains province. Due to Cenozoic cover between the two arc terranes, correlation is difficult. Early studies of the terranes by Brooks and Vallier (1978), Mullen and Sarewitz (1983), and White et al. (1992) suggested that the Wallowa arc terrane and the Olds Ferry arc terrane were genetically related, either as part of the same complex arc system or as arcs with a similar origin. Structural trends within the Wallowa arc and the Olds Ferry arc converge toward the northwest. Similar lithologies and color changes suggest matching oxidation states through evolution and both arcs have undergone low greenschist metamorphism (Brooks and Vallier, 1978). The differences in volcanic activity between the Wallowa and Olds Ferry arcs were accounted for by a shift in subduction polarity in the Late Triassic (Vallier et al., 1977; Brooks and Vallier, 1978; White et al., 1992; Vallier, 1995). Mullen and Sarewitz (1983) made many of the same observations, indicating a relationship in arc origins but also considered paleomagnetic data that suggested both terranes might have an exotic origin. Alternatively, Brooks and Vallier (1978) suggested that the two arcs might be tectonically distinct terranes separated by the oceanic mélange of the Baker terrane. Middle Jurassic sediments unconformably overlie sediments of both the Wallowa and Olds Ferry terranes, suggesting that by at least the Middle Jurassic the terranes were connected (Brooks and Vallier, 1978; White et al., 1992). However, these models state that whether the Wallowa terrane and the Olds Ferry terrane are part of the same arc or two separate arcs, they were

intra-oceanic arcs that amalgamated together prior to deposition of the Jurassic flysch and subsequent accretion to the North American margin (Brooks and Vallier, 1978; Brooks, 1979; White et al., 1992).

Dickinson and Thayer (1978) and Dickinson (1979) studied the Jurassic sediments located in the John Day region of central Oregon and suggested that the two volcanic arcs were not co-genetic. Thick units of volcaniclastic sediments derived from a volcanic arc were deposited into the John Day inlier in the Late Triassic and Early Jurassic (Dickinson and Thayer, 1978; Dickinson 1979). The Wallowa arc is the only collection of volcanic arc affinity rocks exposed in the Blue Mountains province north of the inlier. Active volcanism within the Wallowa arc occurred between the Permian and Triassic with volcanism shutting down by the *Carnian* (Dickinson, 1979). During the Late Triassic, when arc derived volcaniclastic sediments were being deposited into the John Day inlier, the volcanic rocks of the Wallowa arc were being overlain by marine shales and platform carbonates. Paleontological evidence suggested the Olds Ferry arc retained active volcanism into at least the *Norian*, and with correlations of Jurassic sediments deposited directly onto the upper Huntington Formation of the Olds Ferry arc, it is more likely that the sediments within the John Day inlier were sourced from the Olds Ferry arc to the south (Dickinson and Thayer, 1978; Dickinson, 1979). Dickinson (1979) suggested that evidence from this Late Triassic to Jurassic sedimentary basin exposed in the John Day region indicates the Wallowa arc was a far travelled terrane not proximal enough to source the arc derived sediments. Later collision of the Wallowa terrane with the arc, forearc basin, and accretionary wedge of the Olds Ferry and Baker terranes

terminated the evolution of the forearc basin (Dickinson and Thayer, 1978; Dickinson, 1979).

Further study of the Late Triassic to Middle Jurassic sediments of the Izee basin and deposits on the Wallowa terrane have led to a new tectonic model, which incorporates new age data. Data indicating that volcanic sediments of the lower Huntington Formation of the Olds Ferry terrane overlap in age with the Wild Sheep Creek and Doyle Creek Formations in the Wallowa terrane, suggests that both arcs were simultaneously active in the *Norian*. A shift in subduction polarity in a single-arc system causing simultaneous volcanism within the Wallowa terrane and the Olds Ferry terrane is unlikely (Dorsey and LaMaskin, 2007). Dorsey and LaMaskin (2007) therefore, agree with the second model discussed, that the Blue Mountains province consists of two distinct and separate volcanic arcs over top of subduction zones that dipped in opposite directions (Figure 1.5). The previous model, suggesting two distinct magmatic arcs, does not account for the simultaneous formation of basins on either side of the Baker terrane with conglomerates and olistostrome deposits. Dorsey and LaMaskin (2007) proposed that the Wallowa and Olds Ferry arcs collided in the Late Triassic and Early Jurassic rather than in the Late Jurassic, causing crustal thickening, uplift, and deformation of the accretionary wedges, which resulted in the deposition of sediment in the north and south regions of the Baker terrane (Dorsey and LaMaskin, 2007). Closing of the back arc basin occurred during the first half of the Jurassic with final closure of the Blue Mountains terranes to the North American continent in the latest Jurassic and Early Cretaceous time (Dorsey and LaMaskin, 2007).

Lower greenschist and zeolite facies metamorphism within the Wallowa, Olds Ferry, and younger sediments of the Baker terrane suggest that the Blue Mountains underwent regional metamorphism after amalgamation of the terranes to each other by the Late Jurassic (Armstrong et al., 1977; Brooks and Vallier, 1978; Walker, 1986, 1995; Vallier, 1995; Avé Lallemant, 1995; Gray and Oldow, 2005; Dorsey and LaMaskin, 2007). Earlier phases of regional metamorphism have also been documented within the Wallowa and Olds Ferry terranes (Coward, 1983; Ashley, 1995; Avé Lallemant, 1995; Evans, 1995; Vallier, 1995; Dorsey and LaMaskin, 2007). The Baker terrane has elements of blueschist facies metamorphism as well as the regional greenschist facies overprint most likely due to the complex deformational history associated with accretionary wedges (Bloom and Nestell, 1991; Ferns and Brooks, 1995; Vallier, 1995; Bishop, 1995).

In the latest Jurassic and Early Cretaceous, the Blue Mountains province was intruded by a variety of granodioritic and tonalitic plutons (Walker, 1986). These plutons crosscut Late Jurassic faults, folds, and deformation fabrics throughout all terranes of the Blue Mountains province (Armstrong et al., 1977; Brooks and Vallier, 1978; Walker, 1986; Vallier, 1995; Gray and Oldow, 2005; Dorsey and LaMaskin, 2007). The Late Jurassic to Early Cretaceous plutons lacks any evidence of the metamorphism prevalent throughout the terranes of the Blue Mountains province, constraining the deformation within the region to the Late Jurassic. The middle to late Mesozoic intrusions throughout the Blue Mountains province could be attributed to a westward jump in subduction after the closure of the Blue Mountains province with the North American continent (Manduca et al., 1992, 1993; Dorsey and LaMaskin, 2007). By the middle Cretaceous the western

North American margin is considered a mature Andean type convergent zone that continued into the Eocene (Jordan, 1981; Oldow et al., 1989; Heller and Paola, 1989; Burchfiel et al., 1992; Cowan and Bruhn, 1992; Dickinson, 2004; DeCelles, 2004; Dorsey and LaMaskin, 2007).

In western Idaho and eastern Oregon, rocks of the North American craton are juxtaposed with accreted arc terranes of the Blue Mountains province (Figure 1.4). Rocks greater than a $^{87}Sr/^{86}Sr$ value of 0.706 are considered isotopically enriched and interpreted as cratonal material, while material with a $^{87}Sr/^{86}Sr$ value less than 0.704 are considered to be isotopically juvenile and interpreted to be arc terranes in the Blue Mountains province (Kistler and Peterman, 1973; Kurz, 2010). Armstrong et al. (1977) first characterized abrupt differences in $^{87}Sr/^{86}Sr$ ratios between craton and arc related rocks. The boundary between these two types of rocks is an abrupt, nearly vertical shear zone of highly deformed and variably metamorphosed rocks in western Idaho, and has been termed the Salmon River suture zone by Lund and Snee (1988). The Salmon River suture zone records the juxtaposition of the volcanic rocks of the Blue Mountains province to Precambrian and Paleozoic North American rocks in the Early Cretaceous (Selverstone et al., 1992; McClelland et al., 2000; Gray and Oldow, 2005; Giorgis et al., 2007). The Salmon River suture zone, western Nevada shear zone, and the Mojave-Snow Lake fault, located to the south of the Salmon River suture zone, lie along strike of one another after Cenozoic extension of the Great Basin is restored. Wyld and Wright (2001) suggested that these shear zones are part of a 1000 km structural boundary that has accommodated several hundreds of kilometers of dextral strike-slip motion, shifting all the accreted terranes of the western U.S. Cordillera to the north. In the Late Cretaceous,

significant dextral-oblique shearing has concentrated along the western Idaho shear zone that overprints or reactivates the Salmon River suture zone (Wilson and Cox, 1980; McClelland et al., 2000; Giorgis et al., 2005, 2007, 2008; Bedford et al., 2010; Kurz 2010). By the middle Cretaceous, a magmatic arc was present and modified by transpressional deformation along the western Idaho shear zone (Giorgis et al., 2005).

The Wallowa Terrane

The Wallowa terrane is the northwestern most terrane exposed in the Blue Mountains province that includes rocks of the Wallowa Mountains, Seven Devils Mountains, and Snake River canyon north of the Brownlee dam (Vallier, 1995). The Wallowa terrane is an allochthonous oceanic island arc dominated by early Permian to late Triassic island arc igneous rocks overlain by sedimentary rocks into the Early Cretaceous (Vallier, 1995). Crystalline basement rocks of the Wallowa terrane include a suite of Permian to Late Triassic amphibolites, metagabbros, meta-quartz diorite, hornblende schist, mylonites, and gneissic mylonites (Vallier et al., 1977). Anderson (1930) initially referred to Early to Late Triassic volcanic and volcaniclastic rocks that unconformably overlie Permian supracrustal rocks as the Seven Devil Volcanics. Vallier (1977) redefines the Seven Devils volcanic as the Seven Devils Group that includes four formations. Late Triassic to the Middle Jurassic laterally extensive limestone layers, volcaniclastic sedimentary rocks, and marine flysch sediments overlay rocks of the Seven Devils Group (Vallier, 1977; Vallier, 1995; Tumpane, 2010). The Pittsburg Landing area has the best exposures of the younger Triassic to Jurassic sediments.

The Cougar Creek complex exposed in the Pittsburg Landing area comprises the basement rocks of the Wallowa terrane in this location (White and Vallier, 1994; Vallier,

1995; Kurz, 2010). The Cougar Creek complex is composed of a range of lithologies including gabbros, basalts, diorites, and quartz diorites, to more felsic tonalities and trondjhemites (Vallier, 1995; Kurz and Northrup, 2008; Kurz, 2001, 2010). The structure of the Cougar Creek Complex is defined by greenschist metamorphism and deformation. The deformation within the Cougar Creek complex include: tectonic fabrics primarily striking northeast-southwest with moderate to steep dips, stretching lineations plunging to the southwest and northeast, and ductile shear zones generated by transpressional tectonic environments (White and Vallier, 1994; Vallier, 1995; Avé Lallemant, 1995; Kurz and Northrup, 2008; Kurz, 2001, 2010). High precision U-Pb geochronology on the Cougar Creek Complex by Kurz (2010) and Kurz et al. (2011) indicates the Complex underwent two compositionally and temporally distinct episodes of magmatic activity. From the Middle Permian to the Early Triassic, the Wallowa arc consisted of primarily intermediate calc-alkaline magmatism. After a time of relatively no magmatic activity more mafic to intermediate tholeiitic magmatism initiated in the Late Triassic.

The Windy Ridge Formation comprises the basal units of the supracrustal Seven Devils Group that structurally overlie the basement rocks of the Cougar Creek complex. Dominant rock types in the Windy ridge Formation include grayish-green quartz keratophyre tuffs and tuff breccias, and some rare quartz keratophyre flows (Vallier et al., 1977; Vallier, 1977). The Windy Ridge Formation is considered to be a local accumulation of silicic volcanic rocks based on the high viscosity of the erupted material and the lack of outcrops outside the Windy Ridge area near Oxbow, Oregon. The Hunsaker Creek Formation is a thick sequence of metamorphosed strata dominated by conglomerates, volcanic sandstones, keratophyric water-laid tuffs, mafic breccias, and

spilite flows (Vallier, 1977; Vallier et al., 1977). The Hunsaker Creek Formation is Middle Permian as indicated by the presence of *Leonardian* or *Guadalupian* brachiopod faunas (Vallier, 1977). The Permian rocks of the Wallowa terrane records extensive silicic volcanism, indicating subduction occurred along the arc during this time (Vallier, 1977).

The early Mesozoic rocks overlying the Cougar Creek Complex in the Pittsburg Landing area are the Big Canyon Creek unit of the Wild Sheep Creek Formation and the Kurry unit of the Doyle Creek Formation. The Wild Sheep Creek Formation is a thick succession of metamorphosed basalt, to basaltic andesite and andesite flows and volcaniclastic rocks, greywacke, argillite, and limestones (Vallier, 1977). The Wild Sheep Creek Formation is *Ladinian* (latest Middle Triassic) to early C*arnian* (early Late Triassic) based on species of *Daonella* and ammonites, and unconformably overlies the Hunsaker Formation (Vallier, 1977). The Big Canyon Creek unit is the expression of the Wild Sheep Creek Formation at Pittsburg Landing. The Big Canyon Creek unit is characterized by pillow lava flows and pillow breccia, massive lava flows, and coarse-grained volcaniclastic rocks (White and Vallier, 1994). The volcaniclastic rocks are interbedded with beds of tuff, mudstone, sandstone, conglomerate, and limestones (White and Vallier, 1994).

The Doyle Creek Formation is a thick package of red and green metamorphosed volcaniclastic rocks and volcanic flow rocks and is distinguished from other sediments of the area by its red colors and abundance of epiclastic sediments (Vallier, 1977). The Doyle Creek Formation conformably overlies the Wild Sheep Creek Formation (Vallier, 1977). The rocks are most likely Late Triassic bracketed by the *Carnian* age of the Wild

Sheep Creek Formation and the *Norian* age of the overlying Martin Bridge Formation (Vallier, 1977). At Pittsburg Landing, the Kurry unit represents the Doyle Creek Formation. The Kurry Creek Member of Vallier (1977) was subsequently redefined as belonging to both the Doyle Creek Formation and the Coon Hollow Formation (White and Vallier, 1994). The lower, thinly bedded tuffaceous sandstones and mudstones, argillaceous limestone, and tuff are placed within the Doyle Creek Formation.

The Martin Bridge Limestone stratigraphically overlies the Seven Devils Group. Limestones, dolomites, and limestone breccias dominate the Martin Bridge Limestone, with a basal unit of grayish-green calcareous greywacke, siltstone, and argillaceous limestone (Vallier, 1977). Ammonites of the earliest *Norian* (Late Triassic), indicating a shallow marine environment, are well preserved in the Martin Bridge Limestone (Vallier, 1977; Follo, 1992, 1994). The Hurwal Formation is a shale and limestone unit stratigraphically above the Martin Bridge Limestone. The Hurwal Formation conformably overlies the Martin Bridge Limestone with a sequence of calcareous and volcaniclastic argillite, greywacke, and conglomerates (Follo, 1992, 1994). The lower unit of the Hurwal Formation is made up of metamorphosed mudstone and volcaniclastic rocks containing Late Triassic with some Early Jurassic fossils discovered in the northern Wallowa Mountains (Vallier, 1977). These two units, the Martin Bridge Limestone and the Hurwal Formation, are not exposed at Pittsburg Landing.

At Pittsburg Landing, a sedimentary onlap sequence referred to as the Coon Hollow Formation overlies the volcanic rocks of the Big Canyon Creek unit (Wild Sheep Creek Formation) and the Kurry unit (Doyle Creek Formation) along an angular unconformity (Vallier, 1977; White and Vallier, 1994; White, 1994). The formation has

been divided into four distinct units: a basal red tuff, an alluvial fan and deltaic conglomerate and sandstone unit, marine sandstone and mudstone unit, and a turbidite unit (White and Vallier, 1994). In the south and east, the Formation is truncated by the Klopton Creek thrust fault that juxtaposes rocks of the Cougar Creek Complex onto rocks of the Coon Hollow Formation (White and Vallier, 1994). An abundance of plant fossils within the conglomerate and sandstone unit have allowed for interpretations of paleoenvironment, suggesting this basin developed in a temperate climate (White and Vallier, 1994). Corals, ammonites, bivalves, brachiopod, and pelecypod fossils found in the sandstone and mudstone unit have previously been used to estimate *Bajocian* age for the Coon Hollow Formation (Follo, 1992; Imlay, 1986; Stanley and Beauvais, 1990; White and Vallier, 1994; White, 1994). Recent high precision geochronology within the basal red tuff and the conglomerate and sandstone unit have indicated the lower Coon Hollow Formation was deposited between the *Hettangian/Sinemurian* transition (Early Jurassic) to the *Oxfordian* (early Late Jurassic) (Tumpane, 2010). Miocene volcanics of the Columbia River Basalts unconformably overlie the Coon Hollow Formation at Pittsburg Landing.

The Baker Terrane

The Baker terrane is a sequence of oceanic mélange rocks between the Wallowa and the Olds Ferry volcanic arc terranes. The Baker terrane is structurally the most complex of the terranes and the most extensive within the Blue Mountains province, containing rocks ranging from the Early Permian to the Early Jurassic (Nestell, 1983; Walker, 1986, 1995; Blome and Nestell, 1991; Carpenter and Walker, 1992; Ferns and Brooks, 1995; Nestell et al., 1995; Nestell and Nestell, 1998; Nestell and Orchard, 2000;

Schwartz et al., 2010). Bloom and Nestell (1991) reported differences in fauna, lithology, and metamorphic grade in a portion of the Baker terrane, suggesting that this block, termed the Grindstone terrane, is tectonically distinct from other terranes of the Blue Mountains province. Ferns and Brooks (1995) later showed that Paleozoic fauna in the north portion of the Baker terrane matched affinities within the Grindstone terrane, suggesting an established relationship at least by the late Paleozoic. Vallier (1995) suggested that long distance transport of the terrane-size block is not needed to explain the differences between the Grindstone block and the Baker terrane and claimed they were related in both time and space. Ferns and Brooks (1995) recognized the structural, geochemical, and radiometric age differences within the Baker terrane and suggested the evidence indicated two subterranes: the accretionary wedge-type Bourne subterrane and the forearc high-type Greenhorn subterrane (Figure 1.4). Recent reviews of the Baker terrane have recognize three subterranes (the Bourne, Greenhorn, and Burnt River Schist subterranes) recording the complex geologic history experienced marginal to the Wallowa and Olds Ferry terranes (Ferns and Brooks, 1995; Schwartz et al., 2011b).

Bourne Subterrane

The Bourne subterrane is the northern portion of the Baker terrane that comes in contact with the Wallowa terrane to the north. The Bourne subterrane is characterized by exposures of homogeneous argillite termed the Elkhorn Ridge Argillite (Pardee and Hewett, 1914; Gilluly, 1937; Coward, 1983; Ferns and Brooks, 1995; Schwartz et al., 2011b). The Elkhorn Ridge Argillite consists of dark siliceous argillite, cherts, and local rare sandstone and conglomerate deposits (Ferns and Brooks, 1995). Large blocks of bedded argillite and ribbon chert within the Elkhorn Ridge Argillite are folded and cut by

faults and penetrative cleavages (Schwartz et al., 2010, 2011b). Locally, limestone blocks up to a kilometer in length are present within the Elkhorn Ridge Argillite, and are interpreted as olistoliths that were transported into the enclosing deeper marine sediments (Coward, 1983; Ferns and Brooks, 1995; Schwartz et al., 2010). Middle Devonian to Late Triassic crinoids, fusulinids, conodonts, and corals has been recognized within the Bourne subterrane with both Tethyan and McCloud fusulinids (Bostwick and Nestell, 1965; Vallier et al., 1977; Wardlaw et al., 1982; Nestell, 1983; Nestell et al., 1995; Schwartz et al., 2010). Faulted slabs of oceanic and island arc volcanic rocks are found locally throughout the Bourne subterrane and have been subjected to greenschist metamorphism (Ferns and Brooks, 1995; Schwartz et al., 2010). These metaigneous and metasedimentary rocks have been interpreted as imbricated fragments of the Wallowa island-arc terrane that became incorporated into the Baker terrane after the Late Triassic (Schwartz et al., 2011b; Ferns and Brooks, 1995).

Burnt River Schist Subterrane

The Burnt River Schist is exposed throughout the southern regions of the Bourne subterrane in the Huntington area. This region has been interpreted as a high-grade equivalent to the Elkhorn Ridge Argillite; however, recent Rb-Sr and Sm-Nd isotopic geochemistry has shown these two rock groups do not share the same provenance (Ashley, 1995; Mallioux et al., 2009; Schwartz et al., 2010, 2011b). The Burnt River Schist contains Middle to Late Triassic conodonts where as the Elkhorn Ridge Argillite yields a much longer and more diverse faunal history (Mallioux et al., 2009 Schwartz et al., 2011b). Ashley (1995) concludes that the Burnt River Schist developed in a Permian to Triassic subduction complex and separates the Burnt River Schist into two different

units: the Deer Creek phyllite in the north and the Campbell Gulch phyllite in the south. A significant structural feature termed the Cave Creek fault, which trends east west, separates these two units. The primary difference between the two phyletic units are differing metamorphic grades; however, some slight lithologic diversity has been recognized (Ashley, 1995). The Deer Creek phyllite unit is composed most abundantly of phyllitic quartzite and quartz phyllite; quartzfeldspathic phyllite, pelitic phyllite, calc phyllite, and marble are also present throughout the unit (Ashley, 1995). The Campbell Gulch phyllite unit is primarily pelitic phyllite with thin scattered lenses of quartz-feldspathic phyllite, massive quartzite bodies, and marble (Ashley, 1995). Metamorphosed volcanic and volcaniclastic rocks can be found as interbedded tuffs and flows throughout the Deer Creek unit, with greenstones being the dominate expression in the Campbell Gulch unit (Ashley, 1995).

Greenhorn Subterrane

The Greenhorn subterrane is composed of serpentinite-matrix mélange with large blocks of meta-plutonic rocks, locally pillowed metavolcanic rocks, and chert argillite breccias, all overlain by more clastic sediments (Bishop, 1995; Ferns and Brooks 1995; Schwartz et al., 2010, 2011b). The mélange units have been separated from the Bourne subterrane to the north by a southward dipping thrust fault (Ferns et al., 1983; Evans, 1988; Ferns and Brooks, 1995). The Badger Creek Formation, a conglomerate, sandstone, and argillite, overlies the mélange and limestone unit with altered ultramafic detritus from the serpentinized mélange, indicating that the deposition of this unit occurred after serpentinization (Wheeler, 1976; Mullen, 1978; Ferns and Brooks, 1995; Schwartz et al., 2010). The Greenhorn subterrane contains rocks of moderate to high-pressure

metamorphism and fusulinids of McCloud affinity (Bishop, 1995; Mullen, 1978; Schwartz et al., 2010). The presence of McCloud fusulinids within the Greenhorn subterrane and the Bourne subterrane indicate that the tectonic evolutions of the two subterranes were connected (Ferns and Brooks, 1995; Schwartz et al., 2010). Low and medium grade metamorphosed rocks are present within the Greenhorn subterrane from prenhite to epidote-amphibolite facies (Ferns and Brooks, 1995; Schwartz et al., 2010). A recent study of the Greenhorn and Bourne subterrane suggests they are genetically related as two parts of a paired accretionary wedge-forearc system based on the detrital zircon populations, isotopic signatures, and a shared deformational history (Schwartz et al., 2011b).

The Olds Ferry Terrane

The Olds Ferry volcanic arc is the most inboard terrane of the Blue Mountains province. It is exposed in eastern Oregon and western Idaho. Brooks and Vallier (1978) first describe the Olds Ferry terrane deposits as volcanic tuffs, flows, intercalated coarse volcanic breccias, and conglomerates composed primarily of metabasalts and metarhyolites with interlayering fossiliferous marine limestones metamorphosed to zeolite and greenschist facies. The Olds Ferry terrane comprises the Huntington Formation (formally named in Brooks, 1979) and is typified by continuous exposures along the Burnt River and Snake River in the Huntington area of eastern Oregon (Brooks and Vallier, 1978). Recent studies of the Olds Ferry terrane has divided the Huntington Formation into unconformity-bounded upper and lower members, based on lithologic differences, new high precision geochronology, and isotopic data (Collins, 2000; Dorsey and LaMaskin, 2007; LaMaskin, 2008; Tumpane, 2010). The Weatherby Formation is most

likely composed of forearc basin sediments that were sourced primarily from the Olds Ferry terrane (Brooks, 1979; Dickinson, 1979; White et al., 1992; Avé Lallemant, 1995).

The Huntington Formation is composed primarily of volcanic rocks within a succession of volcanic breccias, interbedded with volcanic sandstones, siltstones, shales, and limestones (Vallier, 1995; Payne and Northrup, 2003; Tumpane, 2010) (Figure 1.6). The rocks of the lower Huntington Formation range in compositions from basalt to rhyolite with andesite being the most abundant composition (Brooks, 1979). Many of the interlayered sandstone and siltstone beds contain marine fossils, indicating that most of the volcanic rocks of the lower Huntington Formation are submarine volcanic deposits (Brooks, 1979; Vallier, 1995). The tuffaceous and rhyolitic rocks of the upper Huntington Formation indicate subaqueous or nearby subaerial deposits. Intrusive plutonic rocks of the Huntington Formation range in age from 210 to 237 Ma (Brooks, 1979; Tumpane, 2010). New high-precision U-Pb zircon geochronology on interlayered volcanic rocks as well as the Brownlee Pluton constrains the deposition of the lower Huntington Formation to between 230 and 220 Ma onto Brownlee plutonic basement (Tumpane, 2010). The Iron Mountain pluton intruded the lower member at 210 Ma followed by a brief erosional hiatus after which the upper member was deposited along an angular unconformity (Tumpane, 2010). In turn, the McChord Butte Conglomerate of the basal Weatherby Formation rests unconformably on the upper Huntington Formation (Brooks, 1979; Tumpane, 2010).

The contact between the upper Huntington Formation of the Olds Ferry terrane and the Weatherby Formation of the Izee strata in the Huntington area of eastern Oregon has been interpreted in contrasting ways. Livingston (1932) interpreted the contact

between the volcanic sediments of the Olds Ferry terrane and the basal sediments of the Izee strata as a thrust fault, which he termed the Bayhorse Overthrust. Livingston (1932) interpreted this structural feature as a thrust fault because the limestone and argillite overlaying the McChord Butte conglomerate of the lower Weatherby Formation were misinterpreted as Early Paleozoic age. The position of these misinterpreted Early Paleozoic rocks apparently placed older rocks directly on top of Jurassic-Triassic rocks. Brooks (1967) described the contact to be an unconformity between the greenstones of the Huntington Formation and the conglomerate of the lower Weatherby Formation. Dickinson (1979) agreed with the interpretation of the Jurassic sediments of the Weatherby Formation resting unconformably on the Huntington Formation and also noted this boundary to be not as prominent structurally as the major structural and stratigraphic discontinuity between the Weatherby Formation and the Mélange (Baker) terrane. More recent studies have continued to recognize the locale detritus found within the lower strata and McChord Butte conglomerate of the Weatherby Formation, suggesting the contact to be an unconformity (Vallier, 1995; Avé Lallemant, 1995; Dorsey and LaMaskin, 2007). Recent studies have interpreted the boundary between the upper Huntington Formation and the Weatherby Formation as a tectonized fault zone that developed along the original depositional boundary (Payne and Northrup, 2003; Dorsey and LaMaskin, 2007). A hiatus in the stratigraphy between the Huntington Formation and the Weatherby Formation along the unconformable boundary has been previously constrained, primarily from fossil evidence, between Late Triassic (late *Carnian* to early *Norian*) of the upper Huntington Formation and Early to late Middle Jurassic (*Sinemurian* to *Callovian*) age of the Weatherby Formation (Brooks, 1979; Imlay, 1980,

1986; LaMaskin, 2008). New high precision geochronological data constrain the hiatus in the unconformity between the rhyolite tuff of the upper Huntington Formation and the lowest volcaniclastic unit of the Weatherby Formation. The unconformity has been constrained to less than 6.4 million years in the Huntington area (Tumpane, 2010). This hiatus could be less or accounted for completely in the forty meters of limestones and conglomerates between the base of the marine flysch of the Weatherby Formation and the top of the Huntington Formation (Tumpane, 2010).

The Izee Basin

The Izee stratigraphy contains a coherent sequence of clastic marine flysch rocks with subordinate limestone and volcanic rocks of Late Triassic to Middle Jurassic age (Brooks and Vallier, 1978). The origin of the Izee sediments has been greatly debated, with many different tectonic interpretations. Brooks (1979) and Brooks and Vallier (1978) considered the Izee sediments as a distinct terrane, but recognize the local derivation of clasts, indicating a forearc environment of deposition. Dickinson (1979) interpreted these sediments as part of a forearc basin between a structural high of ocean seafloor mélange and an uplifted volcanic arc.

In the western-most outcrop belt, the basal units of the late Early to Late Jurassic sediments rest on a marked angular unconformity over the complexly deformed Early Triassic to Early Jurassic Vester Formation and Aldrich Mountains Group (Figure 1.6). The Vester Formation is primarily a chert-pebble conglomerate and chert-grain sandstone with fine-grained dark marine lutite containing *Carnian* mollusk fossils, indicating an Early Triassic deposition (Dickinson and Thayer, 1978; Dickinson, 1979). The *Norian* (Late Triassic) to *Sinemurian* (Early Jurassic) slope deposit sediments of the Aldrich

Mountains Group are composed of four units that are dominantly dark lutites with interbedded andesitic rich turbidite deposits (Dickinson, 1979). The volcanic-rich sediments are interpreted to be correlative with the Huntington Formation exposed in the east (Dorsey and LaMaskin, 2007). The lowest stratigraphic unit in the Jurassic sediments is composed of fossiliferous marine sandstones that fine upward into offshore calcarenite volcaniclastic turbidites and shale of the Mowich Group (Dickinson and Vigrass, 1965; Dickinson and Thayer, 1978; Dorsey and LaMaskin, 2007). The overlying Snowshoe and Trowbridge Formations are a package of thinly bedded turbidites and shales respectively (Dickinson and Thayer, 1978). The Snowshoe Formation and the Trowbridge Formation package coarsen upward into the Lonesome Formation fan turbidites sourced from a mixed volcanic and sedimentary provenance (Dickinson and Thayer, 1978). This succession has been interpreted as a relatively conformable sequence of Jurassic volcaniclastic sediments becoming younger to the southeast (Dickinson and Thayer, 1978). Small exposed intervals of slightly dipping Cretaceous sediments unconformably overlie the older rocks, indicating uplift and erosion during the Late Jurassic and the Early Cretaceous (Dickinson and Thayer, 1978). These sediments have been weakly metamorphosed and remain non-deformed, allowing for preservation of stratigraphic detail in the Izee area (Brooks, 1979).

The sediments of the Izee basin in its eastern most exposures near Huntington, along the Oregon-Idaho border, consist of the Weatherby Formation (Figure 1.6). The eastern Izee rocks have not been as extensively studied as the Izee sediments to the west but appear to be a similar succession of metasedimentary turbidites (Brooks, 1979; Hooper et al., 1995). The Weatherby Formation includes a basal red and green

conglomerate unit consisting of clasts ranging from a centimeter to a few centimeters in diameter, an overlying shallow marine limestone band that varies in thickness across the region, and a succeeding thick section of fine-grained marine flysch with discreet volcaniclastic turbidite horizons (Brooks, 1967; Brooks, 1979; Avé Lallemant, 1983; Imlay, 1986; Dorsey and LaMaskin, 2007). In the southern extent of the eastern Izee sub-basin, the Weatherby Formation rests on top of the upper Huntington Formation of the Olds Ferry terrane along an angular unconformity. In the northern extent of the eastern Izee sub-basin, the Baker terrane overthrusts the Weatherby Formation along the Connor Creek fault. The Weatherby Formation was deformed in the Late Jurassic contemporaneous with the Nevadan orogeny.

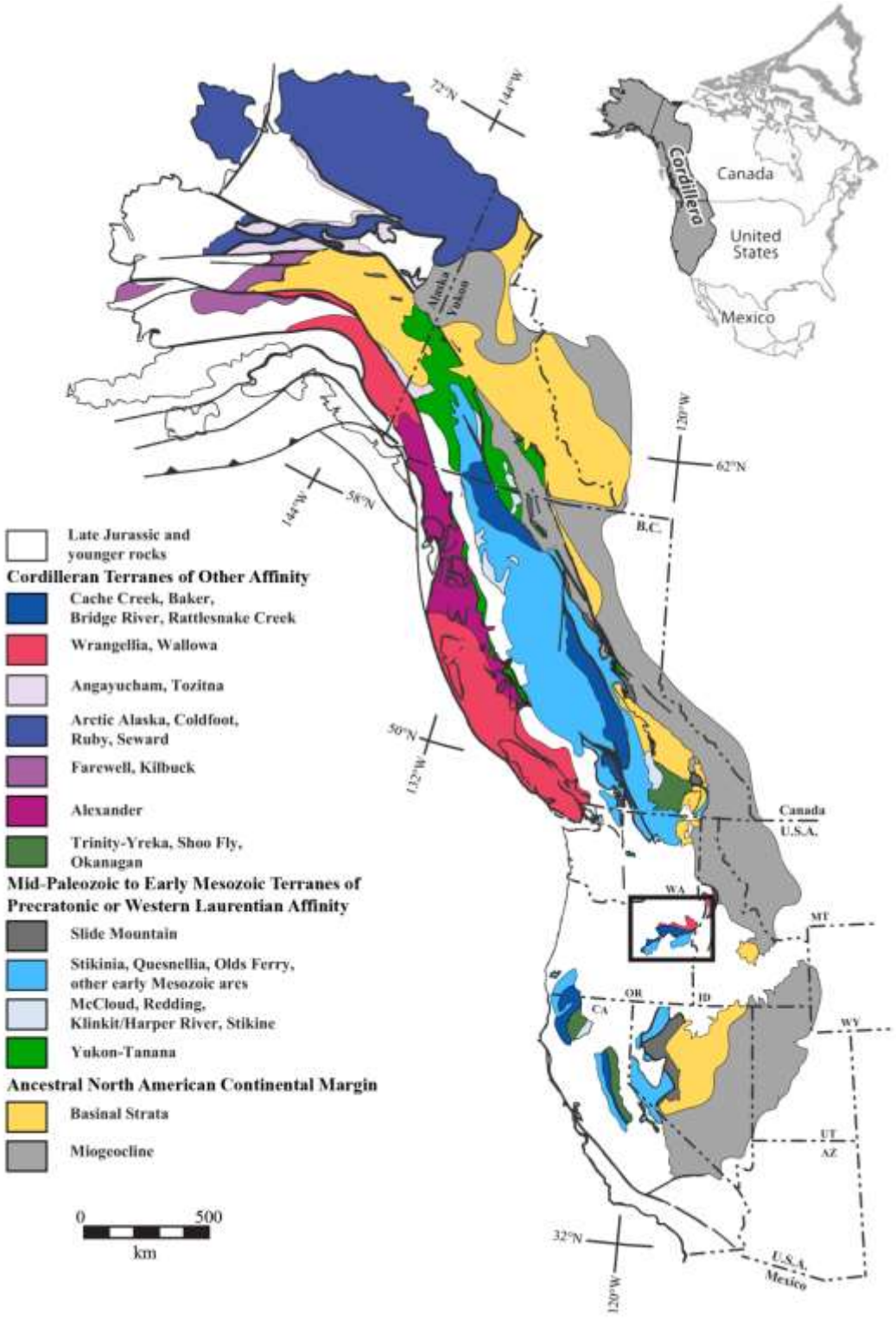

Figure 1.1: A simplified terrane map of the North American Cordillera. Terranes are grouped based on rock type affinity and origins. The Blue Mountains province is outlined in black (Figure 1.4). Redrafted from Colpron and Nelson (2009). B.C. – British Columbia, CA – California, NV – Nevada, AZ – Arizona, UT – Utah, OR – Oregon, WA – Washington, MT – Montana, WY – Wyoming.

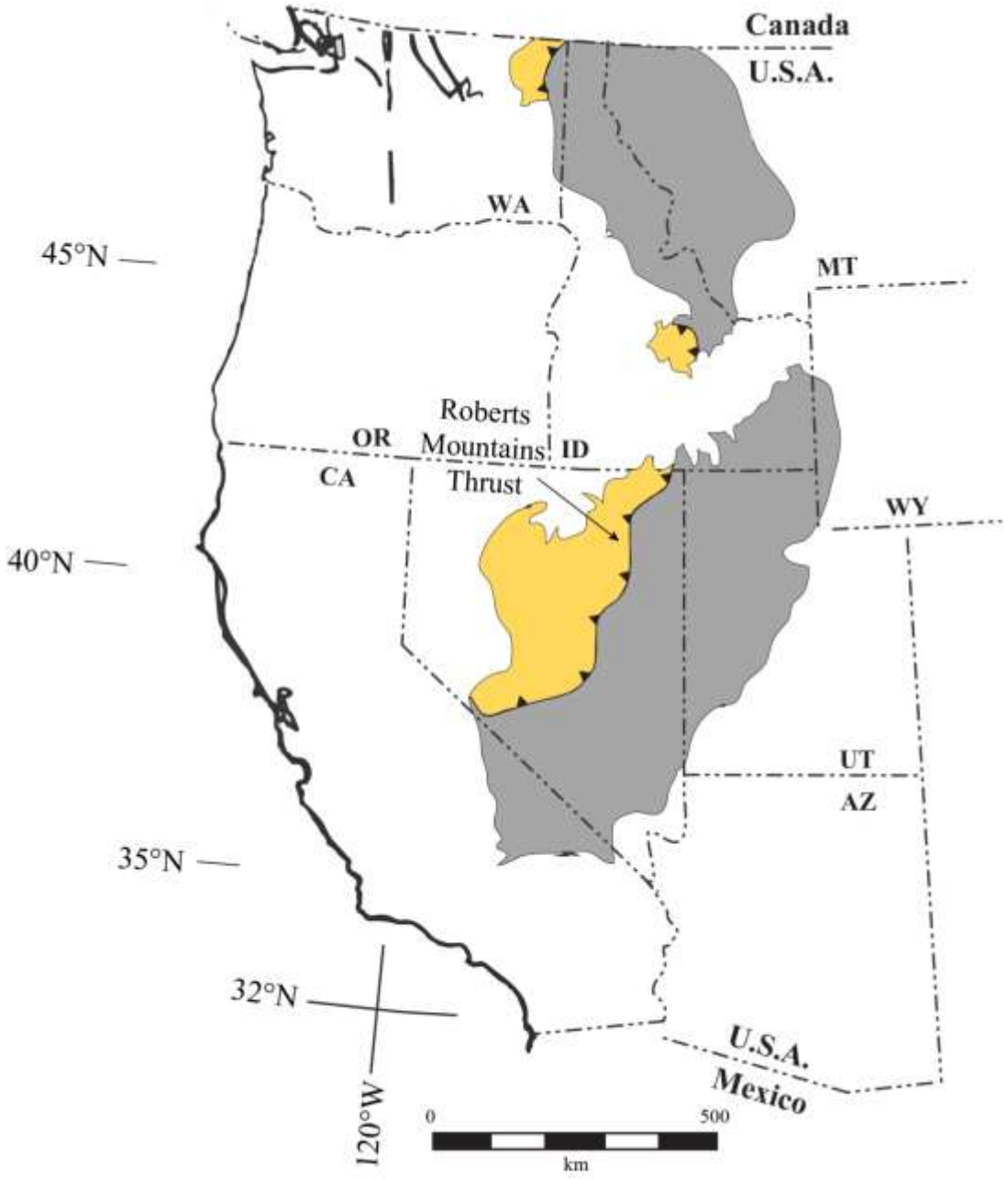

Figure 1.2: Tectonic elements of the Antler orogeny. Yellow indicates Devonian offshore allochthonous material. Grey represents miogeoclinal sediments of the Windermere Group. Redrafted from Burchfiel et al. (1992).

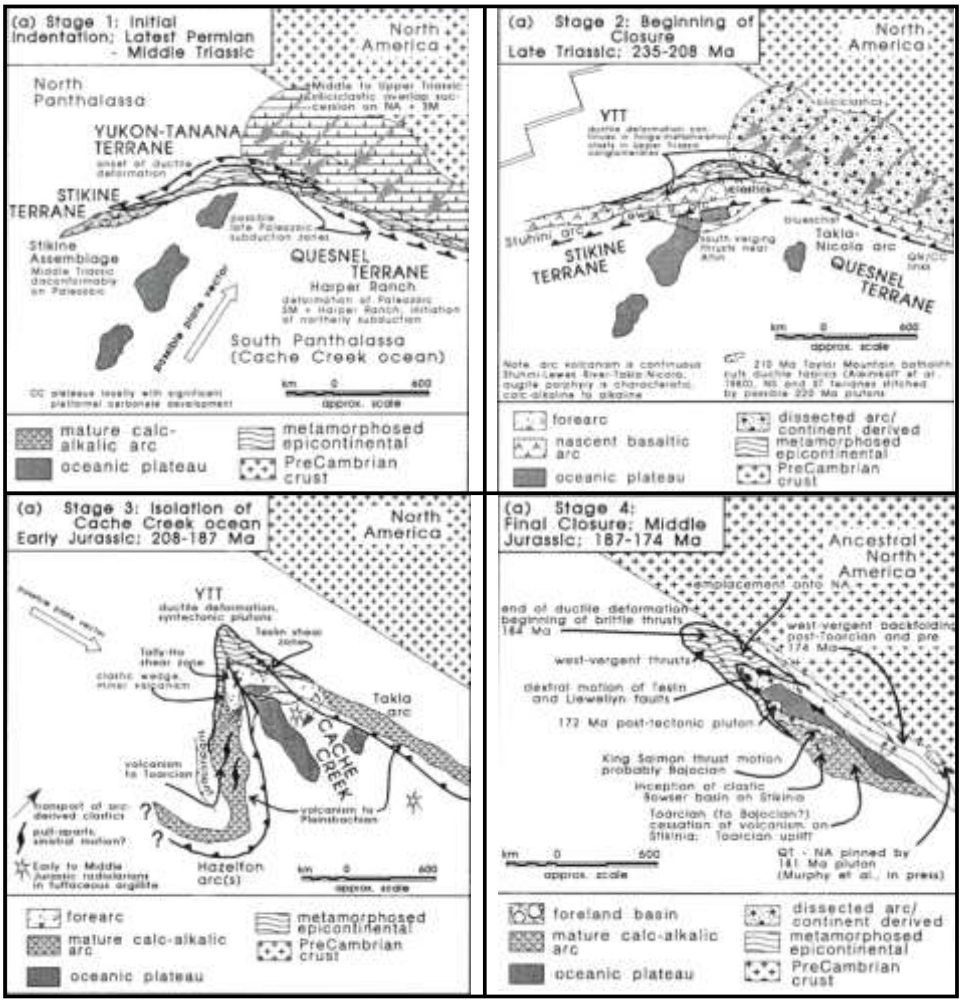

Figure 1.3: [Stage 1]: Late Permian to Middle Triassic arrangement of the Stikine and Quesnel terranes. [Stage 2]: Late Triassic assemblage of Stikine and Quesnel terranes showing collision of the Cache Creek oceanic platforms. [Stage 3]: Early Jurassic closure of the Cache Creek Ocean. [Stage 4]: Middle Jurassic configuration of terranes during amalgamation. Taken from Mihalynuk et al. (1994). HR - Harper Ranch Assemblage.

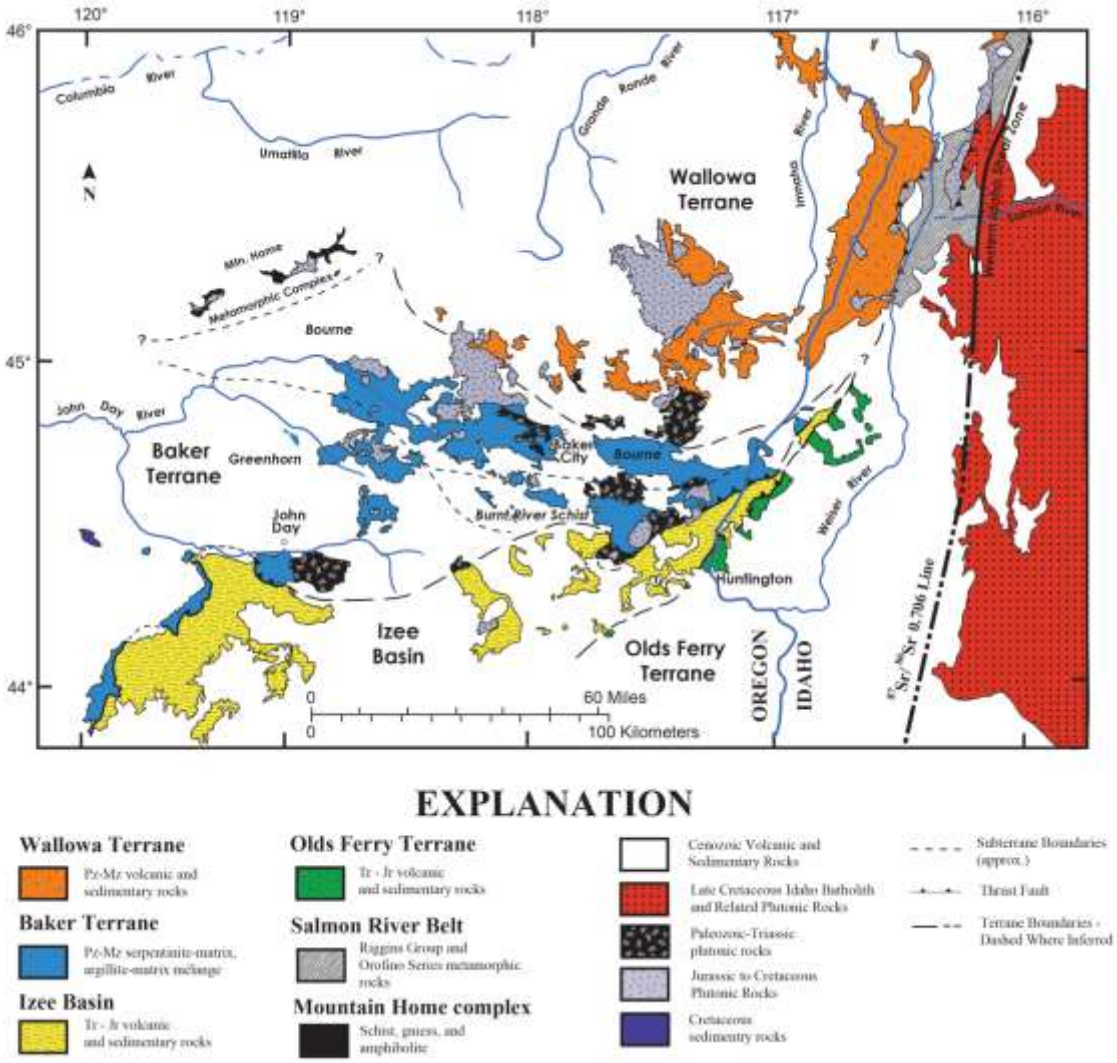

Figure 1.4: Geologic map of the Blue Mountains province showing the three major terranes, the Izee basin, intrusive elements, as well as Cenozoic cover. Modified from LaMaskin et al. (2011b) and Schwartz et al. (2011b). Initial Sr. 0.706 line modified from Armstrong et al. (1977).

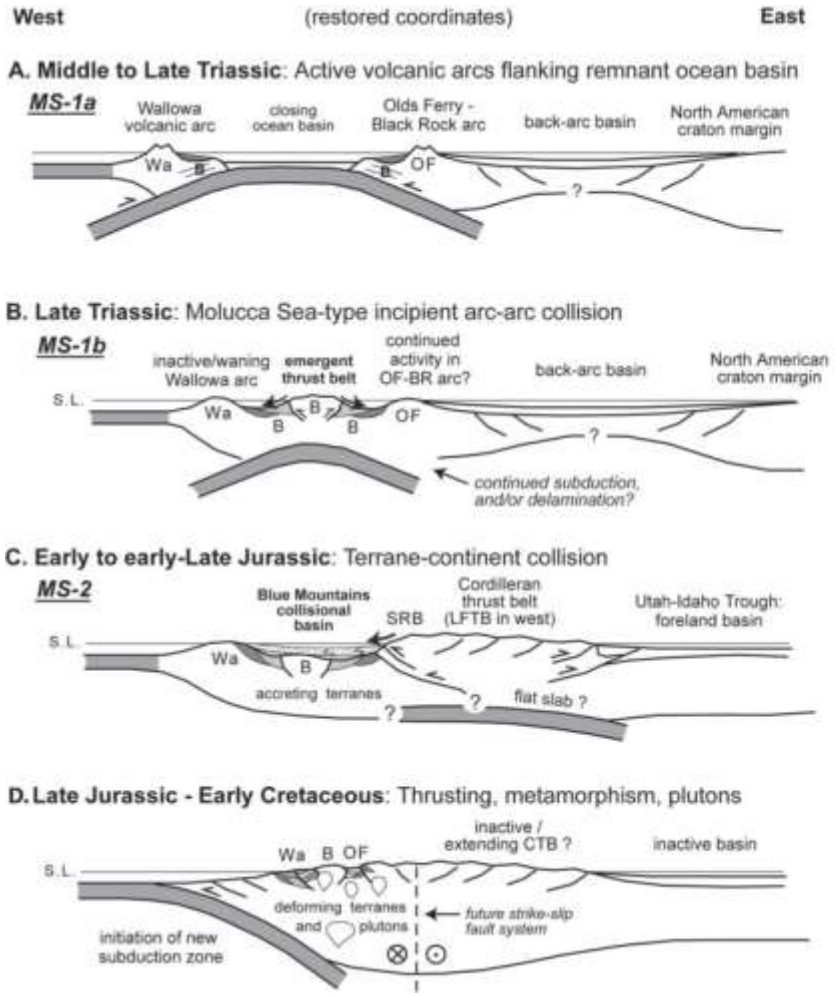

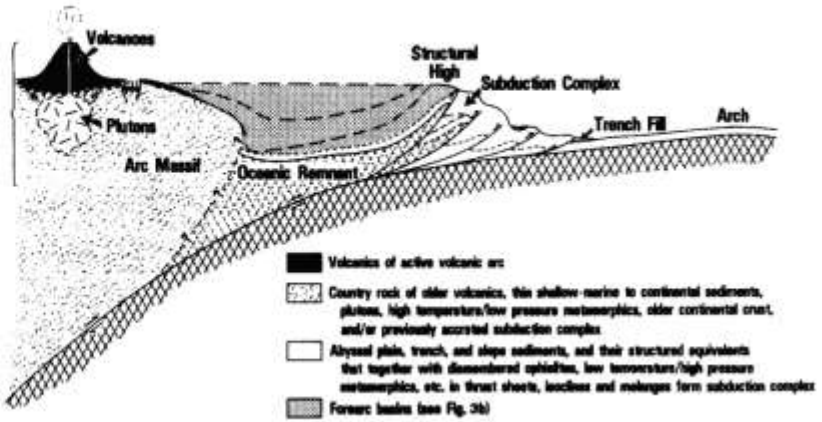

Figure 1.5: Schematic illustrations of the collisional basin model (A – C) and a forearc basin model for the Izee basin (D). Wa - Wallowa, B - Baker, OF - Olds Ferry. Collisional basin model from Dorsey and LaMaskin (2007), forearc basin model form Dickinson and Seely (1979).

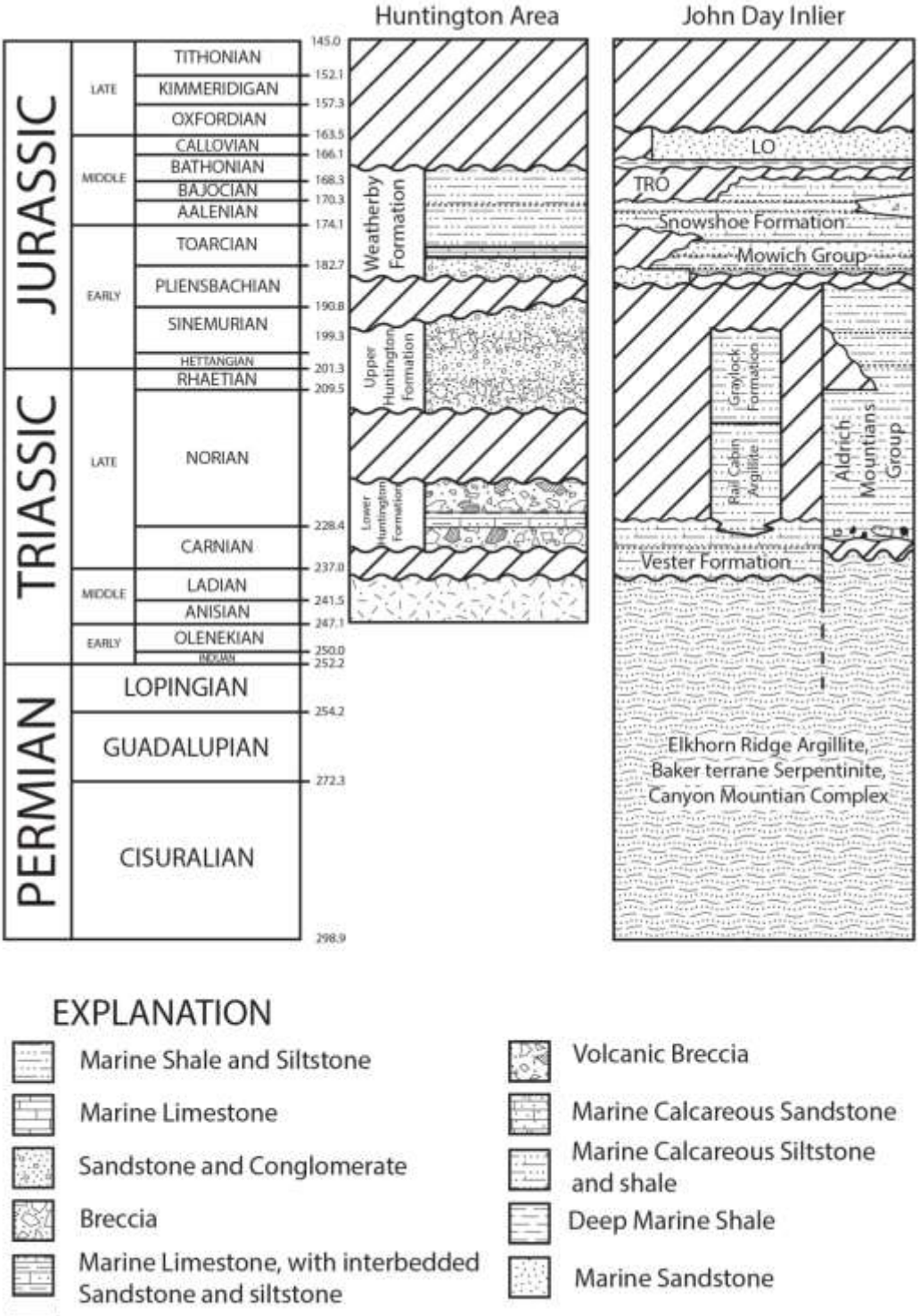

Figure 1.6: Revised chronostratigraphic columns for the Huntington and Weatherby Formations in the Huntington area and the Izee stratigraphy in the John Day Inlier. Huntington Formation data taken from Tumpane (2010) and data for the John Day Inlier taken from Dorsey and LaMaskin (2007). LO - Lonesome Formation, TRO - Trowbridge Formation. Geologic Timescale 2012 (Gradstein et al. 2012).

CHAPTER TWO: THE DEPOSITIONAL AND DEFORMATIONAL EVOLUTION OF THE WEATHERBY FORMATION

Introduction

The North American Cordillera provides the opportunity to study continental growth through collisional, terrane accretion processes. The North American Cordillera hosts a number of tectonic terranes that have accreted to the western margin of North America since the Late Paleozoic revealing elements and timescales of growth. These terranes are exposed extensively in Alaska and Canada, as well as in erosional windows like the Blue Mountains of Oregon and Idaho, and the Klamath Mountains of California and western Nevada (Figure 2.1). These terranes have been investigated and correlated from Alaska to southern British Columbia; however, correlating the tectonic history of the Canadian Cordillera and western U.S. Cordillera has been problematic due to extensive Cenozoic volcanic and sedimentary cover in the Pacific Northwest. Existing correlation models pose interesting problems for the geologic framework in the vicinity of the Blue Mountains province of eastern Oregon. For example, the Blue Mountains province lacks Stikinia equivalent rocks, contains the southernmost exposures of exotic Insular superterrane elements, and accommodates the only exposures in the North American Cordillera that juxtapose exotic Insular superterrane rocks and Quesnellian-type continental fringing arcs separated by intervening Cache Creek accretionary complex rocks.

The pre-Cenozoic rocks of the Blue Mountains province have been divided into three distinct accreted terranes. From north to south, these are the Wallowa volcanic arc terrane, the Baker mélange terrane, and the Olds Ferry volcanic arc terrane. An overlying sedimentary overlap sequence termed the Izee basin was deposited onto supracrustal sequences of the Olds Ferry and Baker terranes (Figure 2.2). The Wallowa terrane is a far travelled allochthonous oceanic island arc dominated by Late Permian to Early Triassic island arc igneous rocks overlain by extensive Triassic volcanic and volcaniclastic rocks (Brooks and Vallier, 1978; Dickinson and Thayer, 1978; Brooks, 1979). The Baker terrane is composed of an assemblage of highly deformed and metamorphosed late Devonian to Early Jurassic mafic igneous and marine sedimentary rocks (Brooks and Vallier, 1978; Dickinson and Thayer, 1978; Brooks, 1979; Vallier, 1995, Schwartz et al., 2010). The Olds Ferry terrane is composed of a wide compositional range of Middle Triassic to Early Jurassic volcanic and plutonic arc rocks and associated volcaniclastic sediments (Brooks and Vallier, 1978; Dickinson and Thayer, 1978; Brooks, 1979; Vallier, 1995; Avé Lallemant 1995, Tumpane, 2010).

The tectonic history of the Izee basin has been widely debated since the first investigations into the terranes of the Blue Mountains province. The Izee stratigraphy consists of forearc sediments exposed as discreet inliers in the John Day, Ironside Mountain, and Huntington areas of central and eastern Oregon (Figure 2.2); correlations between the western and the eastern sub-basins have been difficult to determine. The Izee basin was first interpreted as a distinct tectonostratigraphic terrane between the Baker and Olds Ferry terranes (Brooks and Vallier, 1978; Brooks, 1979). Studies of the Izee sediments exposed in the John Day area interpreted the deposits as forearc sediments

locally derived from the Baker and Olds Ferry terranes (Dickinson and Thayer, 1978; Dickinson, 1979). The eastern Izee stratigraphy has not been as well studied or constrained as the western Izee sediments exposed in the John Day area. Understanding the depositional and deformational history of the eastern Izee sub-basin will lead to a better understanding of internal basin correlations and relationships between Izee sediments as well as potential Olds Ferry and Baker terrane sources.

In the eastern Izee sub-basin, the Weatherby Formation overlies the Huntington Formation along an angular unconformity with a hiatus less than 6.4 million years (Tumpane, 2010). The short time gap in the rock record separating the upper Huntington Formation with the Weatherby Formation is not typical of a terrane boundary. Thus, the Izee sediments have been interpreted as a sedimentary onlap sequence deposited onto the western slopes of the Olds Ferry arc (Dickinson and Thayer, 1978; Dickinson, 1979; Doresy and LaMaskin, 2007; Tumpane, 2010). The Baker terrane is in fault contact with the Weatherby Formation along the Connor Creek fault (Brooks and Vallier, 1978; Brooks, 1979; Avé Lallemant, 1983; Vallier, 1995, Dorsey and LaMaskin, 2007; LaMaskinet al. 2011b).

In this study, a combination of field observations, high precision U-Pb geochronology on primary volcaniclastic layers, and detrital zircon U-Pb geochronology are used to investigate the timing of deposition and deformation of the Weatherby Formation. This study tests and distinguish between two hypotheses regarding the deposition and deformation of the Weatherby Formation: (1) the Weatherby Formation is an upright succession of sediments deposited onto the Olds Ferry terrane that is juxtaposed with oceanic mélange of the Baker terrane in the north by the Connor Creek

fault; or (2) the Weatherby Formation is a synformal remnant of a larger forearc basin deposited onto both the Olds Ferry and Baker terranes, deformed by movement along the Connor Creek fault during amalgamation of the Wallowa and Olds Ferry terranes.

This study provides new evidence that the Weatherby Formation is an Early to Middle Jurassic forearc basin deposited on both the Olds Ferry and Baker terranes. New ages for primary volcaniclastic layers within the Weatherby Formation indicate that the Olds Ferry volcanic arc was active and shedding detritus into the early Middle Jurassic. This study also clarifies the structural orientation and deformation of the Weatherby Formation into a basin-wide synform with overturned beds on the northern limb. The overturning of beds indicates that at least part of the Baker terrane floored the Izee basin and was in relatively close proximity of the Olds Ferry terrane by the Early Jurassic. The new results from the Weatherby Formation are also used to correlate the western and eastern Izee sub-basins, indicating that the two basins are related tectonostratigraphically and temporally. Detrital zircon provenance of sediments within the western and eastern Izee sub-basins both were sourced from Olds Ferry and Baker terrane rocks during the Early to Middle Jurassic. Further correlations suggest extensive basin development all along the North American Cordillera during the late Triassic to Middle Jurassic. These correlations provide for new interpretation of the Izee basin and a greater understanding of the Late Triassic to Middle Jurassic history of the North American Cordillera.

Geologic Setting

The Huntington Formation

The Olds Ferry terrane is predominately expressed as the Huntington Formation exposed along the Snake River in eastern Oregon and west-central Idaho. Lava flows, shallow intrusives, and volcaniclastic rocks dominate the strata of the Huntington Formation (Brooks, 1979; Vallier, 1995) (Figure 2.3). The volcanic rocks range from basalt to rhyolite with an overall increase in silica higher in section (Vallier, 1995; Tumpane, 2010). The interbedding of fossiliferous marine sedimentary rocks suggests most of the volcanic rocks were deposited in subaqueous environments (Vallier, 1995). All of the rocks of the Huntington area have undergone metamorphism to lower greenschist facies (Vallier, 1995). The Huntington Formation has previously been given a late *Carnian* to late *Norian* age based on fossils, primarily ammonites, found within the thin and/or discontinuous sedimentary units (Brooks, 1979; Brooks and Vallier, 1978; Vallier, 1995; Dorsey and LaMaskin, 2007). Recent high precision U-Pb geochronology of the Huntington Formation has provided new age constraints on volcanic strata, giving an age of the Huntington Formation from early *Carnian* (Late Triassic) to the *Pliensbachian* (Early Jurassic) (Tumpane, 2010). Recent studies of the Huntington Formation have divided the formation into two members, the lower Huntington Formation and upper Huntington Formation, based on lithologic characteristics, angular unconformities, and high precision geochronology (Collins, 2000; Dorsey and LaMaskin, 2007; LaMaskin, 2008; Tumpane, 2010).

The lower Huntington Formation is characterized by basaltic andesite to andesite lava flows, interflow breccias, minor volcanic sandstones, rare felsic pyroclastic rocks,

and conformable and olistostromal limestones (Tumpane, 2010). The trondjhemitic Brownlee pluton comprises the basement rocks that the lower Huntington Formation unconformably overlies. The intrusion of basaltic and andesitic dikes and sills through the pluton, along with weathering and brecciation occurring on the surface of the Brownlee Pluton confirm the unconformable contact with the lower Huntington Formation (Tumpane, 2010). The Brownlee Pluton has been dated at 237.77 Ma (Kurz et al., 2008). While the oldest U-Pb age from the lower Huntington Formation is 221.72 Ma, providing further evidence that the Brownlee Pluton did not intrude into the Huntington Formation (Tumpane, 2010). Late *Carnian* ammonites in the *Tropites subbullatus* and *dilleri* ammonite zones shorten the possible unconformity between the lower Huntington Formation and the Brownlee pluton to less than 6 Ma (LaMaskin, 2008; Tumpane, 2010).

The upper Huntington Formation was deposited along an angular unconformity with the lower Huntington Formation (Tumpane, 2010) and the Iron Mountain Pluton that intruded into the lower Huntington Formation at 210.13 Ma (Kurz et al., 2008). Uplift and erosion of the lower Huntington Formation and the Iron Mountain Pluton occurred in the middle Late Triassic, exposing the Iron Mountain Pluton and portions of the Brownlee Pluton on which the upper Huntington Formation was deposited (Tumpane, 2010). The upper Huntington Formation consists of silicic volcanic flows and pyroclastic deposits, volcanic sandstones, turbidites, cobble and boulder conglomerates, and laminate shale deposits (Vallier, 1995; Tumpane, 2010). *Pliensbachian,* ca. 188 to 187 Ma, volcanic units within the upper Huntington Formation indicate that volcanic activity of the Olds Ferry terrane continued into the Early Jurassic (Tumpane, 2010). The Weatherby

Formation of the Izee basin overlies the upper Huntington Formation in the northwest along an unconformity spanning at most 6.4 million years (Vallier, 1995; Avé Lallemant, 1995; Dorsey and LaMaskin, 2007; Tumpane, 2010).

Izee Basin Sediments: Huntington, Oregon

The Jurassic Izee basin sediments exposed north and west of Huntington, Oregon are composed of three units, the McChord Butte conglomerate, the Dennet Creek limestone, and the Big Hill shale (Payne and Northrup, 2003) (Figure 2.3). The McChord Butte conglomerate of the basal Weatherby Formation is made up of primarily rounded fragments of volcanic rocks. The majority of clasts comprise locally derived volcanic rocks eroded from the underlying Huntington Formation (Brooks, 1967; Brooks, 1979), as well as granitic rocks from the plutonic core of the Olds Ferry arc. The presence of granitic pebbles indicates differential uplift and erosion of the Huntington Formation during the deposition of the McChord Butte conglomerate (Brooks, 1979). The McChord Butte conglomerate also contains chert clasts derived from the Baker terrane, indicating uplift and erosion of the Baker terrane by the Early Jurassic (Brooks, 1979). The conglomerate transitions to interlayered siltstones and progressively more carbonate rich marl layers into the Dennet Creek limestone (Brooks, 1979; Avé Lallemant, 1983). The Dennet Creek limestone is a massive shallow marine limestone layer deposited on top of the McChord Butte conglomerate. The Dennet Creek limestone has undergone complete grain recrystallization via shearing and dynamic metamorphism that is apparent in the stretched grains of the McChord Butte conglomerate. Locally, the limestone layer is a convenient marker bed for faulting within the lower section of the Weatherby Formation.

The Weatherby Formation stratigraphy above the red and green basal McChord Butte conglomerate and the variably thick lenses of the Dennet Creek limestone is a thick package of predominantly very fine-grained marine flysch. These sediments include discreet layers of medium to coarse-grained distal volcanic, pyroclastic, and sedimentary material interbedded throughout the fine-grained marine flysch. The area has been affected by greenschist facies metamorphism and a strong shear cleavage that transposes evidence of sedimentary structures and bedding within the fine-grained phyllite (Brooks and Vallier, 1978). Only the variably present graded, coarse-grained layers can be used to recognize bedding of the upper phyllite within the Weatherby Formation.

The fabric of the Weatherby Formation is defined by a pervasive cleavage that strikes dominantly northeast/southwest and dips steeply to the northwest. Previous interpretations have found that the fold axes defined by shear cleavage and bedding intersections have suggested that the cleavage resulted from a compressional deformation event that occurred during sedimentation (Brooks and Vallier, 1978). Southerly verging, kilometer wavelength folding of the Weatherby Formation has been recognized (Schwartz et al., 2010). A recent study in the western most exposures of the Weatherby Formation and the Baker terrane near Pedro Mountain reported extensive Oligocene and Miocene normal faults that disrupted many of the Mesozoic boundaries in the area (Starns, 2011). Cenozoic normal faulting has also been recognized in the southern portions of the Weatherby Formation and throughout the Huntington Formation. The normal faulting and continuations of normal faults within the Huntington Formation could have affected the Weatherby Formation more extensively than what has been previously recognized, but due to the weathered state and fine-grained nature of the

Weatherby Formation this determination is difficult. The Connor Creek thrust dips steeply to the northwest juxtaposing the Baker terrane mélange and greenstone rocks onto the Olds Ferry terrane and the Jurassic marine flysch of the eastern Izee sub-basin.

Bounding faults and changes in sediment types on either side of the Izee sediments caused the first interpretations of the Izee package of rocks to be a tectonically distinct terrane (Brooks and Vallier, 1978). Recent studies have presented evidence against the Izee stratigraphy being a distinct tectonic terrane. Studies of rock units within the Weatherby Formation have shown that the composition of the sediments suggest a local provenance; locally derived clasts of volcanic and plutonic rocks typical of the Huntington Formation have been recognized within the basal conglomerate, suggesting a depositional boundary instead of a terrane boundary (Brooks, 1979; Dorsey and LaMaskin, 2007; Tumpane, 2010). Coupling this provenance evidence with new U-Pb geochronology of the upper Huntington Formation and overlying Weatherby Formation, the boundary has more recently been interpreted as a variably tectonized, but original depositional boundary (Avé Lallemant, 1983; Payne and Northrup, 2003; Wright, 2005; Dorsey and LaMaskin, 2007; Tumpane, 2010). The hiatus of the unconformity between the upper Huntington Formation and the basal conglomerate of the Weatherby Formation has been recognized as being no more than a few million years (Tumpane, 2010). The age difference across the unconformity of the upper Huntington Formation and the basal Weatherby Formation is more typical of a depositional hiatus than the large contrasts expected between terranes.

Izee Basin Sediments: Ironside Mountain Inlier

The Mesozoic sediments exposed in the Ironside Mountain area of central Oregon are made up dominantly of the Weatherby Formation (Figure 2.2). The sediments in this area are strongly folded with many Cretaceous and younger intrusions primarily along the anticlinal axis of the exposed area (Hooper et al., 1995). The Weatherby Formation in this inlier is composed of lithic wacke and arenites, slates, silty limestones, and some siltstones (Engh, 1984; Hooper et al., 1995). The rocks in the northern area of the inlier still contain wacke and siltstone deposits but also become coarser with the appearances of conglomerate deposits (Hooper et al., 1995). Clasts derived from the Baker terrane are prominent within the Weatherby sediments of the Ironside Mountain Inlier. Although the sediments are in fault contact with the Baker terrane in the northern section of the inlier, the abundant presence of chert clasts within the Weatherby Formation suggest the sediments were originally laid down along an unconformity with the mélange of the Baker terrane (Hooper et al., 1995).

Izee Basin Sediments: John Day Inlier

The sediments of the Izee basin, in its western most exposures near the town of Izee in east-central Oregon, are much more diverse than those in the eastern outcrop belt near Huntington, Oregon (Figure 2.3). Two units of primarily turbidite deposits spanning the Middle Triassic to Early Jurassic were deposited onto the mélange of the Baker terrane (Figure 2.3). The Vester Formation rest unconformably on the Baker terrane and is primarily a chert-pebble conglomerate and chert-grain sandstone interbedded in areas with fine-grained, dark marine lutite (Dickinson and Thayer, 1978; Dickinson, 1979). An abundance of chert clasts as well as Archean, Paleoproterozoic, and Paleozoic detrital

zircons suggests the unit is primarily derived from erosion of uplifted mélange located to the northwest of the Vester Formation (Dickenson and Thayer, 1978; Dickinson, 1979; LaMaskin et al., 2011b). The Vester Formation was deposited in the early Late Triassic evidenced by *Carnian* mollusk fossils found within the formation (Dickinson, 1979). The Aldrich Mountains Group is deposited unconformably above the Vester Formation. The Aldrich Mountains Group is composed of four different formations of overlapping wedges with a total thickness of about 10,000 m (Dickinson and Thayer, 1978). The sediments of the group are primarily a dark lutite with interbedded andesite rich turbidite deposits (Dickenson, 1979). These deposits are interpreted as *Norian* (Late Triassic) to *Sinemurian* (Early Jurassic) slope deposits with some slope channels still preserved (Dickinson and Thayer, 1978). Mélange influences have decreased with minor erosional debris primarily near the basal contact with the Vester Formation. Detrital zircons display a shift to primarily Silurian and Devonian grains with Late Paleoproterozoic and Mesoproterozoic influences as well as a lower appearance of Permo-Triassic grains (LaMaskin et al., 2011b). Volcaniclastic greywacke and calcarenitic turbidites compose the upper units of the Aldrich Mountain Group. The Vester Formation experienced a significant amount of deformation before the Aldrich Mountain Group was deposited (Dickinson and Thayer, 1978; Dickinson, 1979). Later compressional deformation caused complex folding and faulting of the Vester Formation and Aldrich Mountains Groups placing some area of the Vester Formation in direct fault contact with the Aldrich Mountains Group (Dickinson and Thayer, 1978; Dickinson, 1979). Deformation to both units caused fault blocks of the Baker terrane to thrust up into the basal sediments of these units (Dickinson and Thayer, 1978; Dickinson, 1979). This compressional

deformation caused complex folding and faulting of the Vester Formation and Aldrich Mountains Groups (Figure 2.4.C)

Late Early to Late Jurassic weakly metamorphosed and primarily non-deformed sediments rest with a marked angular unconformity on the complexly deformed Vester Formation and the Aldrich Mountains Group (Figure 2.4. C). The Mowich Group is the lowest stratigraphic unit in the Jurassic sediments composed of a varied shelf assemblage including fossiliferous marine sandstones that fine upward into offshore calcarenite, volcaniclastic turbidites, and shale (Dickinson and Vigrass, 1965; Dickinson and Thayer, 1978; Dorsey and LaMaskin, 2007) (Figure 2.3). The lower Mowich Group hosts basal 10 – 25 m thick conglomerate layers, limestone layers 2 – 12 m thick, and massive volcanic sandstones with thin sheets of calcareous sandstones and sandy calcarenite (Dickinson and Thayer, 1978). A thick succession of sparingly fossiliferous black shales and volcaniclastic turbidites compose the upper Mowich Group (Dickinson and Thayer, 1978). Fossil evidence suggests the Mowich Group ranges from *Pliensbachian* (middle Early Jurassic) in the lower units to lower *Toarcian* (late Early Jurassic) in the upper most units (Imlay, 1968). Izee sediments of the Huntington area have been correlated to the Mowich Group due to the similar fashion the Weatherby Formation overlie sediments of the Huntington Formation. The overlying Snowshoe Formation and Trowbridge Formations are a package of thinly bedded turbidites and shales respectively (Dickinson and Thayer, 1978). The Snowshoe Formation is dominantly volcaniclastic turbidites composed of thick lenses of volcanic conglomerates and sandstones interbedded with dark lutites (Dickinson and Thayer, 1978). The Snowshoe Formation overlaps the Mowich Group and is deposited directly onto the Greenhorn subterrane in the Suplee area

of central Oregon (Dickinson and Thayer, 1978). The Snowshoe Formation is primarily Middle Jurassic (*Bajocian*) in age with some upper *Toarcian* and lower *Callovian* beds (Imlay, 1973). Overlying the Snowshoe Formation, conformably in places and unconformably in others, is the dominantly black lutite Trowbridge Formation (Dickinson and Thayer, 1978). Volcaniclastic strata and volcanic sandstones in the lower sections grade upward to volcaniclastic tuff and then into the massive black lutite (Dickinson and Thayer, 1978). The Lonesome Formation is a thick (3000 m) unit that progrades overtop the Trowbridge Formation (Dickinson and Thayer, 1978). This succession has been interpreted as a relatively conformable upward succession of basin-plain, outer-fan, sand-rich lobe, and mid-fan channel deposits of *Callovian* (late Middle Jurassic) sediments (Imlay, 1964; Dickinson and Thayer, 1978). Detrital zircon analyses of the Late Triassic to Middle Jurassic sediments of the John Day Inlier indicate a shift in provenance to primarily Mesozoic grains with early Precambrian influences (LaMaskin et al., 2011b). This shift in detrital zircon ages suggests a more local volcanic source emerged in the Late Triassic and provenance shifted from the west-northwest in the Vester Formation and Aldrich Mountains Group to an east-southeastern direction at that time (LaMaskin et al., 2011b). Cretaceous sediments unconformably overlie all the Triassic and Jurassic sediments of the John Day Inlier, indicating uplift and erosion in central Oregon around the Jurassic-Cretaceous boundary (Dickinson and Thayer, 1978).

Many volcanic arc rock fragments have been recognized in the southwestern portion of the Izee stratigraphy as well. The stratigraphy in this area is much more extensive, weakly metamorphosed, and not very deformed making this an ideal spot to study the stratigraphy of the forearc deposits (Brooks, 1979). Throughout the John Day

area of the Izee strata the Mesozoic sandstones contain sedimentary detritus of typical volcanic island arcs (Brooks, 1979). An abundance of Late Triassic to Early Jurassic detrital zircon grains in the Mowich Group, Snowshoe Formation, and Lonesome Formation indicate these sediments were heavily influenced by local volcanism. Although the Olds Ferry terrane is not exposed to the southwest of Juniper Mountain in eastern Oregon, Brooks (1979) inferred a southwestern extent of the terrane to exist beneath Tertiary cover that could be the likely source for the arc detritus.

Results

Fieldwork was conducted during the spring, summer, and fall of 2011 and the spring and summer of 2012. A geologic map was created of the Connor Creek drainage, the Dennet Creek drainage, and the vicinity of Lookout Mountain Road, representing sample locations, contact locations, and new structural data. Samples were collected for U-Pb geochronological analyses. Locations of these samples can be found in Table 2.1 and on Figure 2.5, and their stratigraphic relationships summarized in Figure 2.6. Detailed hand sample descriptions, petrographic observations, and photomicrographs of the samples can be found in Appendix A.

Sedimentology and Lithologic Classification of the Weatherby Formation

Rocks that are of a primary volcaniclastic origin, after White and Houghton (2006), will be described using volcanic identifiers such as ash, tuff, and lapilli. Rocks that are sedimentary in origin will be described using sedimentary rock identifiers such as shale, siltstone, and sandstone, as well as terms such as volcanic sandstone and tuffaceous shale if there is a high abundance of volcanic material present. The samples and results of

this study are presented in a structural context using the unconformity between the upper Huntington Formation and the Weatherby Formation as the primary datum, and extending structurally upward to the Connor Creek fault.

The rocks above the basal conglomerate and limestone are primarily fine-grained marine flysch deposits with alternating beds of coarse-grained volcanic-rich layers, siltstones, and argillites that have metamorphosed to phyllite and slates (Brooks and Vallier, 1978). The term flysch was given to these deposits meaning a sedimentary formation derived by the erosion of an uplifted proximal landmass (Brooks and Vallier, 1978). The interbedded coarser grained volcanic-rich event beds in many instances display normal grading; however, some of the coarse-grained horizons are massive and cannot be used as up indicators. The marine flysch section of the Weatherby Formation, due to the primarily fine-grained nature of the deposits, does not resist well to erosion and is expressed as rolling hills with little outcropping throughout the Huntington area.

The marine flysch portions of the Weatherby Formation contain event beds of sub-angular to angular, poorly sorted, coarse-grained material composed primarily of lithic fragments. In previous studies of the Weatherby Formation, these volcanic-rich horizons have been referred to as volcanic wacke, volcaniclastic material, and turbidite deposits (Brookes and Vallier, 1978; Avé Lallemant, 1983; Imlay, 1986; Dorsey and LaMaskin, 2007). In hand sample, the lithic fragments in these event horizons can comprise both of volcanic lapilli and various sedimentary rock fragments, namely andesitic to dacitic volcanic clasts, a minor amount of chert clasts and quartz-rich sandstone clasts. The sizes of these lithic fragments vary from layer to layer but on average are between 2 and 8 mm in diameter with markedly stretched grains in some

locations and no evidence of stretching in others. In the field, variability in the abundance of volcanic lapilli and rounding can be observed between each coarse-grained horizon as well as color variations, most likely attributed to weathering, with primarily green colors observed on clean surfaces. These coarser grained event horizons within the marine flysch will be termed volcaniclastic turbidites, referring to the graded occurrences, or volcaniclastic grain-flow deposits. These volcanic-rich event horizons were targeted for U-Pb geochronology to determine the depositional history and provenance of the Weatherby Formation.

Based on the relative abundance of volcanic lapilli in the lithic load, and degree of rounding of clasts, two different event horizons can be partitioned. Petrographic analyses of the lithic fragments composing these event horizons reveal layers that contain a high abundance of angular juvenile volcanic material with a low abundance of quartz grains as well as layers that contain well rounded, quartzose-rich lithic fragments with a low abundance of volcanic material. The layers that contain a high abundance of volcanic material are dominated by angular plagioclase phenocrysts in addition to volcanic lapilli. These plagioclase phenocrysts support a volcanic origin. Subangular to angular quartz grains within these layers are rare and are present exclusively in the finer grained matrix of the rock. The moderate rounding of the quartz crystals and the presence of holocrystaline clasts suggest that the juvenile lithic fragments had some recycled material incorporated during the accent of the magma to the surface or during the flow over pre-existing rock. Due to the deep marine depositional environment of these sediments, the likelihood of them being primary volcanic deposits such as lava flows or ash falls is

unlikely. However, the angularity and poor sorting of the volcanic lapilli within these horizons suggest this material has not traveled far from the source.

Other layers within the marine flysch contain a high abundance of quartzose lithic fragments and a lesser amount of volcanic material. These horizons are dominated by subangular to rounded quartz fragments and holoclastic material. Plagioclase crystals are absent or rare, and if present are highly altered. The rounded lithic fragments and low abundance of volcanic lapilli suggests these deposits formed from the erosion of previous volcanic deposits, allowing for the presence of epiclastic zircon grains in mineral separates but are not directly related to an eruption event.

There have been many classification schemes for clastic deposits that are rich in volcanic material. Early studies focused primarily on pyroclastic rocks (e.g. Wentworth and Williams, 1932), studies in the late 1950's and early 1960's used classification nomenclature that focused on particle-forming processes (e.g. Fisher, 1961), and more recent studies have used transportation and depositional mechanisms as a basis for classification (McPhie et al., 1993; Cas and Wright, 1987; White and Houghton, 2006). McPhie et al. (1993) make a distinction of deposits that were resedimented during an eruption and epiclastic deposits that were weathered, eroded, reworked, and then deposited. White and Houghton (2006) combine classification terminology of Fisher (1961) with a depositional-origin focus (Cas and Wright, 1987; McPhie et al., 1993). Due to the depositional and transportation focus and terminology from Fisher (1961) of this classification scheme, this nomenclature is used in this study, to make inferences on the genetic origins of the volcanic turbidites and grain-flow deposits within the Weatherby Formation.

White and Houghton (2006) define primary volcaniclastic rocks as accumulations of material that were mobilized and deposited as a direct result of explosive or effusive volcanism that was not stored prior to deposition. White and Houghton (2006) divide the components of a primary volcaniclastic deposit into three broad groups: juvenile material from newly erupted lava, recycled lithic material from the rock that the eruption is deposited on, and material that are mechanical mixtures of both juvenile and recycled material. Using nomenclature form White and Houghton (2006) the volcanic lapilli-rich deposits with an abundance of angular plagioclase phenocrysts are interpreted as primary volcaniclastic deposits, acknowledging that they represent a combination of both predominant juvenile and subordinate recycled material. U-Pb geochronology will be conducted on these volcaniclastic horizons to determine the depositional age of the layer. The coarse-grained layers that are dominated by subangular to rounded quartzose lithic fragments have a lesser amount of volcanic material, and none to rare occurrences of plagioclase grains are considered holoclastic or epiclastic in origin and are considered sedimentary deposits. These deposits comprise components that have been stored prior to mobilization and deposition and thus are more useful for provenance investigation and U-Pb geochronology to determine only the maximum age of deposition.

Structural Observations of the Weatherby Formation

Structural and stratigraphic relations in the Dennet Creek area suggest that these beds retain the original orientation of deposition. This orientation would be expected in a forearc depositional environment where material was sourced from arc volcanic sediments and deposited on the shelf and slope of the Olds Ferry volcanic arc. Although the thick package of marine flysch is primarily very fine-grained phyllite, there are a

number of coarse-grained event horizons throughout the section. These coarse-grained horizons are composed of both primary volcaniclastic and sedimentary sandstone turbidite and grain-flow deposits. If assumptions are made that the depositional mechanisms behaved under normal grain-flow processes, then the fining directions can be used as up indicators within the formation. For this study, an upright indication was defined by an event horizon fining direction away from the underlying unconformity between the Huntington Formation and Weatherby Formation. Field evidence suggested the Weatherby Formation beds in the area around Big Hill up the Dennet Creek drainage are upright (Figure 2.6a). The beds and cleavage in the southeastern portion of the Weatherby Formation display a high variability of dips ranging from 24 to 58 degrees to the northwest with two peaks ± 5 degrees of 30 and ± 5 degrees of 55 (Figure 2.8). The Weatherby Formation in the area of Dennet Creek is in a stratigraphically simple stack of sediments beginning with the basal Jet Creek Member (McChord Butte conglomerate and the Dennet Creek limestone) overlain by the marine flysch.

New structural field relations suggest that the upper section of the Weatherby Formation has been overturned from its original depositional orientation. Evidence of deposits fining toward the unconformity between the Huntington Formation and the Weatherby Formation are interpreted as overturned bed orientations. On the northern flanks of the basin, in the vicinity of the Connor Creek fault, coarse-grained sediments suggest these beds have been overturned in relation to the upright beds found in the southern flanks of the basin (Figure 2.7). Strike and dip measurements from the northern flanks of the eastern Izee sub-basin display much less variability in dip than those measured in the southern flanks of the basin. The average dip, 66 degrees to the

northwest, of the overturned beds is much steeper than that measured from the upright beds. The overturned beds appear to have been overturned as a result of folding in the footwall of the Connor Creek fault. The mean vector of overturned beds of the Weatherby Formation agrees well with the pole of the Connor Creek fault (Figure 2.8). Overturning of the beds within the Weatherby Formation can be explained by both large-scale folding of the section and as higher frequency folds within the Weatherby Formation. Due to the infrequency of up indicators within the Weatherby Formation, the exact position of the fold axis is difficult to discern from just structural indicators.

U-Pb Geochronology

The increasing precision of U-Pb zircon geochronology in the last couple decades has allowed for greater understandings of time within the rock record and what zircon ages actually mean. This new ability to distinguish time at a higher precision has given geologist the ability to answer much more in-depth and sophisticated questions to new and old problems. Sediments such as the Weatherby Formation composed primarily of marine flysch, metamorphosed to phyllite, with little or no sedimentary structure surviving at present can benefit from these advances in geochronology. The lack of surviving sedimentary structures, uniformity of the sections rock type, and little fossil evidence scattered throughout the area has made constraining the timing of deposition and deformation of the Weatherby Formation difficult. The lack of volcanic flow layers throughout the section has limited much of the geochronology to bracketing by the underlying Olds Ferry terrane, the overlying Baker terrane, and the intrusive igneous elements. To test the structural model, this study uses new high precision capabilities of U-Pb geochronology applied to tuff-rich primary volcaniclastic turbidite horizons and

detrital zircon U-Pb geochronological analyses of secondary volcanic-rich sandstone units within the Weatherby Formation to determine the structural orientation as well as the provenance and timing of deposition and deformation of the Weatherby basin. Cathodoluminescence (CL) images of analyzed zircon grains can be found in Appendix B and a summary of analysis results can be found in Table 2.1. Complete LA-ICPMS U-Pb results can be found in Appendix C, complete CA-TIMS U-Pb results can be found in Table 2.2.

The increased parsing of ages within a single sample due to an increasingly smaller error of ages for each single zircon grain analysis has demanded the need for increasingly more specified language (Miller et al., 2007). To describe the temporal differences, diverse origins, and relation to magma system and history in the individual zircon grains or groups within analyses, we use the terms *inherited grains*, *antecryst*, *xenocryst,* and *autocryst* (Miller et al., 2007). To review, an inherited zircon has been incorporated into a magma chamber or flow from the surrounding country rock. Inheritance can be distinguished from the other zircon grains within the sample usually by it being appreciably older. This happens quite often in the intrusion of plutons into country rock or during the flow of new eruptions over sedimentary or previously lain volcanic rocks due to the high resilience zircons have to anatectic events. An *autocryst* is the zircon grains that are exclusively linked to one magma pulse or increment. In this study, these are the grains that are interpreted as the crystallization age for both intrusive and extrusive elements. *Antecryst* refers to those zircons that have crystallized in an earlier pulse of magma or within discrete reservoirs that have later been incorporated into a larger pulse of magma. These grains will be less temporally different than the inherited

grains and may show similar chemical signatures to autocrystic grains used for the crystallization age of the magma body. *Xenocrysts* are essentially the same as inheritance, referring to a zircon grain that has survived an episode or episodes of partial melting and is usually several million years older as to easily be distinguished as unrelated to the magma system.

The primary sediment type in the Weatherby Formation is a fine-grained flysch that has been metamorphosed to phyllite. The majority of the sediments within the Weatherby Formation are fine-grained silts and shales with interbedded sandy layers and discrete volcanic-rich horizons. The primary volcaniclastic layers only make up a small percentage of the coarser grained event horizons that interbed the marine flysch. Due to the small representation the primary volcaniclastic layers provide, many holoclastic sedimentary layers were collected and analyzed for detrital zircon provenance and maximum deposition age constraints.

Detrital zircon analyses using the LA-ICPMS method do not use chemical abrasion to mitigate lead loss. Large uncertainties are associated with each analysis, giving a typical 10 million years or greater uncertainty. For this study more precision is needed to determine the maximum depositional age throughout the Weatherby Formation. Therefore, to determine if any of the analyzed grains were affected by lead loss and to decrease the uncertainty, a few grains from each sample analyzed using the LA-ICPMS method were chosen for single-grain analyses via CA-TIMS.

Dennet Creek

The Dennet Creek drainage, from the old abandoned mining town of Mineral, Idaho to the Snake River, allows access to the lower Weatherby Formation with

exposures of the basal unconformity, the McChord Butte conglomerate, the Dennet Creek limestone, and the marine flysch of the Big Hill shale (Figure 2.5, 2.7). In the Dennet Creek area, the Huntington Formation and the Weatherby Formation fold to the south with a north/northwest plunging hinge axis. The Dennet Creek area provides excellent exposure of a structurally simple portion of the basal Weatherby Formation along its unconformity with the upper Huntington Formation. Structure data and samples were collected in this area to determine the oldest depositional ages within the Weatherby Formation (Figure 2.7).

The McChord Butte conglomerate is exposed just above the north and south banks of Dennet Creek. To the north, the Dennet Creek limestone outcrops forming a cliff that can be traced along strike for about a kilometer east west. The Dennet Creek limestone is a light grey to grey medium-grained limestone. The thickness of the limestone in this area is about 100m with a gradational lower contact with the McChord Butte conglomerate and a sharp upper contact with the Big Hill shale. The lower gradational contacts transitions from the pebble conglomerate of the McChord Butte conglomerate to a zone of interbedded fine sandstones, siltstones, and marls, and then into the massive Dennet Creek limestone. Locally, within the limestone are thin siltstone and sandstone horizons that are typically tan to orange brown in color. The intermittent sandstone and siltstone sedimentary horizons vary in lateral extent and thicknesses from a few cm to 10s of cm. The limestone dips approximately 30 degrees to the northwest along the north side of Dennet Creek.

Exposed above the Dennet Creek limestone is the marine flysch that forms the majority of the upper Weatherby Formation (Figure 2.7). The sediment is a primarily

green fine-grained phyllite with interbedded sandy horizons. Two samples, DC 07-03 and DC 07-01 (referenced from Tumpane, 2010), were collected from the lower most units of the marine flysch within the Weatherby Formation. DC 07-03 was identified as a crystal tuff within a sequence of coarse-grained, normally graded volcanic sandstone to siltstone beds collected about six meters above the top of the Dennet Creek limestone (Tumpane, 2010). Four of ten zircons analyzed yielded a weighted mean $^{206}Pb/^{238}U$ age of 180.61 ± 0.17 Ma (Table 2.1, Figure. 2.8). DC 07-01 was collected about fifty meters above the top of the limestone and about twenty meters above the transitional zone from the lower sandstone and siltstone unit to the fine-grained flysch that dominate most of the Weatherby Formation. This bed has previously been interpreted as a welded tuff (Tumpane, 2010); however, reanalysis of the thin sections from this sample and its similarity to those collected during this study suggests it is a volcanic-rich turbidite and shall be termed a primary volcaniclastic deposit. Five of eight zircons analyzed yielded a weighted mean $^{206}Pb/^{238}U$ age of 173.91 ± 0.066 Ma (Table 2.1, Figure. 2.8).

DC11-01 was collected in this study, approximately 150 m above the top of the Dennet Creek limestone. The layer is composed of 1 - 5 mm quartz, feldspars, and lithic fragments (possibly pumice clasts) within a very fine-grained phyllitic matrix. This package of coarse-grained horizons strikes 238 degrees and dips 41 degrees to the northwest. The clasts have been stretched, forming a resolvable lineation trending 335 degrees and plunging 43 degrees to the northwest. The overall thickness of this particular coarse-grained horizon is about 25 m with interbedded fine and coarse-grained layers, averaging about 20 cm in thickness. Bedding can clearly be observed between the fine-grained and coarse-grained horizons. The fining direction of these sediments indicates

these beds are still in the original depositional orientation, in relation to deposition onto the Huntington Formation and Dennet Creek limestone. Five out of the seven zircon grains analyzed yielded a weighted mean $^{206}Pb/^{238}U$ age of 173.88 ± 0.07 Ma (Table 2.1, Figure. 2.8). The two grains that were not included in the weighted mean calculation returned older $^{206}Pb/^{238}U$ dates of 180.56 ± 0.27 and 182.33 ± 0.43 Ma. These two grains are considered to be antecrysts from previous magmatism that have been recycled into the eruptive material during the eruption or reworked into the flow during deposition.

Further up Big Hill on the north side of Dennet Creek, the exposures decrease. About 800 meters above Dennet Creek, the slope breaks to a shallower angle up to the top of Big Hill. DC11-04 is from a coarse-grained sandy horizon located about 20 m below the slope break at approximately 3800 feet elevation. The sandstone layer is about 10 cm thick and stratigraphically overlain by a few centimeter thick pure limestone bed. Above the slope break, there are no outcrops of the Weatherby Formation, but subcropping colluvium suggests a possible change in the sediments marked by both lighter colors and a finer grain size (Figure 2.7).

Detrital zircon analysis of DC11-04 (n = 38) yielded a range of $^{206}Pb/^{238}U$ dates from 171 ± 13 Ma to 2361 ± 126 Ma (Table C.1). The zircons can be distinctly separated into two groups of $^{206}Pb/^{238}U$ dates (Figure 2.10). DC11-04 contains an abundance of Precambrian grains dominated by Mesoproterozoic and Neoproterozoic grains (ca. 686-1286). Mesozoic grains form the strongest peak of detrital zircon ages ranging from 195 ± 13 Ma to 171 ± 13 Ma. The Mesozoic grains are interpreted as the primary temporal source to the detritus of DC11-04 with a weighted mean $^{206}Pb/^{238}U$ age of 182.4 ± 2.8 Ma (MSWD = 1.15) calculated from all Mesozoic grains minus any outliers. Due to the

sandy nature and lack of volcanic material in sample DC11-04, the weighted mean has been interpreted as a maximum depositional age. Alternatively, the youngest zircon $^{206}Pb/^{238}U$ date of 171 ± 13 Ma could be a more reliable depositional age than the weighted mean, although we must keep in mind the possibility of lead loss and the large uncertainties of these spot analyses.

To test whether the youngest LA-ICPMS analysis provide a robust maximum age of deposition, three of the youngest zircons were plucked out of the laser mounts for single-grain analyses using the CA-TIMS method. The three grains yielded $^{206}Pb/^{238}U$ dates of 182.41 ± 1.03 Ma, 185.45 ± 0.27 Ma, and 187.86 ± 1.13 Ma (Table 2.1), which are at the older end of the 95% confidence intervals of the laser data, which returned $^{206}Pb/^{238}U$ dates of 177.43 ± 14 Ma, 172.30 ± 12 Ma, and 180.97 ± 14 Ma, respectively (Figure 2.11). The discrepancies in the dates can be readily attributed to minor lead loss affecting the laser spots, which was mitigated during chemical abrasion. On the basis of the youngest CA-TIMS results, the maximum depositional age of the layer is thus interpreted as 182.41 ± 1.03 Ma, which is remarkably similar to the weighted mean laser age.

Wolf Creek

The Wolf Creek and Trail Creek area in Idaho offer a look at the base of the Weatherby Formation in the most southeastern exposures before the Mesozoic rocks are covered by Cenozoic formations (Figure 2.5). The Dennet Creek limestone in this area is a medium-grained, bluish-grey, massive deposit about 100 m in thickness. Locally, interbedded within the limestone is tan to orange, silty to very fine-grained sand sedimentary lenses. The limestone is laterally extensive with exposures on the north

slopes of Trail Creek, south and north slopes of Wolf Creek, and continuing along the west slope of Wolf Creek before disappearing under Columbia River basalts as the drainage hooks north. The limestone strikes 204 degrees and dips 24 degrees west-northwest in this area, displaying a fold to the south compared to the limestone exposed at Dennet Creek. Above the limestone exposure is a block of pebble conglomerate dominated by andesitic and basalt clasts with a minor amount of quartz sandstone pebbles.

The mouth of Trail Creek offers exposures of the typical green marine flysch across the transition to lighter colored sand and silt sediments. The fine-grained deposits are exposed to the northwest and the southeast of the sand and silt deposits. Overlying the Dennet creek limestone is a succession of dark green phyllite alternating between course and fine-grained layers. The coarse horizons are poorly sorted; however, the fine-grained packages dominate the area up Wolf Creek. The exposures in this area are extensively weathered, covered by dust and lichen, and along with pervasive cleavage makes up indicators difficult to determine throughout this site. Stratigraphically above the green marine phyllite to the northwest, the sediment transitions to lighter colored sand and silt deposits. The sandstone layers are primarily massive, fine to very fine-grained, with some boudined quartz veins appearing in one thick sandstone layer. The strike of these beds averages around 235 degrees with the dip of this area progressively steepening from primarily 26 to 52 degrees in the southeast, to 58 to 67 degrees further to the northwest.

Raft Creek

On the north facing slopes of Big Hill, including ridges to the immediate east and west of Big Hill, the slope angle roughly matches that of the sediment bedding, causing

an almost dip slope expression down to Raft Creek in the north (Figure 2.6). The Snake River between Dennet Creek and Raft Creek cuts perpendicular to strike of the upper sediments in the Weatherby Formation. This down cutting and subsequent road cuts along the Snake River allow for access to these lighter colored sediments observed in the colluvium on the upper slopes of Big Hill and outcropping along Trail Creek to the south. Fresh surfaces of the sand appear lighter in color, a light gray to white, with visible rip-up clasts. The sandy horizons are massive, composed primarily of quartz grains with some dark lithic fragments making up about 5% of the composition. Sedimentological observations indicate that these beds are overturned, as evidenced by graded bedding. DC11-05 was collected in a well-exposed region along the banks of the Snake River just south of the Raft Creek drainage. DC11-05 is from a coarse-grained sandy layer with .5 – 2 mm sand particles, and was collected for detrital zircon analysis via LA-ICPMS.

Eighty-eight zircons were analyzed from sample DC11-05, yielding a range of $^{206}Pb/^{238}U$ dates from 157 ± 9 Ma to 1260 ± 116 Ma (Table C.2). Sixty-one of the analyses yielded Mesozoic $^{206}Pb/^{238}U$ dates with over half of those grains falling in the late Early Jurassic to late Middle Jurassic (ca. 186 – 164 Ma). There is a noticeable Precambrian influence in these sediments dominated by Mesoproterozoic and Neoproterozoic grains (ca. 772 – 1260 Ma). This sample yielded a higher abundance of Paleozoic grains (ca. 549 – 350 Ma) than other samples and also yielded the apparently youngest grains in this study, with a weighted mean $^{206}Pb/^{238}U$ age of the Mesozoic group, minus outliers, of 172.3 ± 1.6 Ma (MSWD = 1.11).

The detrital analyses indicated some of the youngest $^{206}Pb/^{238}U$ dates of the Weatherby Formation into the Late Jurassic. These dates could bring the depositional age

of the Weatherby Formation well into the late Middle Jurassic and maybe into the earliest Late Jurassic. Four zircon grains were chosen using the results from the laser analyses to be analyzed via the CA-TIMS method, to test if these ages are truly *Callovian* and *Oxfordian*, or a result of significant lead loss. Three of the four grains yielded a weighted mean $^{206}Pb/^{238}U$ age of 173.01 ± 0.13 Ma (Table 2.1), with one grain giving a much older $^{206}Pb/^{238}U$ date of 191.44 ± 0.50 Ma. Similar to the results of DC11-04, these CA-TIMS analyses are at the older extreme of the 95% confidence limits of the LA-ICPMS analyses (Figure 2.11). This discrepancy again may be attributed to lead loss in the untreated zircon spot analyses, or the random fluctuations in the LA-ICPMS method. The maximum depositional age based upon the CA-TIMS results of < 173.0 Ma is consistent with the weighted mean of the LA-ICPMS analyses.

North of Connor Creek

Along the road that follows the bank of the Snake River north out of Huntington, Oregon, exposures of the Weatherby Formation as the Connor Creek fault is approached can be observed though road cuts. The cleavage becomes more pervasive in the sediments nearer to the Connor Creek fault. The sediments in this area are primarily silts, sands, and shales and are a lighter grey and white color with thin horizons of black very fine-grained layers (Figure 2.7). Due to the extensive cleavage in this area, bedding is difficult to discern and measure. Evidenced by the sediment color changes and grain size differences in areas, the cleavage appears to be along bedding. Cleavage strikes 245 degrees, with very steep dips from 69 to 76 degrees.

Connor Creek

The Weatherby Formation throughout the Huntington area has been heavily weathered, causing the formation to be expressed as rolling hills with large topographic reliefs in some areas and outcroppings almost exclusively limited to road cuts and drainages. The Connor Creek drainage offers significant exposures of the Weatherby Formation up to the Connor Creek fault contact zone (Figure 2.12). Connor Creek flows from the northwest to the southeast perpendicular to strike of the Weatherby units. Field observations were made and samples were collected in this area to obtain a relatively coherent traverse of the Weatherby sediments from the Snake River to the Connor Creek fault. This area is completely within the fine-grained marine flysch sediments of the Weatherby Formation (Figure 2.7).

The structurally lowest portions of the Weatherby Formation exposed at the mouth of the Connor Creek drainage offers the best exposure in this area. The beds dip about 65 ± 5 degrees to the north-northwest and strike west-southwest, east-northeast. A pervasive cleavage is evident throughout all of the Weatherby rocks causing observations of bedding indicators to be difficult, except as evidenced in normally graded sand to siltstone turbidite beds.

Sample LOM11-05 was collected from a coarse-grained turbidite horizon in the well-exposed road cut at the mouth of the Connor Creek drainage. This sample comes from the type section for primary volcaniclastic material within the Weatherby Formation. The coarse-grained material contains an abundance of mm-scale angular quartz, feldspar crystals, and volcanic lithic fragments. The grains are primarily angular to subangular, and petrographic analysis showed many volcanic clasts with subangular

plagioclase phenocrysts, interpreted as de-vitrified relic volcanic lapilli (Figure 2.13). Many of the volcanic lithic fragments appear to be stretched to lengths of 6-7 mm and are interpreted as flattened pumice lapilli; other lithic fragments are holocrystaline, which have been mobilized and resedimented as a turbidite deposit within the marine flysch. A fining direction to the southeast of the coarse material can be easily observed in this layer, indicating an overturned orientation.

Seven zircon grains were analyzed from LOM10-05; five of the seven zircon grains group together with a weighted mean $^{206}Pb/^{238}U$ age of 175.33 ± 0.09 Ma (Table 2.1, Figure 2.9). This analysis showed that the coarser primary volcaniclastic event horizons could be collected for primary deposition analyses. One grain that returned a concordant older $^{206}Pb/^{238}U$ date of 195.29 ± 0.51 Ma is interpreted as an inherited grain from the country rock of the Olds Ferry volcanic arc incorporated as the magma injected. The last grain that was excluded from the weighted mean gave a discordant $^{206}Pb/^{238}U$ date of 368.18 ± 0.32 Ma. The intercept of this discordant zircon grain gives an age of 1170 ± 11 Ma, indicating a Precambrian (late Mesoproterozoic) inheritance into the volcanic deposit.

The nature of the Weatherby Formation changes little along the entire reach of Connor Creek. Two other primary volcaniclastic deposits were collected further up the creek to the northwest. LOM11-11 was collected, on the slopes to the south of Connor Creek, from a discrete 2 to 5 cm horizon that can be traced laterally along strike for more than a meter. A range of clast sizes is present within this sample with the majority less than 1 mm in diameter. The large clasts within the sample are stretched to 6-8 mm and contain primarily holocrystaline and pumiceous volcanic lapilli fragments. LOM11-13

was collected in an area of many outcrops on the slopes to the north of the creek stratigraphically about 350 m to the northwest of LOM11-11. Sample LOM11-13 was taken from a very coarse-grained, poorly sorted, thick event layer. An abundance of coarse-grained fragments included angular quartz and plagioclase grains averaging about 6 mm in diameter. The layer is relatively thick, at least 10 meters; however, the outcrop disappears into hill slope wash before a change can be observed, suggesting this coarse-grained horizon could be much thicker. The clasts within this horizon show no evidence of stretching or any evidence of foliation or lineation. These coarse-grained volcaniclastic event horizons can be subtly different from each other; LOM11-05 is a turbidite type deposit, LOM11-13 is very coarse-grained and poorly sorted layer with a higher abundance of quartz and plagioclase grains than lithic or volcanic fragments, while LOM11-11 is a medium to coarse-grained bed with quartz and plagioclase dominating the smaller grains while sedimentary lithic clasts and volcanic lapilli compose the coarser grained material. These three textural types can be observed throughout the marine flysch.

Six zircon grains were analyzed from sample LOM11-11. Seven of the ten grains yielded a weighted mean $^{206}Pb/^{238}U$ age of 175.66 ± 0.13 Ma (Table 2.1, Figure. 2.8). This is discernibly older than sample LOM10-05 collected to the southeast. The three grains that were excluded from the weighted mean gave all older $^{206}Pb/^{238}U$ dates of 176.18 ± 0.33, 178.15 ± 0.19, and 181.55 ± 1.10 Ma. These grains were interpreted as antecryst from previous magmatism and subsequently incorporated into the magma during the eruption.

Eight grains were analyzed from the primary volcaniclastic sample LOM11-13. Six of the eight grains yielded a weighted mean $^{206}Pb/^{238}U$ age of 178.23 ± 0.094 Ma (Table 2.1, Figure. 2.8). This sample was the structurally highest primary volcaniclastic sample collected in the Weatherby Formation. The grains that were not included in the weighted mean had $^{206}Pb/^{238}U$ dates of 178.51 ± 0.13, and 180.59 ± 0.18 Ma, and were interpreted as an antecryst, indicating some recycled material from previous magmatic activity that were incorporated into the eruption.

As the Connor Creek fault is approached, outcropping of the Weatherby Formation decreases. Much of the sediments that do outcrop are limited to the typical fine-grained flysch sediments that dominate the Weatherby Formation. The topography lessens further up Connor Creek, causing less of the down cutting that allows for the better exposures down the drainage to the southeast. The cleavage becomes increasingly more intense as proximity to the Connor Creek fault increases, causing up indicators to be impossible to discern. Sample LOM11-18 was collected from a thick succession of medium to coarse sandstone on the north slope of Connor Creek. The abundant coarse material in this layer averages about .6 to 1 cm and is dominated by volcanic and sedimentary lithic fragments. There is no evidence of stretched or sheared fragments of coarse grains.

Detrital zircon analyses of thirty-eight zircons of all morphologies were conducted on sample LOM11-18. The group yielded a range of $^{206}Pb/^{238}U$ dates from 171 ± 10 Ma to 1127 ± 101 Ma (Table C.3). The majority of the grains have $^{206}Pb/^{238}U$ dates from 221 ± 19 Ma to 171 ± 10 Ma. The Mesozoic group was used in a calculation of a weighted mean estimation yielding a $^{206}Pb/^{238}U$ age of 181.3 ± 2.9 Ma (MSWD = 1.4).

This is interpreted as a maximum age of deposition; however, these analyses are more useful for provenance speculation. Four Precambrian grains include Mesoproterozoic (ca. 946 - 1127 Ma) and Neoproterozoic (ca. 559 – 915 Ma) ages (Figure 2.10). The four grains that fall in the Paleozoic are each isolated in different periods.

Two zircon grains were plucked from the LOM11-18 laser mounts for CA-TIMS single-grain analyses to determine the youngest dates present in this section. The two grains yielded $^{206}Pb/^{238}U$ dates of 179.98 ± 0.59 Ma and 180.90 ± 0.37 Ma (Table 2.2), compared to laser analyses of 181.59 ± 11 Ma and 174.56 ± 9 Ma, respectively (Figure 2.11). The single-grain zircon analyses fell within error of the laser data for both grains, suggesting that there was not a significant amount of lead loss. The two 180 Ma high precision $^{206}Pb/^{238}U$ dates for this sample are interpreted as a more robust estimation of a maximum age of deposition, agreeing well with the weighted mean calculated for the detrital analyses.

Sample LOM11-17 was the sample collected closest to the Connor Creek fault, located about 800 m southeast of the structure. The unit this sample was collected from consists of poorly sorted sand and siltstone. The medium size sand grains are primarily light colored, grey, with a minor amount of dark lithic material. In this area of the Connor Creek, the coarse-grained layers that are exposed are dominated by sand horizons. The sandy nature of this sample suggested a detrital origin.

Eighty-six zircon grains were separated and analyzed from LOM11-17 yielding a wide range of $^{206}Pb/^{238}U$ dates from 170 ± 12 Ma to 1421 ± 215 Ma with one young outlier of 152 ± 12 Ma (Table C.4). The young outlier, because it was the only grain to yield such a young $^{206}Pb/^{238}U$ date, was interpreted as a grain that had experienced a

significant amount of lead loss and thus not included in the present interpretations and groups. The zircon $^{206}Pb/^{238}U$ dates can easily be separate into two end groups (Figure 2.10). Eleven of the grains group in the Precambrian, dominantly in the Mesoproterozoic (ca. 1103 Ma to 1421 Ma). This sample contained one grain from the upper Neoproterozoic and one grain from the Paleozoic that are not considered for provenance evaluation due to the isolated occurrences of each. There is an almost 700 million year gap between the older group of zircon dates and the Mesozoic group of zircon $^{206}Pb/^{238}U$ dates which ranges from 170 ± 12 Ma to 235 ± 25 Ma. The late Middle Triassic to Middle Jurassic grains are interpreted to be the primary detrital source of these sediments with a weighted mean $^{206}Pb/^{238}U$ age of 187.6 ± 2.2 Ma (MSWD 1.8), interpreted as the maximum age of deposition.

Two grains were selected from the younger $^{206}Pb/^{238}U$ laser dates to be analyzed by the CA-TIMS method to better constrain the youngest zircon dates found within this layer due to this sample proximity to the Connor Creek fault. The two single-grain analyses yielded $^{206}Pb/^{238}U$ dates of 181.52 ± 1.76 Ma and 179.28 ± 0.90 Ma (Table 2.1), compared to laser dates of 179.96 ± 12 Ma and 178.53 ± 10 Ma, respectively. The single-grain analyses fell within the error of the detrital data collected on the ICPMS, suggesting that the lead loss or mixing during analysis was minimal (Figure 2.11). The maximum age of deposition of the Weatherby Formation at this location is thus revised to < 179 ma.

Lookout Mountain Road

Lookout Mountain road traverses up into the mountains north of Huntington, Oregon. This area represents the furthest western extents of this study. Along this road, sediment of the Weatherby Formation, the Burnt River Schist and gabbro of the Baker

terrane, and the Lookout Mountain pluton can be observed. Field relationships of the Connor Creek fault, Weatherby Formation, gabbros and greenstones of the Baker terrane, and the cross-cutting nature of the Lookout Mountain pluton are able to be observed at the head of Morgan Creek (Figure 2.14). Due to the erosive nature of the Weatherby sediments, the exposures away from down cut streams are few and far between, with road cuts providing the best outcrops.

The Weatherby Formation forms much of the steep grass and sage-covered mountains north of Huntington, Oregon. The coarse and fine-grained layers in this area alternate often with an average of about 20 cm thickness. Weathering has caused the Weatherby Formation in this area to appear as much lighter red and tan colors than the typical green observed to the northeast, but fresh surfaces match these green colors that can be observed throughout the rest of the Weatherby Formation. Two samples, LOM11-06a and LOM11-12, were collected from road cuts that expose a succession of fine and coarse-grained phyllite in this region of the Weatherby Formation. Samples LOM11-06a and LOM11-12 in hand sample are very similar; these horizons are poorly sorted with coarser grained material ranging from 1 mm to 1 cm. Both of these samples display slight stretching of the coarse material. Quartz and lithic fragments can be easily recognized in the field. The lithic fragments suggest a volcanic origin or provenance; however, analysis of these samples revealed no angular plagioclase grains and the horizon is interpreted as a holoclastic sandstone deposit (Figure 2.13b).

Forty zircon grains were separated and analyzed from LOM11-12, yielding a range of $^{206}Pb/^{238}U$ dates from 162 ± 12 Ma to 1543 ± 218 Ma (Table C.5). Neoproterozoic (ca. 576 – 911 Ma) and a slight Mesoproterozoic representation (ca. 1142

– 1543 Ma) dominate the Precambrian group of zircons. The majority of zircons $^{206}Pb/^{238}U$ dates are from 162 ± 12 Ma to 220 ± 16 Ma, yielding a weighted mean $^{206}Pb/^{238}U$ age of 182.7 ± 3.4 Ma (MSWD = 1.3). The Mesozoic grains are dominantly from the Jurassic (ca. 162 – 200 Ma) with only a few grains falling into the Late Triassic (Figure 2.10). This weighted mean age could be a minor overestimation of the maximum depositional age of the sediments do to the large MSWD and large range of dates used for the calculation.

Sample LOM11-12 was originally collected for primary volcaniclastic analysis, but after petrographic review this sample was identified as a holoclastic sedimentary deposit. Four zircon grains were initially analyzed yielding a range of $^{206}Pb/^{238}U$ dates from 181.34 ± 0.18 Ma to 190 ± 0.16 Ma (Table 2.2). After detrital analyses were conducted with the LA-ICPMS method, two of the younger grains were plucked and analyzed with the CA-TIMS method to determine if lead loss or mixing affected the laser analysis. The two grains plucked from the laser mount yielded $^{206}Pb/^{238}U$ dates of 170.40 ± 10 Ma and 175.24 ± 10 Ma using the LA-ICPMS method and $^{206}Pb/^{238}U$ dates of 181.83 ± 0.48 Ma and 184.02 ± 0.13Ma on the TIMS, respectively (Figure 2.11). For this sample, the CA-TIMS analysis fell outside and within the outer limits of the laser error, respectively. The discrepancy between the two methods of analyses can be attributed to lead loss that was not mitigated until the grain was subjected to chemical abrasion for ID-TIMS analysis. The maximum depositional age based upon CA-TIMS analysis is ca. 181 Ma.

Sample LOM11-06a was collected not far to the southwest from LOM11-12 almost along strike down Lookout Mountain Road, and shows many similarities from

textures, grain types, zircon morphology, and $^{206}Pb/^{238}U$ dates. Sixty-six zircon grains were separated and analyzed, fifty-three grains with Mesozoic ages (ca. 163 – 211 Ma) (Table C.6) are interpreted as being the primary source age for the detrital grains found in sample LOM11-06a, and have a weighted mean $^{206}Pb/^{238}U$ age of 183.1 ± 2.1 Ma (MSWD 1.16). This weighted mean is interpreted as a maximum deposition age of these sediments. All Precambrian zircon grains are restricted to the Mesoproterozoic (ca. 1048 – 1427 Ma) and Neoproterozoic (ca. 539 – 717Ma) ages (Figure 2.10). Three grains are represented in the Paleozoic with each grain isolated to different periods.

Four single-grain zircon CA-TIMS analyses were conducted on sample LOM11-06a before detrital analysis, yielding a range of $^{206}Pb/^{238}U$ dates from 181.31 ± 0.19 Ma to 186.93 ± 0.26 Ma (Table 2.2). Once detrital analyses were completed, two of the younger grains were plucked for CA-TIMS single-grain analysis to further constrain the age of deposition. The grains plucked for additional analyses yielded $^{206}Pb/^{238}U$ dates of 191.56 ± .08 Ma and 198.92 ± 4.62 Ma, while the laser $^{206}Pb/^{238}U$ dates returned by these two zircons were 172.85 ± 12 Ma and 186.36 ± 14 Ma, respectively (Figure 2.11). Even with the relatively large error on the 198 Ma grain, the laser error barely falls into range. The differences in the analyses can be attributed to lead loss that was mitigated during chemical abrasion for the CA-TIMS analyses and not the LA-ICPMS analyses. Similar to sample LOM11-12, the maximum depositional age from CA-TIMS analysis is ca. 181 Ma.

A very fine black shale unit can be laterally traced for at least 500 meters through outcrops around the intersection between Jordan Creek and Lookout Mountain roads. Bedding planes reveal a northeast-southwest strike dipping to the northwest, matching

orientations of the surrounding Weatherby Formation. Bedding strike and dip is close to equivalent with the cleavage strike and dip, with a slightly steeper cleavage dip at times. The unit is at least 30 meters thick but could be covered or eroded to the south. Correlation of the black shale beyond what is exposed along road cuts is difficult due to the easily weathering nature of the unit and surrounding area. Prostka (1967) continues the unit for at least another two kilometers to the east; however, expression of the unit on the map cuts along valleys and ridges, suggesting an almost vertical orientation, which does not agree with measurements made during this study.

Located structurally to the north of the black shale unit is a massive grey volcanic horizon exposed along a road cut made by Lookout Mountain road. Sample LOM11- 07 was collected from the volcanic horizon about 20 meters north from the uppermost exposure of the black shale. This unit is composed of very fine-grained grey material that weathers to a tan/orange color. Small (a millimeter or less in length) black crystals appear to be present throughout the unit. Petrographic analysis shows the presence of plagioclase within a matrix dominated by fine quartz and white mica (Figure 2.15). Due to the massive nature of this deposit, bedding could not be obtained; however, the unit looks to be conformable with the black shale unit to the south dipping to the west. Again, this volcanic horizon is only exposed through road cuts along Jordan Creek and Lookout Mountain roads.

LOM11-07 is a volcanic layer located in what has previously been interpreted as the Weatherby Formation. LOM11-07 is the closest sample collected to the Connor Creek fault in this study. All of the zircons plucked and imaged display a uniform morphology and zoning pattern (Figure B.18). Four zircons were plucked and analyzed

from this sandstone layer yielding a weighted mean $^{206}Pb/^{238}U$ age of 192.07 ± 0.08 Ma (Table 2.1, Figure 2.9). The age determined for this volcanic is significantly older than what has been previous accepted for the Weatherby Formation and falls within ages of volcanic layers of the upper Huntington Formation. All four grains returned the same age and were included in the weighted mean calculation. Due to the homogeneous zircon population, the euhedral nature of the zircons, and consistent ages this layer has been interpreted to be derived from a single volcanic event that has not travelled far from the source.

Discussion

Timing of Deposition within the Weatherby Formation

Early age estimates of the Weatherby Formation, and much of the Blue Mountains province, were primarily based on fossils (Brooks and Vallier, 1978; Brooks, 1979; Imlay, 1986; Vallier, 1995). The thick package of marine flysch that overlies the McChord Butte conglomerate contains ammonites of middle and late *Sinemurian* to early late *Bajocian* ages (Imlay, 1980, 1986) (Figure 2.3). The ammonites that have been used to determine the age of the Weatherby Formation have been found in only a few locations that are widely separated from one another. With fossil locations spread out and nearly no sedimentary structures visible, these ages cannot be well placed structurally within the package of rocks, making the timing constraints of deposition weak. This study introduces new U-Pb high precision geochronology of primary volcaniclastic horizons and detrital zircon U-Pb geochronology on sandstone deposits within the Weatherby Formation to determine the constraints of deposition on the eastern Izee sub-basin.

The age of the upper Huntington Formation places a maximum age on the deposition of the Weatherby Formation. The Weatherby Formation unconformably, with variable amounts of later tectonized motion, overlies the upper Huntington Formation in eastern Oregon and western Idaho (Avé Lallemant, 1983; Payne and Northrup, 2003; Wright, 2005; Dorsey and LaMaskin, 2007; Tumpane, 2010). Late *Pliensbachian* ammonites, pelecypods, and corals occur in thin calcareous greywacke associated with round non-sheared clast within the lower units of the McChord Butte conglomerate (Imlay, 1980). Geochronologic analyses of rhyodacite and rhyolite tuff units at the top of the Huntington Formation place the youngest ages of volcanism and deposition in the formation to the Early Jurassic (early *Pliensbachian*) at 188.45 Ma and 187.03 Ma, respectively (Tumpane, 2010). Tumpane (2010) also found that the unconformity between the upper Huntington and the base of the Weatherby has a maximum hiatus of about 6.4 Ma. This places an earliest estimate of ~ 181 Ma (latest *Pliensbachian* to earliest *Toarcian*) on the initiation of marine basin deposition within the eastern Izee sub-basin, agreeing well with the fossils found in the lower McChord Butte conglomerate.

New U-Pb geochronology (Table 2.1) from the thick package of fine-grained phyllite and slate provides evidence for deposition of the Weatherby Formation at least into the early Middle Jurassic (*Aalenian*). The progression of ages from the base of the Weatherby to the uppermost primary volcaniclastic unit suggests deposition of varying rates from at least 180.61 Ma (Tumpane, 2010) to 173.88 Ma. A maximum age of deposition due directly to volcanism of the Weatherby Formation can now be placed at 173.88 Ma (Figure 2.9). A detrital sandstone horizon, sample DC11-05, collected in Idaho along the shore of the Brownlee Reservoir just south of Raft Creek was the

stratigraphically highest sample collected within the Weatherby Formation during this study. Field observations suggest these sediments to be on the overturned limb of the synform and detrital zircons provide a slightly younger maximum age constraint of 172.75 Ma (Table 2.1), consistent with the reported presence of late *Aalenian* to *Bajocian* fossils in the marine flysch sediments (Imlay, 1980).

The youngest sediments from the Weatherby Formation suggest deposition within the basin continued after ~ 173 Ma. The thickness of the Weatherby Formation above the final primary volcaniclastic horizon is difficult to determine due to the synformal folding of the section. However, *Bajocian* (Imlay, 1986) ammonites and the appearance of reworked detrital zircons in sediments stratigraphically above the last primary volcaniclastic layer suggest the deposition continued to as young as about 168 Ma.

A black shale layer located up Dennet Creek west of the abundant town of Mineral, Idaho contain, as identified by Imlay (1986), *Callovian* ammonites. This black shale is located in direct contact with the rhyolite tuff of the upper Huntington Formation. Stratigraphic relationships between the rhyolite tuff and the black shale are not clearly exposed or understood. U-Pb high precision geochronology from the upper Huntington Formation (Tumpane, 2010) as well as new U-Pb high precision and detrital zircon geochronology from the Weatherby Formation indicate *Pliensbachian* to *Aalenian* ages. This new geochronology suggests the stratigraphic relationship between the *Callovian* black shale and the *Pliensbachian* rhyolite tuff is unconformable, indicating this ammonite age determination does not indicate depositional ages of the Weatherby Formation.

The *Callovian* black shale could, however, provide further constraints on deformation of the Weatherby Formation. The stratigraphic location of the *Callovian* black shale indicates erosion downcutting into the upper Huntington Formation occurred in the *Callovian*, depositing the black shale into direct contact with the rhyolite tuff. Movement of the Connor Creek fault causing deformation of the Weatherby basin offers a possible tectonic scenario causing erosion to occur in this area and subsequent deposition of this black shale unit. Due to new depositional constraints, suggesting deposition of the Weatherby Formation ceased ca. 168 Ma as a result of deformation, this black shale unit must have been deposited after the start of deformation within the Weatherby Formation, thus providing a minimum age of deformation within the Weatherby Formation.

Structural Evolution of the Weatherby Formation

New U-Pb geochronology of the area along the Connor Creek and Dennet Creek drainages coupled with new field relations from the Weatherby Formation provide evidence for more structural complexity within the Weatherby Formation than previously mapped. To further test the suggestions made from the field evidence and address the questions of to what extent the Weatherby Formation had been overturned, many samples were collected up the Raft and Dennet Creek drainages in Idaho and the Connor Creek drainage in Oregon. Depositional ages within the Weatherby Formation indicate the basin has been subjected to large-scale folding (Figure 2.16). Sediments from the northern section of the Izee basin yielded ages comparable to sediments located stratigraphically within 150 m of the Dennet Creek limestone in the southern area of the basin. DC11-01 was a primary volcaniclastic sample collected about 150 m above the Dennet Creek

limestone with a radiometric age of 173.88 Ma (Figure 2.9). Structural field observations of the event bed, where sample DC11-01 was collected, indicate an upright bed orientation. The structurally higher primary volcaniclastic sample LOM10-05, which was collected 4.25 km above the Dennet Creek limestone, yields a radiometric age of 175.33 Ma (Figure 2.9). Structural observation of the coarse-grained event horizon, where sample LOM11-05 was collected, indicated this bed is overturned. The ages of these two horizons with relation to the structural position within the Weatherby Formation corroborates the new structural evidence of overturned beds that place older rocks structurally above younger ones.

The Connor Creek runs perpendicular to strike of the Weatherby beds in the area northwest of the Snake River, providing access to a traverse that cuts up section to the Connor Creek fault. Radiometric dates of a primary volcaniclastic horizon and a detrital sandstone layer collected within 2 km southeast of the Connor Creek fault indicate depositional ages of these sediments between 179 and 180 Ma (Table 2.1). The horizons sampled in the northern flanks of the basin are the same age as sediments collected in the lowest portions of the Weatherby Formation along the southern flanks of the basin (Figure 2.7). The new U-Pb geochronology indicate what was previously interpreted as the highest sediments of the Weatherby Formation are the overturned repetition of basal sediments recognized in the unstructured, normal stratigraphic section of the Weatherby seen in the south.

The structural complexity within the Weatherby Formation could be greater than a simple single large-scale fold. Depositional rates within a forearc basin and slope and shelf environment can vary significantly. In the Connor Creek region, the interpreted

deposition age ranges between sample locations LOM10-05 and LOM11-11 is at least 300,000 years with a geographical distance of about 1000 m. The thickness of sediments between these two locations is difficult to explain simply by deposition, even if an estimated high sedimentation rate of ~ 400 m/Ma is considered, which has been observed in an outer fan and basin plains region of a forearc basin in California (Ingersoll, 1979). Small folds and/or thrust repetition within the fine-grained marine sediments during final deformation could explain the proximity in age and large distance between these two locations (Figure 2.12a). This question is hard to address in this area due to the low preservation of strain indicators in the fine-grained flysch, in part due to later metamorphism.

The presence of a 192 Ma volcanic structurally above a black shale horizon in the northern portions of the Weatherby Formation indicates further structural complexity present within the Weatherby basin (Figure 2.14a). In the Dennet Creek drainage in west-central Idaho, the contact between the Huntington Formation and the Weatherby Formation has been documented very well. High precision geochronology demonstrates deposition of the upper Huntington Formation ranged from 210 – 187 Ma (Kurz et al., 2008; Tumpane, 2010). The youngest units placed in the Huntington Formation are demarcated by a formation capping rhyolite unit dated at 187 Ma (Tumpane, 2010). Relying on age alone, this would place the 192 Ma volcanic well into the upper Huntington Formation rather than the Weatherby Formation. We interpret this unit as a fault-bounded slice of the upper Huntington Formation imbricated in the overturned basal sediments of the Weatherby Formation along a fault splay of the Connor Creek fault.

Localized strain accommodation with a reverse sense can be observed in the basal McChord Butte conglomerate and Dennet Creek limestone. However, field evidence and geochronologic analyses suggests the southern portion of the basin remains a structurally simple and stratigraphically coherent area of the Weatherby Formation. The hiatus between the upper Huntington Formation and the basal McChord Butte conglomerate of the Weatherby Formation has been constrained to most likely less than a few million years (Tumpane, 2010). Above the McChord Butte conglomerate and the Dennet Creek limestone, the deep marine sediments appear to thicken to the southwest (Figure 2.5). It is entirely possible that the northern flanks of the basin experienced more deformation than the lower flanks. This deformation thickened the section due to the synformal folding as well as shrunk the overall area of the eastern Izee sub-basin during compression as the Blue Mountains province completed amalgamation.

The Connor Creek fault strikes southwest/northeast juxtaposing mélange of the Baker terrane with sediments of the Weatherby Formation in the northern extents of the eastern Izee sub-basin. Previous work has interpreted the contact between the Baker terrane and the Weatherby Formation as a faulted contact based primarily on the observation of older (Permian to Early Jurassic) Baker terrane material structurally above younger (early Middle – late Middle Jurassic) Weatherby material (Brooks and Vallier, 1978). New U-Pb geochronology and structural observations, indicating northern limbs of the Weatherby Formation have been overturned, bring into question the relationship between the Baker terrane and the Weatherby Formation. The overturning of the Weatherby sediments that come in direct contact with the Baker terrane now allow for multiple possible geologic relationships between these two packages of rocks. An

unconformable depositional contact between the Baker terrane and the Weatherby Formation that was later tectonized is one possible explanation based on the observations and new age relations between these two packages of rocks. The similarity of dip orientations of the overturned Weatherby sediments and the Connor Creek fault suggests that the deformation of the Weatherby Formation is related to movement along the Connor Creek fault (Figure 2.8). However, the oblique nature of the fault cuts much of the overturned limb of the Weatherby sediments out in the area of Raft Creek, Idaho (Figure 2.5), suggesting the Connor Creek fault, at least locally, has broken through sediments of the Weatherby Formation.

The Izee sediments in the John Day region of central Oregon display a relatively continuous and coherent stratigraphic section into the *Oxfordian*. These sediments are relatively non-deformed, resting unconformably onto highly deformed Late Triassic rocks of the Vester Formation and Aldrich Mountains Group as well as the oceanic mélange of the Baker terrane (Dickinson and Thayer, 1978; Dickinson, 1979; Dorsey and LaMaskin, 2007; LaMaskin, 2009). The lack of *Oxfordian* sediments in the Weatherby Formation could be due to tectonic reorganization, shutting off deposition into the eastern Izee sub-basin while deposition was able to continue in the western Izee sub-basin. One tectonic explanation is the eastern Izee sub-basin was shortened due to the propagation of reverse faults in the accretionary prism (Baker terrane) into the basin, selectively shutting off deposition to localized areas. The eastern Izee sub-basin was over thrust by a propagating fault (Connor Creek fault) juxtaposing the Burnt River Schist with the Weatherby Formation, deforming the sediments, and shortening the basin from what is observed in the western Izee sub-basin ca. 168 Ma. The Wallowa and Olds Ferry terranes

were linked by the *Oxfordian* evidenced by the reinitiating of magmatism at 162 Ma, the continued deposition in the western Izee sub-basin, cessation of deposition in the eastern Izee sub-basin, and the initiation of Late Jurassic sediments on the Wallowa terrane (Coon Hollow Formation) (Imlay, 1964; Dorsey and LaMaskin, 2007; Schwartz and Johnson, 2009; Kurz, 2010; Tumpane, 2010).

Deformation of the Connor creek fault can now be directly constrained between the Middle Jurassic (*Bajocian*) and the Early Cretaceous (*Barremian*). Deposition of the Weatherby Formation continued into the *Bajocian* ca. 168 Ma. Deformation of the eastern Izee sub-basin indicates movement of the Connor Creek fault occurred after the deposition of the Weatherby Formation. Intrusion of non-deformed calk-alkaline plutons, one of which cross cuts the Connor Creek fault, into the southern Blue Mountains province between 129-123 Ma (data presented in Chapter 3) suggests movement had ceased by the Early Cretaceous. If the movement along the Connor Creek fault is responsible for shutting down deposition into the Weatherby basin, then movement along the fault can be constrained further to beginning between 168 and 163 Ma.

This study proposes a model of basin-scale synformal folding of the Weatherby Formation (Figure 2.17). The sediments of the Weatherby Formation progress to younger depositional ages to a central axis of the sub-basin. Sedimentation of the Weatherby Formation continued into the *Bajocian*, evidenced by the presence of recycle zircons present in samples collected near the fold hinge and fossil evidence from Imlay (1986). The thickness of the Weatherby Formation is likely on the order of about 7000 m thick or less, half the thickness of previous estimates by Brooks and Vallier (1978), Brooks (1979), and Vallier (1995). The eastern Izee sub-basin evolved in the Early Jurassic as a

stable arc, forearc, accretionary wedge system that fringed the North American continent. Deformation of the Weatherby Formation is attributed to the collision of the Wallowa terrane with the Olds Ferry terrane starting in the late Middle Jurassic. New detrital zircon ages, U-Pb geochronology of fault stitching plutons from the Greenhorn and Bourne subterranes, and deformation observations suggest collision could have continued into the early to middle Late Jurassic, with 159 – 157 Ma contractional deformation between the Baker and Wallowa terranes and 159 – 154 Ma deformation between the Bourne and Greenhorn subterranes (Schwartz et al., 2011, 2011b).

Middle Jurassic Volcanism of the Olds Ferry Arc

Early studies of the Blue Mountains province placed a Late Triassic (*Carnian – Norian*) age of active volcanism within the Olds Ferry arc based on fossil evidence from limestone pods and lenses (Brooks, 1979; Vallier, 1995; Dorsey and LaMaskin, 2007). These limestone horizons that ammonite fossils were collected are intermittently developed, forming a very small portion of the unit providing poor age constraints on the Huntington Formation. Tumpane (2010) provided new insights into the volcanic activity within the Olds Ferry arc, from which this study builds from evidence found within the Weatherby Formation.

The Olds Ferry volcanic arc was active from as early as 237 Ma (Kurz et al., 2008), evidenced by the basement Brownlee Pluton of the area, well into the Early Jurassic, evidenced by new U-Pb geochronology from primary volcaniclastic layers of the Weatherby Formation. Tumpane (2010) found that the Weatherby Formation unconformably overlies the upper Huntington Formation, indicating that volcanism from the Olds Ferry arc continued at least until the age of the Mineral Rhyolite at 187 Ma. U-

Pb geochronology of the rhyodacite and rhyolite tuff at the top of the upper Huntington Formation provided very precise time constraints on Olds Ferry volcanism into the *Pliensbachian* (middle Early Jurassic). These upper units of the Huntington Formation push Olds Ferry volcanism much later than what has been interpreted from fossils (Figure 2.3).

The presence of primary volcaniclastic layers within the Weatherby Formation suggest that deposition due directly to volcanic activity continued after the deposition of the upper Huntington Formation. This study recognizes coarse-grained horizons within the marine flysch of the Weatherby Formation that have been deposited as a direct result of a volcanic eruption. The youngest primary volcaniclastic layers present in the Weatherby Formation are from sample DC11-01, giving a crystallization age of 173.88 Ma (Figure 2.9), thus extending the activity of Olds Ferry arc volcanism into the middle *Aalenian* (early Middle Jurassic). Detrital zircons in sandstones extend this youngest age of volcanism only slightly to 172.8 Ma.

The continuation of Olds Ferry volcanism into the *Aalenian* implies subduction beneath the Olds ferry arc continued into the Middle Jurassic. By the Middle Jurassic, the ocean basin between the Wallowa and Olds Ferry terranes closed as initial amalgamation began. The cessation of magmatism within the Olds Ferry arc can be correlated with the end of convergent accommodation by means of subduction. After the closure of the ocean basin, collisional stress may have been accommodated by propagation of faults towards the Olds Ferry terrane, for example, initiating the movement of the Connor Creek fault closing off deposition into the eastern Izee sub-basin. The subduction zone migrated to the west-northwest, outbound of the amalgamated Blue Mountains terranes; re-initiating

magmatism evidenced by the pluton emplacement in the Late Jurassic, ca. 162 Ma (Johnson et al., 2007; Parker et al., 2008; Johnson and Schwartz, 2009).

Previous models have operated under the assumption that volcanic activity within the Olds Ferry arc ceased in the latest Triassic to earliest Jurassic. These previous models of the Blue Mountains province can be categorized into two groups. One group of models consider the Wallowa and Olds Ferry terranes as a single island arc complex that experienced a change in subduction polarity in the Late Triassic (Vallier, 1977; Brooks and Vallier, 1978; Passagno and Blome, 1986; White et al., 1992; Vallier, 1995). Recent age data from the lower Huntington Formation of the Olds Ferry terrane and the Wild Sheep Creek and Doyle Creek Formations of the Wallowa terrane indicate simultaneous volcanic activity within both arcs during the Late Triassic (Kurz, 2010; Tumpane, 2010). Overlapping volcanic activity from the Wallowa and Olds Ferry arcs is inconsistent with subduction polarity changes. The second group of models considers the Wallowa and Olds Ferry arcs as two separate magmatic arcs that converge closing an intervening ocean basin (Dickinson and Thayer, 1978; Dickinson, 1979; Avé Lallemant et al., 1980, 1985; Mortimer, 1986; Follo, 1992; Avé Lallemant, 1995; Dorsey and LaMaskin, 2007). Early models from this group interpret the Izee sedimentary basin as a long-lived forearc basin between the Olds Ferry and Baker terranes with amalgamation of the two arcs occurring in the Later Jurassic during a time of strong regional shortening, penetrative deformation, and regional metamorphism (Dickinson, 1979, Avé Lallemant, 1983, 1995). A recent model proposed by Dorsey and LaMaskin (2007) interpret the Jurassic sediments in the Wallowa terrene and the Izee basin as a collisional basin after the amalgamation of the Blue Mountains terranes in the Late Triassic to Early Jurassic. A recent discovery has

been made of Tethyan reefal, coral-sponge fauna within the upper Huntington Formation (LaMaskin et al., 2011). The appearance of Tethyan fauna in the Olds Ferry terrane and in the Martin Bridge limestone of the Wallowa terrane could indicate the Olds Ferry terrane was spatially distant form the North American margin and connected to the Wallowa terrane by the Late Triassic, Early Jurassic; however, appearances of these taxa in other Cordilleran terranes suggest they are diverse in there localities, making them not good for proximity interpretations (LaMaskin et al., 2011).

New age data from the Weatherby Formation, indicating the Olds Ferry arc was active into the Middle Jurassic provides new implications on the tectonic evolution of the Blue Mountains province. The collisional basin model operates under the assumption that arc volcanism in the Olds Ferry terrane ceased in the Late Triassic, interpreting that this cessation in arc magmatism is attributed to the closing of the ocean basin, termination of subduction, and initial collision of the Wallowa and Olds Ferry arcs. Continued volcanism of the Olds Ferry terrane into the Middle Jurassic suggests subduction continued much later than the collisional model allows. The new constraints on Olds Ferry volcanism support the forearc basin model and a late Jurassic collision of the Wallowa and Olds Ferry arcs. This requires continued eastward subduction underneath the Olds Ferry terrane into the Middle Jurassic, suggesting the intervening ocean basin between the Wallowa and Olds Ferry terranes did not close in the Late Triassic.

Provenance of the Weatherby Formation

The dominant provenance signal in the Weatherby Formation sediments is from Late Triassic to the early Middle Jurassic volcanics (Figure 2.10). Brooks and Vallier (1978) describe the Izee basin as flysch that was derived from the erosion of an adjacent

uplifted landmass. The abundant latest Triassic to Middle Jurassic zircon grains within the Weatherby Formation further indicates the Olds Ferry arc was active and the dominant source of detritus into the basin. LaMaskin et al. (2011b) conducted detrital zircon U-Pb geochronological analyses on two samples from the marine flysch succession of the Weatherby Formation. These samples were collected to the west of this studies western-most limit. Age comparisons of detrital zircons from LaMaskin et al. (2011b) and the new detrital zircon U-Pb geochronology from this study indicate strikingly similar trends (Figure 2.18).

The presence of Precambrian grains suggests the depocenter of the Weatherby Formation was close to the continental margin (Figure 2.10). One process that could put Precambrian zircons into a portion of the sediment deposited into the Izee basin is the derivation of direct erosion from exposed North American craton material to the east. The material could have been transported to the basin through rivers or streams mixing Precambrian zircons from the rifted Rodinian margin with Mesozoic zircons of the arc volcanic sediments. The Precambrian zircon grains could also have been incorporated into magmatic sources within the Olds Ferry terrane. Zircons that were inherited into Olds Ferry magma chambers, as they injected through the rifted North American margin, were later erupted and deposited into the basin. Rocks of the Belt Supergroup are interpreted to being deposited in the Mesoproterozoic evidenced by the display of a strong peak of zircon ages in the Early Mesoproterozoic (*Calymmian*) (Lewis et al., 2010). Windermere Supergroup rocks primarily display younger detrital zircon peaks than the Belt Supergroup, in the Neoproterozoic from the southern Canadian Cordillera to more prominently the southwestern United States (Ross and Bowring, 1990; Lewis et al.,

2010). The Neoproterozoic and Mesoproterozoic modes in the provenance signal match well with proximal Windermere and Belt Supergroup rocks on the North American craton. By contrast, the Paleozoic zircons in the Weatherby sediments are more enigmatic. We suggest that these zircons are not sourced from the North American cratonic margin, but instead were derived from the Baker terrane.

The collisional basin model proposed by Dorsey and LaMaskin (2007) interpret an emergent thrust belt uplifting the Baker terrane, allowing for chert detritus to be shed into marine foredeep basins on both the Wallowa and Olds ferry arcs. The forearc basin model interprets the chert clast in the basal sediments of the basin as a result of a structural high between the forearc basin sediments and the accretionary wedge. The presence of chert clasts in the basal conglomerate coupled with new age data from the Weatherby Formation indicates Baker terrane uplift occurred in the Early Jurassic (*Pliensbachian*). The dominance of detrital zircon provenance signals from the Mesozoic and the Precambrian indicate detritus shedding into the basin was, however, primarily from the Olds Ferry arc, further implementing the forearc basin model over the emergent thrust belt of the collisional basin model.

Eastern and Western Izee Sub-Basin Correlations

The Izee basin occupies an area of approximately 10,000 square kilometers in central and eastern Oregon (Figure 2.2). Cenozoic volcanic and sediment cover has limited the exposure of the Izee sediments to three primary locations: the John Day Inlier in the west, the Ironside Inlier in the central zone of exposures, and the Huntington area in the east. The Izee sediments of the John Day Inlier remain relatively non-deformed and present a coherent and continuous stratigraphy of late Early Jurassic to Late Jurassic

sediments (Brooks, 1979; Dickinson and Thayer, 1978; Dorsey and LaMaskin, 2007). The Ironside Mountain Inlier is composed dominantly of strongly folded Weatherby Formation sediments (Hooper et al., 1995). The structure of the Jurassic Izee sediments in the Huntington area has been difficult to determine due to the fine-grained nature of the majority of the sediments found. Many attempts at correlation from previous studies have been made. This study uses new U-Pb geochronology on primary volcaniclastic sediments and detrital sediments coupled with field observations of the Weatherby Formation to correlate the Izee sediments in the east to the Izee sediments in the western extents.

Early Late Triassic highly deformed sediments in the John Day Inlier rest unconformably on the Baker terrane (Figure 2.4C). Detrital zircon analyses from the Brisbois Member of the Vester Formation suggest an age in the early Late Triassic evidenced by *Carnian* and *Norian* grains, in agreement with mollusk fossils present within the Vester Formation (LaMaskin et al., 2011b). High precision U-Pb geochronologic studies in the Huntington Formation have better constrained the timing of deposition for the strata that the eastern portion of the Izee basin overly. The Brownlee pluton, 237.77 Ma, provides the basement on which the lower Huntington Formation was deposited (Figure 2.3) (Kurz et al., 2008; Tumpane, 2010). Constrains, by a combination of fossil evidence and high precision U-Pb geochronology, on the lower Huntington Formation indicates an earliest *Carnian* to late *Norian* deposition (Tumpane, 2010). The late Middle Triassic intrusion of the Brownlee pluton and Late Triassic deposition of lower Huntington sediments occurred at the same time as the deposition of the Vester Formation in the John Day inlier (Figure 2.3). The Vester Formation is composed

primarily of detritus from the mélange, whereas the lower Huntington Formation is composed primarily of andesitic volcanic rocks containing no mélange detritus. Therefore, in the early Late Triassic, the Vester Formation was being deposited onto and sourced from uplifted Baker oceanic mélange in the west while volcanic arc sediments of the lower Huntington Formation are being deposited in the east. The lack of volcanic detritus in the Vester Formation and the lack of mélange material in the lower Huntington Formation indicate these two areas were not proximal to cause a mix of sources in the early Late Triassic. These two formations record the early stages of subduction and first steps toward the development of an accretionary wedge, forearc basin, and volcanic arc system.

The upper units of the Aldrich Mountains Group deposited contemporaneously with the deposition of the upper Huntington Formation. The Aldrich Mountains Group shows a shift from the deposition of mélange detritus in the lower units to volcanic detritus in the upper units. The appearance of volcanic debris in the Aldrich Mountains Group suggests a more proximal position to the Olds Ferry arc by the middle Late Triassic. The sediments of the Aldrich Mountains Group in the John Day Inlier are deposited directly onto mélange of the Baker terrane, whereas the Huntington Formation is deposited directly onto crystalline basement of the Olds Ferry terrane. The upper Huntington Formation was deposited unconformably onto the 210.13 Ma Iron Mountain granodiorite (Kurz et al., 2008; Tumpane, 2010). The Iron Mountain granodiorite intruded the sediments of the lower Huntington Formation, providing the basement for the deposition of the upper Huntington Formation. The U-Pb zircon age constraints from the upper most volcanics of the Huntington Formation extend volcanism and deposition

of the Olds Ferry terrane into the Early Jurassic (Tumpane, 2010). Compression between the accretionary wedge and the Olds Ferry volcanic arc continued in the Early Jurassic evidenced by folding in the Huntington Formation, Vester Formation, and Aldrich Mountains Group. This new U-Pb geochronology strengthens the correlations between the pre-onlap sediments in the west with the Huntington Formation in the east, suggesting that the eastern portion of the basin followed a depositional history much like that observed in the west.

Recent high precision U-Pb geochronology around the unconformity between the Weatherby Formation and the Huntington Formation provide further correlations with the onlap sediments of the John Day Inlier (Figure 2.3). An angular unconformity separates the Aldrich Mountains Group from the Jurassic onlap sequences in the west (Dickinson and Thayer, 1978; Dorsey and LaMaskin, 2007). The Mowich Group began deposition in the *Pliensbachian* (Early Jurassic), suggesting the hiatus in sediments is limited to a few million years between the Mowich Group and the Aldrich Mountains Group (Imlay, 1968). In the Huntington area, an unconformity demarcates the boundary between the upper Huntington Formation and the Weatherby Formation (Figure 2.3) (Vallier, 1995; Avé Lallemant, 1995; Dorsey and LaMaskin, 2007; Tumpane, 2010). A recent study constrained the unconformable hiatus between the upper Huntington Formation and the Weatherby Formation to less than 6.4 million years (Tumpane, 2010). Again, the chronostratigraphic correlations between the Mowich Group and basal Weatherby Formation are striking.

New U-Pb geochronology from the Weatherby Formation extends deposition in the Huntington area into the late *Aalenian* to *Bajocian* (early Middle Jurassic). By

contrast, the youngest sediments found in the John Day Inlier in the Lonesome Mountain Formation are deposited into the late Middle Jurassic, *Callovian* to earliest *Oxfordian* (Imlay, 1964; Dickinson and Thayer, 1978). The Jurassic marine sediments in the western Izee sub-basin are relatively non-deformed, providing better stratigraphic detail to this area of the western Izee sub-basin than in the eastern Izee sub-basin. Evidence suggests the structural orientation of the Weatherby Formation is a result of folding in the footwall of the Connor Creek fault. The movement along the Connor Creek fault could attest for the lack of *Bathonian* sediments in the eastern Izee sub-basin. Sedimentation was cut off into the eastern Izee sub-basin during propagation of the fold and thrust belt as a result of collision between the Wallowa and Olds Ferry volcanic arcs.

The eastern sediments of the Izee basin are more highly deformed than the Izee stratigraphy in the John Day inlier. The deformation of the Weatherby Formation is expressed as a synform in the easternmost extents and isoclinal folds in the western most extents (Figure 2.4). The collection of Izee sediments in the John Day inlier are non-deformed resting horizontally along an angular unconformity with the Aldrich Mountains Group. The along strike variation in the degree of deformation within the Izee basin could be caused by the termination of the Wallowa/Wrangellia arc. The collision of the southernmost extents of Wrangellia with the Olds Ferry terrane in the late Middle Jurassic resulted in the deformation of the Izee basin. The termination of Wrangellia can account for the more intense deformation present in the eastern Izee sub-basin leaving the central basin moderately deformed and the western Izee sub-basin undeformed.

Typical volcanic island arc rock fragments recognized in the Mesozoic sandstones of the southwestern portion of the Izee stratigraphy suggest that the Izee sediments of the

John Day Inlier were being locally sourced from a volcanic arc of that region (Brooks, 1979). The majority of coarse-grained event horizons that interbed the marine flysch of the eastern Izee sub-basin are composed primarily of volcaniclastic rocks, suggesting volcanic arc provenance, due to this areas proximity, most likely to the Olds Ferry arc. Detrital zircon analysis of the John Day Inlier by LaMaskin et al. (2011b) and sandstone petrography by Dickinson et al. (1979) suggested a major change in sediment provenance from the direction of the Baker terrane in the Triassic to Late Triassic to an eastern, possibly more local, provenance in the Late Triassic to the Late Jurassic. LaMaskin et al. (2011b) found a marked increase in Neoproterozoic and Mesoproterozoic grains beginning in the Late Triassic continuing into the early Late Jurassic, suggesting a change in provenance and/or an increase in local magmatism. All samples collected from the Weatherby Formation contained an appreciable amount of Precambrian detrital zircon grains (Figure 2.10) all from the Mesoproterozoic and Neoproterozoic. The presence of no grains older than the Mesoproterozoic in the eastern Izee sub-basin suggests the eastern and western Izee sub-basin sediments were being sourced from the same area during the Jurassic (Figure 2.19). The primary volcaniclastic layers within the Weatherby Formation and evidence that the Olds Ferry arc was active from the early Late Triassic to the Middle Jurassic suggest that the dominant source area for the Late Triassic and Jurassic sediments of both the western and eastern Izee sub-basin was the Olds Ferry arc.

North American Cordilleran Basin Correlations

Correlations between the Canadian Cordillera and the Western U.S. Cordillera are problematic due to extensive Cenozoic volcanic and sedimentary cover from northern Washington to southern Oregon. The Blue Mountains province allows the only access to

the southernmost exposures of Wrangellia affinity rocks as well as the only exposures in the Cordillera of Cache Creek affinity rocks in direct contact with North American and exotic affinity rocks. To gain a better understanding of north-south correlations within the North American Cordillera, this study correlates the Izee basin of the Blue Mountains province with marine and non-marine basins within the Canadian Cordillera.

The Whitehorse Trough

The Whitehorse Trough is an early Mesozoic arc-marginal forearc basin deposited on the eastern extends of Stikinia juxtaposed by the Cache Creek terrane in the east (English et al., 2005) (Figure 2.1). Stikinia is the largest accreted terrane in the Canadian Cordillera and is composed of lower Devonian to Middle Jurassic sedimentary, volcanic, and plutonic rocks (Johannson et al., 1997). The primary rock types are those created during arc magmatism of Stikinia during late Middle Triassic to the Middle Jurassic as the complex subducted crust to the west, during migration toward the North American margin (Dickinson, 2004). The Stuhini and Hazelton arcs were active during the Middle Triassic to the Middle Jurassic, depositing the subalkaline volcanic and pyroclastic rocks of the Stuhini and Hazelton Groups (English et al., 2005). The Cache Creek terrane is interpreted as a suture zone of oceanic mélange between arc rocks of Quesnellia and Stikinia. The Whitehorse Trough extends over 400 km in southern Yukon and northern British Columbia and is interpreted to be submarine-fan deposits sourced primarily from Stikinia to the west and southwest (English et al., 2005; Lowey et al., 2009).

Sediment sources for the Whitehorse Trough were specifically the Stuhini and Hazelton Groups composing the upper members of Stikinia in the east (English et al., 2005; Lowey et al., 2009). The Stuhini Group is deposited directly onto the Devonian to

Permian Stikine assemblage (English and Johnston, 2005) (Figure 2.20). The Stuhini Group is composed of subalkaline volcanic flows and pyroclastic rocks, coarse arc-derived alluvial clastic strata, and shallow marine conglomerates that were emplaced or erupted onto the Stikine middle and late Paleozoic basement rocks (English et al., 2005). In the uppermost sediments, Sinwa Formation, of the Stuhini Group limestone layers occur and are commonly greater than 500 m thick (Souther, 1971; English et al., 2005). In the Yukon, the Stuhini Group is referred to as the Lewes River Group.

The Laberge Group overlies the Stuhini/Lewes River Group along an approximate 5 Ma unconformity (Lowey et al., 2009). The Laberge Group is composed of conglomerates, sandstones, siltstones, and shales in the west and a succession of interbedded sandstone, shale, and siltstone in the east (English et al., 2005) (Figure 2.20). The Inklin Formation is composed of lower *Sinemurian* to upper *Pliensbachian* strata making up the basal units of the forearc basin (Figure 2.20). The succession is characterized by 100 m thick planar-bedded sheet sand turbidites ranging in size from fine sand to minor zones of coarse conglomeratic sands (Johannson et al., 1997). Subordinate sediments found within the Inklin Formation are thin bedded, fine sands and siltstone-mudstone couplets that are interpreted as deposits formed in the transitional zone between the fan-fringe and basin-plain environments (Dickie and Hein, 1995; Johannson et al., 1997; English et al., 2005). Fine-grained sediments dominate the *Sinemurian* deposits with an overall coarsening up section to sandier strata dominating the *Pliensbachian* sediments (Johannson, 1994; English et al., 2005). The western-most conglomeratic layers onlap onto the Triassic Stuhini Group making up only a minor volume of sediment within the Whitehorse Trough (English et al., 2005; English and

Johnston, 2005). The *Pliensbachian* to *Bajocian* (late Early Jurassic to Middle Jurassic*)* conglomerates are thickest closest to Stikinia and thin and become finer grained outbound into the basin (English et al., 2005). Composing the finer grained western most proximal sediments, including the fossiliferous conglomerates, are interbedded sandstones, siltstones, and mudstones referred to as the Takwahoni Formation (Johannson et al., 1997; Shirmohammad et al., 2007). The Takwahoni Formation is dominated by volcanic clasts in its basal deposits (Shirmohammad et al., 2007). Some areas of the Whitehorse Trough lake sediments do not include the Takwahoni Formation and are composed strictly of coarse conglomerates in the west and the Inklin Formation in the east.

The Whitehorse Trough is more extensively exposed in the Yukon with similar lithologies recognized however split into three different formations within the Yukon Laberge Group (Figure 2.20). The western sediments contain the Tanglefoot Formation in the Yukon and are correlated with the Takwahoni Formation in British Columbia. Interbedded coal bearing sandstones, and mudstones ranging from *Sinemurian* to *Bajocian* in age characterize the sediments of the Tanglefoot Formation (Lowey et al., 2009). The Tanglefoot Formation is interpreted as a deltaic depositional environment (Lowey et al., 2009). The Richthofen Formation is correlated with the Inklin Formation in British Columbia. In the Yukon, the Richthofen Formation is composed of *Sinemurian* to *Bajocian* thin beds of graded siltstone and very fine sandstone and mudstone turbidites much like that observed in British Columbia (Lowey et al., 2009). The Richthofen Formation composes the southern half of the basin, which is interpreted as the most outbound, deepest deposits within the Whitehorse Trough. Conglomeratic deposits can be found interbedded in both the Tanglefoot and Richthofen Formations (Lowey et al.,

2009). Rocks of the Nordenskiold Formation are crystal-rich volcaniclastics occurring as massive isolated layers in the center and western margins of the Whitehorse Trough (Lowey et al., 2009). U-Pb zircon analyses were conducted on the Nordenskiold Formation, yielding a range of ages from 188.5-182.5 Ma (Colpron and Friedman, 2008). Some of the volcanic material can be observed reworked into sediments of both the Tanglefoot and Richthofen Formations (Lowey, 2008; Lowey et al., 2009)

The Whitehorse Trough is bounded on the southeast and west by structurally significant faults. The Sinwa Formation and the lower Jurassic sediments of the Inklin Formation are thrust over more proximal sediments of the Laberge Group along the King Salmon fault (English et al., 2005). The Nahlin Fault bounds the basin in the northeast, juxtaposing the Cache Creek terrane onto the Inklin Formation (English et al., 2005; English and Johnston, 2005). Folding is common throughout the Whitehorse Trough with dominantly southwest-verging trends (English and Johnston, 2005).

The Stuhini and Hazelton Groups, strata of the Whitehorse Trough, and the Cache Creek terrane form the components of a magmatic arc, forearc, and accretionary wedge, respectively. Volcanic activity within arcs of Stikinia occurred during the Middle Triassic into the Middle Jurassic. The Early Jurassic to Middle Jurassic Laberge Group sediments is deposited onto volcanic strata of the Stuhini Group. The Laberge Group is primarily composed of interbedded siltstones, shales, and fine sands with minor amounts of conglomerates and sandstones (English et al., 2005; Lowey et al., 2009). Temporal correlations of forearc deposits in the Whitehorse Trough and the eastern Izee sub-basin suggest coeval basin formation in the northern-most Canadian Cordillera and the Blue Mountains province (Figure 2.20).

The Bowser Basin

The Bowser basin is a Middle Jurassic to mid-Cretaceous marine and non-marine extensive area of sedimentation onto Stikinia in the central Canadian Cordillera (Ricketts et al., 1992, Evenchick et al., 2010) (Figure 2.1). The Bowser basin represents greater than 6 km of sediments deposited onto the Early to Middle Jurassic Hazelton trough (Gagnon et al., 2009, Evenchick et al., 2010). Many models based on stratigraphic relations and tectonic setting have been presented for the Bowser basin; from flexural subsidence due to overthrusting of the Cache Creek terrane (Eisbacher, 1985; Ricketts et al., 1992), crustal stretching do to rifting on Stikinia (Anderson, 1993; Thorkelson et al., 1995) and amplified accommodation space due to sediment loading (Gagnon et al., 2009), a forearc setting (Dickinson, 1976), strike-slip setting (Greig et al., 1991), or processes caused by the obduction of the Cache Creek terrane (Evenchick et al., 2007).

The Middle Jurassic to mid-Cretaceous sediments of the Bowser basin is deposited onto Stikine sediments of the Hazelton Group in the north and the Spatsizi Group in the south (Ricketts et al., 1992; Gagnon et al., 2009). The Hazelton Group represents the last widespread volcanism in the Stikine arc and has accumulated in a northwest-southeast oriented intra-arc basin: the Hazelton trough. The upper Hazelton Group unconformably overlies calc-alkaline volcanic rocks of the *Hettangian* to early *Pliensbachian* lower Hazelton Group (Gagnon et al., 2009; Evenchick et al., 2010). *Pliensbachian* to *Toarcian* volcanic and shallow-marine sediments compose the upper Hazelton Group marking a change in volcanic dominated deposition to a subsiding sedimentary basin with a decrease in local volcanism (Gagnon et al., 2009). The Bowser

Lake Group overlies the *Aalenian* sediments of the upper Hazelton Group in the south and the north (Ricketts et al., 1992; Gagnon et al. 2009; Evenchick et al., 2010).

The Jurassic to Cretaceous Bowser Lake Group consists of marine and nonmarine mudstones, siltstones, sandstones, and conglomerates with localized volcanic rocks (Evenchick et al., 2010). The Bowser Lake Group ranges in age from the *Bajocian* to the mid-Cretaceous with a diachronous deposition onto the upper Hazelton Group, younging to the center of the Bowser basin (Evenchick et al., 2010). Radiolarian chert clasts abundant throughout the Bowers Lake Group relate a provenance link between the Cache Creek terrane and Stikinia by the Middle Jurassic (Gagnon et al., 2009; Evenchick et al., 2010).

The forearc portion of the Bowser basin is composed of the Hazelton Group. The Hazelton Group was deposited from the *Pliensbachian* to *Aalenian* contemporaneously with the Weatherby Formation in the Blue Mountains. Volcanism in the Bowser basin and Huntington/Izee basin waned in the late Early Jurassic and early Middle Jurassic, shifting from primarily volcanic sediments to dominantly shallow marine sediments. The subsidence of the Bowser Lake Group began at the cessation of the Early to Middle Jurassic forearc sedimentation. The Cache Creek terrane and Stikine arc were proximal by the *Bajocian*, evidenced by the presence of chert detritus in the sediments of the Bowser Lake Group.

The Ashcroft Basin

The Ashcroft Basin is interpreted as an early Mesozoic outer arc basin that provides implications for the accretion of the Cache Creek terrane to Quesnellia. The Ashcroft Basin is located in south-central British Columbia in the Intermontane Belt of

the Canadian Cordillera (Figure 2.1). The Ashcroft basin is deposited unconformably on the upper Triassic Nicola Group in the east (Travers, 1978). In the west, strata of the Nicola Group and the Ashcroft Formation lie on the mélange of the Cache Creek terrane (Travers, 1978). The series of rocks are considered to be an arc, forearc, and accretionary wedge system active during the Late Triassic to Middle Jurassic (Travers, 1978).

Isolated blocks of deformed limestone, basalt, serpentinite, variably serpentinized ultramafic rocks, greenstones, lithic sands, thin-bedded cherts, argillite, and phyllite constitute the Cache Creek Group in this area (Travers, 1978). Foliation and relic bedding trend north-northwest and are near vertical with intense deformation visible in small-scale folding of thin chert horizons (Travers, 1978). Permian fusulinids are found in the limestone layers near the town of Cache Creek, mid-Pennsylvanian limestones are recognized farther north, and Middle to Late Triassic fauna have been discovered south of the town of Cache Creek (Sada and Danner, 1974; Danner, 1975; Travers, 1978).

The Nicola Group is interpreted as calc-alkaline to alkaline volcanic arc related sediments deposited directly on to basement rocks of Quesnellia. Rocks within this group consist of dark, andesitic volcanic flows, chert, argillite, sandstone, calcarenite, conglomerates, sharpstone, and pebbly mudstones (Travers, 1978) (Figure 2.20). The upper units of the Nicola Group are weakly altered; however, much of the lower units of the Nicola Group have been heavily altered by hydrothermal metamorphism, turning the Nicola rocks into a greenish color (Travers, 1978). Exposures of the Nicola Group in the Ashcroft area represent deposition in the *Carnian* and *Norian* (Travers, 1978). The volcanic flows of the Nicola Group show local metamorphism due to the intrusion of the Guichon Creek Batholith (McMillian, 1975; Travers, 1978).

Carbonaceous, silty shale beds with interbedded siltstone, graded sandstone, some conglomerates, and rare argillaceous limestone construct the strata of the Ashcroft Formation (Travers, 1978) (Figure 2.20). Grading, cross bedding, and bottom marks are prevalent within the western Ashcroft sediments, allowing for a great understanding of the sediments up direction (Travers, 1978). Conglomerate clasts in the north and northwestern areas of the basin contain mafic and intermediate volcanic clasts with no felsic volcanic material present in any abundance (Travers, 1978). In the southern and southeastern portions of the basin, felsic material resembling the Guichon Creek Batholith appears in the basal conglomerates (Travers, 1978). Conglomerates are more common in the basal members of the Ashcroft Formation; however, shale dominates most of the strata. The shale units are interbedded with lenses of sandstones and siltstone (Travers, 1978). The Ashcroft strata have experienced significant soft sediment slumping and local folding to thicken the appearance of the section (Travers, 1978). Fossil evidence within the Ashcroft Formation suggests that the age of the basin ranges from Early Jurassic to Middle Jurassic (*Sinemurian* to *Callovian*) (Travers, 1978).

The Nicola Group and the Ashcroft Formation lay on the older Cache Creek mélange along both depositional and faulted contacts. The Nicola Group is overturned with a steep westward dip along a sharp contact with serpentinite, argillite, and chert of the Cache Creek terrane (Travers, 1978). Uniform large-scale folding and faulting are present within the Nicola sediments with overturning of the beds occurring during the deposition of the Ashcroft Formation (Travers, 1978). Pre-lithification deformation occurs in the deformed lower units of the Ashcroft Formation overlain by relatively non-deformed *Callovian* sediments (Travers, 1978). The contact between the Nicola Group

and Ashcroft Formation is complexly deformed with both folding and faulting, placing all different orientations of strata between the two rock groups (Travers, 1978).

The Nicola Group of Quesnellia, the Ashcroft Formation, and the Cache Creek Group comprised the elements of a magmatic arc, forearc basin, and accretionary wedge, respectively. The Ashcroft basin shares all of the temporal correlations made with the Whitehorse Trough in the north and the Izee basin in the south (Figure 2.20). The Nicola Group records active volcanism along the western edges of Quesnellia during at least the Middle Triassic to the Late Triassic (Travers, 1978). Along with temporal correlations with Olds Ferry volcanic activity, both groups are composed of calc-alkaline – alkaline volcanic arc rocks, suggesting some amount of continental influences (Travers, 1978; Kurz et al., 2008; Tumpane, 2010). The Ashcroft Formation is composed of Early Jurassic basal conglomerates, with the bulk of the Ashcroft strata consisting of interbedded silts, sands, and shales with occasional limestone horizons. Deformation of the Ashcroft basin ceased before the *Callovian,* evidenced by non-deformed *Callovian* sediments overlaying earlier deformed material, comparable with the cessation of deposition and deformation of the eastern Izee sub-basin in the *Bajocian*. The Ashcroft Basin and the Izee basin share lithologic and temporal correlations, suggesting a comparable depositional environment.

Correlations between the Whitehorse Trough, Bowser basin, Ashcroft basin, and Izee basin suggest synchronous basin subsidence in the Cordillera during the Triassic and Jurassic. All four of the basins begin with ca. 245 – 237 Ma volcanic arc activity and strata, transitioning into ca.190 – 182 Ma coarse-grained proximal deposits to basin-plain fine-grained marine and shallow marine deposits typical of a forearc environment (Figure

2.20). This change of tectonic environments indicates a fundamental reorganization along the entire Cordilleran margin. The fundamental change records the initiation of terrane accretion to the North American margin shutting down the stable accretionary wedge, forearc, and volcanic arc system of the Late Triassic to Middle Jurassic. The Bowser basin was deposited more inland than the other three basins, possibly being the cause for continued deposition into the Early Cretaceous. The Whitehorse trough is an eastward-facing forearc basin deposited on the flanks of Stikinia in the west, whereas the Izee basin and the Ashcroft basin are northwest-western basins deposited on the flanks of Quesnellia to the east. This suggests that coeval basin formation was occurring on both side of the enclosing oceanic basin. If the Mihalynuk et al. (1994) oroclinal model is considered, then these basins could all be forearc basins developing on fringing arcs off the North American continent.

Conclusion

New field and geochronological evidence presented for the Weatherby Formation of the eastern Izee sub-basin offer better constraints on the timing of deposition and structural orientation of this Mesozoic forearc basin. Active deposition within the Weatherby Formation occurred at a minimum estimation of 180 Ma - 172 Ma, middle *Toarcian* to the late *Aalenian*, agreeing well with previous estimations from ammonite fossils found in the region. The thickness of the McChord Butte conglomerate and the Dennet Creek limestone suggest that the oldest depositional ages within the Weatherby Formation are older than 180 Ma. There is a significant thickness of sediments between the upper-most units analyzed and what is interpreted in this study, to be the top of the Weatherby Formation, suggesting that deposition continued into the *Bajocian*. The

transition from fine-grained marine flysch interbedded with volcanic-rich turbidites to more deltaic sands, silts, and shales suggests that the Olds Ferry magmatic arc shut off around the time of the last primary volcanic deposits in the Weatherby Formation. The Olds Ferry arc was active into the middle *Aalenian*, evidenced by primary volcaniclastic layers within the Weatherby Formation and the recycling of early 170 Ma age detrital zircons from secondary sandstone sediments stratigraphically above the youngest primary volcaniclastic horizon. Continued subduction below the Olds Ferry terrane continued well into the Middle Jurassic, suggesting collision between the Wallowa and Olds Ferry terrane occurred by the Middle Jurassic, shutting down subduction.

The presence of Precambrian and a majority of Mesozoic zircons in secondary sandstone deposits of the Weatherby Formation display an Olds Ferry volcanic arc and Laurentian influence into the eastern Izee sub-basin. The strong Mesozoic influences suggest that the Olds Ferry terrane provided the majority of the sediment to the Izee forearc basin. The Precambrian grains were likely eroded from proximal continental North America and deposited into the basin by streams and rivers. The Olds Ferry arc experienced significant uplift during the late Early and Middle Jurassic causing major erosion into the forearc region.

New structural relations, high precision U-Pb geochronology, and detrital zircon U-Pb geochronology of the Weatherby Formation show the eastern Izee sub-basin is a synfomal remnant of a larger forearc basin trending northeast/southwest. New field relations show overturned beds within the northern flanks of the eastern Izee sub-basin and upright bedding present in the southern flanks of the basin. Geochronology of primary volcaniclastic and detrital sediments within the Weatherby Formation display a

younging progression to the center of the basin. Geochronology in the northern flank of the eastern Izee sub-basin indicates further structural complexity.

The new age constraints on both the Weatherby Formation and the Huntington Formation allow for greater correlations between the eastern Izee sub-basin and the western Izee sub-basin. The deposition of the lower Huntington Formation deposited onto the Olds Ferry terrane contemporaneously as the Vester Formation deposited on the Baker terrane. New constraints on the youngest deposits of the Weatherby Formation indicate the deposition of the basal onlap sediments from the John Day Inlier began around the same time as deposition of the McChord Butte conglomerate in the Huntington area.

Greater constraints on the timing of deposition within the Izee basin allows for temporal correlations to forearc basins in the Canadian Cordillera. Evidenced by the Whitehorse Trough, Bowser basin, Ashcroft basin, and Izee basin, the North American Cordillera experienced a massive tectonic reorganization from arc volcanics to basin subsidence in the Early Jurassic.

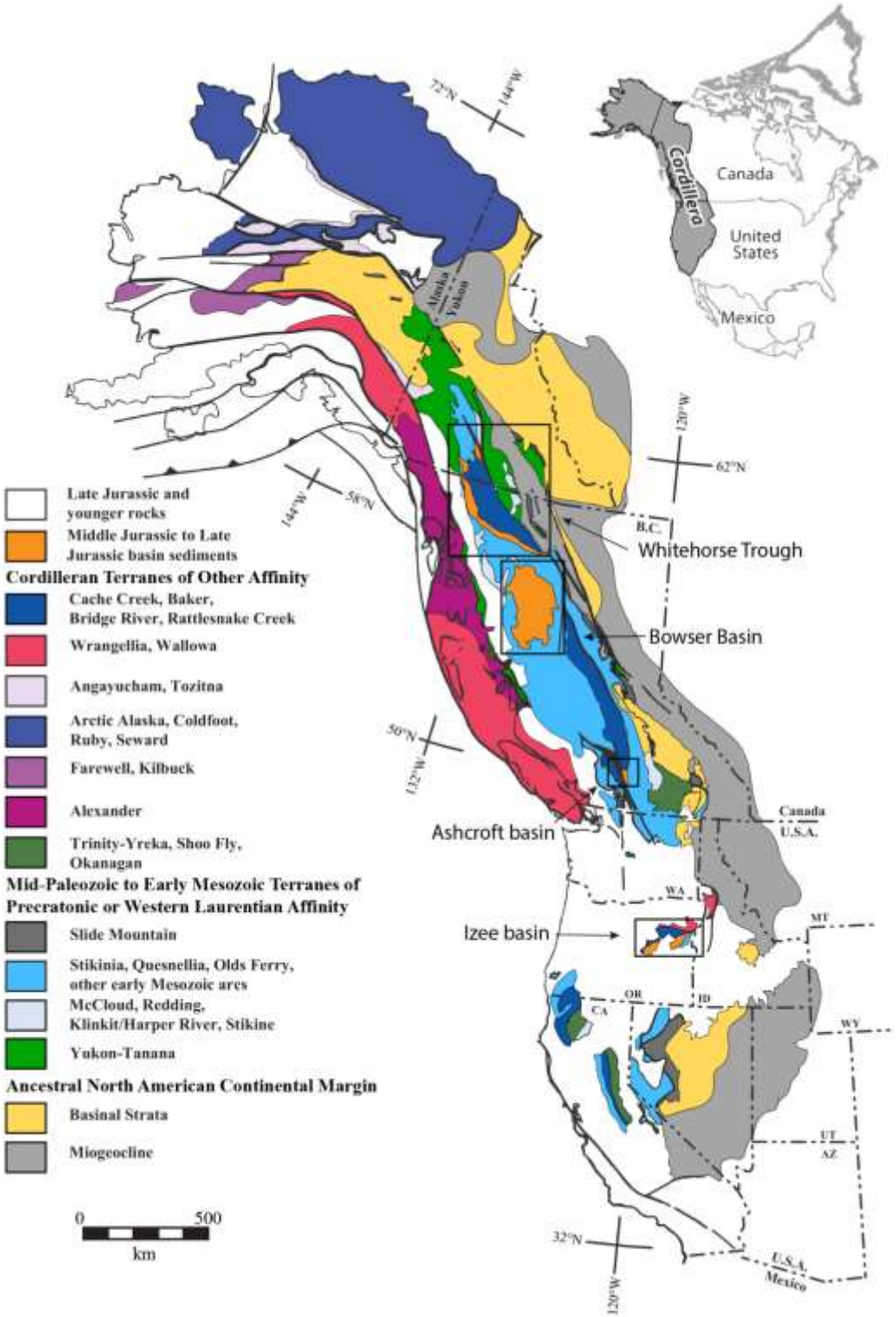

Figure 2.1: Paleozoic and Mesozoic terrane map of the North American Cordillera. Terranes are grouped based on rock type affinity and origins. Location from south to north the Izee basin, Ashcroft basin, Bowser basin and Whitehorse Trough are outlined in black. Modified from Colpron and Nelson (2009). B.C. - British Columbia, CA - California, NV - Nevada, AZ - Arizona, UT - Utah, OR - Oregon, WA - Washington, MT - Montana, WY - Wyoming.

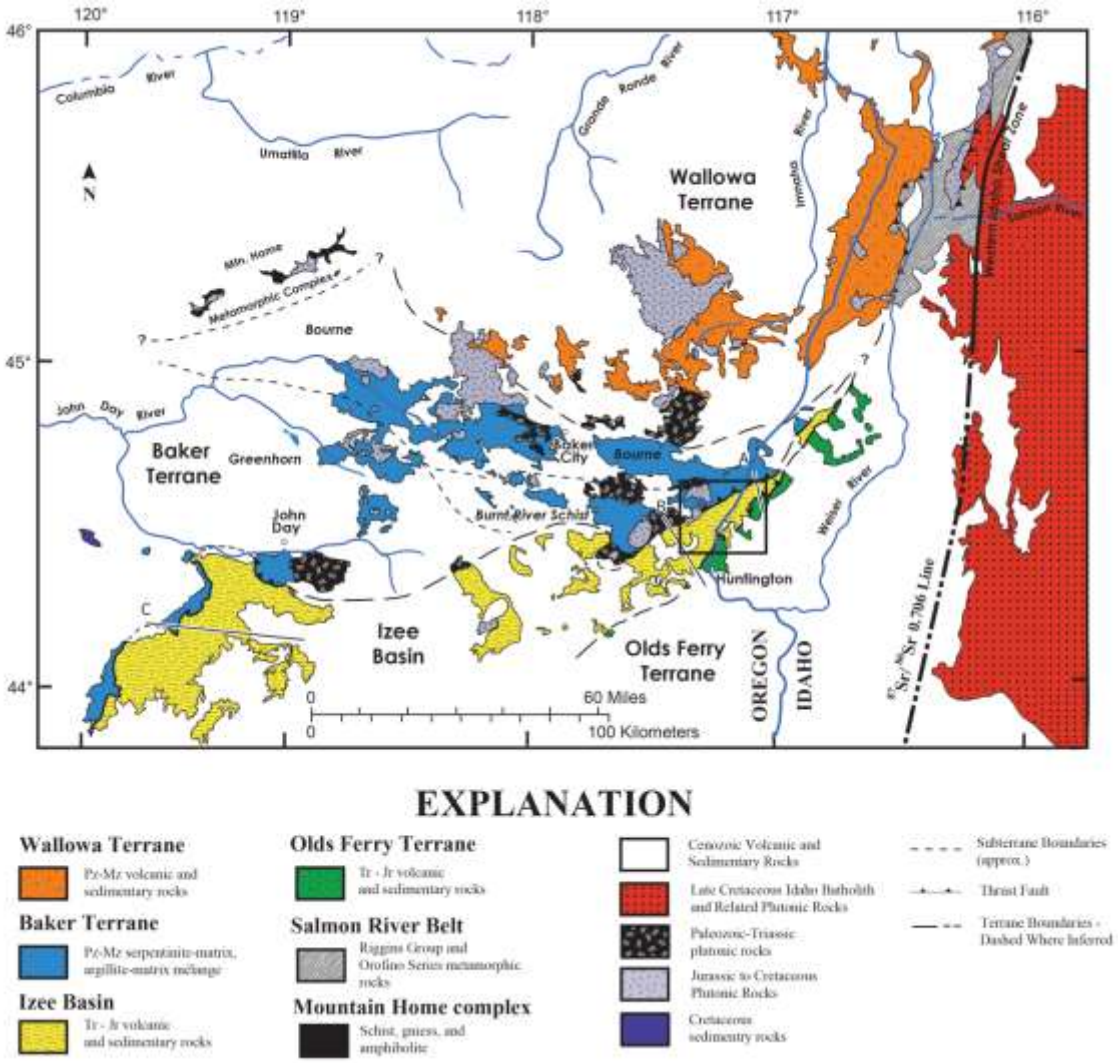

Figure 2.2: Geologic map of the Blue Mountains province divided into the three tectonic terranes, the Izee forearc basin, and also showing other prevalent rock types. Study area is shown in black box (Figure 2.5). Modified from LaMaskin et al. (2011b) and Schwartz et al. (2011b).

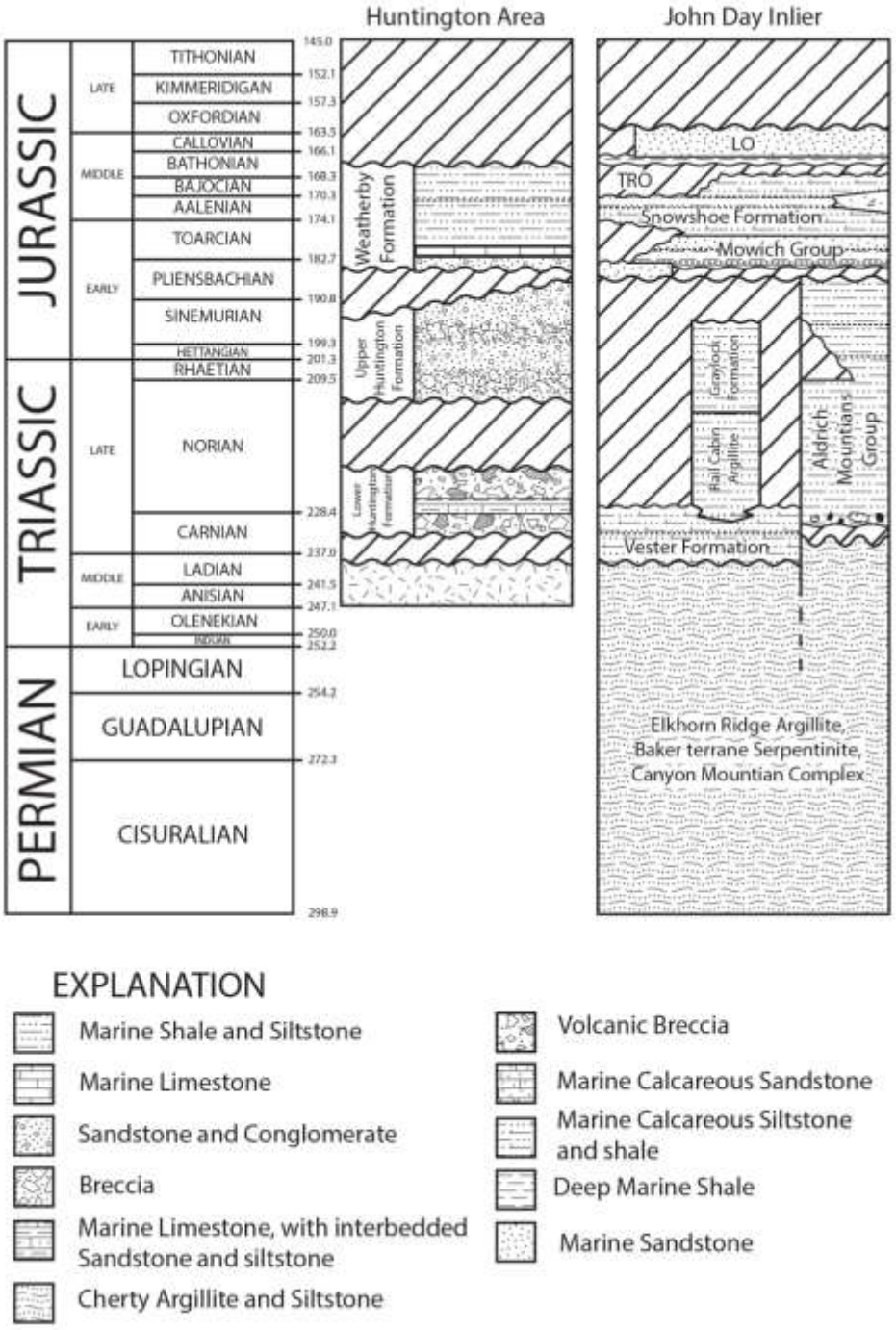

Figure 2.3: Revised chronostratigraphic column for the stratigraphy in the Huntington and the John Day areas. Huntington Formation data taken from Tumpane (2010); John Day stratigraphy taken from Dorsey and LaMaskin (2007). Geologic Timescale 2012, Gradstein et al. (2012).

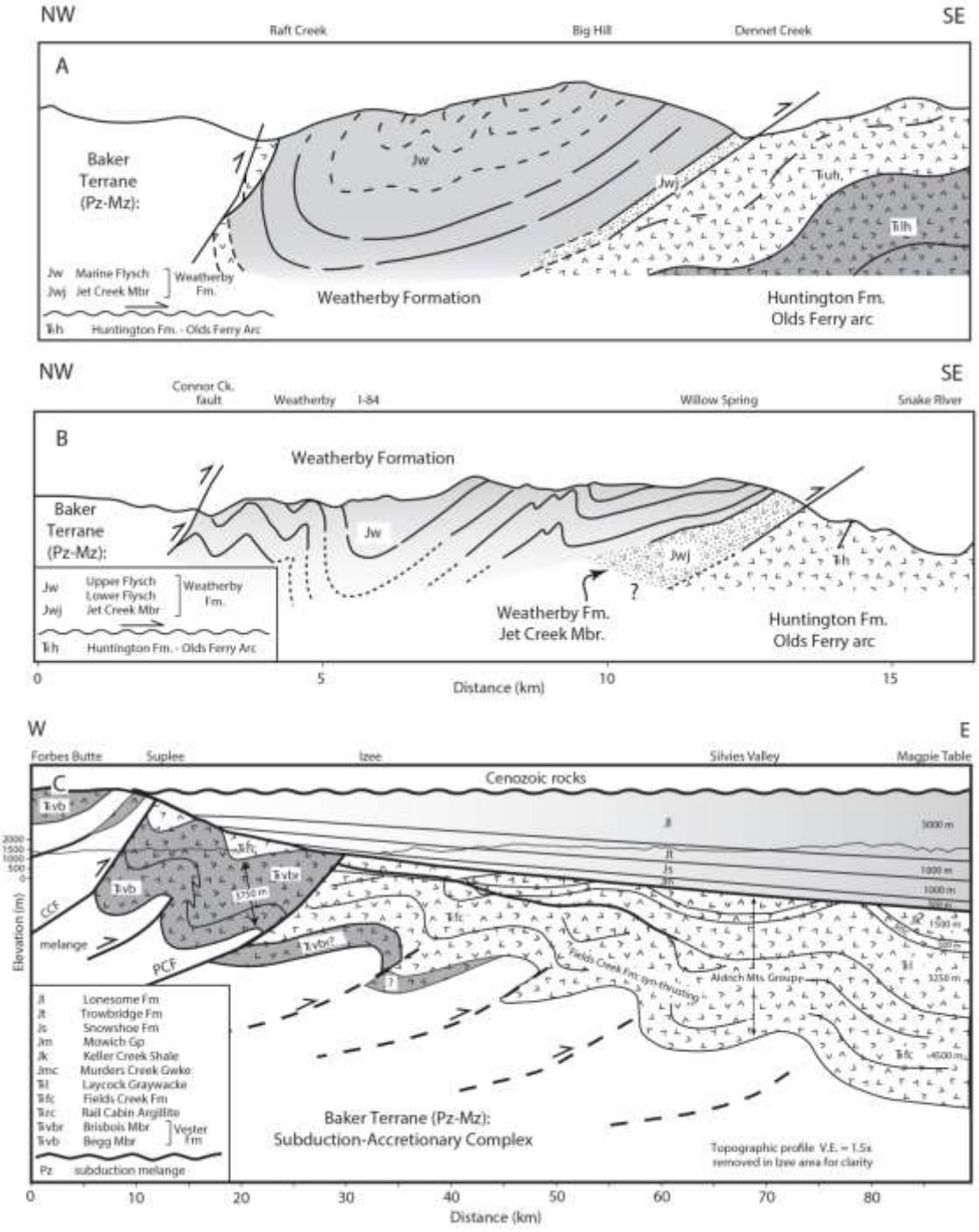

Figure 2.4: Schematic cross-sections of the Izee basin. (A) Cross-section of the Weatherby Formation in the easternmost extents of the Izee basin. (B) Cross-section of the Weatherby Formation in the central Izee basin. Taken from LaMaskin et al. (2011b). (C) Cross-section of the John Day sediments in the western Izee sub-basin. Redrafted from LaMaskin et al. (2011b).

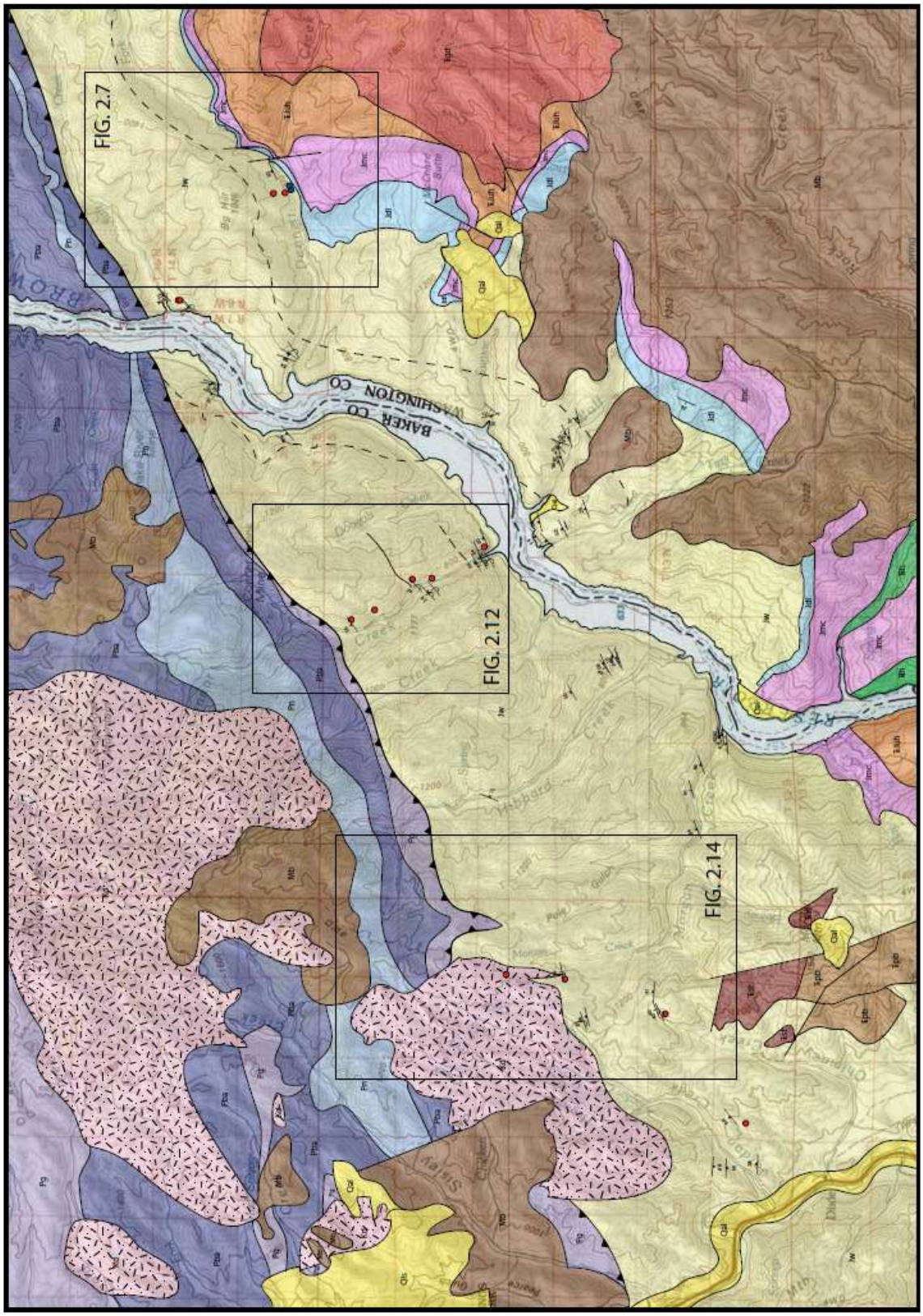
FIG. 2.7
FIG. 2.12
FIG. 2.14
BAKER CO
WASHINGTON CO

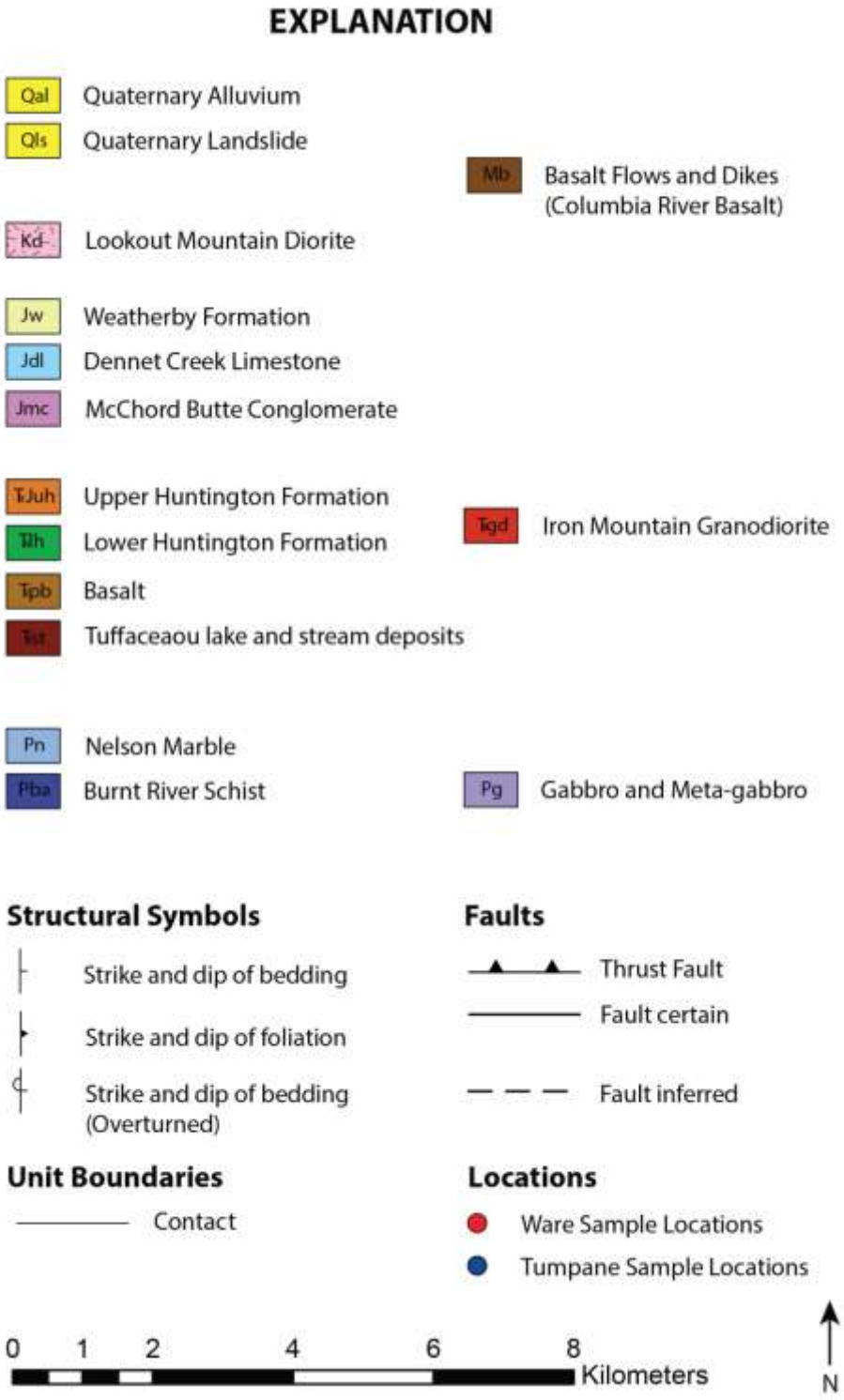

Figure 2.5: Full field area map of the Weatherby Formation, Original geology complemented by Prostka (1967), Brooks et al. (1978), Brooks (1979), and Payne and Northrup (2003).

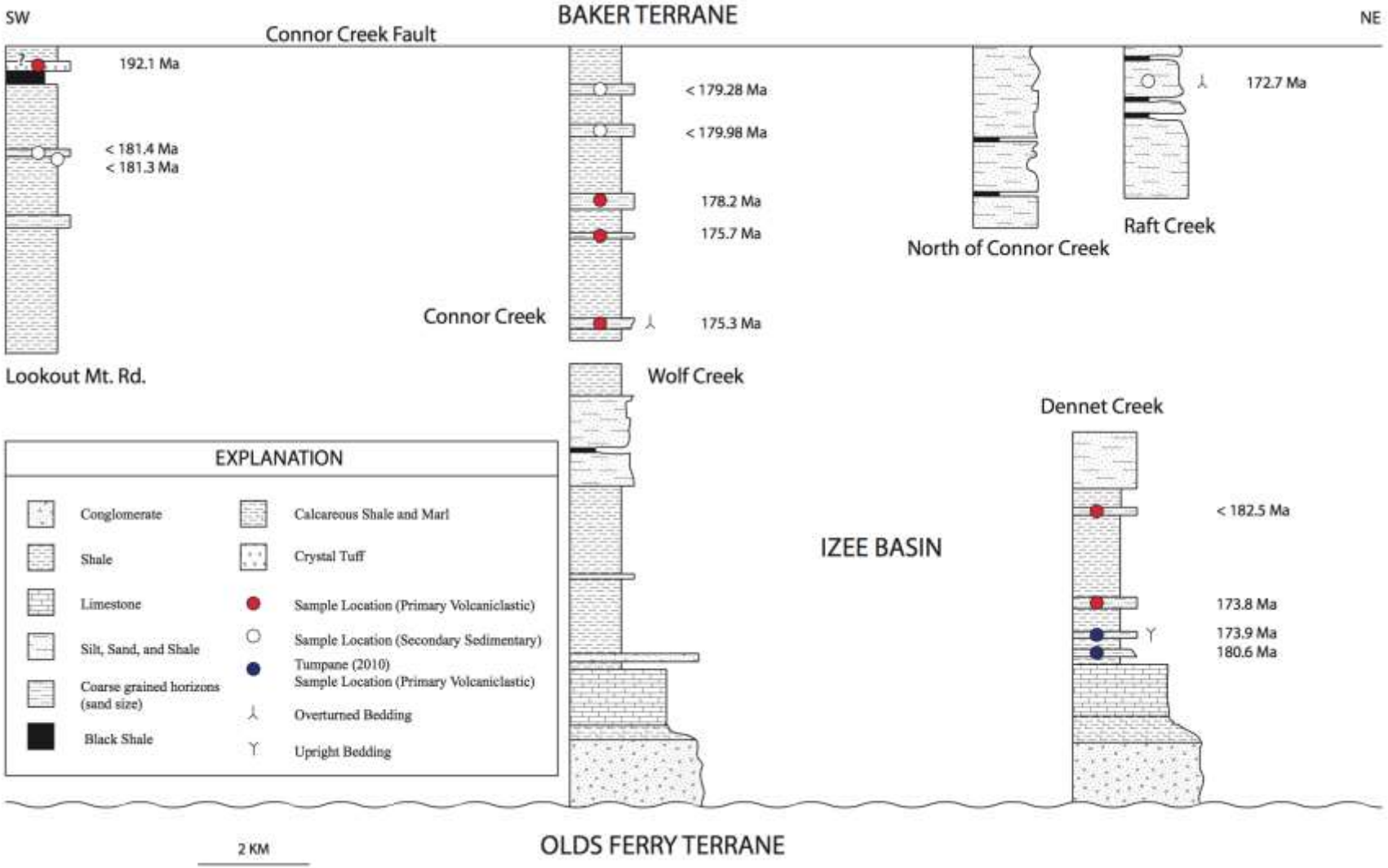

Figure 2.6: Stratigraphic columns of east west traverses spanning the field area of this study. Ages are both CA-TIMS single-grain zircon analyses and LA-ICPMS detrital zircon analyses (denoted by a < symbol).

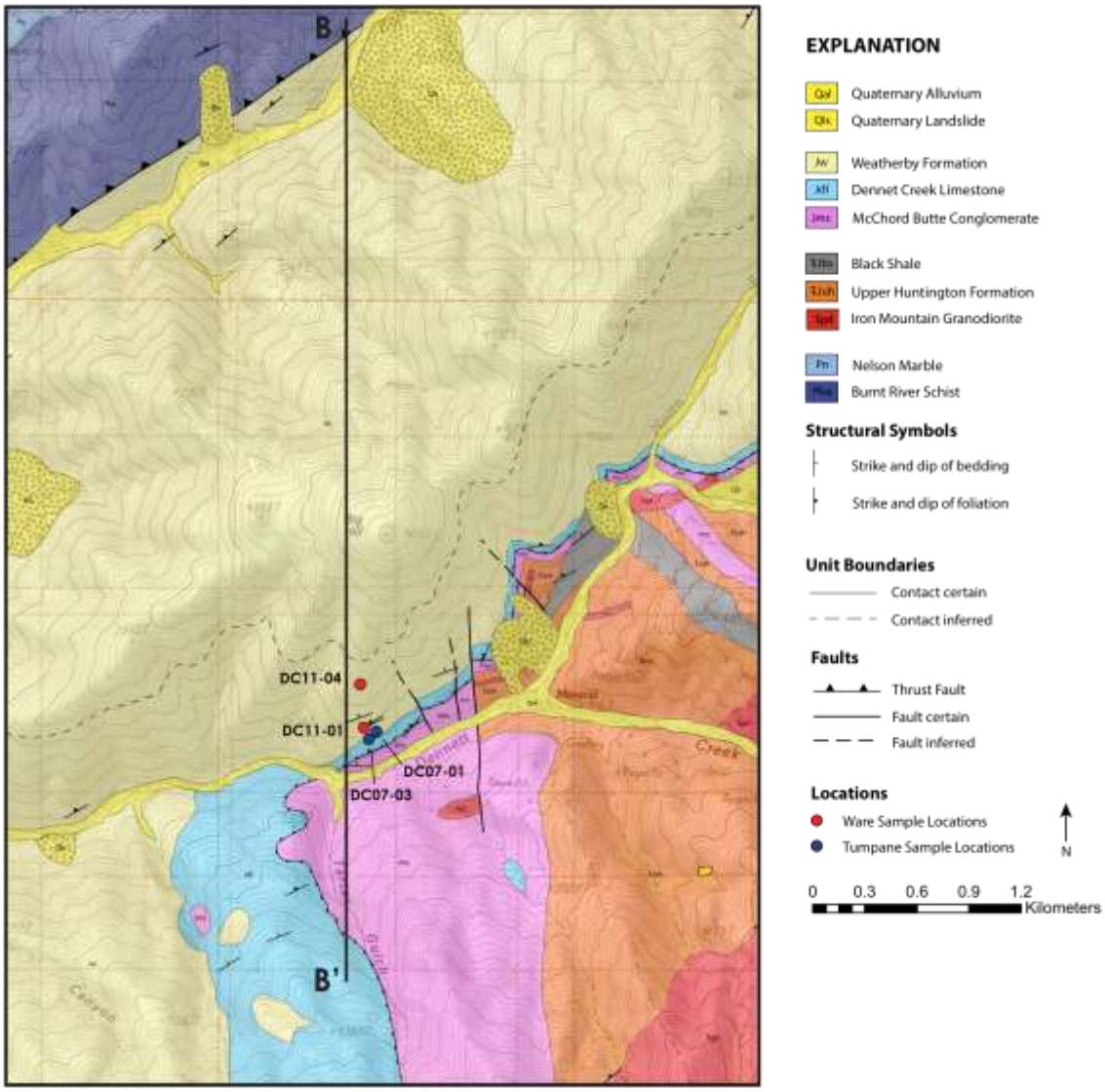

Figure 2.7: Geologic field map of the Dennet Creek field site. Huntington Formation and Baker terrane geology taken from Payne and Northrup (2003). Cross-section line location for Figure 2.7a shown.

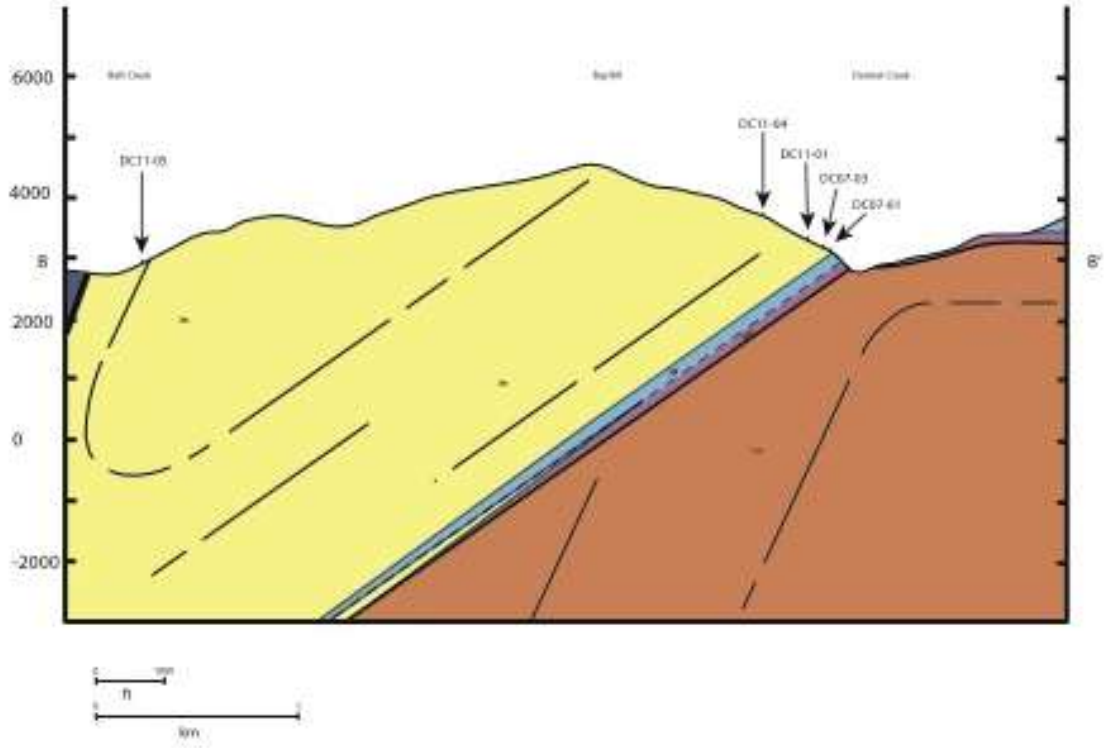

Figure 2.7a: Geologic cross-section of Dennet Creek (B – B') with sample locations. Jw – Marin Flysch, Jdl – Dennet Cree Limestone, Jmc – McChord Butte Conglomerate, T_RJuh – upper Huntington Formation, Pba – Burnt River Schist.

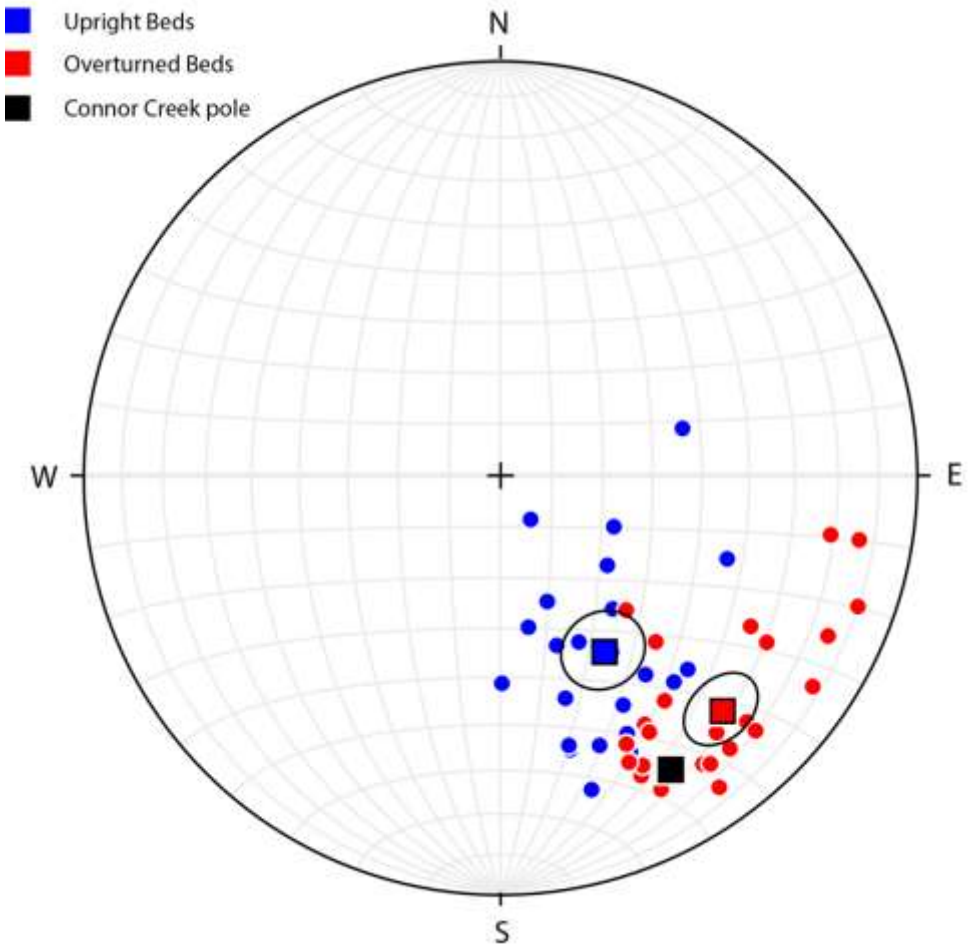

Figure 2.8: Stereonet displaying poles to bedding within the Weatherby Formation. The pole of the Connor Creek fault is also shown to display the dip similarity with the overturned beds.

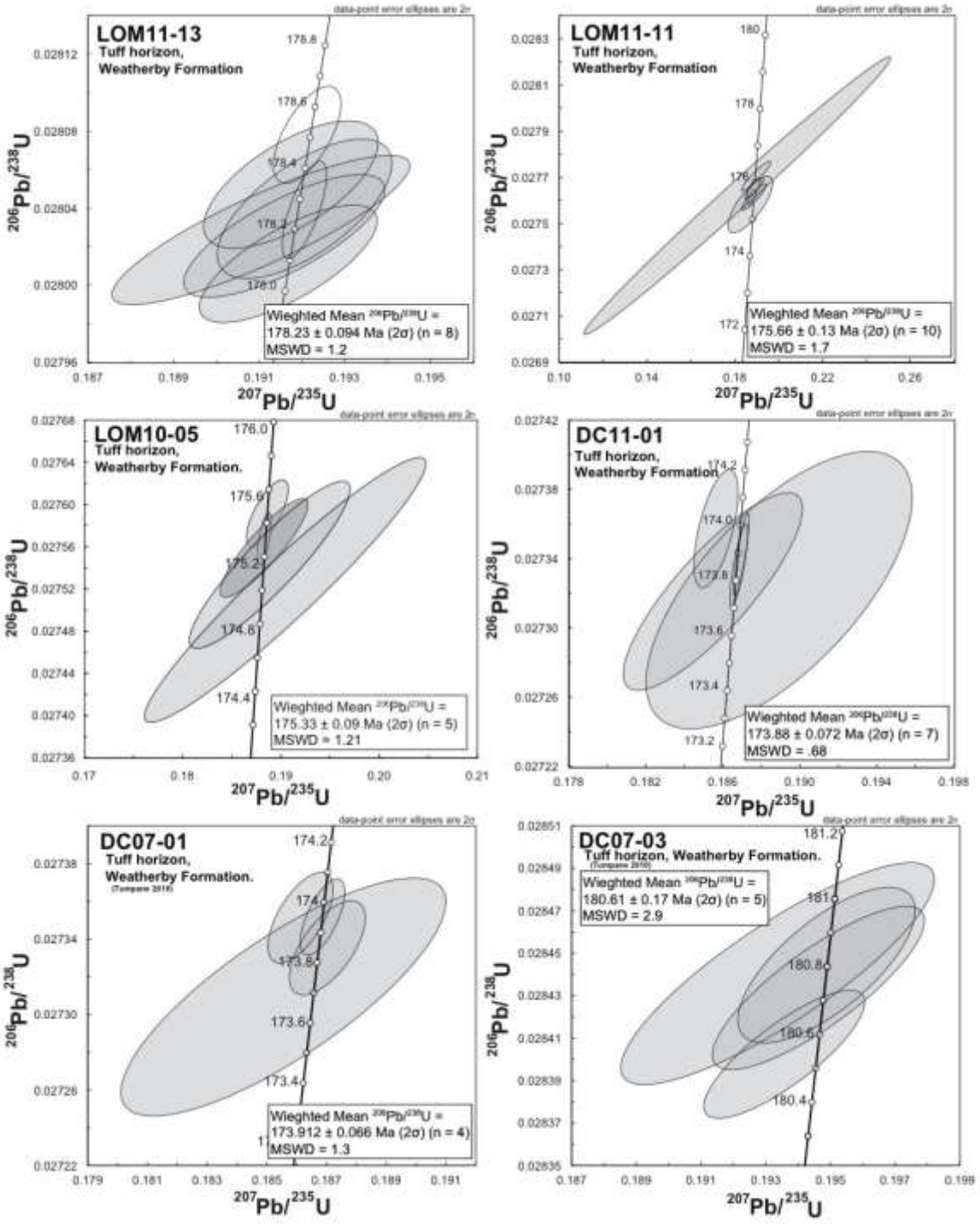
LOM11-13
Tuff horizon,
Weatherby Formation
Wieghted Mean 206Pb/238U =
178.23 ± 0.094 Ma (2σ) (n = 8)
MSWD = 1.2
LOM11-11
Tuff horizon,
Weatherby Formation
Wieghted Mean 206Pb/238U =
175.66 ± 0.13 Ma (2σ) (n = 10)
MSWD = 1.7
LOM10-05
Tuff horizon,
Weatherby Formation.
Wieghted Mean 206Pb/238U =
175.33 ± 0.09 Ma (2σ) (n = 5)
MSWD = 1.21
DC11-01
Tuff horizon,
Weatherby Formation
Wieghted Mean 206Pb/238U =
173.88 ± 0.072 Ma (2σ) (n = 7)
MSWD = .68
DC07-01
Tuff horizon,
Weatherby Formation.
Wieghted Mean 206Pb/238U =
173.912 ± 0.066 Ma (2σ) (n = 4)
MSWD = 1.3
DC07-03
Tuff horizon, Weatherby Formation.
Wieghted Mean 206Pb/238U =
180.61 ± 0.17 Ma (2σ) (n = 5)
MSWD = 2.9
data-point error ellipses are 2σ
206Pb/238U
207Pb/235U

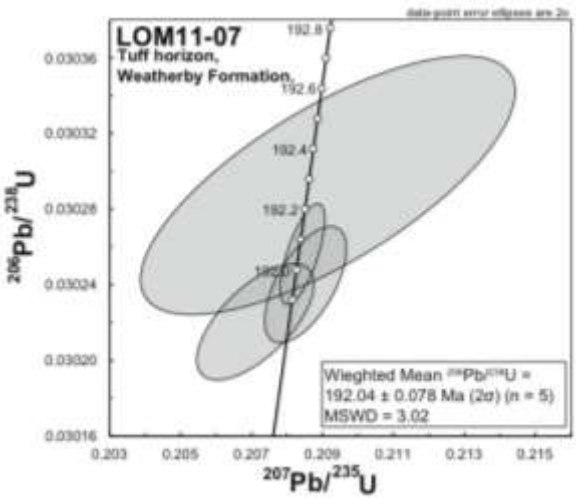

Figure 2.9: Concordia diagrams for all primary volcaniclastic samples, as well as the 192 Ma volcanic, showing chemically abraded zircon single-grain analyses. Shaded ellipses denote analyses used in the weighted mean age calculations. Data point error ellipses are 2σ. DC07-01 and DC07-03 taken from Tumpane (2010).

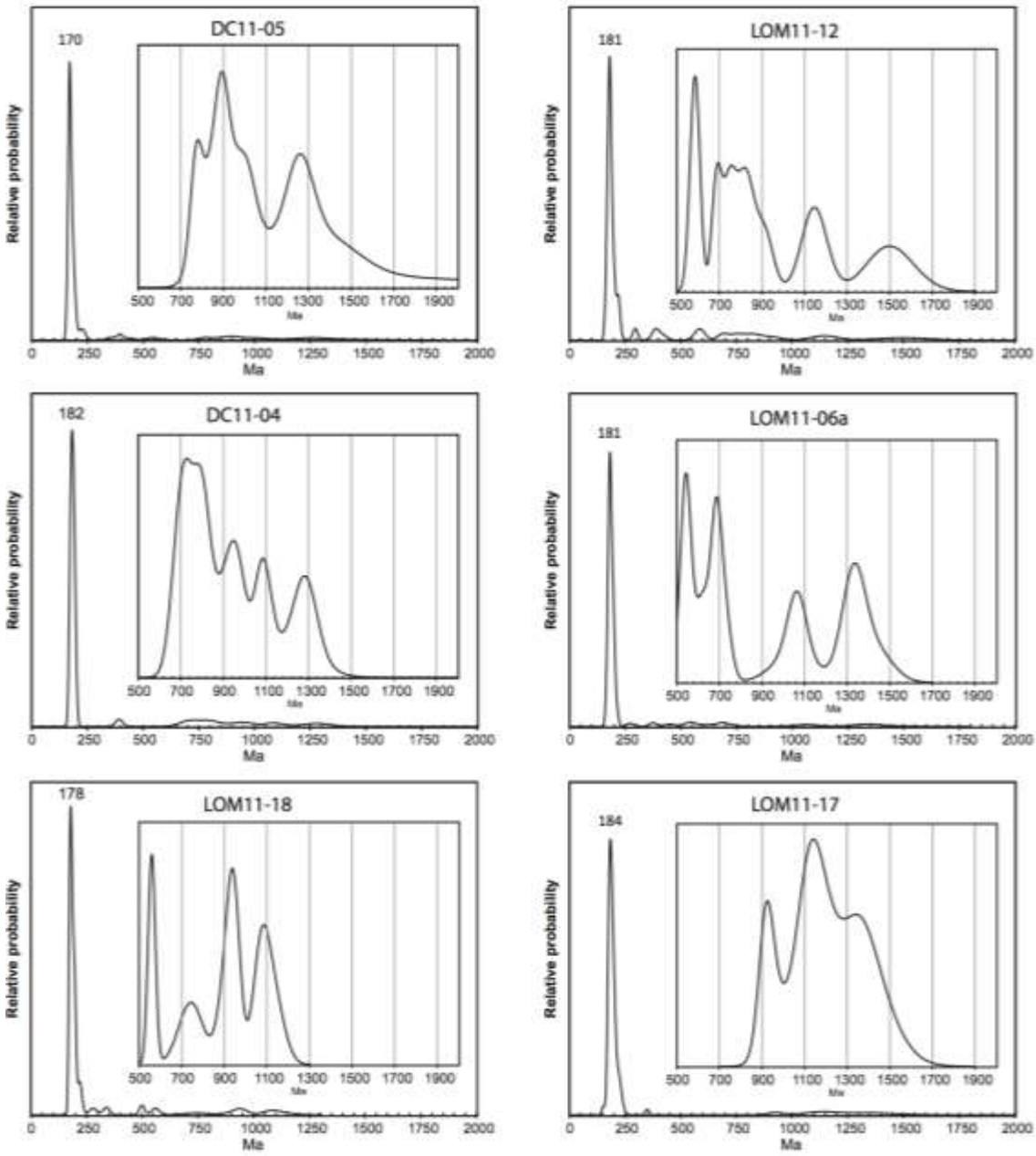

Figure 2.10: Density probability diagrams of all detrital samples representing the peaks in the late Early and Middle Jurassic; inset graphs showing peaks in the Mesoproterozoic and Neoproterozoic.

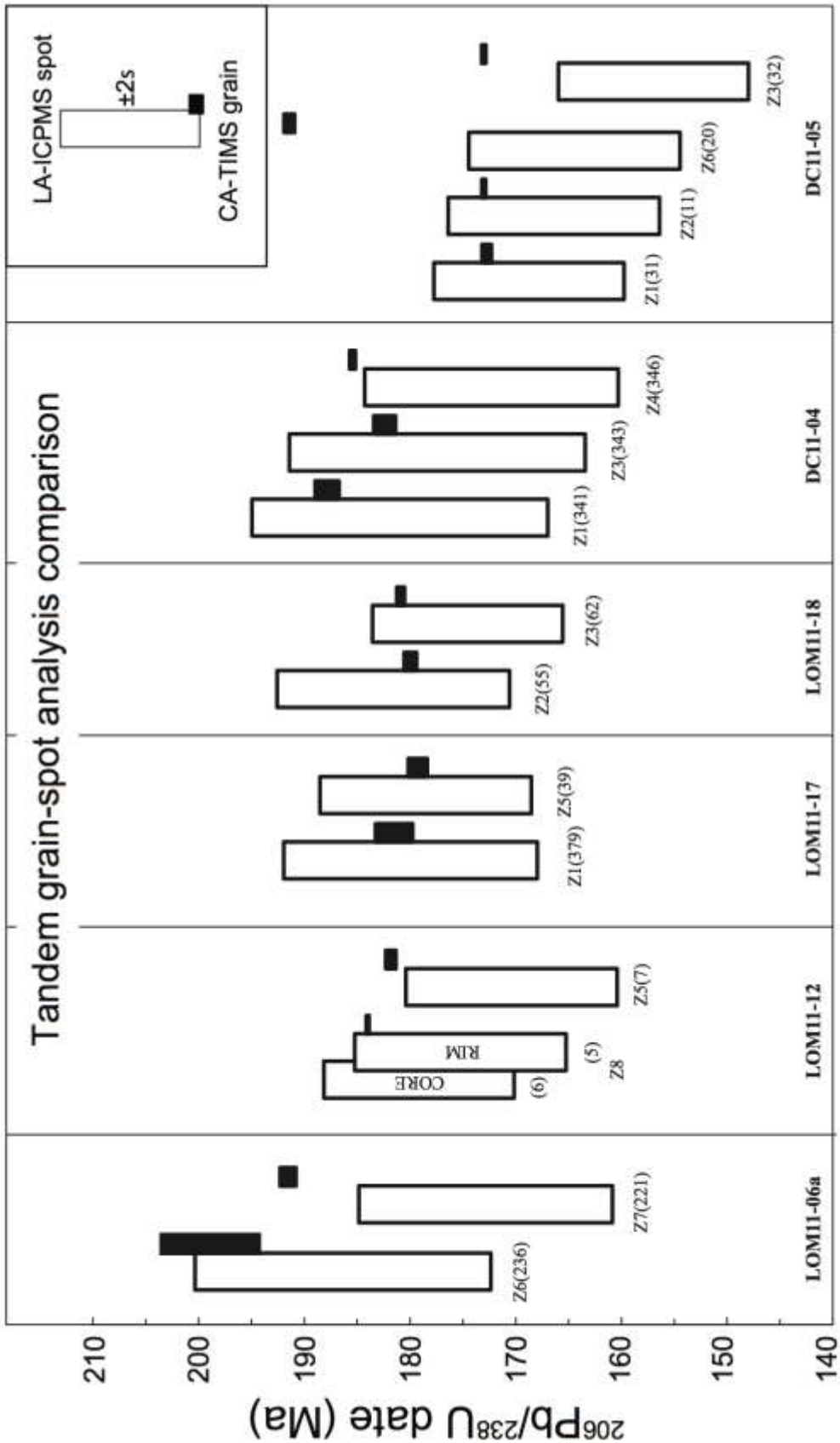
Tandem grain-spot analysis comparison
LA-ICPMS spot
±2s
CA-TIMS grain
$^{206}Pb/^{238}U$ date (Ma)
210
200
190
180
170
160
150
140
LOM11-06a
Z6(236)
Z7(221)
LOM11-12
CORE
RIM
(6)
(5)
Z8
Z5(7)
LOM11-17
Z1(379)
Z5(39)
LOM11-18
Z2(55)
Z3(62)
DC11-04
Z1(341)
Z3(343)
Z4(346)
DC11-05
Z1(31)
Z2(11)
Z6(20)
Z3(32)

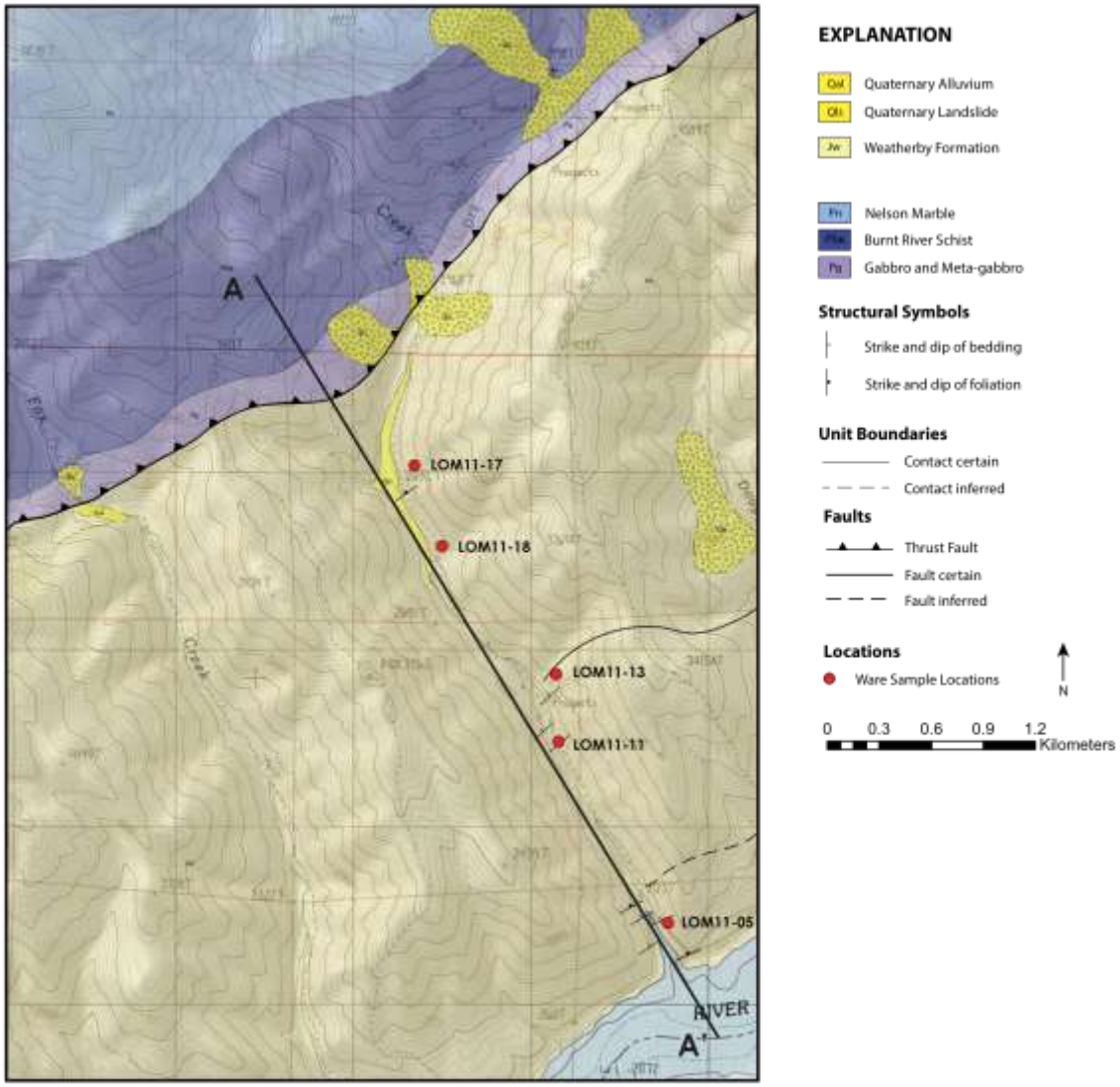

Figure 2.12: Geologic field map of the Connor Creek field site. Baker terrane geology taken from Brooks (1979). Cross-section line location for Figure 2.12a is shown.

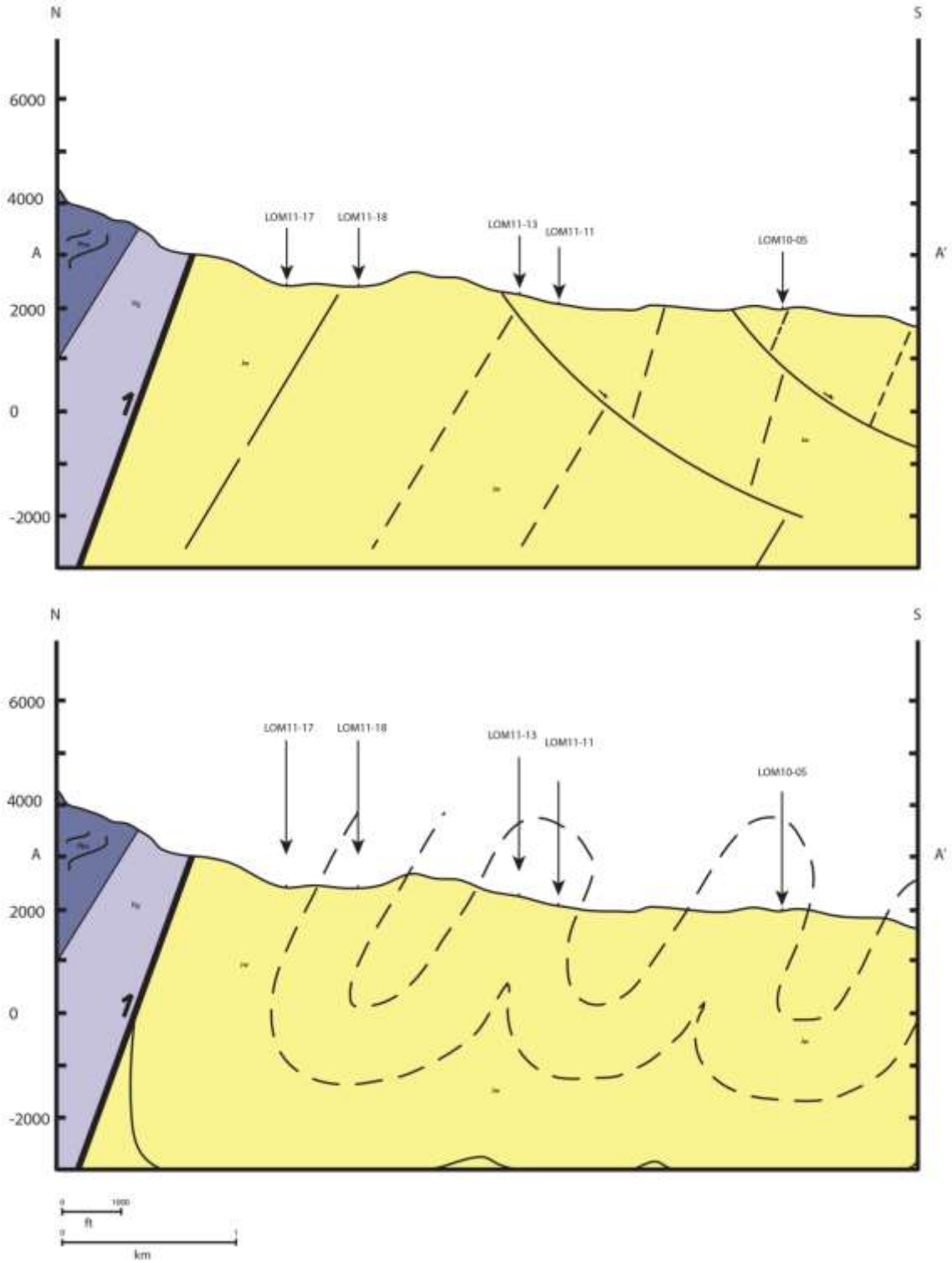

Figure 2.12a: Two possible geologic cross-sections of Connor Creek (A – A') with sample locations. Jw – Weatherby Formation, Pg – Gabbro, Pba – Burnt River Schist.

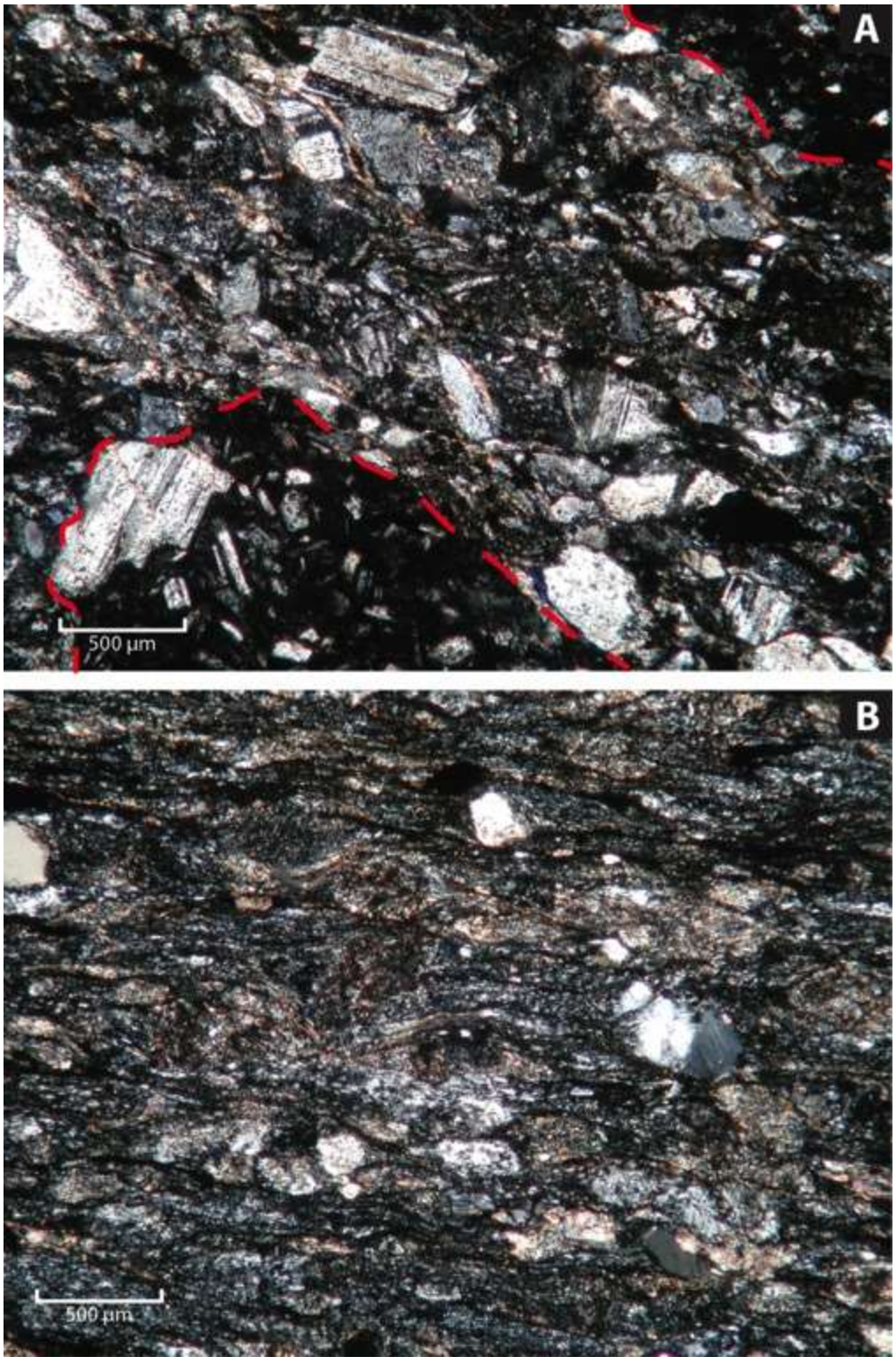

Figure 2.13: Photomicrographs of LOM10-05 (A), type sample for primary volcaniclastic textures displaying subangular plagioclase grains and volcanic lapilli outlined in red; and LOM11-12 (B), an example of a secondary sedimentary deposit displaying subangular to rounded quartz grains and a lack of plagioclase grains.

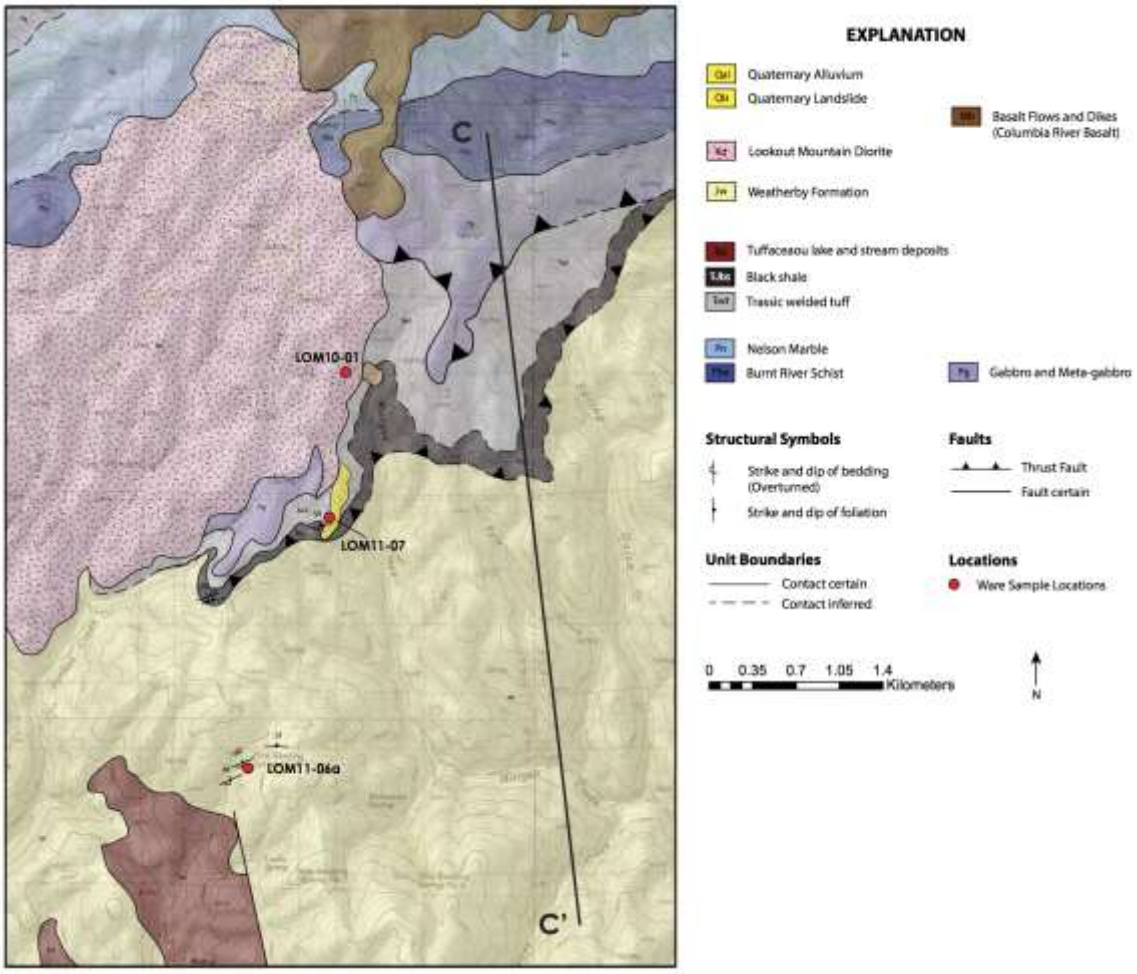

Figure 2.14: Geologic field map representing relationships of the Connor Creek fault, cross-cutting Lookout Mountain pluton, the Baker terrane, and the Weatherby Formation with sample locations and new structure data. Cross-section line for Figure 2.14a is shown. Baker terrane geology taken from Prostka (1967).

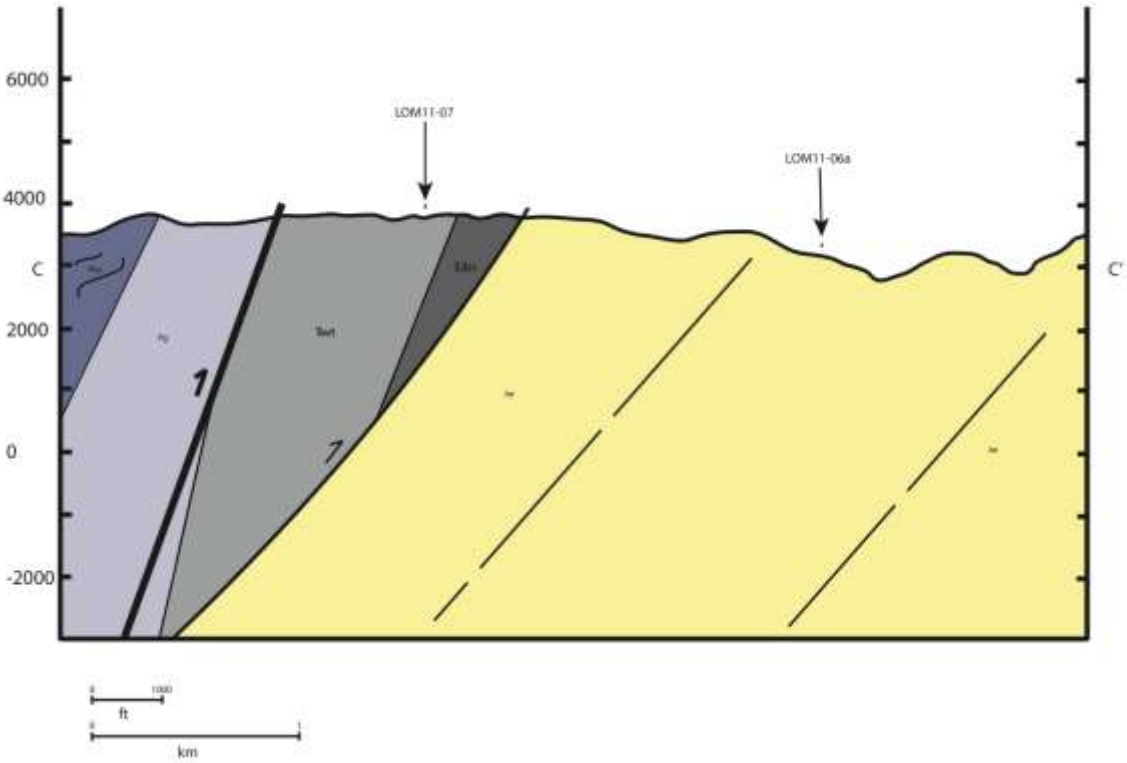

Figure 2.14a: A geologic cross-section of the area around the southern stock of the Lookout Mountain pluton with sample locations. Jw – Weatherby Formation, Pg – Gabbro, Pba – Burnt River Schist, $T_R$wt – 192 Ma volcanic, T_RJbs – Black Shale.

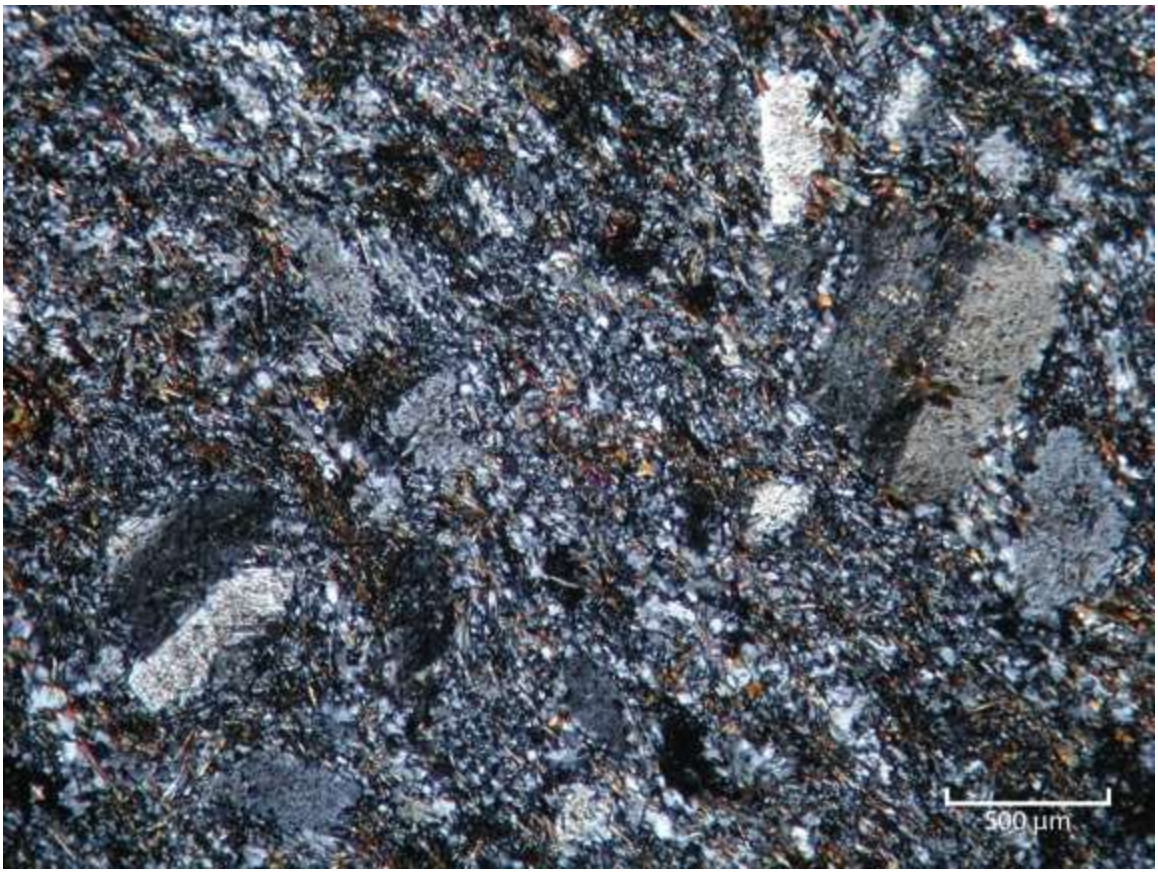

Figure 2.15: Photomicrographs of the 192 Ma volcanic (LOM11-07). An abundance of subrounded to rounded plagioclase grains can be observed, as well as primary and secondary white micas, in a quartz-rich matrix.

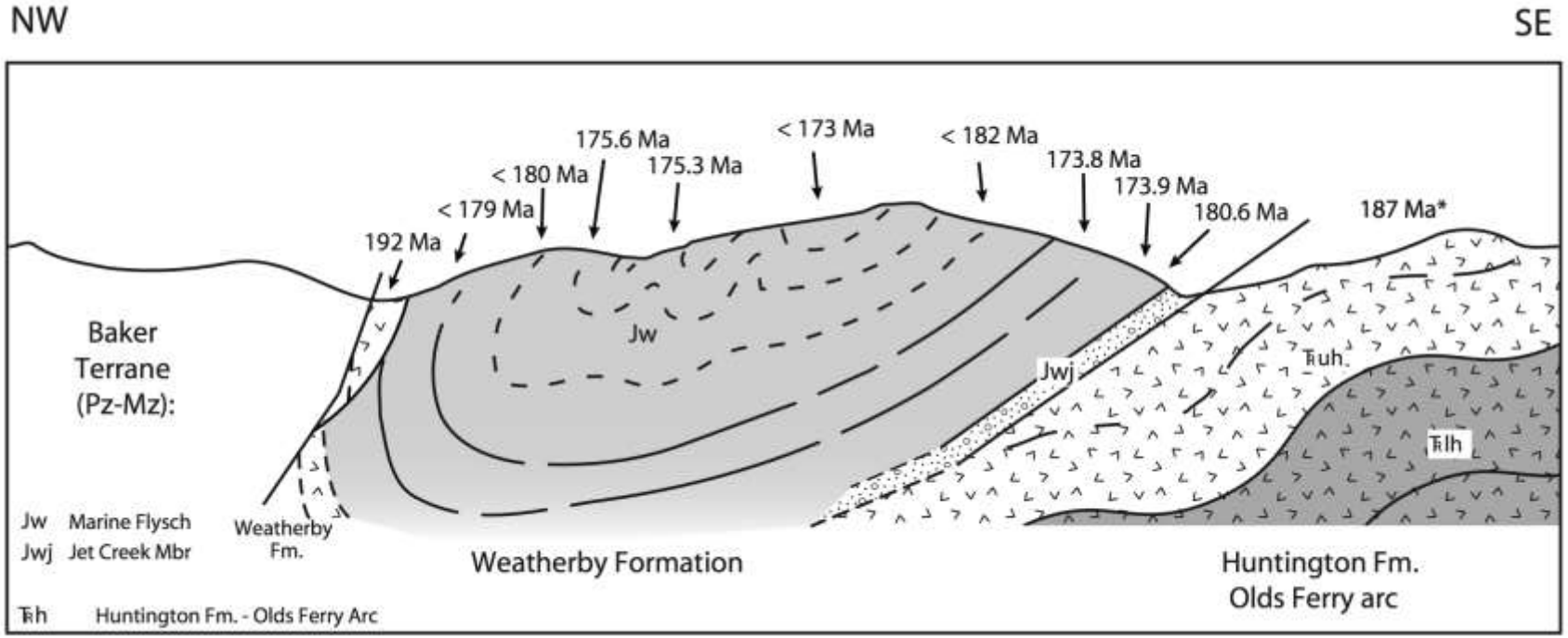

Figure 2.16: Schematic cross-section of the Weatherby Formation with CA-TIMS and LA-ICPMS (italics) ages from volcanic-rich turbidite horizons within the thick package of marine flysch. * Represents CA-TIMS zircon age data from a rhyolite unit in the upper Huntington Formation (Tumpane 2010).

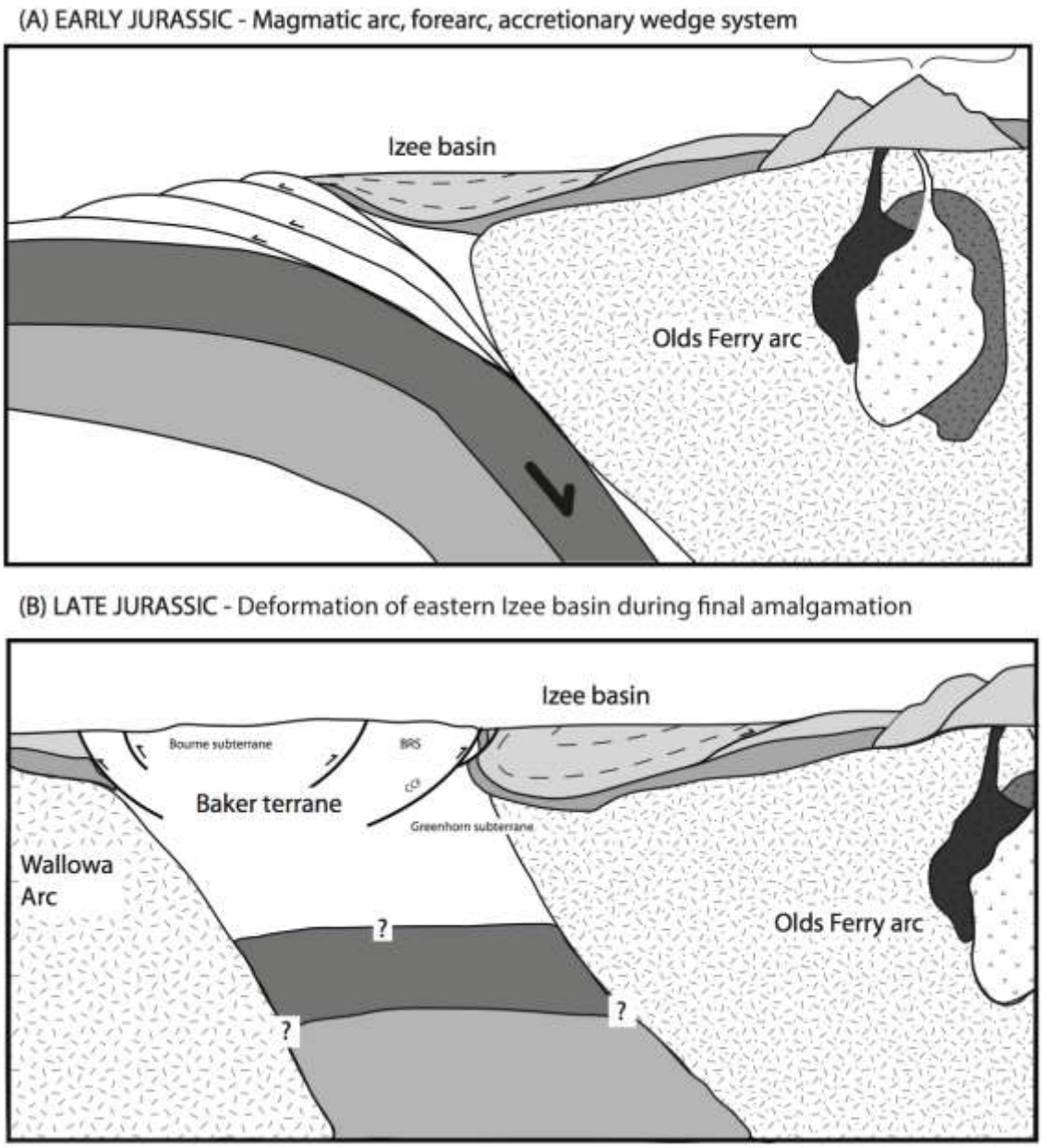

Figure 2.17: Proposed tectonic model of the eastern Izee sub-basin. (A) Formation of the eastern Izee basin on the flanks of both the Olds Ferry terrane and the Baker terrane modeled after the western Izee sub-basin. (B) Structural orientation of the eastern Izee sub-basin after cessation of subduction beneath the Olds Ferry arc and Late Jurassic deformation. CCF - Connor Creek fault.

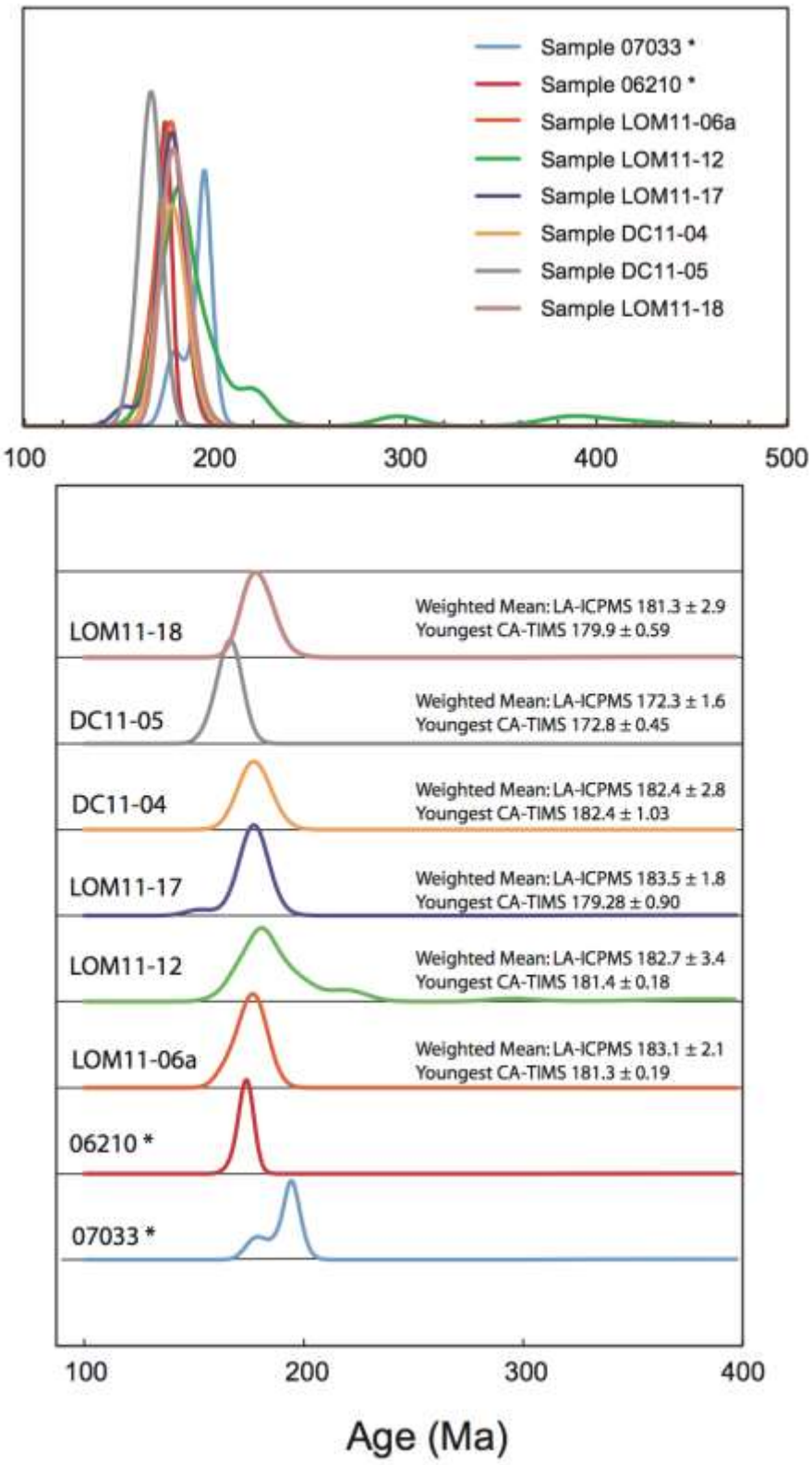

Figure 2.18: Density probability diagrams of all samples analyzed within the marine flysch of the Weatherby Formation. * Indicates data from LaMaskin et al. (2011b).

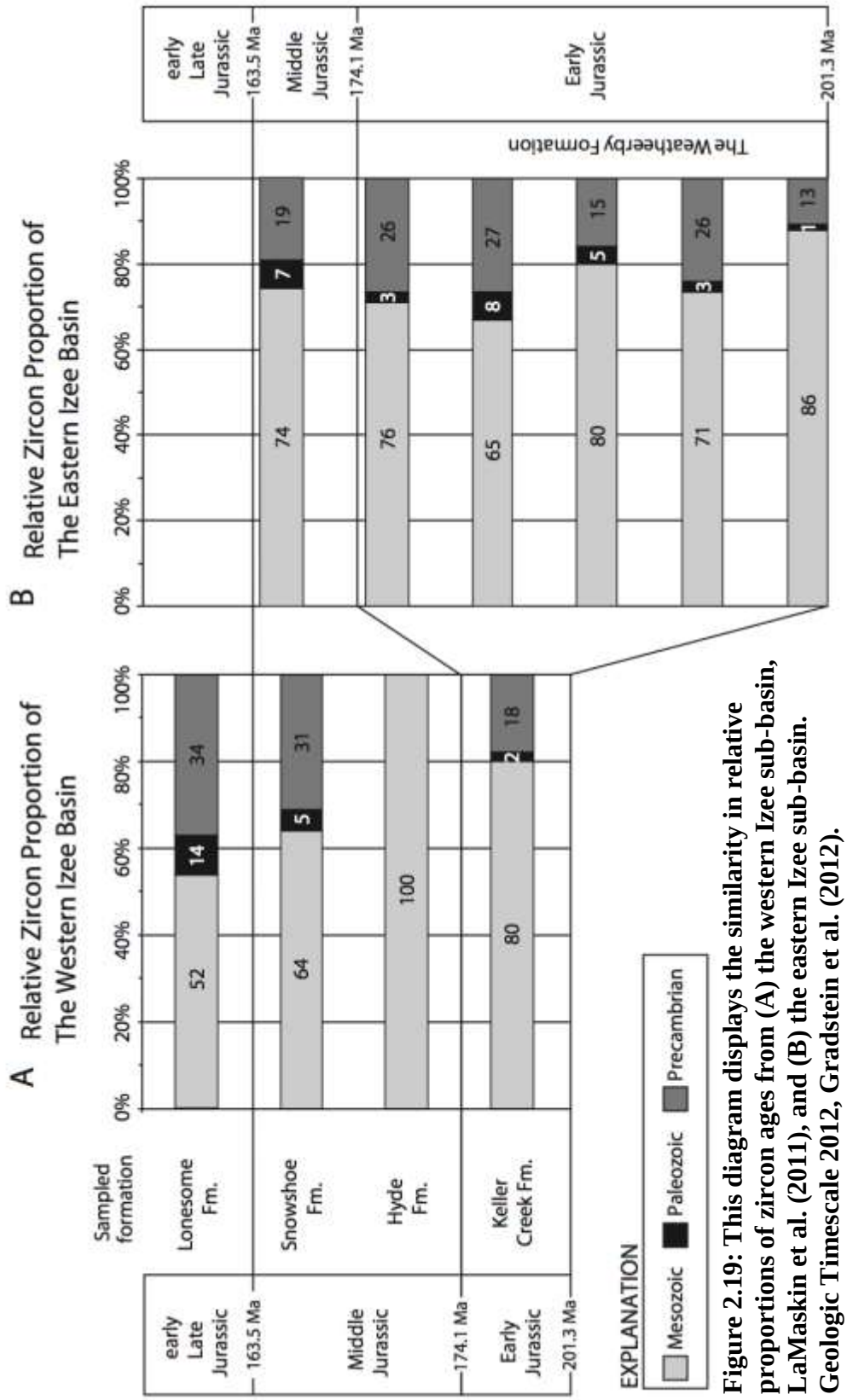

Figure 2.19: This diagram displays the similarity in relative proportions of zircon ages from (A) the western Izee sub-basin, LaMaskin et al. (2011), and (B) the eastern Izee sub-basin. Geologic Timescale 2012, Gradstein et al. (2012).

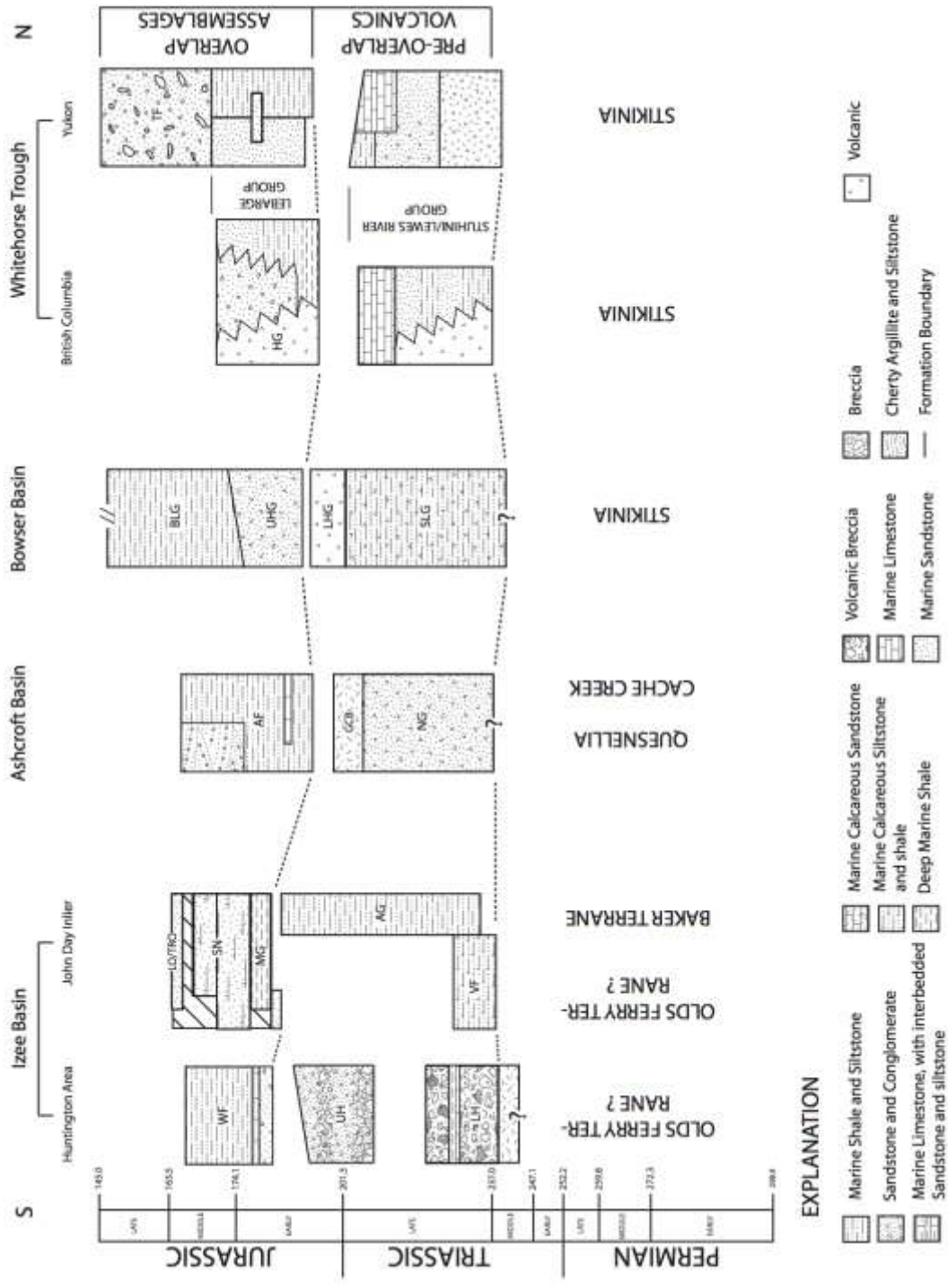
N
S
Whitehorse Trough
Yukon
British Columbia
Izee Basin
Huntington Area
John Day Inlier
Bowser Basin
Ashcroft Basin
OVERLAP ASSEMBLAGES
PRE-OVERLAP VOLCANICS
LEIARGE GROUP
STUHINI/LEMES RIVER GROUP
STIKINIA
STIKINIA
STIKINIA
QUESNELLIA
CACHE CREEK
BAKER TERRANE
OLDS FERRY TER-RANE ?
OLDS FERRY TER-RANE ?
HG
BLG
UHG
LMG
SLG
AF
GCb
NG
AG
VF
WF
UH
LH
LO/TRO
SN
MG
JURASSIC
TRIASSIC
PERMIAN
1410
1655
1741
2013
2370
2471
2522
2596
2723
2884
EXPLANATION
Marine Shale and Siltstone
Sandstone and Conglomerate
Marine Limestone, with interbedded Sandstone and siltstone
Marine Calcareous Sandstone
Marine Calcareous Siltstone and shale
Deep Marine Shale
Volcanic Breccia
Marine Limestone
Marine Sandstone
Breccia
Cherty Argillite and Siltstone
Formation Boundary
Volcanic

Figure 2.20: Schematic stratigraphic sections of the Izee basin, Ashcroft basin, Bower basin, and Whitehorse Trough. Basement is denoted below each column with question marks where inferred. WF - Weatherby Fm., UH - upper Huntington Fm., LH - lower Huntington Fm., VF - Vester Fm., AG - Aldrich Mt. Group, MG - Mowich Group, SN - Snowshoe Fm., LO/TRO - Trowbridge Fm. and Lonesome Fm., HG - Hazelton Group, LHG - Lower Hazelton Group, UHG - Upper Hazelton Group, BLG - Bowser Lake Group, SLG - Stuhini/Lewes River Group, TF - Tantalus Fm., AC - Ashcroft Fm., NG - Nicola Group GCB - Guichon Creek Batholith. Compiled from Tumpane (2010), Dorsey and LaMaskin (2007), English et al. (2005), Lowey et al. (2009), and Travers (1978). Geologic Timescale 2012, Gradstein et al. (2012).

Table 2.1 CA-TIMS U-Pb age summary

Sample	Formation	Location	UTM $^{206}Pb/^{238}U$ age	Weighted mean (2σ)	± X	MSWD	N
Primary Volcaniclastic Turbidites							
LOM11-07		Lookout Mountain Rd	11T0477176, 4928843	192.07	± 0.084	2.63	4 of 4
LOM11-13	Weatherby	Connor Creek, OR	11T0485079, 4931460	178.23	± 0.094	1.2	6 of 8
LOM11-11	Weatherby	Connor Creek, OR	11T0485079, 4931460	175.66	± 0.13	1.7	8 of 10
LOM10-05	Weatherby	Connor Creek, OR	11T0485700, 4930435	175.33	± 0.09	1.21	5 of 7
DC11-01	Weatherby	Big Hill, ID	11T0492706, 4934345	173.88	± 0.072	0.68	5 of 7
DC07-01*	Weatherby	Big Hill, ID	11T0492809, 4934266	173.91	± 0.066	1.3	5 of 8
DC07-03*	Weatherby	Big Hill, ID	11T0492770, 4934213	180.61	± 0.17	2.9	4 of 10
Secondary Volcanic Sandstones							
LOM11-12	Weatherby	Connor Creek, OR	11T0474331, 4925278	< 181.83	± 0.43		z5
LOM11-06a	Weatherby	Lookout Mountain Rd	11T0476490, 4926855	< 181.31	± 0.19		z2
LOM11-18	Weatherby	Connor Creek, OR	11T0484420, 4932560	< 179.98	± 0.59		z2
LOM11-17	Weatherby	Connor Creek, OR	11T0484262, 4933020	< 179.28	± 0.90		z5
DC11-05	Weatherby	Raft Creek, ID	11T0490572, 4936471	< 172.75	± 0.45		z2
DC11-04	Weatherby	Big Hill, ID	11T0492685, 4934590	< 182.47	± 1.03		z3

Notes:

* Samples from Kyle Tumpane's thesis "Age and Isotopic Investigations of the Olds Ferry Terrane and its Relations to Other Terranes of the Blue Mountains province, Eastern Oregon and West-Central Idaho." (2010)

Table 2.2 CA-TIMS U-Pb Isotopic Data

								Radiogenic Isotope Ratios								Radiogenic Isotope Dates					
	Th	^{206}Pb*	mol %	Pb*	Pbc	^{206}Pb	^{208}Pb	^{207}Pb		^{207}Pb		^{206}Pb		corr.	^{207}Pb		^{207}Pb		^{206}Pb	
Grain	U	x10^{-13} mol	^{206}Pb*	Pbc	(pg)	^{204}Pb	^{206}Pb	^{206}Pb	% err	^{235}U	% err	^{238}U	% err	coef.	^{206}Pb	±	^{235}U	±	^{238}U	±
(a)	(b)	(c)	(c)	(c)	(c)	(d)	(e)	(e)	(f)	(e)	(f)	(e)	(f)		(g)	(f)	(g)	(f)	(g)	(f)
LOM11-07: Volcanic Tuff																				
z1	**0.230**	**1.5422**	**98.51%**	**19**	**1.92**	**1233**	**0.073**	**0.050013**	**0.406**	**0.208531**	**0.452**	**0.030240**	**0.083**	**0.618**	**195.62**	**9.43**	**192.32**	**0.79**	**192.05**	**0.16**
z2	**0.261**	**0.8121**	**98.82%**	**24**	**0.80**	**1561**	**0.083**	**0.049703**	**0.601**	**0.207103**	**0.652**	**0.030220**	**0.083**	**0.654**	**181.14**	**13.99**	**191.12**	**1.14**	**191.93**	**0.16**
z3	**0.238**	**1.5144**	**99.65%**	**80**	**0.44**	**5230**	**0.076**	**0.049965**	**0.202**	**0.208441**	**0.244**	**0.030256**	**0.072**	**0.685**	**193.37**	**4.69**	**192.24**	**0.43**	**192.15**	**0.14**
z4	**0.279**	**0.3160**	**91.24%**	**3**	**2.50**	**210**	**0.089**	**0.050076**	**1.935**	**0.209156**	**2.065**	**0.030293**	**0.184**	**0.727**	**198.54**	**44.93**	**192.84**	**3.63**	**192.38**	**0.35**
LOM11-13: Volcaniclastic Tuff																				
z1	**0.336**	**3.3047**	**99.68%**	**89**	**0.88**	**5696**	**0.107**	**0.049676**	**0.176**	**0.192052**	**0.220**	**0.028039**	**0.073**	**0.713**	**179.88**	**4.10**	**178.38**	**0.36**	**178.26**	**0.13**
z2	0.506	0.6076	97.72%	13	1.17	805	0.161	0.049635	1.145	0.194428	1.225	0.028410	0.102	0.804	177.95	26.69	180.40	2.03	180.59	0.18
z3	**0.325**	**0.5535**	**98.36%**	**17**	**0.76**	**1121**	**0.103**	**0.049629**	**0.823**	**0.191678**	**0.886**	**0.028011**	**0.089**	**0.734**	**177.67**	**19.18**	**178.06**	**1.45**	**178.09**	**0.16**
z4	**0.393**	**0.3357**	**98.44%**	**19**	**0.44**	**1174**	**0.125**	**0.049677**	**0.804**	**0.192057**	**0.869**	**0.028040**	**0.105**	**0.656**	**179.89**	**18.73**	**178.38**	**1.42**	**178.27**	**0.19**
z7	**0.297**	**0.3892**	**97.29%**	**10**	**0.90**	**676**	**0.094**	**0.049432**	**1.393**	**0.191037**	**1.489**	**0.028029**	**0.113**	**0.864**	**168.39**	**32.53**	**177.51**	**2.43**	**178.20**	**0.20**
z8	0.333	1.6947	99.43%	51	0.80	3228	0.106	0.049625	0.294	0.192118	0.335	0.028078	0.073	0.634	177.45	6.85	178.43	0.55	178.51	0.13
z10	**0.350**	**1.0793**	**98.16%**	**15**	**1.67**	**996**	**0.111**	**0.049579**	**0.934**	**0.191584**	**1.002**	**0.028026**	**0.093**	**0.757**	**175.32**	**21.78**	**177.98**	**1.64**	**178.18**	**0.16**
z11	**0.340**	**0.6193**	**98.46%**	**19**	**0.80**	**1193**	**0.108**	**0.049572**	**0.810**	**0.191740**	**0.870**	**0.028052**	**0.096**	**0.658**	**174.99**	**18.89**	**178.11**	**1.42**	**178.35**	**0.17**
LOM11-11: Volcaniclastic Tuff																				
z1	**0.262**	**1.2176**	**99.34%**	**42**	**0.67**	**2770**	**0.083**	**0.049534**	**0.349**	**0.188558**	**0.392**	**0.027608**	**0.074**	**0.639**	**173.17**	**8.15**	**175.40**	**0.63**	**175.56**	**0.13**
z2	0.296	0.5035	94.73%	5	2.31	348	0.094	0.049652	2.721	0.189683	2.896	0.027707	0.189	0.933	178.76	63.41	176.36	4.69	176.18	0.33
z3	**0.338**	**0.1525**	**95.69%**	**6**	**0.57**	**426**	**0.108**	**0.049550**	**2.261**	**0.188677**	**2.410**	**0.027617**	**0.168**	**0.891**	**173.95**	**52.75**	**175.50**	**3.88**	**175.62**	**0.29**
z4	**0.374**	**0.2012**	**96.70%**	**9**	**0.57**	**557**	**0.119**	**0.049533**	**1.771**	**0.188869**	**1.890**	**0.027655**	**0.136**	**0.884**	**173.13**	**41.32**	**175.66**	**3.05**	**175.85**	**0.24**
z5	**0.263**	**0.3879**	**92.32%**	**3**	**2.66**	**239**	**0.083**	**0.049191**	**4.190**	**0.187085**	**4.458**	**0.027584**	**0.362**	**0.759**	**156.92**	**98.04**	**174.14**	**7.13**	**175.41**	**0.63**
z6	**0.395**	**0.3246**	**98.54%**	**20**	**0.40**	**1255**	**0.125**	**0.049305**	**0.765**	**0.187741**	**0.825**	**0.027617**	**0.093**	**0.679**	**162.34**	**17.88**	**174.70**	**1.32**	**175.61**	**0.16**
z7	0.295	0.2385	83.35%	1	3.93	110	0.093	0.049537	9.736	0.195093	10.345	0.028563	0.614	0.992	173.32	227.16	180.97	17.15	181.55	1.10
z9	**0.329**	**0.2741**	**97.77%**	**13**	**0.52**	**822**	**0.105**	**0.049460**	**1.216**	**0.188606**	**1.302**	**0.027657**	**0.117**	**0.754**	**169.71**	**28.39**	**175.44**	**2.10**	**175.86**	**0.20**
z10	**0.411**	**0.0747**	**63.27%**	**1**	**3.58**	**50**	**0.126**	**0.047559**	**29.754**	**0.181125**	**31.515**	**0.027622**	**1.775**	**0.992**	**77.37**	**706.66**	**169.03**	**49.07**	**175.65**	**3.07**
z11	0.309	0.5321	97.53%	11	1.11	743	0.099	0.049797	1.253	0.192396	1.341	0.028022	0.108	0.818	185.52	29.18	178.67	2.20	178.15	0.19

Table 2.2. CA-TIMS U-Pb Isotopic Data Cont.

							Radiogenic Isotope Ratios								Radiogenic Isotope Dates					
	Th	^{206}Pb*	mol %	Pb*	Pbc	^{206}Pb	^{208}Pb	^{207}Pb		^{207}Pb		^{206}Pb		corr.	^{207}Pb		^{207}Pb		^{206}Pb	
Grain	U	x10^{-13} mol	^{206}Pb*	Pbc	(pg)	^{204}Pb	^{206}Pb	^{206}Pb	% err	^{235}U	% err	^{238}U	% err	coef.	^{206}Pb	±	^{235}U	±	^{238}U	±
(a)	(b)	(c)	(c)	(c)	(c)	(d)	(e)	(e)	(f)	(e)	(f)	(e)	(f)		(g)	(f)	(g)	(f)	(g)	(f)
LOM10-05: Volcaniclastic Tuff																				
z1	**0.394**	**1.3818**	**99.51%**	**60**	**0.56**	**3771**	**0.125**	**0.049573**	**0.256**	**0.188424**	**0.298**	**0.027567**	**0.074**	**0.650**	**175.02**	**5.97**	**175.28**	**0.48**	**175.30**	**0.13**
z3	**0.473**	**0.2331**	**96.51%**	**8**	**0.69**	**526**	**0.151**	**0.049584**	**1.802**	**0.188407**	**1.923**	**0.027559**	**0.139**	**0.880**	**175.52**	**42.02**	**175.27**	**3.10**	**175.25**	**0.24**
z4	0.448	0.5256	99.00%	31	0.44	1838	0.170	0.067669	0.375	0.548398	0.429	0.058776	0.090	0.669	858.44	7.78	443.95	1.54	368.18	0.32
z5	**0.551**	**0.3352**	**98.42%**	**19**	**0.44**	**1162**	**0.176**	**0.049608**	**0.855**	**0.188724**	**0.920**	**0.027591**	**0.094**	**0.719**	**176.67**	**19.94**	**175.54**	**1.48**	**175.46**	**0.16**
z6	0.656	0.1207	92.65%	4	0.79	250	0.214	0.051298	3.784	0.217552	4.034	0.030758	0.267	0.943	254.23	86.99	199.87	7.32	195.29	0.51
z7	**0.664**	**0.0671**	**93.92%**	**5**	**0.36**	**302**	**0.212**	**0.049761**	**3.298**	**0.188972**	**3.510**	**0.027543**	**0.235**	**0.905**	**183.85**	**76.81**	**175.75**	**5.66**	**175.15**	**0.41**
z8	**0.399**	**0.0756**	**89.65%**	**3**	**0.72**	**177**	**0.129**	**0.050214**	**5.747**	**0.190527**	**6.102**	**0.027519**	**0.373**	**0.954**	**204.93**	**133.30**	**177.08**	**9.92**	**175.00**	**0.64**
DC11-01: Volcaniclastic Tuff																				
z1	0.497	0.3966	95.38%	6	1.59	391	0.160	0.050366	1.017	0.197264	1.110	0.028406	0.150	0.656	211.94	23.57	182.81	1.86	180.56	0.27
z2	**0.521**	**0.2746**	**92.26%**	**4**	**1.91**	**233**	**0.165**	**0.049234**	**1.910**	**0.185465**	**2.051**	**0.027321**	**0.170**	**0.838**	**158.97**	**44.69**	**172.75**	**3.26**	**173.76**	**0.29**
z3	0.366	0.3774	87.92%	2	4.30	150	0.117	0.049894	2.698	0.197356	2.894	0.028688	0.237	0.839	190.04	62.76	182.89	4.84	182.33	0.43
z5	**0.369**	**0.0570**	**91.14%**	**3**	**0.46**	**204**	**0.119**	**0.050147**	**2.835**	**0.188911**	**2.989**	**0.027322**	**0.239**	**0.667**	**201.81**	**65.81**	**175.70**	**4.82**	**173.77**	**0.41**
z6	**0.407**	**1.3955**	**99.72%**	**104**	**0.33**	**6442**	**0.130**	**0.049589**	**0.122**	**0.186948**	**0.176**	**0.027343**	**0.071**	**0.846**	**175.76**	**2.84**	**174.02**	**0.28**	**173.89**	**0.12**
z7	**0.542**	**1.1307**	**99.48%**	**59**	**0.49**	**3494**	**0.173**	**0.049565**	**0.153**	**0.186814**	**0.204**	**0.027336**	**0.072**	**0.800**	**174.62**	**3.56**	**173.91**	**0.33**	**173.85**	**0.12**
z8	**0.507**	**0.3933**	**98.95%**	**28**	**0.35**	**1712**	**0.160**	**0.049212**	**0.448**	**0.185630**	**0.503**	**0.027357**	**0.102**	**0.612**	**157.94**	**10.48**	**172.89**	**0.80**	**173.99**	**0.17**
LOM11-12: Secondary Volcanic Sandstone																				
z1	0.360	0.8249	98.97%	28	0.71	1789	0.115	0.049849	0.514	0.200593	0.562	0.029185	0.081	0.637	187.95	11.96	185.63	0.95	185.45	0.15
z2	0.407	0.5624	98.28%	17	0.81	1069	0.130	0.050015	0.868	0.205933	0.935	0.029862	0.094	0.744	195.71	20.16	190.13	1.62	189.69	0.17
z3	0.431	0.7454	98.76%	24	0.77	1484	0.136	0.049567	0.660	0.204968	0.715	0.029991	0.087	0.672	174.73	15.39	189.32	1.23	190.49	0.16
z4	0.550	0.3895	98.15%	16	0.60	993	0.174	0.049500	0.980	0.194765	1.055	0.028537	0.101	0.762	171.59	22.87	180.69	1.75	181.38	0.18

Table 2.2. CA-TIMS U-Pb Isotopic Data Cont.

							Radiogenic Isotope Ratios								Radiogenic Isotope Dates					
	Th	^{206}Pb*	mol %	Pb*	Pbc	^{206}Pb	^{208}Pb	^{207}Pb		^{207}Pb		^{206}Pb		corr.	^{207}Pb		^{207}Pb		^{206}Pb	
Grain	U	x10^{-13} mol	^{206}Pb*	Pbc	(pg)	^{204}Pb	^{206}Pb	^{206}Pb	% err	^{235}U	% err	^{238}U	% err	coef.	^{206}Pb	±	^{235}U	±	^{238}U	±
(a)	(b)	(c)	(c)	(c)	(c)	(d)	(e)	(e)	(f)	(e)	(f)	(e)	(f)		(g)	(f)	(g)	(f)	(g)	(f)
LOM11-12: Secondary Volcanic Sandstone Cont.																				
z5	0.405	0.0748	92.78%	4	0.48	254	0.127	0.048942	3.928	0.193047	4.175	0.028607	0.265	0.934	145.08	92.12	179.23	6.86	181.83	0.48
z8	0.397	2.7319	99.81%	156	0.42	9772	0.126	0.049697	0.120	0.198428	0.171	0.028958	0.071	0.819	180.86	2.80	183.79	0.29	184.02	0.13
LOM11-06a: Secondary Volcanic Sandstone																				
z1	0.260	0.7696	97.36%	10	1.72	697	0.083	0.049685	0.797	0.196433	0.861	0.028674	0.102	0.662	180.26	18.56	182.10	1.44	182.25	0.18
z2	0.359	0.4996	97.23%	10	1.17	663	0.114	0.049598	1.198	0.195072	1.282	0.028525	0.106	0.811	176.19	27.93	180.95	2.12	181.31	0.19
z3	0.407	0.2387	87.11%	2	2.91	143	0.128	0.049297	2.742	0.199073	2.913	0.029288	0.249	0.711	161.97	64.10	184.34	4.91	186.09	0.46
z4	0.558	0.2233	97.26%	11	0.52	669	0.177	0.049832	1.470	0.202148	1.572	0.029422	0.143	0.736	187.14	34.20	186.94	2.68	186.93	0.26
z6	2.208	0.0159	57.16%	1	0.98	43	0.723	0.051703	71.274	0.223403	72.464	0.031338	2.361	0.516	272.28	1633.52	204.74	134.36	198.92	4.62
z7	0.471	0.0911	90.45%	3	0.79	192	0.153	0.051293	5.609	0.213308	5.930	0.030161	0.395	0.826	254.02	128.95	196.32	10.59	191.56	0.75
LOM11-18: Secondary Volcanic Sandstone																				
z2	0.361	0.1471	83.82%	2	2.34	114	0.116	0.050109	4.100	0.195616	4.362	0.028313	0.334	0.797	200.04	95.20	181.41	7.25	179.98	0.59
z3	0.551	0.0812	94.99%	6	0.35	366	0.172	0.048762	2.734	0.191345	2.911	0.028460	0.207	0.866	136.39	64.22	177.78	4.75	180.90	0.37
LOM11-17: Secondary Volcanic Sandstone																				
z1	0.317	0.0225	77.16%	1	0.55	80	0.096	0.047157	20.908	0.185687	21.614	0.028558	0.982	0.730	57.21	498.43	172.94	34.37	181.52	1.76
z5	0.474	0.0788	83.51%	2	1.28	112	0.152	0.050019	7.687	0.194493	8.162	0.028201	0.507	0.941	195.88	178.60	180.46	13.49	179.28	0.90
DC11-04: Secondary Volcanic Sandstone																				
z2	0.549	0.2226	96.44%	8	0.68	515	0.172	0.049110	1.872	0.197621	1.997	0.029185	0.147	0.860	153.07	43.84	183.11	3.35	185.45	0.27
z3	0.426	0.0433	85.58%	2	0.60	127	0.131	0.047940	10.436	0.189706	10.901	0.028700	0.571	0.823	96.30	246.98	176.38	17.65	182.41	1.03
z4	0.561	0.0362	85.34%	2	0.51	125	0.171	0.047643	11.663	0.194253	12.114	0.029571	0.608	0.754	81.58	276.77	180.25	20.01	187.86	1.13
DC11-05: Secondary Volcanic Sandstone																				
z1	0.366	0.5095	98.17%	16	0.78	1001	0.117	0.049615	0.949	0.186110	1.019	0.027206	0.104	0.703	176.99	22.12	173.30	1.62	173.03	0.18
z2	0.472	0.2589	88.81%	2	2.68	165	0.149	0.049018	2.435	0.183569	2.595	0.027161	0.267	0.635	148.70	57.06	171.13	4.09	172.75	0.45

Table 2.2. CA-TIMS U-Pb Isotopic Data Cont.

							Radiogenic Isotope Ratios								Radiogenic Isotope Dates					
Grain (a)	Th/U (b)	$^{206}Pb^*$ x10^{-13} mol (c)	mol % $^{206}Pb^*$ (c)	Pb^*/Pbc (c)	Pbc (pg) (c)	$^{206}Pb/^{204}Pb$ (d)	$^{208}Pb/^{206}Pb$ (e)	$^{207}Pb/^{206}Pb$ (e)	% err (f)	$^{207}Pb/^{235}U$ (e)	% err (f)	$^{206}Pb/^{238}U$ (e)	% err (f)	corr. coef.	$^{207}Pb/^{206}Pb$ (g)	± (f)	$^{207}Pb/^{235}U$ (g)	± (f)	$^{206}Pb/^{238}U$ (g)	± (f)
DC11-05: Secondary Volcanic Sandstone Cont.																				
z3	0.596	4.0782	99.33%	46	2.26	2761	0.189	0.049417	0.174	0.185363	0.239	0.027205	0.115	0.726	167.67	4.07	172.66	0.38	173.03	0.20
z6	0.497	0.1089	93.09%	4	0.67	265	0.160	0.050702	3.647	0.210725	3.886	0.030143	0.268	0.902	227.32	84.25	194.16	6.87	191.44	0.50

Notes:

(a) z1, z2 etc. are labels for fractions composed of single zircon grains or fragments; all fractions annealed and chemically abraded after Mattinson (2005).

(b) Model Th/U ratio calculated from radiogenic $^{208}Pb/^{206}Pb$ ratio and $^{207}Pb/^{235}U$ age.

(c) Pb* and Pbc represent radiogenic and common Pb, respectively; mol % $^{206}Pb^*$ with respect to radiogenic, blank and initial common Pb.

(d) Measured ratio corrected for spike and fractionation only. Fractionation estimated at 0.15 +/- 0.03 %/atomic mass unit for Daly analyses, based on analysis of NBS-981 and NBS-982.

(e) Corrected for fractionation, spike, and common Pb; up to 1 pg of common Pb was assumed to be procedural blank: $^{206}Pb/^{204}Pb = 18.35 \pm 1.5\%$; $^{207}Pb/^{204}Pb = 15.60 \pm 0.5\%$; $^{208}Pb/^{204}$ Pb = 38.08 ± 1.0% (all uncertainties 1-sigma).

Excess over blank was assigned to initial common Pb, using the Stacey and Kramers (1975) two-stage Pb isotope evolution model at the nominal sample age.

(f) Errors are 2-sigma, propagated using the algorithms of Schmitz and Schoene (2007).

(g) Calculations are based on the decay constants of Jaffey et al. (1971). $^{206}Pb/^{238}U$ and $^{207}Pb/^{206}Pb$ ages corrected for initial disequilibrium in $^{230}Th/^{238}U$ using Th/U [magma] = 3.

CHAPTER THREE: NEW HIGH PRECISION (CA-TIMS) U-Pb ZIRCON GEOCHRONOLOGY OF SOUTHERN INTRUSIVE ELEMENTS WITHIN THE BLUE MOUNTAINS PROVINCE, EAST-CENTRAL AND EASTERN OREGON

Introduction

The Blue Mountains province is composed of Paleozoic and Mesozoic accreted terranes exposed in eastern Oregon, west-central Idaho, and southeastern Washington (Vallier et al., 1977; Hamilton, 1978; Brooks and Vallier, 1978; Brooks, 1979; Dickinson, 1977, 1979; Coney et al., 1980; Silberling et al., 1984; Vallier, 1995; Avé Lallemant, 1995; Dorsey and LaMaskin, 2007; Schwartz et al. 2010, 2011a,b). Uplift of the area and erosion by the Snake River and its tributaries have exposed the Paleozoic and Mesozoic rocks in an erosional window through extensive overlying Cenozoic volcanic and sedimentary deposits. The exposure of these pre-Cenozoic terranes has allowed for further investigation into the evolutional history of the North American Cordillera.

The Blue Mountains are divided into three tectonic elements (Figure 3.1): from northwest to southeast, the intra-oceanic Wallowa arc terrane, the Baker terrane accretionary complex, and the continental fringing Olds Ferry arc terrane (Vallier et al., 1977; Hamilton, 1978; Brooks and Vallier, 1978; Brooks, 1979; Dickinson, 1977, 1979; Coney et al., 1980; Silberling et al., 1984; Vallier, 1995; Avé Lallemant, 1995; Dorsey

and LaMaskin, 2007). The Izee basin is a Jurassic forearc onlap sequence that has been deposited onto the Baker and Olds Ferry terrane.

Throughout the Blue Mountains province, intrusive igneous rocks of varying ages are exposed. Earliest arc magmatism is evidenced by a suite of Permian – Triassic plutons exposed in the Wallowa and Olds Ferry terranes (Brooks and Vallier, 1979; Vallier, 1995; Kurz et al., 2008; Kurz, 2010; Tumpane, 2010). A Middle Jurassic to Early Cretaceous pulse of magmatism emplaced an abundance of plutons into the terranes of the Blue Mountains province after the cessation of volcanism in both the Wallowa and Olds Ferry volcanic arcs and before the intrusive episodes that created the Idaho Batholith in the Late Cretaceous (Walker, 1986, 1989, 1995; Johnson and Barnes, 2002; Johnson et al., 2007; Unruh et al., 2008; Johnson and Schwartz, 2009; Schwartz and Johnson, 2009; Schwartz et al., 2011a,b).

Many field petrologic, and geochemical studies (Taubeneck, 1957, 1995; Hamilton, 1963, 1969; Vallier, 1995; Johnson et al., 2007; Parker et al. 2008; Schwartz and Johnson, 2009; Schwartz et al., 2011a) of this Middle Jurassic to Early Cretaceous plutonism within the Blue Mountains province have documented the type of rocks intruded and the relationships of different groups of intrusions, but the timing of intrusions is only weakly constrained. Early radiometric dating of the intrusive elements within the Blue Mountains province utilized K-Ar and $^{40}Ar/^{39}Ar$ analyses (Armstrong et al., 1977), or multi-crystal isotope dilution thermal ionization mass spectrometry (ID-TIMS) U/Pb zircon geochronology (Walker, 1986, 1989, 1995). Most recent single crystal U-Pb zircon geochronology using a sensitive high resolution ion microprobe (SHRIMP) has focused on the high abundant plutons intruded into the Baker and

Wallowa terranes (Johnson and Barnes, 2002; Johnson et al., 2007; Unruh et al., 2008; Kurz et al., 2008; Johnson and Schwartz, 2009; Schwartz and Johnson, 2009; Kurz, 2010; Tumpane, 2010; Schwartz et al., 2011a,b), leaving studies of the southern plutons intruded into the Izee basin and Baker terrane largely lacking.

In this study, four plutons from the southern region of the Blue Mountains province were analyzed to determine crystallization and emplacement age. Plutonic samples for this study were collected on the bases of their geographic relationship to the Weatherby Formation and previous studies of the intrusive igneous rocks of the Blue Mountains province. New chemical abrasion thermal ionization mass spectrometry (CA-TIMS) U-Pb zircon geochronology for plutonic rocks of the southern Blue Mountains province have added greater precision to the few existing emplacement ages, and now show a resolvable younging of crystallization ages from the southwest to the northeast. The cessation of deposition within the Weatherby Formation and the intrusion of these southern plutons constrain the metamorphic and deformational history of the southern Blue Mountains province to within an interval of 44 million years. Movement along the Connor Creek fault can be constrained to occurring within this 44 million year time window, as evidenced by the stitching nature of the Lookout Mountain pluton. The new high precision U-Pb geochronology of these plutons adjusts the age of the final pulse of Early Cretaceous magmatism in the Blue Mountains, as well as estimates for accretion of the Blue Mountains province to the North American margin.

Geologic Setting

The variably deformed and metamorphosed sedimentary, volcaniclastic, and volcanic rocks of the Blue Mountains province are intruded by a number of gabbroic to

granodioritic plutons. Plutonism within the Blue Mountains province represents a dynamic magmatic history from the late Permian to the Early Cretaceous (Armstrong et al., 1977; Walker, 1986; Vallier, 1995; Dickinson, 2004). The Wallowa terrane contains arc-related plutonic rocks of primarily tholeiitic to calc-alkaline affinities emplaced during two pulses of magmatism in the late Permian – Early Triassic and in the Late Triassic (Vallier, 1995; Kurz, 2010). Pluton emplacement within the Olds Ferry terrane occurred during at least two pulses, one at the Middle-Late Triassic boundary and another in the late *Norian* (late Triassic) (Tumpane, 2010; Kurz et al., 2008). The Baker terrane also includes a number of Paleozoic to early Mesozoic igneous bodies as part of the complexly deformed mélange. During the late Mesozoic, large volumes of evolved granodiorite to granitic rocks were emplaced into the Blue Mountains province and throughout the western margin of North America (Armstrong et al., 1977).

Reinitiation of magmatism in the Middle Jurassic to Early of Cretaceous, after the conclusion of the Wallowa and Olds Ferry arc volcanism, is recorded throughout the Blue Mountains. These Jurassic-Cretaceous plutons are chemically different than those intruded during late Permian to Triassic arc volcanism of the Wallowa and Olds Ferry terranes, displaying a higher concentration of potassium and other large-ion-lithophile elements, as well as enriched rare earth element patterns particularly in the light rare earth elements (Walker, 1986). This Middle Jurassic to Early Cretaceous magmatism can be separated into three distinct pulses from 162 to 154 Ma, 148 to 141 Ma, and 125 to 111 Ma (Walker, 1986, 1989, 1995; Johnson and Barnes, 2002; Johnson et al., 2007; Unruh et al., 2008; Johnson and Schwartz, 2009; Schwartz and Johnson, 2009; Schwartz et al., 2011 a & b).

The initial pulse is characterized by a northeast – southwest trend of late Middle to Late Jurassic plutons exposed in the Wallowa terrane, Bourne subterrane as localized stocks comprising the Bald Mountain Batholith, and the Greenhorn subterrane (Johnson et al., 2007; Parker et al., 2008; Unruh et al., 2008, Schwartz et al., 2011a). The southwestern-most plutons in this NE – SW belt across the Wallowa and Baker terranes indicate renewed magmatism in the Blue Mountains as early as ca. 162 Ma to as late as 154 Ma (Johnson et al., 2007; Parker et al., 2008; Johnson and Schwartz, 2009, Schwartz et al., 2011a). Intrusions in this group are characterized by magnesian, calc-alkalic, metaluminous plutons ranging from gabbro to quartz diorite. This suite of plutons have low Sr/Y values, LILE enrichment, negative Nb anomalies, and strongly positive epsilon Hf values, suggesting these plutons formed by hydrous partial melting of a depleted mantle peridotite or mafic-arc crust source (Schwartz et al., 2011a). Late Jurassic faulting and folding interpreted to signify collision of the Wallowa and Olds Ferry island arcs has caused propylitic alteration in this suite of plutonic rocks as well as in folded volcanogenic sedimentary rocks (Avé Lallemant, 1995; Schwartz et al., 2010, 2011a & b).

The next pulse of magmatism occurred after approximately a 6 million year lull in magmatism emplacing plutons of the Bald Mountain Batholith and the Wallowa Batholith as well as intrusive bodies into the Greenhorn subterrane (Schwartz et al., 2011a & b) (Figure 3.3). This pulse of dominantly tonalite and granodiorite magmatism emplaced into the pre-Cenozoic rocks of the Blue Mountains province from 148 to 141 Ma (Johnson and Schwartz, 2009; Schwartz and Johnson, 2009; Schwartz et al., 2011a). Voluminous low Sr/Y magmatism dominates the intrusions in the Baker and Wallowa

terranes, however a suite of plutons emplaced around the Dixie Butte area intruded between 148 – 145 Ma have high Sr/Y values. Schwartz et al. (2011a) suggest the temporal association and bimodal low and high Sr/Y values may have been caused by the closure of the Salmon River suture zone allowing for dehydration partial melting of the mantle wedge and mafic underplating beneath the Baker terrane. The Bald Mountain Batholith intrudes along the contact of the Baker and Wallowa terranes. Detailed mapping of the Bald Mountain Batholith was done by Taubeneck (1957, 1995), however the timing of magmatism was not well constrained during these studies. U-Pb geochronological analyses by Schwartz et al. (2011b) constrain the emplacement of the various plutons that construct the composite Bald Mountain Batholith to a first phase of intrusions from 157 to 154 Ma, falling within the first pulse of magmatism, and a second phase of intrusions from 147 to 140 Ma emplacing the core of the batholith, falling into the second pulse of magmatism. Plutons associated with the second pulse of magmatism are much less affected by greenschist metamorphism than the first pulse plutons are (Schwartz et al., 2011a). Anisotropy of magnetic susceptibility studies on plutons found within the Dixie Butte area and the Sunrise Butte area indicate a change in tectonic regime between the first and second pulses of magmatism (Žák et al., 2012).

The final stage of magmatism within the Blue Mountains province and prior to the intrusion of the Idaho Batholith occurred between approximately 125 to 111 Ma (Johnson and Schwartz, 2009). Plutonism of the last pulse of magmatism intruded in three regions: late elements of the Wallowa Batholith intruding ca. 125 Ma, with a satellite body intruding at 122 Ma (Johnson et al., 2011); a NE-SW trending belt of metaluminous hornblende-biotite tonalite plutons intruding into the Izee basin and across

the Izee-Olds Ferry-Baker terrane boundary between 124 – 120 Ma; and a third group of peraluminus tonalite and trondjhemite plutons intruding subparallel to the initial Sr isotopic 0.706 line in western Idaho at a minimum age of 118 Ma (Walker, 1986; Manduca et al. 1993; Schwartz et al., 2011b) (Figure 3.3). Early studies of these plutonic bodies described them as western outliers of the Idaho Batholith (Hamilton, 1978); however, the limited preexisting dating, done extensively by Richard Armstrong and William Taubeneck in the late 50's to late 70's, indicated a need for more complicated origins. The Salmon River Suture zone demarks the separation of Precambrian North American crust and the accreted terranes of the Blue Mountains province (Lund and Snee, 1988). The plutons emplaced in this region have been split into two groups; an epidote-bearing suite of intrusive rocks composed of orthogneiss, tonalite and trondjhemite (the Hazard Creek Complex), and a suite of interlayered dioritic to granitic orthogneisses with minor amounts of metamorphosed supracrustal rocks (Little Goose Creek Complex) (Manduca et al., 1993). Geochemistry from these rocks suggests an origin as arc margins formed over a subduction zone between, at minimum, 125 Ma to 90 Ma (Manduca et al., 1993; Lee, 2004; Snee et al., 2007; Schmidt et al., 2009).

Determining the time at which the Blue Mountains terranes accreted fully to the western margin of North America has also been difficult. These intrusive elements within the Blue Mountains province can help to constrain the timing of terrane amalgamation prior to accretion onto the ancient North American western boundary. Avé Lallemant et al. (1980) and Avé Lallemant (1983) suggest that the accretion of the amalgamated Blue Mountains terranes occurred during the Late Jurassic into the Early Cretaceous as evidenced by deformation within the terranes. Lund (1984) and Lund et al. (1985)

suggest the accretion of the Blue Mountains occurred in the Early Cretaceous along a right lateral transcurrent fault, displacing the oceanic and volcanic arc rocks northward. Walker (1986) interpreted the appearance of an abundance of plutonic bodies in the terranes of the Blue Mountains to indicate that the accretion of the oceanic and volcanic terranes onto the North American margin did not occur until after 120 Ma.

Recent studies of the Jurassic to Cretaceous intrusive igneous rocks of the Blue Mountains province have presented geochemical analyses to further constrain the accretion of the Blue Mountains province to the North American margin. Middle to Late Jurassic plutons within the Wallowa and Baker terranes have subduction-related trace element signatures, and match what is expected from derivation in an arc or back-arc setting (Johnson and Barnes, 2002; Johnson et al., 2007). By contrast, the Early Cretaceous plutonic bodies, such as the Wallowa Batholith and possibly the Bald Mountain Batholith, are interpreted as the result of partial melting of island arc terrane crust that has been overthickened from collision of the Blue Mountains terranes to the western North American margin (Johnson and Schwartz, 2009; Schwartz et al., 2011b). Getty et al. (1993) used petrologic observations and Sm-Nd dating of garnets to constrain the tectonic burial and heating at 128 ± 3 Ma, correlating metamorphism to the final suturing of the Blue Mountain terranes to the continental margin. These geochemical and petrological studies suggest the amalgamated Blue Mountains terranes accreted to the continent in the Early Cretaceous (Getty et al., 1993; Johnson and Barnes, 2002; Johnson and Schwartz, 2009; Johnson et al., 2007).

Field Observations and Sampling

Fieldwork was conducted during the spring, summer, and fall of 2011 and the spring and summer of 2012. U-Pb geochronological analyses and locations of collected samples can be found in Table 3.1 and 3.2. A detailed hand sample description, petrographic observation, and photomicrographs of the Lookout Mountain pluton, sample LOM10-01, can be found in Appendix A. Cathodoluminescence (CL) images of zircon grains analyzed are presented in Appendix B. Intrusive rocks will be described using typical International Union of Geological Sciences (IUGS) pluton rock classification terminology for rocks derived from magmatic sources such as granite, diorite, and granodiorite. Dr. Basil Tikoff and Dr. Richard Gaschnig provided samples for Pedro Mountain, Amelia, and Tureman Ranch plutons.

Intrusive Elements

Lookout Mountain road intersects exposures of the Lookout Mountain pluton north of Morgan Creek. Field relations of the Lookout Mountain pluton demonstrate the intrusion of the igneous body into the sediments of the Izee basin's Weatherby Formation, the Burnt River Schist and Nelson Marble of the Baker terrane, and across the Connor Creek fault (Figure 3.3). The Lookout Mountain pluton is a non-deformed, unmetamorphosed, tonalite. Finer grained mafic xenoliths or enclaves composed primarily of hornblende and plagioclase are present near the edges of the pluton. The Weatherby Formation has undergone greenschist metamorphism and deformation. Field observation and thin-section analyses of sample LOM10-01 from the Lookout Mountain pluton shows little evidence of metamorphism and deformation at the grain scale. The relatively unaltered nature of the Lookout Mountain pluton suggests the emplacement

occurred after the significant metamorphism and deformation of the Blue Mountains terranes. The cross-cutting relationships of the pluton with the Connor Creek fault makes the crystallization of this igneous body an important constraint on the timing of deformation along the fault. Granitic dikes intrude the Weatherby sediments that are interpreted as radiating dykes or feeder dykes of the Lookout Mountain Pluton. Aplite dikes ranging from a few centimeters to 20-30 cm, in diameter, are prevalent throughout the Lookout Mountain Pluton.

U-Pb Geochronology

We use the terms *inherited grains*, *antecryst*, *xenocryst*, and *autocryst* as defined by Miller et al. (2007) to describe the temporal differences, diverse origins, and relations between crystals and their host magmas. To review, an inherited zircon has been incorporated into a magma chamber or flow from the surrounding country rock. Inherited grains can be distinguished from the other crystals within the sample by usually being appreciably older. This happens quite often in the intrusion of plutons into country rock or during the flow of new eruptions over sedimentary or previously lain volcanic rocks due to the refractory nature of zircon. An autocryst is a zircon grain that is exclusively linked to one magma pulse or increment. In this study, these are the grains that are interpreted as the crystallization age for both intrusive and extrusive elements. Antecryst refers to those zircons that have crystallized in an earlier pulse of magma or within discrete reservoirs that have later been incorporated into a larger pulse of magma. These grains will be less temporally different than inherited grains, but may show distinctive age and chemical signatures compared to autocrystic grains used for the crystallization age of the magma body. Xenocrysts are essentially the same as inheritance, referring to a

zircon grain that has survived an episode or episodes of partial melting and is usually several million years older as to easily be distinguished as unrelated to the magma system. CL images are used in zircon-grain selection to mitigate the selection of xenocrystic and antecrystic grains. During CL image analyses, zircon grains with consistent textures, such as similar zoning patterns, and similar morphologies are identified for further analyses under the assumption that these dominant grains represent the autocrystic component.

Tureman Ranch Pluton

Sample 10RMG024 of granodiorite from the Tureman Ranch area is located furthest to the southwest of all the pluton samples collected. The Tureman Ranch pluton is non-deformed and intrudes entirely into Izee sediments about ten kilometers southwest of Ironside, Oregon. Nine single zircon crystals selected on the basis of CL patterns return equivalent $^{206}Pb/^{238}U$ dates with a weighted mean $^{206}Pb/^{238}U$ age of 129.40 ± 0.04 Ma (Table 3.1; Figure 3.2). The grains are interpreted as autocrystic zircons dating the igneous crystallization of the pluton. The lack of any older ages can be attributed to the efficiency of grain selection by the use of cathodoluminescence images to avoid inherited grains, the mitigation of Pb loss through the method of chemical abrasion, or because of a lack of antecrystic or xenocrystic grains within the pluton.

Amelia Pluton

Sample 10RMG030 collected about 4 km east of Malheur city, Oregon intrudes into Paleozoic to Triassic plutonic rocks of the Baker terrane yielding concordant U-Pb dates ranging from 125.01 ± 0.367 Ma to 126.02 ± 0.106 Ma (Table 3.2; Figure 3.2).

Seven of the eight zircons analyzed yield equivalent $^{206}Pb/^{238}U$ dates and a weighted mean $^{206}Pb/^{238}U$ age of 125.59 ± 0.053 Ma (Table 3.1). These grains have been interpreted as autocrysts and thus dating the igneous crystallization of this pluton. The older grain returned a $^{206}Pb/^{238}U$ age of 126.02 ± 0.106 Ma and was just outside of error to be included into the weighted mean calculation. This grain was interpreted as an antecryst that crystallized in a slightly earlier pulse of magma or primary reservoir at 126 Ma and then incorporated into the magma during injection.

Pedro Mountain Pluton

The Pedro Mountain pluton intrudes sediments of both the Baker terrane and Izee basin stitching the Connor Creek fault. Seven zircon grains of sample 10RMG032, collected about twenty kilometers west of Dixie, Oregon, were analyzed and yielded concordant U-Pb dates ranging from 124.82 ± 0.10 Ma to 125.95 ± 0.27 Ma (Table 3.2). The sample had 6 of 7 zircons with equivalent $^{206}Pb/^{238}U$ dates and a weighted mean $^{206}Pb/^{238}U$ age of 124.91 ± 0.056 Ma (Table 3.1; Figure 3.2); these are interpreted as autocrysts and the igneous crystallization age of the pluton; the one outlier that was not included in the weighted mean calculation yielded a $^{206}Pb/^{238}U$ date of 126.07 ± 0.18 Ma. The million-year difference suggests that this older grain is most likely an antecryst that crystallized in an earlier pulse of magma and was later entrained into the magma during intrusion.

Lookout Mountain Pluton

The Lookout Mountain pluton is the most northeastern pluton, and crosscuts the Connor Creek fault, intruding both the Burnt River Schist and the Weatherby Formation.

Eight zircon crystals selected from the tonalite sample LOM10-01 from the Big Lookout Mountain area yielded equivalent $^{206}Pb/^{238}U$ dates with a weighted mean $^{206}Pb/^{238}U$ age of 123.84 ± 0.042 Ma (Table 3.1; Figure 3.2). The results are interpreted all as autocrysts and the igneous crystallization age of the pluton. There were no older age zircons from this sample.

Discussion

Intrusive History of the Southern Blue Mountains Province

New high precision U-Pb zircon ages of plutons from the southern portion of the Blue Mountains province tightly constrain magmatism to between 129.4 and 123.8 Ma, and reveal resolvable differences in the pluton crystallization ages evident from the southwest to the northeast (Figure 3.3). Our results for the Pedro Mountain pluton differ from those presented by Walker (1986), suggesting a crystallization age about five million years older than previously recognized. The analyses of non-abraded bulk fractions of zircons by Walker (1986) would be prone to Pb-loss, which can explain the differences between studies. This reanalysis of the southern plutons indicate the last pulse in magmatism lasted longer and began earlier than the initial 124 to 120 Ma estimation of magmatism.

With the increase in precision and accuracy of the CA-TIMS U-Pb ages of this study, the differences in the crystallization ages between each pluton can now be resolved. The Tureman Ranch, Amelia, Pedro Mountain, and Lookout Mountain plutons were intruded along a southwest to northeast trend younging from the Tureman Ranch pluton in the southwest (129.40 ± 0.04 Ma) to the Lookout Mountain pluton in the

northeast (123.84 ± 0.04 Ma) (Figure 3.2). The rate of migration of plutonism for this middle Early Cretaceous pulse remained relatively constant. These four plutons represent a line of the southwestern most intrusions within the final pre-Idaho Batholith pulse of magmatism.

Intrusions to the northwest of the four plutons sampled for this study represent further extensions to the final pulse of Late Jurassic to Early Cretaceous plutonism. The Wallowa Batholith contains at least one pluton in the main collection of intrusions and a satellite body emplaced at 125 Ma and 122 Ma, respectively (Johnson et al., 2011). Similarities in the compositional characteristics (metaluminous to peraluminous tonalities and trondjhemites) suggest these intrusions are related to the NE-SW trending plutons located in the southern Blue Mountains. The possibly last plutons emplaced in this final pulse are represented by rocks along, and to the west of, the Salmon River Suture zone. Plutons of the Salmon River suture zone, specifically the ca.118 ± 5 Ma tonalite intrusives of the Hazard Creek complex, are temporally related and compositionally related, in part, to the pulse of plutonism in the southern Blue Mountains province. Tonalite and trondjhemite compose most of the Hazard Creek complex and is much less deformed than the older orthogneisses. Manduca et al. (1993) reports a 118 Ma age for the Hazard Creek complex; this is most likely a minimum age due to Pb-loss. The Hazard Creek complex in the past has been considered as related to the Salmon River suture zone or western extents of the Idaho Batholith. A new perspective is offered here due to the striking similarities in rock type, deformation state, and minimum age of the Hazard Creek complex with the plutons exposed in the southern Blue Mountains; therefore, this study considers the Hazard Creek complex as representing the youngest extents of the

final pre-Idaho Batholith stage of Early Cretaceous magmatism. The Little Goose Creek complex is compositionally different and geochronological younger than the NE-SW trend of middle Early Cretaceous tonalite and trondjhemite plutons and thus considered part of the Salmon River suture zone magmatics.

The final pulse began at 129.4 Ma in the southwest, emplacing the plutons in the southern Blue Mountains province, emplacing at least two plutons at 125 and 122 Ma in the Wallowa Batholith, and ending with late Early Cretaceous intrusions of the ca. 118 Ma Hazard Creek complex. This shifts the previous interpreted final pulse of pluton emplacement from 124 – 111 Ma to 129 – 118 Ma.

Geochemical analyses of plutons from the first pulse of magmatism contain low Sr/Y values, which suggest derivation from partial melting of shallow mafic arc crust and/or depleted mantle and emplacement into relatively thin arc crust (Schwartz et al., 2011a). Geochemical studies from the second pulse of magmatism indicate intrusions containing high and low Sr/Y values, suggesting bimodal tectonic environments. The compositionally restricted (tonalite-trondjhemite-granodiorite) high Sr/Y plutons most likely intruded thickened crust after the collision of the Wallowa and Olds Ferry terranes (Schwartz et al., 2011a). Compositional similarities of these high Sr/Y plutons from the second pulse of magmatism with plutons from this study could suggest these plutons are most likely derived from thickened crust caused by the accretion of the Blue Mountains province to the North American margin. High Sr and low Y values have been found in the Hazard Creek Complex of the Salmon River suture zone (Table 3, Manduca et al., 1993; Schwartz et al., 2011a). This study proposes igneous rocks from the Hazard Creek Complex are part of the finale pulse of pre-Idaho Batholith magmatism further suggesting

formation of these southern Blue Mountains plutons could be a result of thickened crust. Determination of exact formation factors for these four southern plutons in the Blue Mountains province is difficult to discern solely from the present data set of high precision U-Pb geochronology done on single zircon grains. Geochemical analysis of these plutons is needed for further interpretations on derivation environments for the suite of southern plutons of the Blue Mountains province.

The pulse in magmatism in the mid to late Early Cretaceous could be due to subduction of oceanic crust to the west-northwest of the orogenic thickened Blue Mountains province (Hamilton, 1978). After the accretion to continental North America the subduction zone jumped westward outside of the amalgamated Blue Mountains. The differences in crystallization ages in the southern Blue Mountains plutons display a constant rate of arc magma migration from the southwest to the northeast. These plutons, emplaced between 129 and 118 Ma, lie along a north-south trend when approximately 50-60° of Eocene rotation of the Blue Mountains province is back rotated (Figure 3.4) (Wilson and Cox, 1980; Heller et al., 1987; Dickinson, 2002, 2004). Along arc magma migration has been documented in many arc complexes around the world: such as Southwest Japan, South America along the Peruvian margin, Eastern Asia, Northwest Mexico, and Turkey; to name a few (Kinoshita, 1999; Valencia-Moreno et al., 2004; Cengiz Cinku et al., 2010; Choi et al., 2011; Boekhout et al., 2012). Magma migration has been shown to occur due to the subduction of spreading centers (Kinoshita, 1999) or dip changes of the subducting slab (Valencia-Moreno et al., 2004; Cengiz Cinku et al., 2010; Choi et al., 2011).

Lomize and Luchitskaya (2012), in studying the subduction of the contemporary Chile Ridge, suggests the subduction of a spreading ridge displays characteristic complexes and structures as well as varying compositions in proximal and distal magmatism. Late Mesozoic subduction of the Pacific plate beneath Japan resulted in a Cordilleran-type orogen (Nakajima, 1992; Kinoshita, 1999). Nakajima (1992) and Kinoshita (1999) suggest increased magmatism and magmatic migration in this area are due to the subduction of a spreading center. If this process can relate to the Early Cretaceous magmatism in the Blue Mountains province, then a compositional difference would be expected along trend due to changes in magma generation characteristics as the slab window subducts (Lomize and Luchitskaya, 2012). This is probably not the case in the Blue Mountains province due to the similarity in pluton compositions throughout the 129 – 118 Ma NE-SW suite.

If the subduction zone in the Early Cretaceous is more to the northwest rather than west of the Blue Mountains province, then a simple steepening of the subduction zone could explain the south to north migration of arc magmatism. A progression of shallower to steeper slap dips from 129 – 118 Ma would cause distance differences between the trench and the Benioff zone, causing a migration of arc magmatism. This would result in older plutons located closer to the continent side (to the south in the case of the Blue Mountains) and younger plutons located closer to the oceanic side (more north in the Blue Mountains). This type of migration has been documented in Late Cretaceous plutons in NW Mexico (Valencia-Moreno et al., 2004).

Constraints on Terrane Amalgamation and Accretion to North America

The Lookout Mountain pluton crosscuts the Connor Creek fault, indicating that the movement along the fault plane was complete before the intrusion of the Lookout Mountain pluton at 124 Ma. New U-Pb geochronology of the Weatherby Formation, as well as on a suite of related plutons trending in a line to the southwest of Lookout Mountain pluton, can place tighter constraints on deformation along the Connor Creek fault as well as terrane amalgamation and accretion to the western North American margin.

The minimum age of deformation in the southern Blue Mountains province can be constrained by metamorphic fabric comparisons between the Late Jurassic to Early Cretaceous plutons and the surrounding country rock as well as the crosscutting nature of various intrusions. The southern margin of the Baker terrane is comprised of the Burnt River Schist, a primarily quartzose phyllite with variable amounts of marble, greenstones, and metavolcanic and metavolcaniclastic rocks (Walker, 1995). Studying plutons that showed textural evidence of metamorphism and deformation as well as non-deformed and non-metamorphosed plutons in the southern-most region of the Burnt River Schist, Walker (1995) constrained the timing of deformation and metamorphism of the Burnt River Schist to a minimum age of 124 Ma. A new age constraint on the minimum age of deformation and metamorphism can now be placed at 129 Ma, evidenced by the similarities in geochemistry and the crystallization evolution of the NE-SW trending plutons intruding the Izee basin and Baker terrane.

Renewed magmatism within the Blue Mountains province coupled with new depositional and deformational evidence within the Izee basin can provide further

constraints on the timing of arc-arc collision (Figure 3.5). The lack of deformation in the 129 to 124 Ma plutons suggest that much of the deformation associated with contraction of the Blue Mountains terranes was complete by 129 Ma. Sedimentation within the Weatherby basin ceased ca. 168 Ma as a result of movement along the Connor Creek fault; resulting in basin-wide deformation as the Wallowa terrane began collision with the Olds Ferry terrane. The southern termination of the Wallowa terrane caused deposition to cease and deformation to occur within the eastern Izee sub-basin while allowing deposition to continue into the *Oxfordian* with no deformation in the western Izee sub-basin. Interpretations of Middle to Late Jurassic intrusions suggest the amalgamation of the Wallowa and Olds Ferry terranes was completed by 162 Ma (Schwartz and Johnson, 2009), which agrees well with the new data and interpretations made from the Weatherby Formation.

Much of the plutonism within the first pulse was localized primarily within the Greenhorn subterrane and western extents of the Wallowa terrane. The Greenhorn subterrane has been interpreted to be a subduction complex structural high on the western extents of an arc (Olds Ferry volcanic arc), forearc (Izee basin), and accretionary wedge (Baker oceanic mélange – Greenhorn subterrane) system (Dickinson and Thayer, 1978; Dickinson, 1979). The intrusion of geochemically and temporally related plutons within these two portions of the Blue Mountains province would indicate the evolutional history of the Wallowa and Olds Ferry arcs are related by 162 Ma. Dorsey and LaMaskin (2007) propose a model, suggesting the Wallowa and Olds Ferry terranes were linked by about 180 Ma (Tumpane, 2010) with a coeval evolution by the early Late Jurassic, prior to deposition within the Izee terrane. New U-Pb geochronology from the Weatherby

Formation, of the Izee basin, indicates deformation of the eastern Izee sub-basin occurred after the *Bajocian* ca. 168 Ma. The western Izee sub-basin remains relatively non-deformed, displaying continued deposition into the Oxfordian. This data coupled with 162 – 154 Ma intrusions suggest amalgamation of the Wallowa and Olds Ferry terranes occurred in the early Late Jurassic, much later than the estimated late Early Jurassic collision made by Dorsey and LaMaskin (2007).

The intrusion of these plutons signifies the movement of the trench to the west-northwest of the Blue Mountains province after the amalgamation of terranes was complete. Getty et al. (1993) correlated metamorphism history of garnets to the final suturing age of the Blue Mountains province to the North American margin at 128 ± 3 Ma. The final pulse of magmatism intruded into all terranes of the Blue Mountains province. The non-deformed nature of these intrusions suggests this suite of plutons was emplaced post amalgamation and deformation of the Blue Mountains province. Therefore, the final pulse of magmatism constrains the amalgamation of the Blue Mountains terranes to the North American margin. The oldest pluton emplaced into the Izee basin at 129.4 Ma indicates deformation within the Blue Mountains province was complete. The intrusion of the Pedro Mountains pluton by 129 Ma suggests the Blue Mountains province had accreted to the North American margin by that time, agreeing well with the interpretations made by Getty et al. (1993).

Conclusions

New high precision geochronology of the southernmost plutons within the Blue Mountains province constrains the deformation and metamorphism of the Izee basin and Baker terrane to less than 44 million years. This age can be pushed to a smaller interval

by the amount of younger sediment present above the stratigraphically youngest volcanic unit in the Weatherby Formation, the presence of *Bajocian*, *Callovian*, and *Oxfordian* fossils found in the western Izee sub-basin and not in the eastern Izee sub-basin, as well as the relatively non-deformed nature of plutons from the Late Jurassic to the Early Cretaceous.

Analysis of four Cretaceous plutons in the southern portion of the Blue Mountains province indicates a consistent younging of crystallization ages from the southwest to the northeast, 129.4 – 123.8 Ma. The western most pluton analyzed, Tureman Ranch pluton, indicates that by the early *Barremian* (Early Cretaceous), the North American arc shifted northwestward from the Blue Mountains province. This location change of the western North American subduction zone suggests that the amalgamation of the Blue Mountains had completed by this time. Further evidence that the Blue Mountains province was no longer a zone of terrane accretion during the Early Cretaceous is the intrusion of the Lookout Mountain pluton stitching the Connor Creek fault.

The high precision U-Pb results have also indicated a timeframe adjustment to the last pulse of Middle Jurassic – Early Cretaceous magmatism. The age range from the Tureman Ranch pluton to the Lookout Mountain Pluton progressively youngs from 129.4 to 123.8 Ma. This new data shifts the age of the final pulse from the previous interpretation of activity between 124 -120 Ma to 129.4 -123.8 Ma. With the addition of satellite stocks near the Wallowa Batholith and plutons along the Salmon River suture zone, the last pulse continued at minimum to 118 Ma. These new ages agree well with the interpretation from garnet growth (Getty et al., 1993) and geochemical signature

(Manduca et al. 1992; Schwartz et al., 2011a) of the plutons that the accretion of the Blue Mountains province occurred shortly before the intrusion of these plutonic bodies.

The stitching nature of the Lookout Mountain pluton and evidence suggesting these four plutons are from the same pulse of magmatism place constraints on the deformation along the Connor Creek fault. The youngest sediments within the Weatherby Formation indicate deposition continued into the Middle Jurassic (*Bajocian*) ca. 168 Ma. Sediments within the Weatherby Formation have adopted cleavage dip angles in accord to the dip of the Connor Creek fault, indicating movement along the fault occurred post deposition of the eastern Izee sub-basin. The initiation and crosscutting relations of some of the intrusive bodies constrain the movement of the Connor Creek fault between the Middle Jurassic (*Bajocian*) ca. 168 Ma and the Early Cretaceous (*Aptian*) 129.4 Ma. Although the early Late Jurassic pulse of magmatism does not cross-cut the Connor Creek fault, this intrusive episode has been interpreted as magmatism related to crustal thickening due to the amalgamation of the Wallowa and Olds Ferry terranes thus possibly constraining movement of the Connor Creek fault between ca. 168 Ma and 162 Ma.

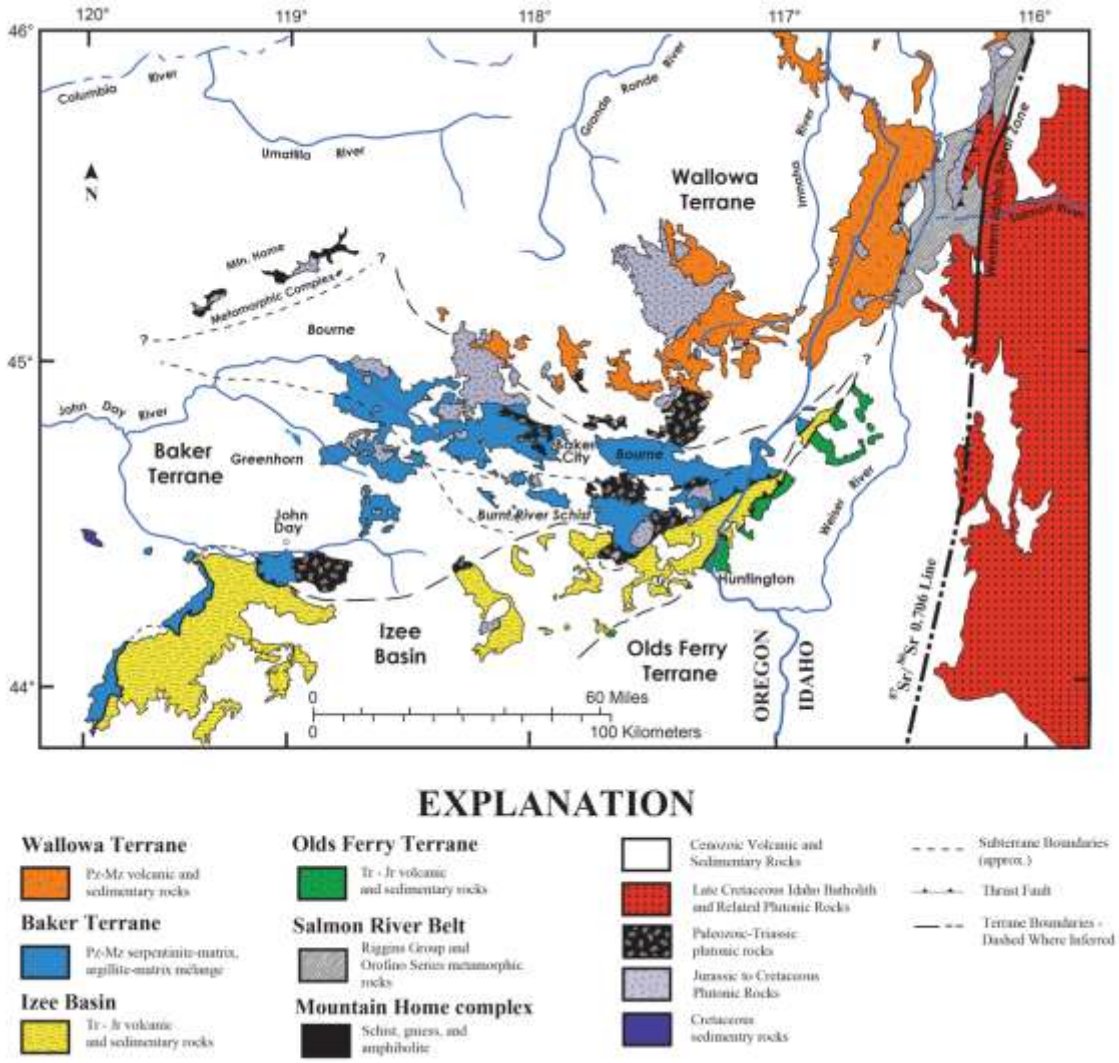

Figure 3.1: Geologic map of the Blue Mountains province showing the three tectonic terranes, the Izee forearc basin, and the Jurassic to Cretaceous intrusive elements. Modified from LaMaskin et al. (2011b) and Schwartz et al. (2011b).

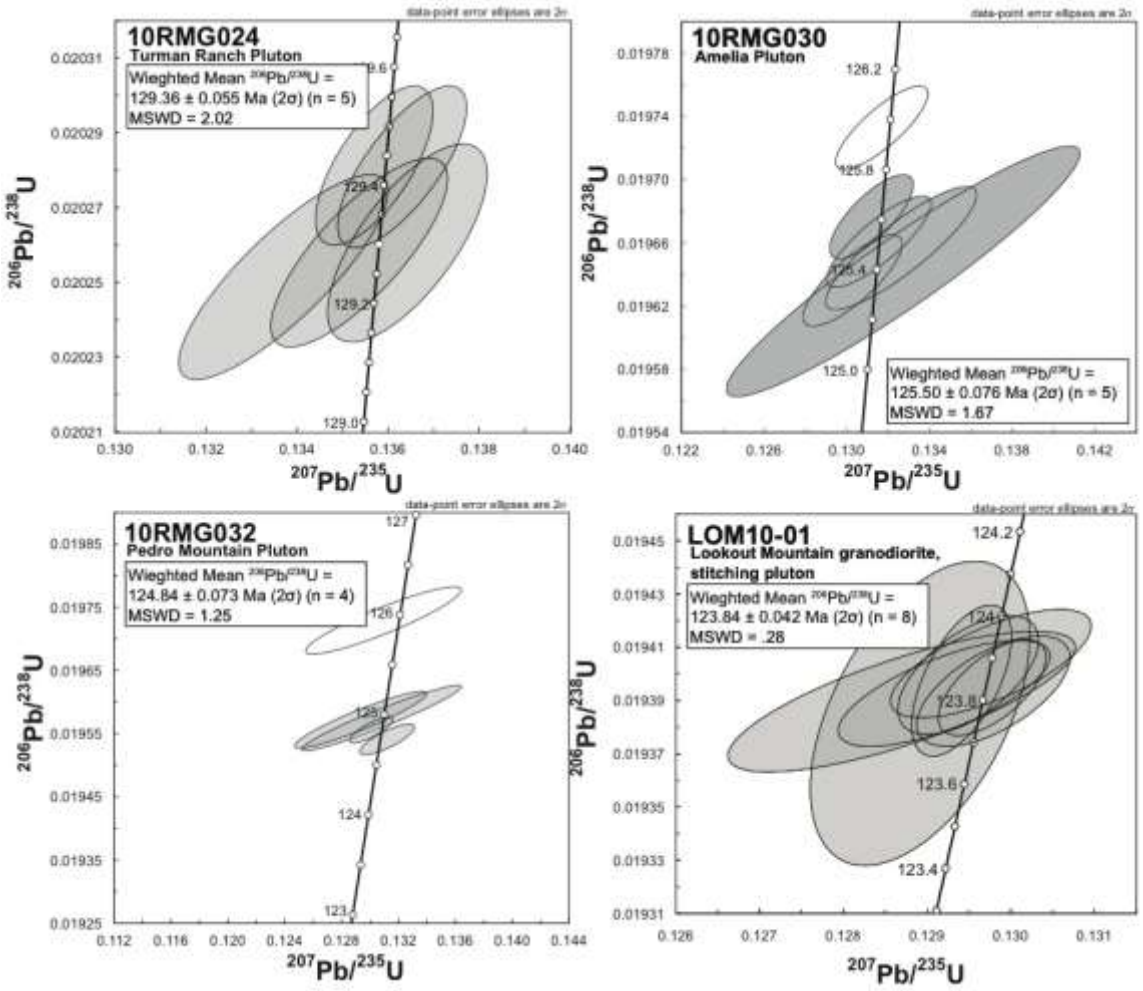

Figure 3.2: Concordia diagrams for all plutonic samples from the Blue Mountains province showing chemically abraded zircon single-grain analyses. Shaded ellipses denote analyses used in the weighted mean age calculations. Data point error ellipses are 2σ.

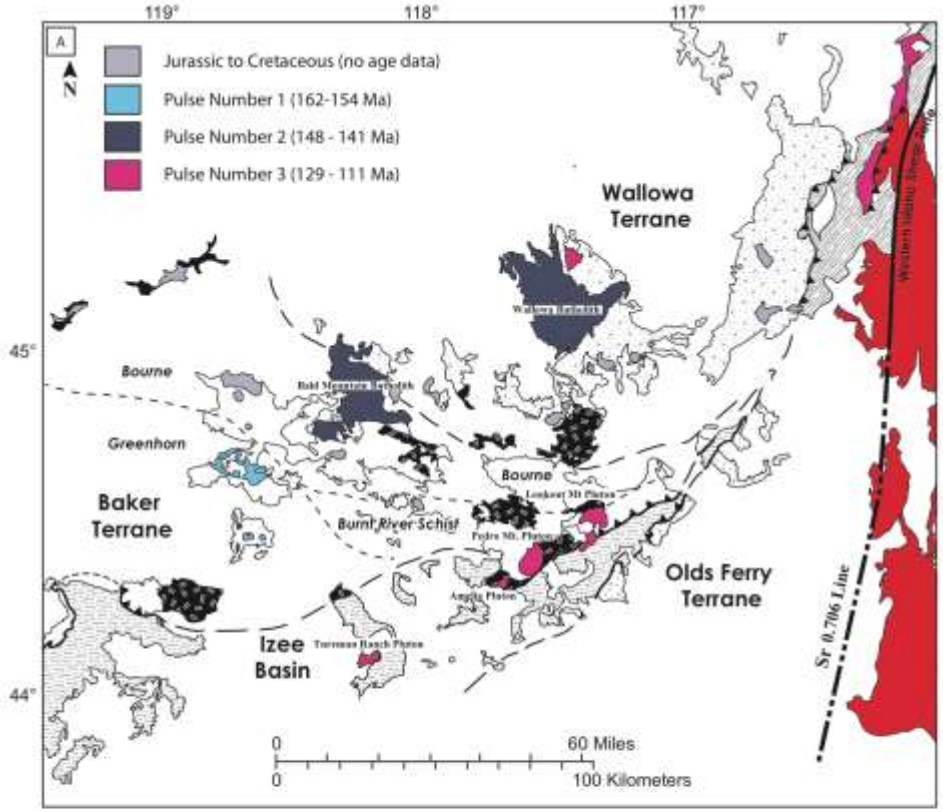

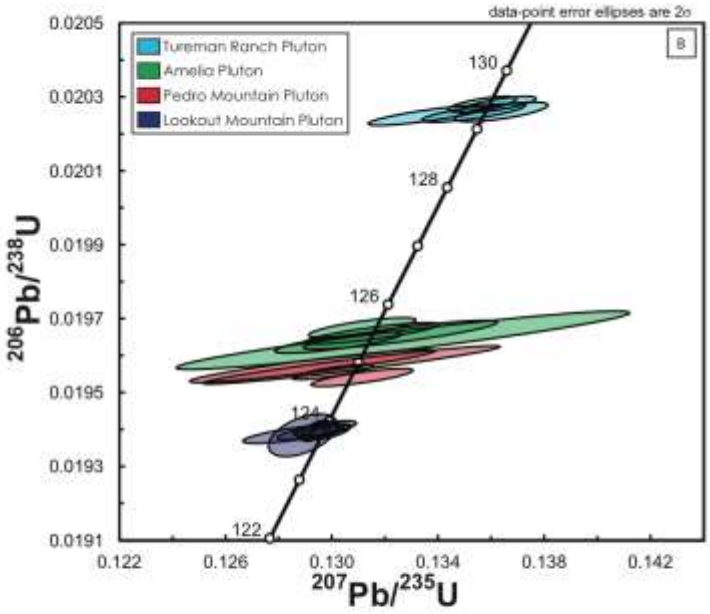

EXPLANATION

Wallowa Terrane
Pz-Mz volcanic and sedimentary rocks

Baker Terrane
Pz-Mz serpentinite-matrix, argillite-matrix mélange

Subterrane Boundaries (approx.)

Olds Ferry Terrane
Tr - Jr volcanic and sedimentary rocks

Izee Basin
Tr - Jr volcanic and sedimentary rocks

Terrane Boundaries - Dashed Where Inferred

Salmon River Belt
Riggins Group and Orofino Serie metamorphic rocks

Cenozoic Volcanic and Sedimentary Rocks

Mountain Home complex
Schist, gneiss, and amphibolite

Paleozoic-Triassic plutonic rocks

Jurassic to Cretaceous Plutonic Rocks

Late Jurassic Plutonic Rocks

Thrust Fault

Late Cretaceous Idaho Batholith and Related Plutonic Rocks

late Early Cretaceous Plutonic Rocks

Early Cretaceous Plutonic Rocks

Figure 3.3: (A) Terrane map of the Blue Mountains province showing the Wallowa, Baker, and Olds Ferry terranes, the Izee basin, and highlighting the Late Jurassic to Cretaceous plutons. Modified from LaMaskin et al. (2011b) and Schwartz et al. (2011b). (B) Concordia diagram of chemically abraded zircon single-grain analyses showing the progressively younger ages from west to east of the four plutons analyzed from the southern Blue Mountains province.

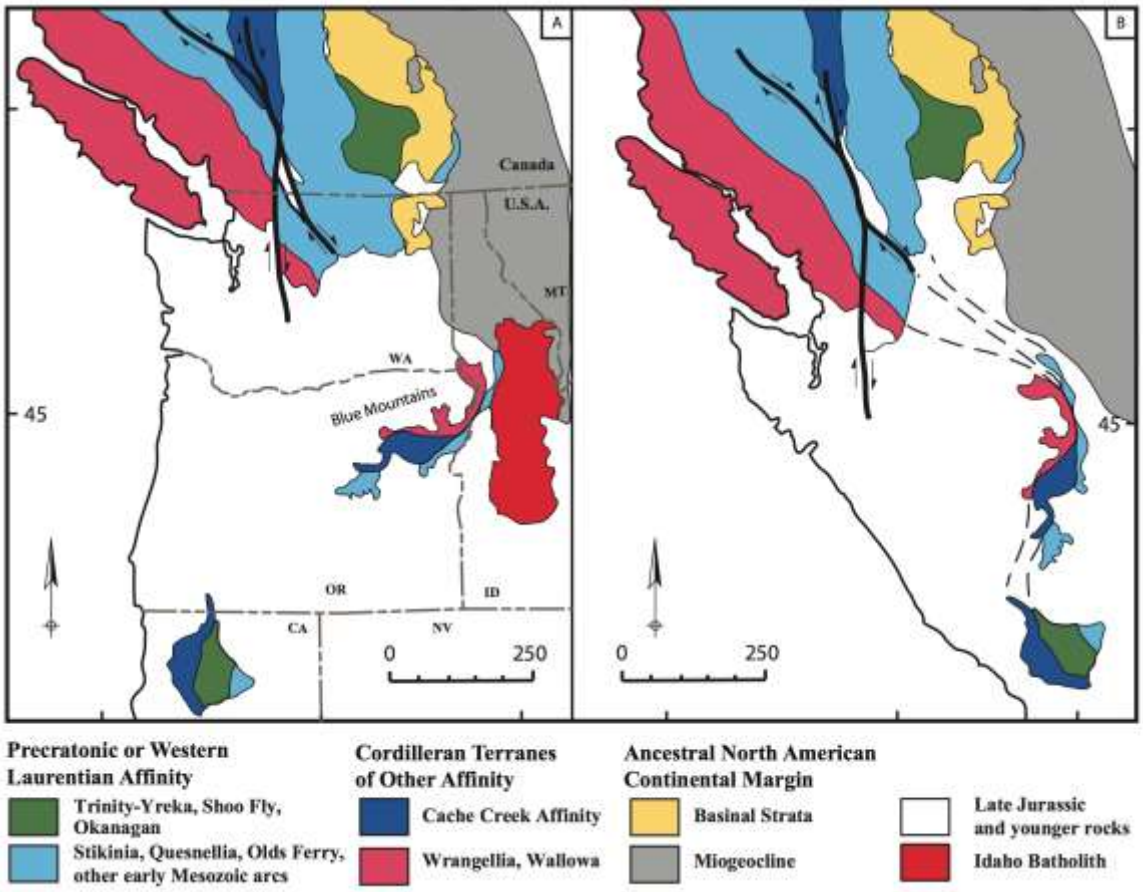

Figure 3.4: Pre-Oligocene geotectonic features in the Pacific Northwest (USA) and adjacent Canada at present (A) and as reconstructed before clockwise rotations of the Oregon-Washington Coast Range and Blue Mountains provinces, and before dextral slip on branching faults near the USA-Canada border (B). Modified from Dickinson (2004).

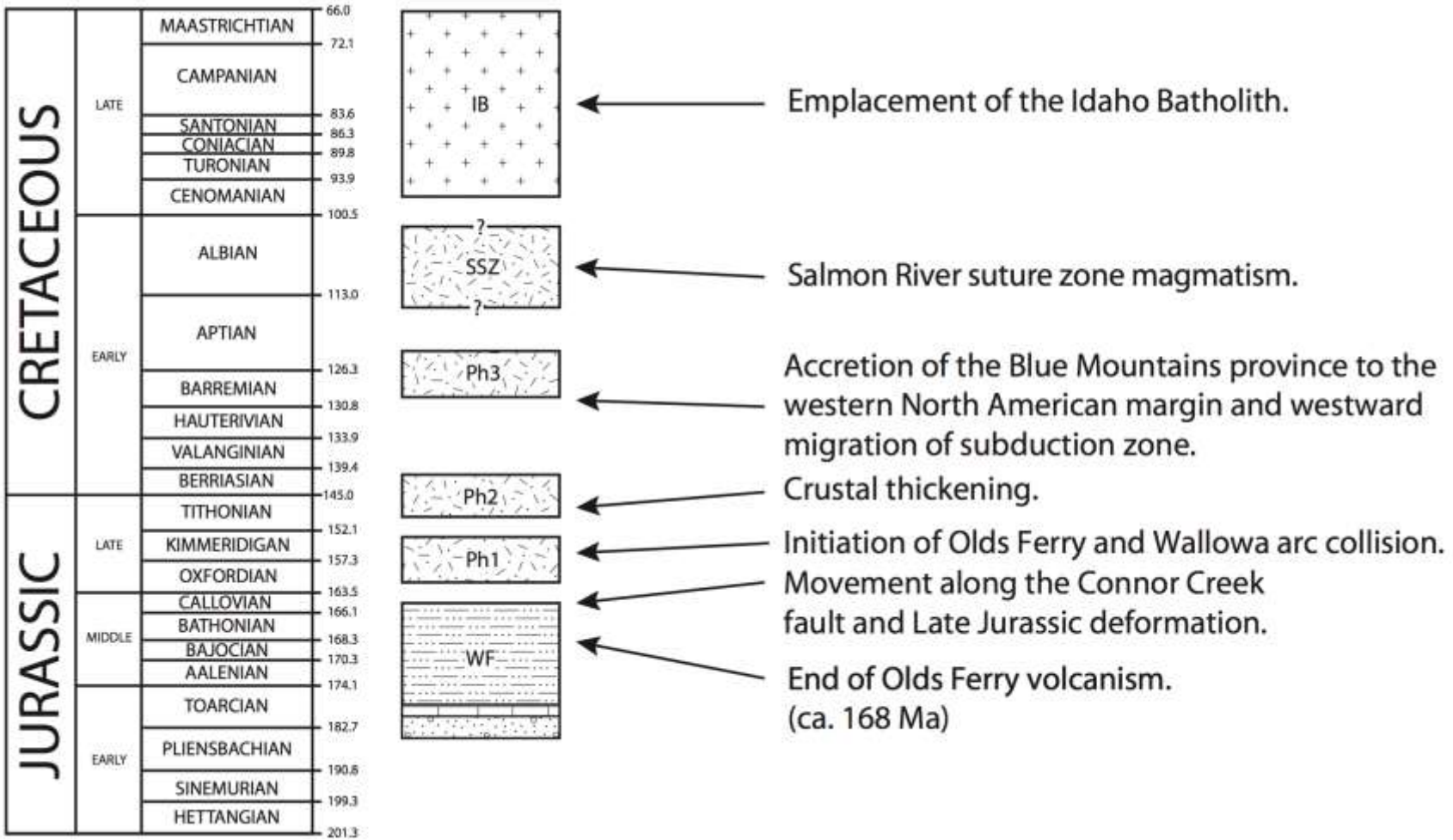

Figure 3.5: Timeline of Jurassic through Cretaceous magmatism in the Blue Mountains province, with tectonic interpretations on the right and emplacement and deposition ages on the left. Ph1 Ph2, Ph3 = Phase 1,2, and 3 reinitation of magmatism post Wallowa and Olds Ferry arc activity. SSZ - Salmon River suture zone, inferences form Manduca et al. (1993). Idaho Batholith emplacement ages inferred from Manduca et al. (1993), Gaschnig et al. (2011). Geologic Timescale 2012, Gradstein et al. (2012).

Table 3.1 Plutonic CA-TIMS U-Pb age summary

Sample	Location	UTM	Weighted mean $^{206}Pb/^{238}U$ age	± X (Y) [Z] (2σ)	MSWD	N
10RMG024	Tureman Ranch	11T0409590, 4896041	129.40	± 0.04 (0.08) [0.16]	1.45	9 of 9
10RMG030	Amelia	11T0448044, 4916603	125.59	± 0.053 (0.08) [0.16]	1.07	7 of 8
10RMG032	Pedro Mountain	11T0457691, 4920480	124.91	± 0.056 (0.08) [0.16]	1.74	6 of 7
LOM10-01	Lookout Mountain	11T0477260, 4929998	123.86	± 0.042 (0.13) [0.19]	0.26	8 of 8

Table 3.2 Plutonic U-Pb Isotopic Data

								Radiogenic Isotope Ratios								Radiogenic Isotope Dates					
Grain	Th/U	$^{206}Pb^*$ x10^{-13} mol	mol % $^{206}Pb^*$	Pb^*/Pbc	Pbc (pg)	$^{206}Pb/^{204}Pb$	$^{208}Pb/^{206}Pb$	$^{207}Pb/^{206}Pb$	% err	$^{207}Pb/^{235}U$	% err	$^{206}Pb/^{238}U$	% err	corr. coef.	$^{207}Pb/^{206}Pb$	±	$^{207}Pb/^{235}U$	±	$^{206}Pb/^{238}U$	±
(a)	(b)	(c)	(c)	(c)	(c)	(d)	(e)	(e)	(f)	(e)	(f)	(e)	(f)		(g)	(f)	(g)	(f)	(g)	(f)
10RMG024 Tureman Ranch Pluton																				
z3	**0.352**	**0.7021**	**98.50%**	**19**	**0.89**	**1203**	**0.112**	**0.048781**	**0.370**	**0.136444**	**0.421**	**0.020286**	**0.076**	**0.722**	**137.32**	**8.68**	**129.87**	**0.51**	**129.465**	**0.098**
z4	**0.328**	**0.7358**	**92.71%**	**4**	**4.80**	**247**	**0.105**	**0.048624**	**1.680**	**0.135899**	**1.800**	**0.020271**	**0.141**	**0.864**	**129.73**	**39.50**	**129.38**	**2.19**	**129.365**	**0.180**
z5	**0.425**	**1.7125**	**98.92%**	**27**	**1.56**	**1663**	**0.136**	**0.048590**	**0.269**	**0.135893**	**0.314**	**0.020284**	**0.074**	**0.693**	**128.09**	**6.32**	**129.38**	**0.38**	**129.449**	**0.094**
z7	**0.334**	**0.4110**	**90.57%**	**3**	**3.55**	**191**	**0.107**	**0.048839**	**2.219**	**0.136534**	**2.374**	**0.020275**	**0.177**	**0.881**	**140.11**	**52.09**	**129.95**	**2.90**	**129.397**	**0.227**
z8	**0.293**	**0.1279**	**96.36%**	**8**	**0.40**	**495**	**0.094**	**0.047978**	**1.076**	**0.134013**	**1.162**	**0.020258**	**0.119**	**0.750**	**98.18**	**25.44**	**127.70**	**1.39**	**129.288**	**0.152**
z9	**0.321**	**0.3345**	**98.72%**	**22**	**0.36**	**1407**	**0.103**	**0.048555**	**0.404**	**0.135809**	**0.450**	**0.020286**	**0.078**	**0.645**	**126.40**	**9.51**	**129.30**	**0.55**	**129.462**	**0.100**
z10	**0.316**	**0.6823**	**96.81%**	**9**	**1.86**	**566**	**0.101**	**0.048928**	**0.799**	**0.136779**	**0.865**	**0.020275**	**0.100**	**0.692**	**144.40**	**18.74**	**130.17**	**1.06**	**129.39**	**0.13**
z11	**0.309**	**0.4104**	**98.01%**	**14**	**0.69**	**906**	**0.099**	**0.048512**	**0.570**	**0.135550**	**0.627**	**0.020265**	**0.085**	**0.706**	**124.32**	**13.41**	**129.07**	**0.76**	**129.33**	**0.11**
z12	**0.342**	**0.1372**	**97.80%**	**13**	**0.26**	**819**	**0.109**	**0.047935**	**0.784**	**0.133900**	**0.851**	**0.020259**	**0.091**	**0.761**	**96.09**	**18.55**	**127.60**	**1.02**	**129.29**	**0.12**
10RMG030 Amelia Pluton																				
z1	0.273	0.4801	97.53%	11	1.01	730	0.087	0.048458	0.610	0.131902	0.666	0.019742	0.085	0.702	121.70	14.36	125.80	0.79	126.022	0.106
z2	**0.267**	**0.0884**	**91.45%**	**3**	**0.69**	**211**	**0.085**	**0.049243**	**2.512**	**0.133577**	**2.678**	**0.019674**	**0.203**	**0.828**	**159.44**	**58.75**	**127.31**	**3.20**	**125.592**	**0.253**
z4	**0.276**	**0.3300**	**80.24%**	**1**	**6.74**	**92**	**0.088**	**0.048479**	**3.959**	**0.130886**	**4.221**	**0.019581**	**0.296**	**0.892**	**122.72**	**93.23**	**124.89**	**4.96**	**125.008**	**0.367**
z5	**0.263**	**0.2543**	**96.01%**	**7**	**0.88**	**452**	**0.084**	**0.048354**	**0.932**	**0.131233**	**1.007**	**0.019684**	**0.100**	**0.772**	**116.65**	**21.97**	**125.21**	**1.19**	**125.656**	**0.124**
z6	**0.268**	**0.2374**	**88.42%**	**2**	**2.58**	**156**	**0.086**	**0.048358**	**2.844**	**0.131028**	**3.037**	**0.019651**	**0.233**	**0.840**	**116.84**	**67.03**	**125.02**	**3.57**	**125.452**	**0.290**
z7	**0.258**	**0.1536**	**82.15%**	**1**	**2.77**	**101**	**0.083**	**0.048151**	**4.745**	**0.130112**	**5.054**	**0.019598**	**0.346**	**0.901**	**106.71**	**112.06**	**124.20**	**5.91**	**125.114**	**0.428**
z9	**0.263**	**0.5028**	**97.91%**	**13**	**0.89**	**863**	**0.084**	**0.048401**	**0.640**	**0.131362**	**0.699**	**0.019684**	**0.093**	**0.666**	**118.93**	**15.09**	**125.32**	**0.82**	**125.658**	**0.116**
z10	**0.259**	**0.1779**	**97.54%**	**11**	**0.37**	**732**	**0.083**	**0.048174**	**0.776**	**0.130566**	**0.840**	**0.019657**	**0.097**	**0.697**	**107.83**	**18.32**	**124.61**	**0.99**	**125.49**	**0.12**
z11	**0.258**	**0.3609**	**97.26%**	**10**	**0.84**	**659**	**0.082**	**0.048589**	**0.698**	**0.131781**	**0.759**	**0.019670**	**0.091**	**0.708**	**128.05**	**16.41**	**125.70**	**0.90**	**125.57**	**0.11**
z12	**0.261**	**0.2485**	**96.13%**	**7**	**0.83**	**466**	**0.083**	**0.049029**	**1.036**	**0.132974**	**1.120**	**0.019670**	**0.117**	**0.741**	**149.22**	**24.27**	**126.77**	**1.33**	**125.57**	**0.15**
10RMG032 Pedro Mountain Pluton																				
z7	**0.230**	**0.3482**	**93.35%**	**4**	**2.06**	**271**	**0.073**	**0.048870**	**1.925**	**0.131938**	**2.049**	**0.019581**	**0.256**	**0.533**	**141.59**	**45.16**	**125.84**	**2.43**	**125.006**	**0.318**
z8	**0.246**	**0.0648**	**89.37%**	**2**	**0.64**	**170**	**0.079**	**0.048498**	**3.261**	**0.130991**	**3.439**	**0.019589**	**0.261**	**0.706**	**123.65**	**76.76**	**124.99**	**4.04**	**125.058**	**0.323**
z9	**0.246**	**0.1545**	**95.17%**	**6**	**0.65**	**374**	**0.078**	**0.048044**	**1.402**	**0.129736**	**1.500**	**0.019585**	**0.122**	**0.824**	**101.42**	**33.13**	**123.86**	**1.75**	**125.032**	**0.151**
z10	**0.229**	**0.1951**	**92.91%**	**4**	**1.24**	**254**	**0.073**	**0.048348**	**2.524**	**0.130534**	**2.682**	**0.019582**	**0.135**	**1.164**	**116.31**	**59.49**	**124.58**	**3.14**	**125.01**	**0.17**

Table 3.2 Plutonic U-Pb Isotopic Data Cont.

								Radiogenic Isotope Ratios								Radiogenic Isotope Dates					
	Th	^{206}Pb*	mol %	Pb*	Pbc	^{206}Pb	^{208}Pb	^{207}Pb		^{207}Pb		^{206}Pb		corr.	^{207}Pb		^{207}Pb		^{206}Pb	
Grain	U	x10^{-13} mol	^{206}Pb*	Pbc	(pg)	^{204}Pb	^{206}Pb	^{206}Pb	% err	^{235}U	% err	^{238}U	% err	coef.	^{206}Pb	±	^{235}U	±	^{238}U	±
(a)	(b)	(c)	(c)	(c)	(c)	(d)	(e)	(e)	(f)	(e)	(f)	(e)	(f)		(g)	(f)	(g)	(f)	(g)	(f)
10RMG032 Pedro Mountain Pluton																				
z11	**0.190**	**0.3831**	**97.91%**	**13**	**0.68**	**863**	**0.061**	**0.048733**	**0.538**	**0.131371**	**0.594**	**0.019551**	**0.082**	**0.709**	**134.98**	**12.65**	**125.33**	**0.70**	**124.82**	**0.10**
z12	**0.208**	**0.4541**	**98.45%**	**18**	**0.59**	**1166**	**0.066**	**0.048269**	**0.511**	**0.130191**	**0.567**	**0.019562**	**0.074**	**0.782**	**112.47**	**12.06**	**124.27**	**0.66**	**124.89**	**0.09**
z13	0.253	0.1404	94.34%	5	0.70	319	0.081	0.048275	1.600	0.131457	1.708	0.019750	0.144	0.765	112.78	37.75	125.41	2.02	126.07	0.18
LOM10-01 Lookout Mountain Pluton																				
z1	**0.304**	**0.6461**	**99.33%**	**43**	**0.36**	**2712**	**0.097**	**0.048547**	**0.185**	**0.129836**	**0.236**	**0.019397**	**0.074**	**0.778**	**126.00**	**4.34**	**123.95**	**0.28**	**123.84**	**0.09**
z2	**0.231**	**0.3229**	**98.72%**	**22**	**0.35**	**1409**	**0.074**	**0.048534**	**0.349**	**0.129877**	**0.401**	**0.019408**	**0.079**	**0.711**	**125.39**	**8.22**	**123.99**	**0.47**	**123.91**	**0.10**
z3	**0.263**	**0.6298**	**99.12%**	**32**	**0.46**	**2047**	**0.084**	**0.048435**	**0.243**	**0.129573**	**0.297**	**0.019402**	**0.092**	**0.690**	**120.55**	**5.73**	**123.71**	**0.35**	**123.88**	**0.11**
z4	**0.267**	**0.6641**	**99.43%**	**49**	**0.32**	**3156**	**0.085**	**0.048403**	**0.174**	**0.129466**	**0.244**	**0.019399**	**0.119**	**0.748**	**118.99**	**4.10**	**123.62**	**0.28**	**123.86**	**0.15**
z5	**0.256**	**1.2072**	**98.55%**	**19**	**1.47**	**1246**	**0.082**	**0.048579**	**0.338**	**0.129927**	**0.388**	**0.019398**	**0.086**	**0.652**	**127.56**	**7.96**	**124.03**	**0.45**	**123.85**	**0.11**
z6	**0.239**	**0.4698**	**98.61%**	**20**	**0.55**	**1299**	**0.076**	**0.048361**	**0.337**	**0.129341**	**0.387**	**0.019397**	**0.077**	**0.704**	**116.97**	**7.96**	**123.51**	**0.45**	**123.85**	**0.09**
z7	**0.266**	**0.3447**	**98.72%**	**22**	**0.37**	**1409**	**0.085**	**0.048268**	**0.416**	**0.129039**	**0.519**	**0.019389**	**0.239**	**0.621**	**112.41**	**9.80**	**123.23**	**0.60**	**123.80**	**0.29**
z8	**0.288**	**0.5250**	**95.52%**	**6**	**2.04**	**403**	**0.092**	**0.048281**	**1.043**	**0.129160**	**1.129**	**0.019402**	**0.115**	**0.772**	**113.08**	**24.61**	**123.34**	**1.31**	**123.88**	**0.14**

Notes:

(a) z1, z2 etc. are labels for fractions composed of single zircon grains or fragments; all fractions annealed and chemically abraded after Mattinson (2005).

(b) Model Th/U ratio calculated from radiogenic ^{208}Pb/^{206}Pb ratio and ^{207}Pb/^{235}U age.

(c) Pb* and Pbc represent radiogenic and common Pb, respectively; mol % ^{206}Pb* with respect to radiogenic, blank and initial common Pb.

(d) Measured ratio corrected for spike and fractionation only. Fractionation estimated at 0.15 +/- 0.03 %/atomic mass unit for Daly analyses, based on analysis of NBS-981 and NBS-982.

(e) Corrected for fractionation, spike, and common Pb; up to 1 pg of common Pb was assumed to be procedural blank: ^{206}Pb/^{204}Pb = 18.35 ± 1.5%; ^{207}Pb/^{204}Pb = 15.60 ± 0.5%; ^{208}Pb/^{204} Pb = 38.08 ± 1.0% (all uncertainties 1-sigma).

Excess over blank was assigned to initial common Pb, using the Stacey and Kramers (1975) two-stage Pb isotope evolution model at the nominal sample age.

(f) Errors are 2-sigma, propagated using the algorithms of Schmitz and Schoene (2007).

(g) Calculations are based on the decay constants of Jaffey et al. (1971). ^{206}Pb/^{238}U and ^{207}Pb/^{206}Pb ages corrected for initial disequilibrium in ^{230}Th/^{238}U using Th/U [magma] = 3.

REFERENCES

Anderson, A. L., (1930) The geology and mineral resources of the region about Orofino, Idaho: Idaho Bureau of Mines and Geology Pamphlet v. 34 63 p.

Anderson, R.G., (1993) A Mesozoic stratigraphic and plutonic framework for northwestern Stikinia (Iskut River Area), northwestern British Columbia, Canada: *in* Mesozoic Paleogeography of the Western United States-II. Dunne, G., and McDougall, K., (eds.). Society of Economic Paleontologists and Mineralogists, Pacific Section, v. 71, p. 477–494.

Armstrong, R. L., Taubeneck, W. H., and Hales, P.O., (1977) Rb-Sr and K-Ar geochronometry of Mesozoic granitic rocks and their Sr isotopic composition, Oregon, Washington, and Idaho: Geological Society of America Bulletin v. 88 p 397-411

Ash, C.H., (1994) Origin and tectonic setting of ophiolitic ultramafic and related rocks in the Atlin area, British Columbia (NTS 104N): British Columbia Ministry of Energy, Mines and Petroleum Resources, Bulletin 94.

Ashley, R.P., (1995) Petrology and deformation history of the Burnt River Schist and associated plutonic rock in the Burnt River Canyon area, northeastern Oregon: *in* Vallier, T.L., and Brooks, H. C., (eds.), Geology of the Blue Mountains Region of Oregon, Idaho, and Washington: Petrology and Tectonic Evolution of Pre-Tertiary, Blue Mountains Province USGS Professional Paper 1438, p. 457-496

Avé Lallemant, H. G., (1983) The kinematic insignificance of mineral lineations in a Late Jurassic thrust and fold belt in eastern Oregon, U.S: Tectonophysics v. 100 p.389-404

Avé Lallemant, H. G., (1995) Pre-Cretaceous tectonic evolution of the Blue Mountains province, northeastern Oregon: *in* Vallier, T.L., and Brooks, H. C., (eds.), Geology of the Blue Mountains Region of Oregon, Idaho, and Washington: Petrology and Tectonic Evolution of Pre-Tertiary, Blue Mountains Province USGS Professional Paper 1438, p. 271-304

Avé Lallemant, H. G., Phelps, D. W., Sutter, J. F., (1980) ^{40}Ar-^{30}Ar ages of some pre-Tertiary plutonic and metamorphic rocks of eastern Oregon and their tectonic relationships: Geology, v. 8 p. 371-374

Avé Lallemant, H. G., Schmidt, W. J., Kraft, J. L., (1985) Major Late Triassic strike-slip displacement in the Seven Devils terrane, Oregon and Idaho – A result of left oblique plate convergence?: Tectonophysics v. 119, p. 299-328

Bedford, B., Crowley, J., Schmitz, M., Northrup, C. J. and Tikoff, B., (2010) Mesozoic magmatism and deformation in the northern Owyhee Mountains, Idaho: Implications for along-zone variations for the western Idaho shear zone: Lithosphere v. 2 p. 93-118

Bishop, E. M., (1995) High-pressure, low-temperature schistose rocks of the Baker terrane, northeastern Oregon: *in* Vallier, T.L., and Brooks, H. C., (eds.), Geology of the Blue Mountains Region of Oregon, Idaho, and Washington: Petrology and Tectonic Evolution of Pre-Tertiary, Blue Mountains Province USGS Professional Paper 1438, p. 211-219

Bloom, C. D., and Nestell, M. K., (1991) Evolution of a Perm-Triassic sedimentary mélange, Grindstone terrane, east-central Oregon: Geological Society of America Bulletin v. 103 p. 1280-1296

Blome, C.D., Jones, D.L., Murchey, B.L., and Liniecki, M., (1986) Geologic implications for radiolarian-bearing Paleozoic and Mesozoic rocks from the Blue Mountains Province, eastern Oregon: *in* Vallier, T.L., and Brooks, H.C., (eds.), Geology of the Blue Mountains Region of Oregon, Idaho, and Washington—Geological Implications of Paleozoic and Mesozoic Paleontology and Biostratigraphy, Blue Mountains Province, Oregon and Idaho: U.S. Geological Survey Professional Paper 1435, p. 79–101.

Boekhout, F., Spikings, R., Sempere, T., Chiaradia, M., Ulianov, A., Schaltegger, U., (2012) Mesozoic arc magmatism along the southern Peruvian margin during Gondwana breakup and dispersal: Lithos v. 146-147. p. 48-64

Bostwick, D. A. and Nestell, M. K., (1965) A new species of *polydiexodina* from central Oregon: Journal of Paleontology v. 39 p. 611-614

Brooks, H. C., (1967) Distinctive conglomerate layer near Lime, Baker County, Oregon: The Ore Bin v. 29, No. 6, p. 113-128

Brooks, H. C., (1979) Plate tectonics and the geologic history of the Blue Mountains: Oregon Geology v. 41 n. 5 p. 69-80

Brooks, H. C., (1985) Mélanges and associated rocks of northeast Oregon; implications for timing of terrane assembly: Proceedings of the Pacific division, American Association for the Advancement of Science v.4 p29

Brooks, H. C., Vallier, T. L., (1978) Mesozoic rocks and tectonic evolution of Eastern Oregon and Western Idaho: *in* Howell, D.G., and McDougall, K.A., (eds.), Mesozoic paleogeography of the Western United States, Pacific Coast Paleogeography Symposium 2: Los Angeles, Pacific Section, Society of Economic Paleontologists and Mineralogists, p. 133-145

Brooks, H. C., McIntyre, J.R., Walker, G. W., (1978) Geology of the Oregon Part of the Baker 1-degree by 2-degree Quadrangle: State of Oregon, Oregon Department of Geology and Mineral Industries, Geologic Map Series, GMS-7, Scale 1:250,000.

Burchfiel, B. C, Cowen, D. S, Davis, G. A., (1992) Tectonic Overview of the Cordilleran Orogen in the Western United States: The Geology of North America. v. G-3 The Cordilleran Orogen: Conterminous U.S. The Geologic Society of America Chapter 8 p.407-479

Carpenter, P.S., and Walker, N.W., (1992) Origin and tectonic significance of the Aldrich Mountains serpentinite matrix mélange, northeastern Oregon: Tectonics v. 11, p. 690–708, doi: 10.1029/91TC03013.

Cas, R. F. and Wright, J. V., (1987) Volcanic successions: Modern and ancient: London, Allen & Unwin, 528 p.

Cengiz Cinku, M., Ustaomer, T., Hirt, A. M., Hisarli, Z. M., Heller, F., (2010) Southward migration of arc magmatism during latest Cretaceous Associated with Slab Steepening, East Pontides, North Turkey, New Paleomagnetic Data from the Amasya Region: Physics of the Earth and Planetary Interiors. v. 182 no. 1-2 p. 18-29.

Choi, T., Lee, Y. I., Orihashi, Y., (2011) Mesozoic detrital zircon U-Pb ages of modern river sediments in Korea: implications for migration of arc magmatism in the Mesozoic East Asian continental margin: Terra Nova v. 24 p. 156-165i

Collins, A.Q., (2000) Regional implications defined by the petrogenesis of the Huntington Formation, Olds Ferry terrane, Baker County, Oregon [B.S. thesis]: Boise, Idaho, Boise State University, 43 p.

Colpron, M. and Friedman, R.M., (2008) U-Pb zircon ages for the Nordenskiold Formation (Laberge Group) and Cretaceous intrusive rocks, Whitehorse Trough,

Yukon: *in*. Yukon Exploration and Geology 2007. D.S. Emond, L.R. Blackburn, R.P. Hill and L.H. Weston (eds.), Yukon Geological Survey, p. 179–197.

Colpron, M., and Nelson, J. L., (2009) A Palaeozoic Northwest Passage: incursion of Caledonian, Baltican and Siberian terranes into eastern Panthalassa, and the early evolution of the North American Cordillera: *in*. Earth Accretionary Systems in Space and Time. Cawood, P. A., and Kroner, A., (eds.), The Geologic Society, London, Special Publications. v. 318. P. 273-307

Coney, P. J., Jones, D. L., Monger, J. W. H. (1980) Cordilleran suspect terranes: Nature. v. 288 p. 329-333

Cowan, D. S. and Bruhn, R. L., (1992) Late Jurassic to early Late Cretaceous geology of the U.S. Cordillera: *in* Burchfiel B. C., Lipman P. W., and Zoback M. L., (eds.), The Cordilleran Orogen: Conterminous U. S.: Geological Society of America , The Geology of North America, v. G-3 p. 169-203

Coward, R. I., ms., (1983) Structural geology, stratigraphy, and petrology of the Elkhorn Ridge Argillite in the Sumpter area northeastern Oregon: [Ph. D. Dissertation] Houston, Texas, Rice University. 144 p.

Danner, W. R., (1975) Notes on the Cache Creek Group: Mimeograph sheet for a field trip to the western Intermontane Belt, 4 p.

DeCelles, P. G., (2004) Late Jurassic to Eocene Evolution of the Cordilleran Thrust Belt and Foreland Basin System, Western U.S.A: American Journal of Science. v. 304 p.105-168

Dickie, J. R., and Hein, F. J., (1995) Conglomeratic fan deltas and submarine fans of the Jurassic Laberge Group, Whitehorse Trough, Yukon Territory, Canada: fore-arc sedimentation and unroofing of a volcanic island arc complex. Sedimentary Geology, v. 98, p. 263-292.

Dickinson, W.R., (1976) Sedimentary basins developed during evolution of Mesozoic-Cenozoic arc-trench system in western North America. Canadian Journal of Earth Sciences, v. 13, no. 9, p. 1268–1287.

Dickinson, W., (1977) Paleozoic Plate Tectonics and the Evolution of the cordilleran Continental Margin: *in* Stewart, J.H., Stevens, C.H., and Fritsche, A.E., (eds.), Paleozoic paleogeography of the western United States: Pacific Coast Paleogeography Symposium 1: Los Angeles, Society of Economic Paleontologists and Mineralogists, Pacific Section, p. 137-155.

Dickinson, W., (1979) Mesozoic Forearc Basin in central Oregon: Geology v. 7 p.166-170

Dickinson, W., (2002) The Basin and Range province as a composite extensional domain: Int. Geol. Rev. v. 44 p. 1-38

Dickinson, W., (2004) Evolution of the North American Cordillera: Annual Review Earth and Planetary Science v. 32 p13-45

Dickinson, W. R., Helmold, K. P., and Stein, J. A., (1979) Mesozoic lithic sandstones in central Oregon: Journal of Sedimentary Petrology v. 49 no. 2 p. 0501-0516

Dickinson, W.R., and Seely, D.R., (1979) Structure and stratigraphy of forearc regions: American Association of Petroleum Geologists Bulletin, v. 63, p. 2-31

Dickinson, W.R., and Thayer, T.P., (1978) Paleogeographic and paleotectonic implications of Mesozoic stratigraphy and structure in the John Day Inlier of central Oregon: *in* Howell, D.G., and McDougall, K.A., (eds.), Mesozoic paleogeography of the Western United States, Pacific Coast Paleogeography Symposium 2: Los Angeles, Pacific Section, Society of Economic Paleontologists and Mineralogists, p. 147-161

Dickinson, W. R., and Vigrass, L. W., (1965) Geology of the Suplee-Izee area Crook, Grant, and Harney Counties, Oregon: Oregon Department of Geology and Mineral Industries Bulletin 58 109 p.

Dorsey, R, and LaMaskin, T., (2007) Stratigraphic record of Triassic-Jurassic collisional Tectonics in the Blue Mountains province, northeastern Oregon: American Journal of Science v. 50 p.1167- 1193

Dostal, J., Church, B. N., and Höy, T., (2001) Geological and geochemical evidence for variable magmatism and tectonics in the southern Canadian Cordillera: Paleozoic to Jurassic suits, Greenwood, southern British Columbia: Canadian Journal of Earth Sciences v. 38 p. 75-90

Eisbacher, G. H., (1985) Pericollisional strike-slip faults and synorogenic basins, Canadian Cordillera, in Biddle K. T., and Christie-Blick, N., (eds.), Strike-slip deformation, basin formation, and sedimentation: Society of Economic Paleontologists and Mineralogists Special Publication 37, p. 265 - 282

Engh, K. R., (1984) Structural geology of the Rastus Mountain area, east-central Oregon: [M.S. Thesis] Pullman, Washington, Washington State University 78p.

English, J. M., Johannson, G. G., Johnston, S. T., Mihalynuk, M. G., Fowler, M., Wight, K. L., (2005) Structure, stratigraphy, and petroleum resource potential of the Central Whitehorse Trough, Northern Canadian Cordillera: Bulletin of Canadian Petroleum Geology v. 53 n. 2 p. 130-153

English, J. M., and Johnston, S. T., (2005) Collisional orogenesis in the northern Canadian Cordillera: Implications for Cordilleran crustal structure, ophiolites emplacement, continental growth, and the terrane hypothesis: Earth and Planetary Science Letters v. 232 p. 333-344

English, J. M., Mihalynuk, M. G., Johnston, S. T., (2010) Geochemistry of the northern Cache Creek terrane and implication for accretionary processes in the Canadian Cordillera: Canadian Journal of Earth Sciences. v. 47 p. 13 - 34

Evans, J. G., (1986) Geologic map of the North Fork John Day river roadless area, Grant County, Oregon: U. S. Geological Survey miscellaneous field studies map MF 1581-C, scale 1:48,000

Evans, J. G., (1995) Pre-Tertiary deformation in the Desolation Butte quadrangle, northeastern Oregon: *in* Vallier, T.L., and Brooks, H. C., (eds.), Geology of the Blue Mountains Region of Oregon, Idaho, and Washington: Petrology and Tectonic Evolution of Pre-Tertiary, Blue Mountains Province USGS Professional Paper 1438, p. 305 - 330

Evenchick, C. A., McMechan, M.E., McNicoll, V.J. and Carr, S.D., (2007) A synthesis of the Jurassic-Cretaceous tectonic evolution of the central and southeastern Canadian Cordillera: exploring links across the orogen: *in* Sears, J. W., Harms, T. A., & Evenchick, C. A., (eds.), Whence the Mountains? Inquiries into the Evolution of Orogenic Systems: A Volume in Honor of Raymond A. Price. Geological Society of America, Special Papers, 433, 117–145.

Evenchick, C. A., Poulton, T. P., and McNicoll, V. J., (2010) Nature and significance of the diachronous contact between the Hazelton and Bowser Lake Groups (Jurassic), north-central British Columbia: Bulletin of Canadian Petroleum Geology. v. 58 no. 3 p. 235 - 257

Ferns, M.L. and Brooks, H.C., (1995) The Bourne and Greenhorn subterranes of the Baker terrane, north-eastern Oregon: Implications for the evolution of the Blue Mountains island-arc system: *in* Vallier, T.L., and Brooks, H. C., (eds.), Geology of the Blue Mountains Region of Oregon, Idaho and Washington. Petrology and Tectonic Evolution of Pre-Tertiary Rocks of the Blue Mountains Region: U.S. Geological Survey Professional Paper 1438, p.331-358

Ferns, M.L., Brooks, H.C., and Avery, D.G., (1983) Geology and Gold Deposits Map of the Greenhorn Quadrangle, Baker and Grant Counties, Oregon: Oregon Department of Geology and Mineral Industries Geological Map Series GMS-28, scale 1:24,000.

Ferns, M.L., Brooks, H.C., Avery, D.G., and Blome, C.D., (1987) Geology and Mineral Resources Map of the Elkhorn Peak Quadrangle, Baker County, Oregon: Oregon Department of Geology and Mineral Industries Geological Map Series GMS–41, scale 1:24,000, 1 sheet.

Fisher, R.V., (1961) Proposed classification of volcaniclastic sediments and rocks: Geological Society of America Bulletin, v. 72 p. 1409-1414

Follo, M.F., (1992) Conglomerates as clues to the sedimentary and tectonic evolution of a suspect terrane: Wallowa Mountains, Oregon: Geological Society of America Bulletin, v. 104, p. 1561-1576.

Follo, M.F., (1994) Sedimentology and stratigraphy of the Martin Bridge Limestone and Hurwal Formation (upper Triassic to lower Jurassic) from the Wallowa terrane, Oregon, in Vallier, T.L., and Brooks, H.C., (eds.), Geology of the Blue Mountains region of Oregon, Idaho and Washington: Stratigraphy, physiography, and mineral resources of the Blue Mountains region: U.S. Geological Survey Professional Paper 1439, p. 1-27.

Gabrielse, H., Monger, J. W. H., Wheeler, J. O. and Yorath, C. J., (1991) Part A: Morphogeological belts, tectonic assemblages, and terranes: *in* Gabrielse, H., and Yorath, C.J., (eds.),Geology of the Cordilleran orogen in Canada: Geological Survey of Canada, Geology of Canada, no. 4, and Geological Society of America, Geology of North America, v. G-2 p. 15–28.

Gagnon, J. F., Evenchick, C.A., Waldron, J.W.F., Cordey, F. and Poulton, T.P., (2009) Jurassic subsidence history of the Hazelton Trough–Bowser Basin in the area of Todagin Mountain, north-central British Columbia, Canada. Bulletin of Canadian Petroleum Geology, v. 57, p. 430–448.

Gardner, M., Bergman, S., Cushing, G., MacKevett, E. M., Plafker, G., Campbell, R., Dodds, C., McClelland, W., Mueller, P., (1988) Pennsylvanian Pluton Stitching of Wrangellia and the Alexander Terrane, Wrangell Mountains, Alaska: Geology. v. 16 p. 967-971

Gashnig, R. M., Vervoort, J. D., Lewis, R. S., Tikoff, B., (2011) Isotopic Evolution of the Idaho Batholith and Challis Intrusive Province, Northern US Cordillera:

Journal of Petrology. v. 52, no. 12, p. 2397-2429

Getty, S. R., Selverstone, J., Wernicke, B. P., Jacobson, S. B., Aliberti, E., Lux, D. R., (1993) Sm-Nd dating of multiple garnet growth events in an arc-continent collision zone, northwestern U.S. Cordillera: contributions Mineral Petrology v. 115 p. 45-57

Ghosh, D.K., (1995) Nd-Sr isotopic constraints on the interactions of the Intermontane superterrane with the western edge of North America in the southern Canadian Cordillera: Canadian Journal of Earth Sciences, v. 32, p. 1740–1758.

Gilluly, J., (1937) Geology and Mineral Resources of the Baker Quadrangle, Oregon: U.S. Geological Survey Bulletin 879, 199 p.

Giorgis, S., Tikoff, B., and McClelland, W., (2005) Missing Idaho arc: Transpressional modification of the $^{87}Sr/^{86}Sr$ transition on the western edge of the Idaho Batholith: Geology v. 33 p. 496-472

Giorgis, S., Tikoff, B., and McClelland, W., (2007) Field forum report: Tectonic significance of vertical boundaries in the Cordillera: GSA Today v. 17 p. 27

Giorgis, S., McClelland, W., Fayan, A., Singer, B. S. and Tikoff, B., (2008) Timing of Deformation and Exhumation in the western Idaho shear zone, McCall, Idaho: Geological Society of America Bulletin v. 120 p. 1119-1133

Gradstein, F M., Ogg, J. G., Schmitz, M. D., Ogg, G. M., (2012) The Geologic Time Scale. Amsterdam: Elsevier, p. 731-791

Gray, K., and Oldow, J., (2005) Contrasting structural histories of the Salmon River belt and Wallowa terrane: Implications for terrane accretion in northeastern Oregon and west-central Idaho: GSA Bulletin v. 117 no 5/6 p.687-706

Greig, C. J., Gehrels, G.E., Anderson, R.G. and Evenchick, C.A., (1991) Possible transtensional origin of the Bowser Basin, British Columbia. In: Geological Society of America, Abstract with Programs, v. 23, no. 2, p. 30.

Hamilton, W., (1963) Hamilton, W., 1963, Metamorphism in the Riggins region, western Idaho: U.S. Geological Survey Professional Paper 436, 95 p.

Hamilton, W., (1969) Reconnaissance geologic map of the Riggins quadrangle, west-central Idaho: U.S. Geological Survey Miscellaneous Geologic Investigations Series Map I–579, scale 1:125,000.

Hamilton, W., (1978) Mesozoic tectonics of the western United States: *in* Howell, D. G., and McDougall, K. A., (eds.), Mesozoic paleogeography of the Western United States, Pacific Coast Paleogeography Symposium 2: Los Angeles, Pacific Section, Society of Economic Paleontologists and Mineralogists, p. 33-70.

Heller, P. L., and Paola, C., (1989) The paradox of lower Cretaceous gravels and the initiation of thrusting in the Sevier orogenic belt, United States Western Interior: Geological Society of America Bulletin v. 101, p. 864-875

Heller, P.L., Tabor, R.W., Suczek CA., (1987) Paleo- geographic evolution of the United States Pacific Northwest during Paleogene time: Canadian Journal of Earth Sciences. v. 24 p. 1652–67

Hooper, P. R., Houseman, M. D., Beane, J. E., Caffrey, G. M., Engh, K. R., Scrivner, J. V., and Watkinson, A. J. (1995) Geology of the Northern Part of the Ironside Mountain Inlier, Northeastern Oregon: *in* Vallier, T.L., and Brooks, H. C., (eds.), Geology of the Blue Mountains Region of Oregon, Idaho, and Washington: Petrology and Tectonic Evolution of Pre-Tertiary, Blue Mountains Province USGS Professional Paper 1438, p.125-209

Imlay, R., (1964) Upper Jurassic mollusks form eastern Oregon and Western Idaho: U. S. Geol. Survey Professional Paper 483-D p. D1-D21

Imlay, R., (1968) Lower Jurassic (Pliensbachian and Toarcian) ammonites from eastern Oregon and California: U. S. Geol. Survey Professional Paper 593-C, p. C1-C151

Imlay, R., (1973) Middle Jurassic (Bajocian) ammonites from eastern Oregon: U. S. Geol. Survey Professional Paper 756, 100 p.

Imlay, R., (1980) Jurassic Paleobiogeography of the Conterminous Unites States in its Continental Setting: Geological Survey Professional Paper 1062. P. 1-134

Imlay, R., (1986) Jurassic Ammonites and Biostratigraphy of Eastern Oregon and Western Idaho: *in* Vallier, T.L., and Brooks, H. C., (eds.), Geology of the Blue Mountains Region of Oregon, Idaho and Washington. Geologic Implications of Paleozoic and Mesozoic Paleontology and Biostratigraphy, of the Blue Mountains Province, Oregon and Idaho: U.S. Geological Survey Professional Paper 1435, p.53-57

Ingersoll, R. V., (1979) Evolution of the Late Cretaceous forearc basin, northern and central California: Geological Society of America Bulletin. V. 90 p. 813-826

Jaffey, A.H., Flynn, K.F., Glendenin, L.E., Bentley, W.C., and Essling, A.M., (1971) Precision measurement of half-lives and specific activities of ^{235}U and ^{238}U: Physical Review c, v.4, p.1889-1906

Johannson, G. G., (1994) Provenance constraints on Early Jurassic evolution of the northern Stikinian arc: Laberge Group, Whitehorse Trough, northwestern British Columbia: [M. S. thesis] Vancouver, British Columbia, University of British Columbia 297 p.

Johannson, G. G., Smith P. L., Gordey S. P., (1997) Early Jurassic evolution of the northern Stikinian arc: evidence from the Laberge Group, northwestern British Columbia: Canadian Journal of Science v. 34 p. 1030-1057

Johnson, K., Barnes, C. G., (2002) Jurassic magmatism prior to and during terrane accretion in the Blue Mountains Province, NE Oregon: Geological Society of America Abstracts with Programs v. 34 no. 5, p. 21-22

Johnson, K., Schwartz, J. J., (2009) Overview of Jurassic-Cretaceous Magmatism in the Blue Mountains Province (NE Oregon & W Idaho); Insights form new Pb/U (SHRIMP-Rg) age determinations: Geologic Society of America Abstracts with Programs. v. 41 no. 7 p. 182

Johnson, K., Schwartz, J. J., Walton, C., (2007) Petrology of the Late Jurassic Sunrise Butte Pluton, eastern Oregon: a record of renewed Mesozoic arc activity? Geological Society of America Abstracts with Programs v. 39 p. 6

Johnson, K., Schwartz, J. J., Wooden, J. L., O'Driscoll, L. J., Jeffcoat, C. R., (2011) The Wallowa Batholith; New Pb/U (SHRIMP-RG) ages place constraints on arc magmatism and crustal thickening in the Blue mountains Province, NE Oregon: Geological Society of America Abstracts with Programs, v. 43 no. 4 p. 5

Jordan, T. E., (1981) Thrust loads and foreland basin evolution, Cretaceous, western United States: American Association of Petroleum Geologist bulletin v. 65 p. 2506-2520

Kinoshita, O., (1999) A migration model of magmatism explaining a ridge subduction, and its details on a statistical analysis of the granite ages in Cretaceous Southwest Japan: The Island Arc v. 8 p. 181–189

Kistler, R. W., and Peterman, Z. E., (1973) Variations in Sr, Rb, Na, and initial $^{87}Sr/^{86}Sr$ in Mesozoic granitic rocks and intruded wall rocks in central California: Geological Society of America v. 84 p. 3489-3512

Kurz, G.A., (2001) Structure and geochemistry of the Cougar Creek complex, northeastern Oregon and west-central Idaho [M.S. Thesis]: Boise, Idaho, Boise State University, 248 p. 66

Kurz, G. A., (2010) Geochemical, Isotopic and U-Pb Geochronological investigations of intrusive basement rocks from the Wallowa and Olds Ferry arc terranes, Blue Mountains province, Oregon-Idaho [Ph. D. Dissertation]: Boise, Idaho, Boise State University, 278 p.

Kurz, G.A., and Northrup, C.J., (2008) Structural analysis of mylonitic rocks in the Cougar Creek Complex, Oregon–Idaho using the porphyroclast hyperbolic distribution method, and potential use of SC'-type extensional shear bands as quantitative vorticity indicators: Journal of Structural Geology, v. 30, p. 1005-1012. doi:10.1016/j.jsg.2008.04.003

Kurz, G. A., Schmitz, M.D., and Northrup, C.J., (2008) Tracer isotope geochemistry and U-Pb zircon geochronology of intrusive rocks from the Wallowa and Olds Ferry arc terranes, Blue Mountains province, northeastern Oregon and west-central Idaho: Geological Society of America Abstracts with Programs, v. 40, p. 87.

Kurz, G. A, Schmitz, M. D, Northrup, C. J, Vallier, T. L., (2011) Preview U-Pb geochronology and geochemistry of intrusive rocks from the Cougar Creek Complex, Wallowa arc terrane, Blue Mountains Province, Oregon-Idaho: Geological Society of America Bulletin v. 124. No. 3-4 p. 578-595.

LaMaskin, T. A., (2008) Late Triassic (Carnian-Norian) mixed carbonate-volcaniclastic facies of the Olds Ferry terrane, eastern Oregon and western Idaho: *in* Blodgert, R. B., and Stanley, G. D. Jr., (eds.), The terrane puzzle: New perspectives on paleontology and stratigraphy form the North American Cordillera: The Geological Society of America, special Paper 442 p. 251-267 doi: 10.1130/2008.442(13)

LaMaskin, T. A., (2009) Stratigraphy, provenance, and tectonic evolution of Mesozoic basins in the Blue Mountains Province, eastern Oregon and western Idaho [Ph. D. Dissertation]: Eugene, Oregon, University of Oregon 232 p.

LaMaskin, T. A., Stanley, Jr. G. D., Caruthers, A. H., Rosenblatt, M. R., (2011) Detrital record of upper Triassic reefs in the Olds Ferry terrane, Blue Mountains province, northeastern Oregon, United States: Palaios v. 26 p. 779-789

LaMaskin, T. A., Vervoort, J. D., Dorsey, R. J., Wright, J. E., (2011b) Early Mesozoic paleogeography and tectonic evolution of the western United States: Insights from

detrital zircon U-Pb geochronology, Blue Mountains Province, northeastern Oregon: Geological Society of America Bulletin v. 123 no. 9-10 p. 1939-1965

Lee, R. G., (2004) the geochemistry, stable isotopic composition, and U-Pb geochronology of tonalite and trondjhemites within the accreted terrane, near Greer, north-central Idaho: [M. S. thesis] Washington State University, Pullman.

Lewis, R. S., Vervoort, J. D., Burmester, R. F., Oswald, P. J., (2010) Detrital zircon analysis of Mesoproterozoic and Neoproterozoic metasedimentary rocks of north-central Idaho: implications for development of the Belt–Purcell basin: Canadian Journal of Earth Science v. 47 p. 1383–1404

Livingston, D. C., (1932) A geologic reconnaissance of the Mineral and Cuddy Mountain mining district Washington and Adams counties, Idaho: Idaho Bureau of Mines and Geology, Pamphlet 13, 24 p.

Lomize, M. G., and Luchitskaya, M. V., (2012) Subduction of Spreading Ridges as a Factor in the Evolution of Continental Margins: Geotectonics, v. 46, no.1, p. 47-68.

Lowey, G. W., (2008) Summary of the stratigraphy, sedimentology, and hydrocarbon potential of the Laberge Group (lower-Middle Jurassic), Whitehorse Trough, Yukon: *in* Yukon Exploration and Geology 2007. D.S. Emond, L. R. Blackburn, R. P. Hill, L. H. Weston, (eds.), Yukon Geological Survey p. 179-197

Lowey, G. W., Long, D. G. F., Fowler, M. G., Sweet, A. R., and Orchard, M. L., (2009) Petroleum source rock potential of Whitehorse trough: a frontier basin in south-central Yukon: Bulletin of Canadian Petroleum Geology v. 57 n. 3 p. 350-386

Lund, K., (1984) The continent-island arc juncture in west-central Idaho – a missing link in the Cordilleran Tectonics [abs.]: Geological Society of America Abstracts with Programs, v. 16, no. 6 p. 580

Lund, K., and Snee, L. W., (1988) Metamorphism, structural development, and age of the continental-island arc juncture in west-central Idaho: *in* Ernst, W. G., (eds.), Metamorphism and crustal evolution of the western United States, Rubey Volume III: Englewood Cliffs, New Jersey, Prentice Hall p. 297-331

Lund, K., and Snee, L. W., Sutter, J. F., (1985) Style and timing of suture-related deformation in island arc rocks of western Idaho [abs.]: Geological Society of America Abstracts with Programs v. 17, no. 6, p. 367

Mailloux, J.M., Starns, E.C., Snoke, A.W., and Frost, C.D., (2009) An isotopic study of

the Burnt River Schist: Implications for the development of the composite Baker terrane, Blue Mountains Province, NE Oregon: Geological Society of America Abstracts with Programs v. 41, no. 7, p. 441.

Manduca, C. A., Silver, L. T., and Taylor, H. P., (1992) $^{87}Sr/^{86}Sr$ and $^{18}O/^{16}O$ isotopic systematic and geochemistry of granitoids plutons across a steeply dipping boundary between contrasting lithospheric blocks in western Idaho: Contributions to Mineralogy and Petrology v. 109 p. 355-372

Manduca, C. A., Kuntz, M. A., and Silver, L. T., (1993) Emplacement and deformation history of the western margin of the Idaho Batholith near McCall, Idaho; influence of a major terrane boundary: Geological Society of America Bulletin v. 105 p. 749-765

Mattinson, J.M., (2005) Zircon U-Pb chemical abrasion ("CA-TIMS") method: Combined annealing and multi-step partial dissolution analysis for improved precision and accuracy of zircon ages: Chemical Geology, v. 220, p. 47-66

McClelland, W. C., Tikoff, B., and Manduca, C. A., (2000) Two-phase evolution of accretionary margins: examples from the North American Cordillera: Tectonophysics v. 326 p. 37-55

McMillian, W. J., (1975) Geology and genesis of the Highland Valley ore deposits and the Guichon Creek Batholith: In Porphyry deposits of the Canadian Cordillera (Part 3). Canadian Institute of Mining and Metallurgy, Special Volume 15, p. 85-104

McPhie, J., Doyle, M., and Allen, R., (1993) Volcanic textures: A guide to the interpretation of textures in volcanic rocks: Hobart, CODES Key Centre, University of Tasmania, 196 p.

Mihalynuk, M.G., (1999) Geology and mineral resources of the Tagish Lake area (NTS 104M/8, 9, 10E, 15 and 104N/12W) northwestern British Columbia: British Columbia Ministry of Energy, Mines and Petroleum Resources, Bulletin 105.

Mihalynuk, M., Nelson, J., and Diakow, L., (1994) Cache Creek terrane entrapment: Oroclinal paradox within the Canadian Cordillera: Tectonics v.13 no. 2 p.575-595

Miller, J.S., Matzel, J.E.P., Miller, C.F., Burgess, S.D., and Miller, R.B., (2007) Zircon growth and recycling during the assembly of a large, composite arc plutons: Journal of Volcanology and Geothermal Research. V. 167, p. 282-299

Monger, J.W.H., (1977) Upper Paleozoic rocks of the western Canadian Cordillera and their bearing on Cordilleran evolution: Canadian Journal of Earth Sciences, v. 14 p. 1832–1859.

Monger, J.W.H., (1985) Structural evolution of the southwestern Intermontane belt, Ashcroft and Hope map area, British Columbia: Geological Survey of Canada, Current Research, Part A, Paper 85–1A, p. 349–358.

Monger, J. W. H., and Irving, E., (1980) Northward displacement of north-central British Columbia: Nature v. 285 p. 289-294

Monger, J. W. H., and Ross, C., (1971) Distribution of Fusulinaceans in the Western Canadian Cordillera: Canadian Journal of Earth Sciences. v. 8 p.259-278

Monger, J.W.H., Price, R.A., and Tempelman-Kluit, D.J., (1982) Tectonic accretion and the origin of the two major metamorphic and plutonic welts in the Canadian Cordillera: Geology, v. 10 p. 70–75.

Monger, J.W.H., Wheeler, J.O., Tipper, H.W., Gabrielse, H., Harms, T., Struik, L.C., Campbell, R.B., Dodds, C.J., Gehrels, G.E., and O'Brian, J., (1991) Part B: Cordilleran terranes, *in* Gabrielse, H., and Yorath, C.J., (eds.), Geology of the Cordilleran orogen in Canada: Geological Survey of Canada, Geology of Canada, no. 4, and Geological Society of America, Geology of North America, v. G-2 p. 281–327.

Mortimer, N., (1986) Late Triassic, arc-related, potassic igneous rocks in the North American Cordillera: Geology, v. 14 p. 1035–1038.

Mortimer, N., (1987) The Nicola Group: Late Triassic and Early Jurassic subduction related volcanism in British Columbia: Canadian Journal of Earth Sciences, v. 4 p. 2521–2536.

Mullen, E. D., (1978) Geology of the Greenhorn Mountains, northeastern Oregon [M.S. Thesis]: Corvallis, Oregon, Oregon State university 372 p.

Mullen, E. D., and Sarewitz, D., (1983) Paleozoic and Triassic terranes of the Blue Mountains northeast Oregon: Discussion and field trip guide. Part 1. A new consideration of old problems: Oregon Geology v. 45 no. 6 p. 65 - 68

Nakanishi, M., Tamaki, K., and Kodama, K., (1992) Magnetic anomaly lineations from Late Jurassic to Early Cretaceous in the west-central Pacific Ocean: Geophysical Journal International v. 109 p. 701–19.

Nestell, M.K., (1983) Permian foraminifera faunas of central and eastern Oregon: Geological Society of America Abstracts and Programs v. 15, no. 5 p. 371

Nestell, M.K., and Nestell, G.P., (1998) Middle Permian conodonts and Tethyan fusulinaceans associated with possible seamount debris in Oregon: Geological Society of America Abstracts with Programs, v. 30, no. 7, p. 151–152.

Nestell, M.K., and Orchard, M.J., (2000) Late Paleozoic and middle Late Triassic conodont assemblages from the Baker terrane, eastern Oregon: Geological Society of America Abstracts with Programs, v. 32, no. 6, p. 59.

Nestell, M.K., Lambert, L. L., and Wardlaw, B. R., (1995) Pennsylvanian conodonts and fusulinaceans of the Baker terrane, eastern Oregon: Geological Society of America Abstracts with Programs v. 27, no. 3 p. 76

Oldow, J. S., Bally, A. W., Avé Lallemant, H. G., and Leeman, W. P., (1989) Phanerozoic evolution of the north American Cordillera: United States and Canada: *in* Bally, A. W., and Palmer, A. R., (eds.), The geology of North America: an overview: Geological Society of America, The Geology of North America, v. A p. 139-232

Orchard, M.J., Struik, L.C., Rui, L., Bamber, E.W., Mamet, B., Sano, H., and Taylor, H., (2001) Paleontological and biogeographical constraints on the Carboniferous to Jurassic Cache Creek terrane in central British Columbia: Canadian Journal of Earth Sciences v. 38 p. 551–578.

Pardee, J.T., and Hewett, D.F., (1914) Geology and Mineral Resources of the Sumpter Quadrangle, Oregon: Oregon Bureau of Mines and Geology v. 1, no. 6, p. 3–128.

Parker, K.O., Schwartz, J.J., Johnson, K., (2008) Petrology and age of Dixie Butte plutonic rocks, Blue Mountains, NE Oregon: Geological Society of America Abstracts with Programs, v. 40, no. 6, p. 154–155.

Passagno, E. A., Jr., and Blome, C. D., (1986) Faunal affinities and tectonogenesis of Mesozoic rocks in the Blue Mountains province of eastern Oregon and western Idaho: *in* Vallier, T.L., and Brooks, H. C., (eds.), Geology of the Blue Mountains Region of Oregon, Idaho and Washington. Geologic Implications of Paleozoic and Mesozoic Paleontology and Biostratigraphy, of the Blue Mountains Province, Oregon and Idaho: U.S. Geological Survey Professional Paper 1435, p.65-78

Payne, J.D., and Northrup, C.J., (2003) Geologic map of the Monroe Butte 7.5 minute quadrangle, Idaho-Oregon: Idaho Geological Survey, Technical Report 03-01, Idaho Geological Survey.

Prostka, H. J., (1967) Preliminary geologic map of the Durkee Quadrangle, Oregon: Oregon Department of Geology and Mineral Industries Geologic Map Series GMS-3.

Ricketts, B. D., Evenchick, C. A., Anderson, R. G., Murphy, D. C., (1992) Bowser Basin, northern British Columbia: Constraints on the timing of initial subsidence and Stikinia-North America terrane interactions: Geology v. 20 p. 1119-1122

Ross, G. M., and Bowring, S. A., (1990) Detrital Zircon Geochronology of the Windermere Supergroup and the Tectonic Assembly of the Southern Canadian Cordillera: The Journal of Geology v. 98 no. 6 p. 879-893

Sada, K., and Danner, W. R., (1974) Early and Middle Pennsylvanian fusulinids from southern British Columbia, Canada, and northwestern Washington, U.S.A. Transactions and Proceeding of the Paleontological Society of Japan, New Series 93, p. 249-265

Saleeby, J., (1983) Accretionary Tectonics of the North American Cordillera: Annual Review Earth and Planetary Sciences. v. 15 p.45-73

Schmidt, K. L., Lewis, R. S., Gaschnig, R. M., Vervoort, J. D., (2009) testing hypotheses on the origin of the Syringia embayment in the Salmon River suture zone, western Idaho, USA: Geological society of America Abstracts with Programs v. 41 p 223

Schmitz, M.D., and Schoene, B., (2007) Derivation of isotope ratios, errors and error correlations for U-Pb geochronology using ^{205}Pb- ^{235}U- (^{233}U-) spike isotope dilution thermal ionization mass spectrometric data: Geochemistry, Geophysics, Geosystems (G^3), v. 8, p. Q08006

Schwartz, J. J., Johnson, K., (2009) Origin of Paired Late Jurassic High and Low Sr/Y magmatic Belts in the Blue Mountains Province, NE Oregon: Geological Society of America Abstracts with Programs v. 41 no. 7 p. 182

Schwartz, J. J., Johnson, K., Miranda, E. A., Wooden, J. L., (2011) The generation of high Sr/Y plutons following ate Jurassic arc-arc collision, Blue Mountains province, NE Oregon: Lithos v. 126 p. 22-41

Schwartz, J. J., Snoke, A., Frost, C., Barnes, C., Gromet, P., Johnson, K., (2010) Analysis of the Wallowa-Baker terrane boundary: Implications for tectonic accretion in the Blue Mountains province, northeastern Oregon: GSA Bulletin v. 122 no.3/4 p.517-536

Schwartz, J. J., Snoke, A. W., Fabrice, C., Johnson, K., Frost, C. D., Barnes, C. G., LaMaskin, T. A., Wooden, J. L., (2011b) Late Jurassic Magmatism, Metamorphism, and Deformation in the Blue Mountains Province, northeastern Oregon: GSA Bulletin v. 123 n. 9/10 p. 2083-2111

Selverstone, J., Wernicke, B. P., and Aliberti, E. A., (1992) Intercontinental subduction and hinged unroofing along the Salmon River suture zone, west-central Idaho: Tectonics v. 11 p. 124-144

Shirmohammad, F., Smith, P. L., Anderson, R. G., McNicoll, V. J., (2007) the involvement of Stikine Terrane in development of the central Whitehorse Trough, NW British Columbia: Abstracts with Programs, Geologic Society of America v. 38. 5

Silberling, N. J., Jones, D. L., Blake, M. C. Jr., and Howell, D. G., (1984) Lithotectonic terrane map of the western conterminous United States: *in* Silberling, N. J., and Jones, D. L., (eds.), Lithotectonic terrane maps of the North American Cordillera: U. S. Geological Survey Open File Report 84-0523, p. C1-C43

Snee, L. W., Davidson, G. F., Unruh, D. M., (2007) Geological, geochemical, and $^{40}Ar/^{39}Ar$ and U-Pb thermochronological constraints for the tectonic development of the Salmon River suture zone near Orofino, Idaho: *in* Kuntz, M. A., and Snee, L. W., (eds.), Geological studies of the Salmon River suture zone and adjoining areas, west-central Idaho and eastern Oregon. US Geological Survey, Professional Papers 1738 p. 51-94

Souther, J. G., (1971) Geology and mineral deposits of Tulsequah map-area, British Columbia: Geological Survey of Canada, Memoir 362, 84 p.

Souther, J.G., (1991) Volcanic regimes, *in* Gabrielse, H., and Yorath, C.J., (eds.), Geology of the Cordilleran orogen in Canada: Geological Survey of Canada, Geology of Canada, no. 4, and Geological Society of America, Geology of North America, v. G-2, p. 459–490.

Stacey, J. S., and Kramers, J. D., (1975) Approximation of terrestrial lead isotope evolution by a two-stage model: Earth and Planetary Science Letters, v. 26 no. 2 p. 207-221.

Stanley, G.D., Jr., and Beauvais, L., (1990) Middle Jurassic corals from the Wallowa terrane, west-central Idaho: Journal of Paleontology, v. 64, p. 352-362.

Starns, E. C., (2011) Structural evolution of the southern margin of the Baker terrane, Blue Mountains Province, northeastern Oregon [M.S. Thesis]: Laramie, Wyoming, university of Wyoming 89 p.

Taubeneck, W. H., (1957) Geology of the Elkhorn Mountains, northeastern Oregon – Bald Mountain Batholith: Geological Society of America Bulletin, v. 68, p. 181-238

Taubeneck, W.H., (1995) A Closer Look at the Bald Mountain Batholith, Elkhorn Mountains, and Some Comparisons With The Wallowa Batholith, Wallowa Mountains, Northeastern Oregon: *in* Vallier, T.L., and Brooks, H. C., (eds.), Geology of the Blue Mountains Region of Oregon, Idaho, and Washington: Petrology and Tectonic Evolution of Pre-Tertiary, Blue Mountains Province USGS Professional Paper 1438, p. 45-125

Tempelman-Kuilt, D. J., (1979) Transported cataclasite, ophiolites, and granodiorite in Yukon: Evidence of arc-continent collision: Pap. Geological Survey Canada v. 79 no. 14, 27p.

Terry, J., (1977) Geology of the Nahlin ultramafic body, Atlin and Tulsequah map-areas, northwestern British Columbia: In Current research. Geological Survey of Canada, pp. 263–266.

Thorkelson, D.J., Mortensen, J.K., Marsden, H. and Taylor, D.C., (1995) Age and tectonic setting of Early Jurassic episodic volcanism along the northeastern margin of the Hazelton Trough, northern British Columbia: *in* Jurassic Magmatism and Tectonics of their North American Cordillera. D.M. Miller, and C.J. Busby, (eds.), Geological Society of America Special Paper 299, p. 83–94.

Travers, W. B., (1978) Overturned Nicola and Ashcroft strata and their relation to the Cache Creek Group, Southwestern Intermontane Belt, British Columbia: Canadian Journal of Earth Sciences v. 15 p. 99-116

Tumpane, K. P., ms., (2010) Age and isotopic investigations of the Olds Ferry terrane and its relations to other terranes of the Blue Mountains province, eastern Oregon and west-central Idaho [M.S. Thesis]: Boise, Idaho, Boise State University, 220 p.

Unruh, D. M., Lund, K., Kuntz, M. A., Snee, L. W., (2008) Uranium-Lead Zircon Ages and Sr, Nd, and Pb Isotope Geochemistry of Selected Plutonic Rocks from Western Idaho: U.S. Geological Survey Open-File Report 2008-1142, 37 p.

Untershutz, J. L. E., Creaser, R. A., Erdmer, P., Thompson, R. I., and Daughtry, K.L., (2002) North American margin origin of Quesnel terrane strata in the southern

Canadian Cordillera: Inferences from geochemical and Nd isotopic characteristics of Triassic metasedimentary rocks: Geologic Society of America Bulletin v. 114 p. 462-475

Valencia-Moreno, M., Iriondo, A., González-León, C., (2004) Temporal constraints on the eastward migration of the Late Cretaceous–early Tertiary magmatic arc of NW Mexico based on new $^{40}Ar/^{39}Ar$ hornblende geochronology of granitic rocks: Journal of South American Earth Sciences v. 22 p. 22–38

Vallier, T. L., (1977) The Permian and Triassic Seven Devils Group, western Idaho and northeastern Oregon: U.S. Geological Survey Bulletin 1437 58 p.

Vallier, T. L., (1995) Petrology of Pre-Tertiary Igneous Rocks in the blue Mountains Region of Oregon, Idaho, and Washington: Implications for the Geologic Evolution of a Complex Island Arc: *in* Vallier, T.L., and Brooks, H. C., (eds.), Geology of the Blue Mountains Region of Oregon, Idaho, and Washington: Petrology and Tectonic Evolution of Pre-Tertiary, Blue Mountains Province USGS Professional Paper 1438, p.125-209

Vallier, T.L., Brooks, H. C., and Thayer, T. P., (1977) Paleozoic rocks of eastern Oregon and western Idaho: *in* Stewart, J. H., Stevens, C. H., and Fritsche, A. E., (eds.), Paleozoic paleogeography of the western United States: Society of Economic Paleontologists and Mineralogists, Pacific Sections: Pacific Coast paleogeography symposium 1, p. 455-466

Walker, N. W., ms, (1986) U/Pb geochronology and petrologic studies in the Blue Mountains terrane, northeastern Oregon and western most-central Idaho; implications for pre-Tertiary tectonic evolution: [Ph. D. Dissertation] Santa Barbara, California, University of California, Santa Barbara, 224 p.

Walker, N. W., (1989) Early Cretaceous initiation of post-tectonic plutonism and the age of the Connor Creek fault, northeastern Oregon [abs]: Geological Society of America Abstracts with Programs, v. 21, no. 5, p. 155.

Walker, N. W., (1995) Tectonic Implications of U-Pb Zircon Ages of the Canyon Mountain Complex, Sparta Complex, and Related Metaplutonic Rocks of the Baker Terrane, Northeastern Oregon: *in* Vallier, T.L., and Brooks, H. C., (eds.), Geology of the Blue Mountains Region of Oregon, Idaho, and Washington: Petrology and Tectonic Evolution of Pre-Tertiary, Blue Mountains Province USGS Professional Paper 1438, p. 247-271

Wardlow, B. R., Nestell, M.K., and Dutro, J.T. Jr., (1982) Biostratigraphy and structural setting of the Permian Coyote Butte Formation of Central Oregon: Geology v. 10 p. 13-16 doi: 10.1130/0091-7613(1982) 10 <13:BASSOT>2.0.CO; 2.

Wentworth, C. K., and Williams, H., (1932) the classification and terminology of the pyroclastic rocks: Bulletin of the National Research council, v. 89, Report of the Commission on Sedimentation p. 19-53

Wheeler, G. R., ms., (1976) Geology of Vinegar Hill Area, Grant County, Oregon [Ph. D. Dissertation]: Seattle, Washington, University of Washington 94 p.

White, J.D.L., (1994) Intra-arc basin deposits within the Wallowa terrane, Pittsburg Landing area, Oregon and Idaho: *in* Vallier, T.L., and Brooks, H.C., (eds.), Geology of the Blue Mountains region of Oregon, Idaho and Washington: Stratigraphy, physiography, and mineral resources of the Blue Mountains region: U.S. Geological Survey Professional Paper 1439, p. 75-89.

White, J. D. L., Houghton, B. F., (2006) Primary volcaniclastic rocks: Geological Society of America. v. 34 no. 8 p. 677-680

White, D. L., and Vallier, T. L., (1994) Geologic Evolution of the Pittsburg Landing Area, Snake River Canyon, Oregon and Idaho: *in* Vallier, T. L., and Brooks, H. C., (eds.), Geology of the Blue Mountains region: U.S. Geological Survey Professional Paper 1439 p. 55-73

White, J., White, D., Vallier, T., Stanley, G., Ash, S., (1992) Middle Jurassic strata link Wallowa, Olds Ferry, and Izee terranes in the accreted Blue Mountains island arc, northeastern Oregon: Geology v. 20 p.729-732

Wilson, D., and Cox, A., (1980) Paleomagnetic evidence for tectonic rotation of Jurassic plutons in Blue Mountains, eastern Oregon: Journal of Geophysical Research, v.85, p. 3681-3689.

Wright, P. J., (2005) Evidence for shear at the contact between the Huntington and Weatherby Formations, eastern Oregon: [B. S. Honors thesis] Eugene, Oregon, University of Oregon, 45 p.

Wyld, S. J., and Wright, J. E., (2001) New evidence for Cretaceous strike-slip faulting in the United States Cordillera and implications for terrane-displacement, deformation patterns, and plutonism: American Journal of Science v. 301 p. 150-181

Žák, J., Verner, K., Johnson, K., Schwartz, J. J., (2012) Magnetic fabric of Late Jurassic arc plutons and kinematics of terrane accretion in the Blue Mountains, northeastern Oregon: Gondwana Research v. 22 p. 341-352

APPENDIX A

Petrographic Analysis

LOM10-01

Geologic Setting

LOM10-01 was collected along Big Lookout Mountain road near the beginning of Morgan Creek. It is an igneous pluton that intrudes the Weatherby Formation, cross cuts the Connor Creek Fault, and the Burnt River schist of the Baker terrane during the Cretaceous. The exact location of this sample is 477260 E, 4929998 N.

Hand Sample Description

This is a medium-grained, non-porphyritic, biotite-hornblende tonalite.

Thin Section Description

Texture

This rock is a phaneritic intrusive igneous rock with no evidence of penetrative foliation.

Mineralogy

Quartz - 40% - Undulose extinction in only a few grains, most crystal boundaries are straight boundaries with only a minor amount of the grains showing irregular crystal boundaries, average size is 1-2 mm.

Plagioclase - 40% - Concentric compositional zoning is present in some grains with twinning over printing in a minor amount of crystals, average size is 2-3 mm.

Biotite - 14% - Pleochroic dark brown and green, average size is 3-4 mm.

Hornblende - 5% - Pleochroic dark and light green, found in close proximity and relation to biotite crystals, average size is 2-3 mm.

Accessory Minerals

Zircon - < 1% - Size is very variable with some as large as .1 mm.

Epidote - <1% - Average size is about 1 mm. The mineral appears to be magmatic in its origin.

Magnetite - <1% - Opaque, average size is about .5 mm.

Alteration

Alteration evidence is minor with only a small number of the crystal boundaries being irregular and only minor undulose extinction in a few of the quartz grains. Many of the plagioclase grains show concentric compositional zoning. The majority of these grains that show this complex zoning are not overprinted with polymorphic twinning as the grains without zoning show. The hornblende tends to appear amongst the biotite crystals.

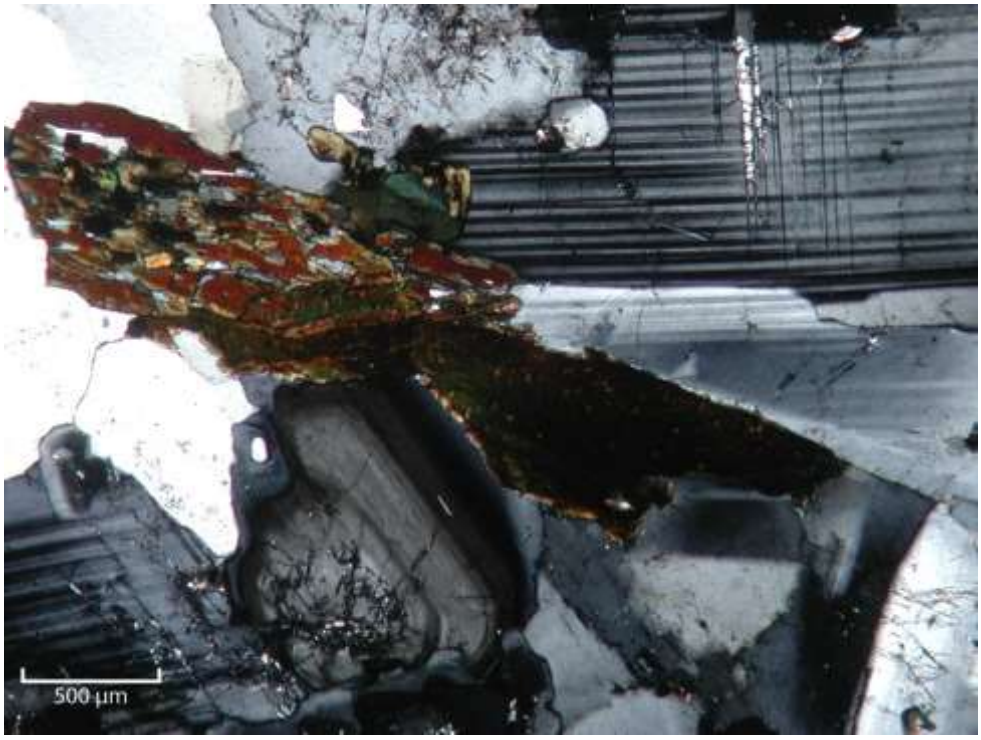

Figure A.1: Cross-polarized view of complexly zoned plagioclase grains a large grain of biotite altering to hornblende that can be distinguished by the differing birefringence. 40x magnification.

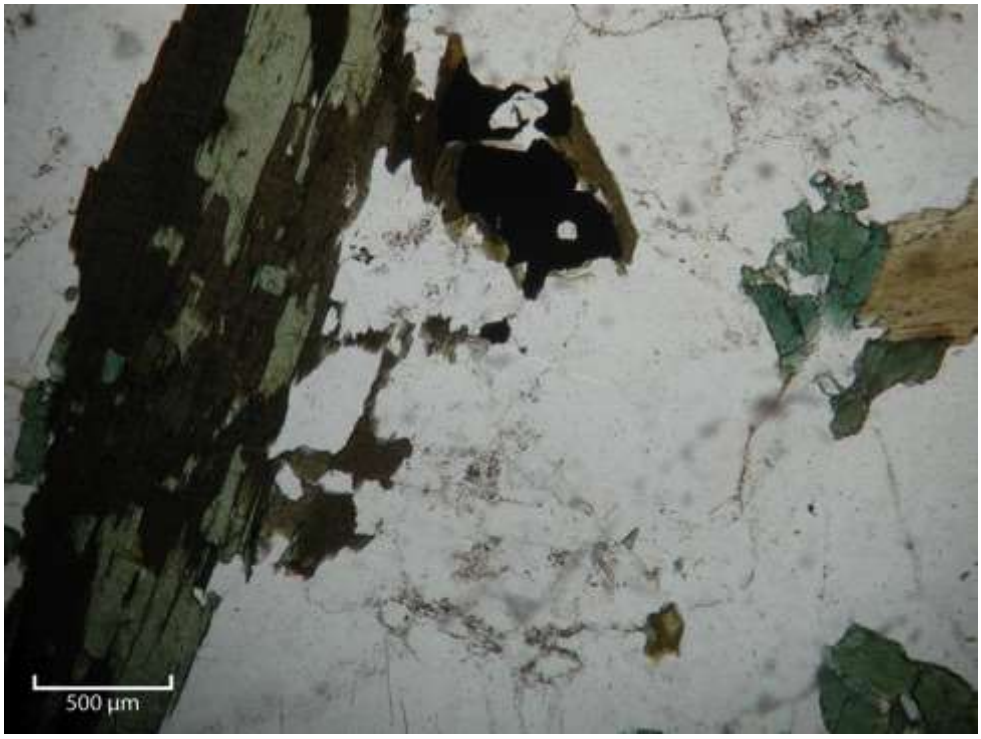

Figure A.2: Plain polarized view of a large biotite and hornblende grain that can be recognized by the different pleochroism; hornblende is pleochroic in shades of green and biotite is brown to green pleochroic.

LOM10-05

Geologic Setting

LOM10-05 was collected in Connor Creek. It is a coarse-grained volcaniclastic deposit within a section of fine-grained marine shales and siltstones deposits metamorphosed to phyllite that composes the upper Weatherby Formation. The exact location of this sample is 485700 E, 4930435 N.

Hand Sample Description

The sample is a poorly sorted, fine – medium-grained, volcanic-rich turbidite termed a primary volcaniclastic.

Thin Section Description

Texture

This sample contains an abundance of crystals and rock fragments full of phenocrysts. The crystals and phenocrysts are primarily plagioclase and quartz, with plagioclase being the most abundant. The phenocrysts present within the volcanic (andesite) lapilli are angular to subangular. Oxides and opaques fill the space between crystals all resting in a phyllitic matrix.

Mineralogy

Quartz -15% - Subhedral crystals, angular to subrounded, average size is .3-.5 mm.

Plagioclase - 60% - Subangular to angular crystals, polysynthetic twinning is present in most grains, wavy extinction in the grains that do not show strong twinning, average size is .3-.5 mm with some 1 mm size crystals present primarily in the volcanic lapilli.

Mica - 10% - elongate grains in areas with other grains filling the between spaces of the quartz and plagioclase, slight clear to brown pleochroism in plain polarized light.

Altered Minerals

Altered Plagioclase - 5% - blue extinction color in cross-polarized light, very low relief, white in plane polarized light.

Altered Pyroxene - 3% - High relief, 3rd order birefringence, brown/orange in plane-polarized light, found only within lithic fragments.

Alteration

The plagioclase phenocrysts do not appear to be heavily altered. The phyllitic groundmass displays a minor foliation.

Figure A.3: Photomicrograph of subangular, twinned plagioclase crystals within volcanic lapilli of LOM10-05. 40x magnification.

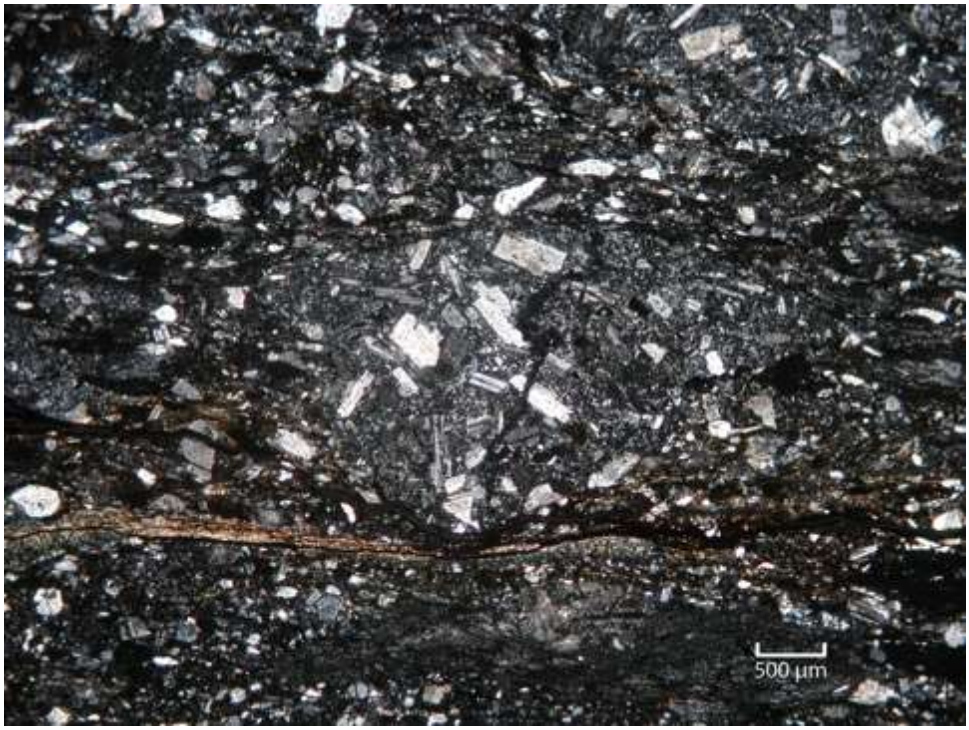

Figure A.4: Photomicrograph of a volcanic lapilli with an abundance of angular to subangular plagioclase phenocrysts. 20x magnification.

LOM11-06a

Geologic Setting

LOM11-06 was collected along Lookout Mountain road. It is a coarse-grained deposit within a section of siltstone and shale marine deposits metamorphosed to phyllite that composes the majority of the Weatherby Formation. This sample was collected low in the section from an area of a high abundance of these coarser grained sections. The exact location of this sample is 476490 E, 4926855 N.

Hand Sample Description

This sample is a secondary sandstone deposit. Sample has a red/brown color on weathered surfaces. Contains stretched medium grains. The grains that do not show evidence of stretching are subangular to angular with an average size of 2-3 mm.

Thin Section Description

Texture

The quartz crystals not heavily deformed or altered with subrounded to angular grains, suggesting that transport of this material was not a great distance from the source. Oxides fill the space between the lithic fragments and inside the lithic fragments. One or two grains of quartz-rich sand grains can be clearly distinguished along with a small abundance of chert grains.

Mineralogy

Quartz - 20% - Angular to subrounded grains, average size is .5 mm with occasional grains at about 1 mm, some in the form of chert clasts.

Accessory Minerals

Altered Pyroxene - < 1% - High relief, high birefringence orange red, green pleochroism average size is .4 cm.

Alteration

Many of the lithic fragments show signs of alteration. Some of the alteration is to a low relief 2nd order birefringence mineral. One large lithic fragment has a reaction ring around the grain with an abundance of rutile phenocrysts. Coarse-grained material rests in a metamorphic groundmass.

Figure A.5: Plain-polarized (left) and cross-polarized (right) view of an altered pyroxene grain within sample LOM11-06, indicating detritus sourced from volcanic material. 40x magnification.

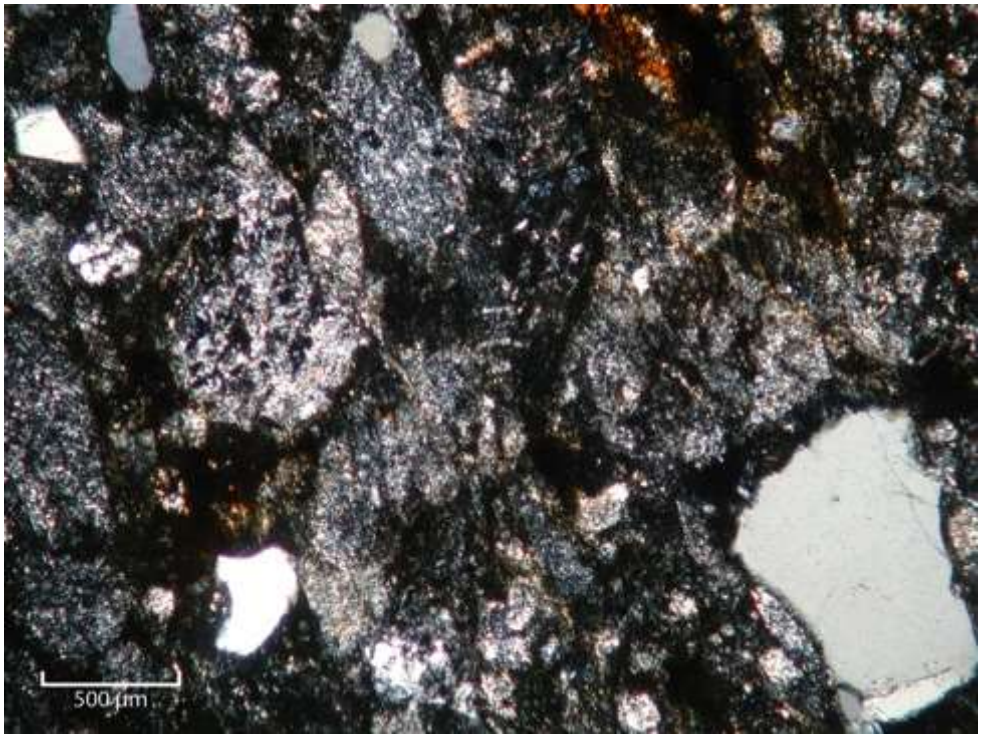

Figure A.6: Photomicrograph showing a typical section from LOM11-06a with subrounded quartz grains visible within a metamorphic phyllite groundmass. Cross Polarized, 40x magnification.

LOM11-07

Geologic Setting

LOM11-07 was collected along Lookout Mountain road. It is a tuffaceous sandstone above a black shale deposit within the area of the Weatherby Formation. This sample was collected in close proximity to the Connor creek fault and Lookout Mountain Pluton. The exact location of this sample is 477176 E, 4928843 N.

Hand Sample Description

This is fine to very fine-grained tuffaceous sandstone. Clean surface is a light grey with darker spots of the same size. Weathered surfaces are primarily tan to rust red with some grey still visible.

Thin Section Description

Texture

Tuffaceous sandstone containing subrounded to rounded plagioclase and rounded quartz grains. Secondary mica crystals are present overprinting the plagioclase grains and quartz matrix.

Mineralogy

Quartz - 20% - large clasts are rounded, majority of the quartz present in this sample makes up the matrix material

Plagioclase - 25% - Subangular to subrounded crystals, carlsbad twinning, moderately altered, average size is .6 – 1 mm.

Mica - 30% - 2^{nd} order birefringence primarily orange and red, clear in plain polarized light

Alteration

All of the plagioclase crystals show evidence of alteration giving them a hazy look in plain polarized light. Primary and secondary mica is present. Some of the mica crystals grow around the plagioclase crystals while some clearly have grown in overprinting the plagioclase crystals. The secondary mica crystals have grown due to the metamorphism that has affected this area post deposition.

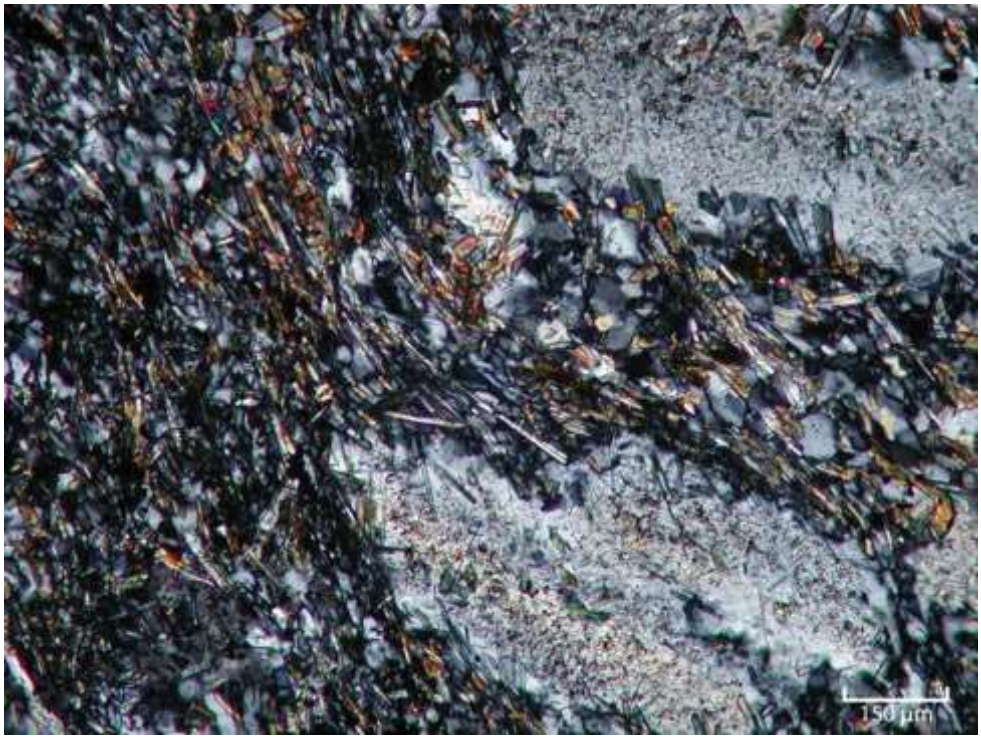

Figure A.7: Cross-polarized view of secondary mica crystals growing within the plagioclase crystals of LOM11-07. 100x magnification.

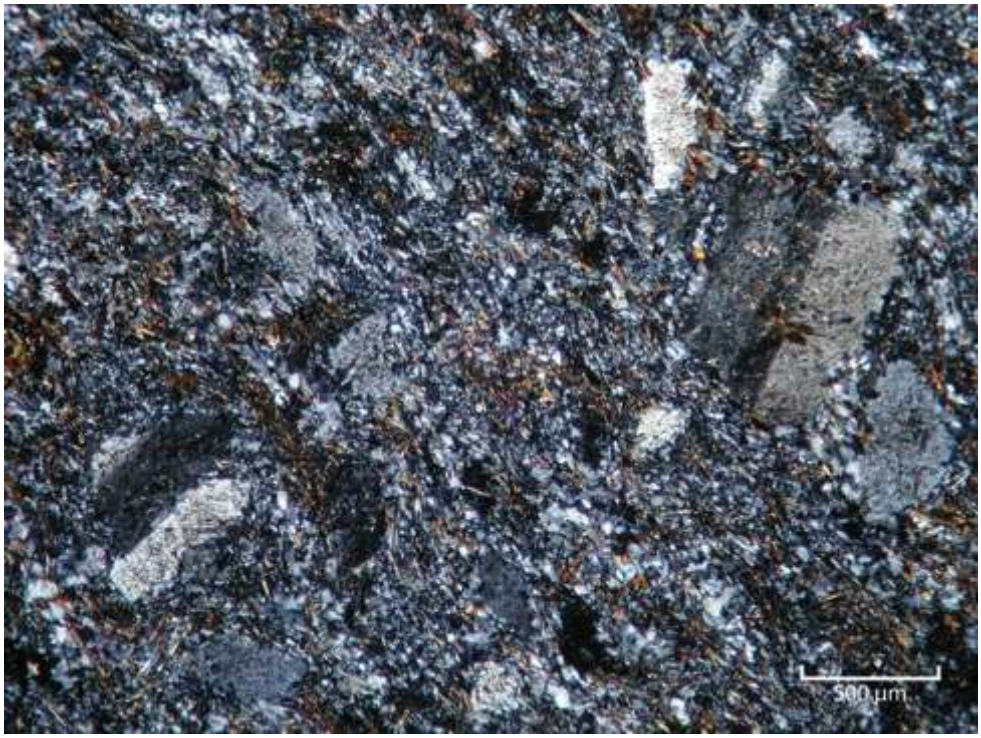

Figure A.8: Photomicrograph from a typical section of LOM11-07 where primary mica crystals can be observed growing around the plagioclase crystals and secondary mica overprinting the Plagioclase crystals. 40x magnification.

LOM11-12

Geologic Setting

LOM11-12 was collected along Big Lookout Mountain road. It is a coarse-grained volcaniclastic deposit within a section of siltstone and shale marine deposits metamorphosed to phyllite that composes the majority of the Weatherby Formation. The exact location of this sample is 474331 E, 4925278 N.

Hand Sample Description

This is a secondary sandstone deposit. Sample is greenish grey weathered to an orange/tan color. Contains stretched opaque lithic fragments and stretched quartz-rich sand grains up to about 1 cm long.

Thin Section Description

Texture

This sample contains stretched chert and remnant volcanic lapilli fragments in a phyllitic texture.

Mineralogy

Quartz - 15%- Subangular to subrounded grains, average size is .5 mm with occasional grains at about 1 mm, some in the form of chert clasts

Alteration Minerals

Calcite - 10% - high order birefringence colors

Alteration

LOM11-12 is recognizable foliated. Occasional quartz grains a scattered throughout the sample with no evidence of heavy deformation, no undulose deformation, grain boundaries are intact, and the grains are subrounded to angular. The shape of the quartz grains suggest that this samples source was not a great distance away. The calcite present in this sample could possibly be altered from plagioclase within lithic fragments. Phyllitic matrix has a defined foliation.

Figure A.9: Chert clast found within sample LOM11-12 within the well defined planar fabric. 40x magnification.

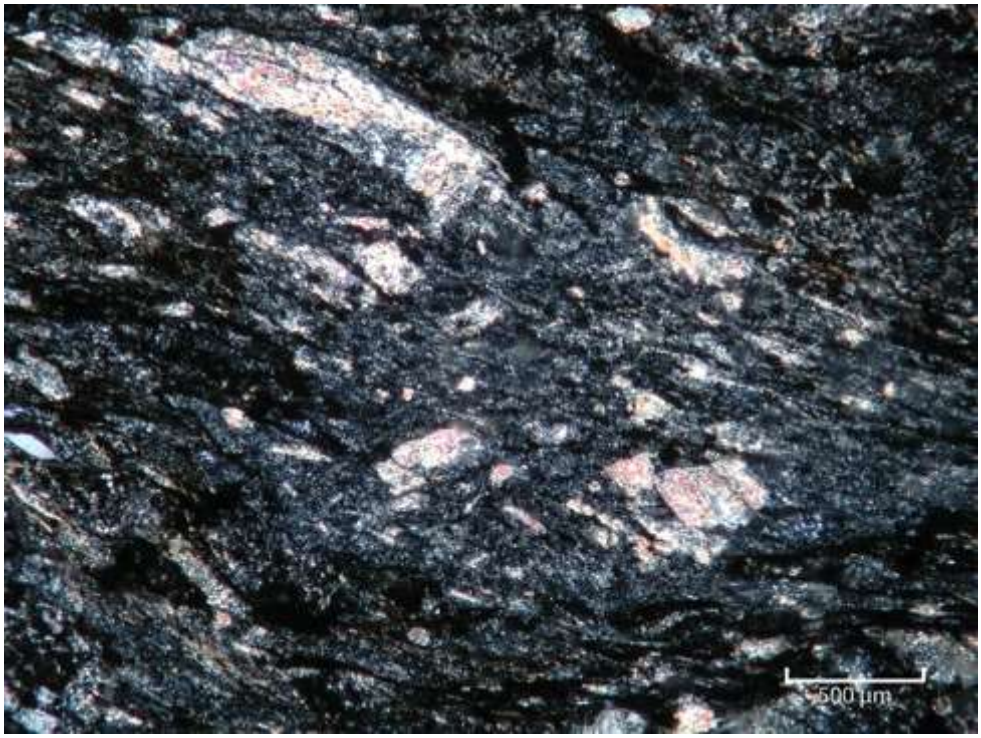

Figure A.10: Photomicrograph from LOM11-12 showing a stretched lithic fragment with an abundance of calcite. 40x magnification.

LOM11-13

Geologic Setting

LOM11-13 was collected in Connor Creek. It is a very coarse-grained poorly sorted volcaniclastic deposit within a section of siltstone and shale marine deposits metamorphosed to phyllite that compose the upper part of the Weatherby Formation. The exact location of this sample is 485066 E, 4931841 N.

Hand Sample Description

This sample is a poorly sorted, medium-grained volcanic-rich turbidite deposit termed primary volcaniclastic.

Thin Section Description

Texture

Volcanic lapilli contain exclusively fragmented plagioclase phenocrysts. No distinguishable foliation is present

Mineralogy

Quartz - 30% - Primary crystal grains that are unaltered and altered fragmented grains with cracks throughout compose the majority, anhedral grains, clear in plane polarized light for the unaltered grains, grey for the altered fragmented grains, average size of crystal grains about .5 mm, average size of fragments 1 mm.

Plagioclase - 15% - Euhedral to subhedral grains, polysynthetic twinning present in majority of grains, highly fragmented and heavily altered, grey in plane polarized light, average size is 1mm outside lithic fragments and .3 mm within the lithic fragments.

Altered Mineralogy

Calcite – 5% - green to tanish color in plan polarized light.

Alteration

All of the plagioclase grains show signs of alteration making them look dirty. The plagioclase and quartz grains that compose the majority of the section are heavily fragmented. Calcite is present in spaces between fragmented plagioclase crystals. Not much foliation or lineation can be observed in this sample.

Figure A.11: Plain polarized view showing the abundance of euhedral quartz and plagioclase crystals within LOM11-13. 40x magnification.

Figure A.12: Cross-polarized view of twinned plagioclase crystals within volcanic lapilli of LOM11-13. 40x magnification.

DC11-01

Geologic Setting

DC11-01 was collected about 150 m stratigraphically above the Dennet creek Limestone in Dennet Creek, Idaho. DC11-01 is a coarse-grained primary volcaniclastic horizon within the primarily flysch sediments of the Weatherby Formation. The exact location of this sample is 492706 E, 4934345N.

Hand Sample Description

This sample is a fine to medium coarse-grained volcanic turbidite deposit termed primary volcaniclastic. Coarse-grained material both lithic and quartz grains within this sample shows significant stretching. Bedding planes can be observed clearly between coarse and fine-grained layers.

Thin Section Description

Texture

Very fine-grained strongly foliated

Mineralogy

Quartz - 5% - rounded, many grains are heavily altered minor amount are not, all have undulose alterations.

Plagioclase - 15% - heavily altered towards clay, light to clear in plain polarized light.

Mica - 10% - elongate grains filling between spaces, dark to light brown pleochroism in plain polarized light.

Accessory Minerals

Magnetite - 3% - Opaque, fill in spaces within fabric

Altered Minerals

Pyroxene - 5% - high relief, 2nd order birefringence colors, clear in plain polarized light, range in size form .3-.5 mm.

Alteration

DC11-01 is a phyllite sample with a minor amount of altered olivine and pyroxene crystals within the metamorphic groundmass primarily composed of mica and quartz. Quartz and calcite veins cross cut the metamorphic foliation. The plagioclase is heavily altered to clay; no twinning within the plagioclase crystals can be viewed. This sample is heavily foliated with the metamorphic groundmass curving around the quartz and plagioclase crystals.

Figure A.13: Photomicrograph from DC11-01 showing an altered pyroxene grain within the heavily foliated texture and planar fabrics. 40x magnification.

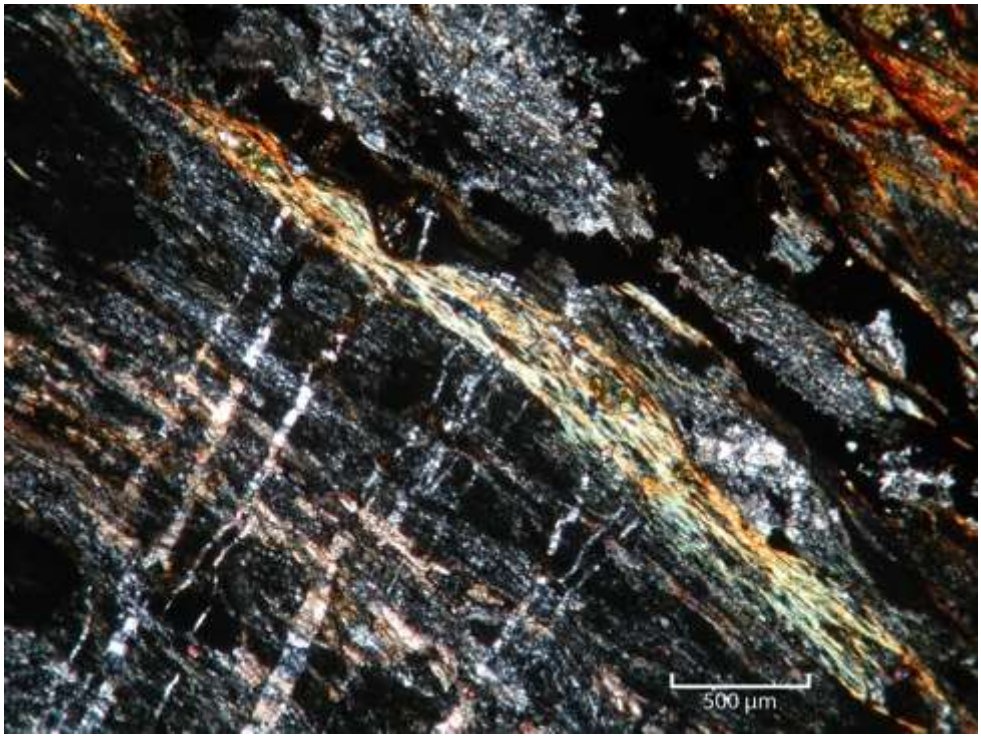

Figure A.14: Photomicrograph from DC11-01 showing the planar fabrics with magnetite within the foliation and later quartz veins cross-cutting the foliation. 40x magnification.

DC11-04

Geologic Setting

DC11-04 was collected up the slopes of Big Hill on the north side of Dennet Creek. DC11-04 is a coarse-grained horizon within the fine-grained phyllite that comprises the majority of the Weatherby Formation. The exact location of this sample is 492685 E, 4934590 N

Hand Sample Description

This is a fine to very fine-grained secondary volcanic sandstone.

Thin Section Description

Texture

This sample displays a heavy foliation. The phyllitic fabric wraps around many of the quartz and plagioclase grains forming shear stress indicators.

Mineralogy

Quartz - 15% - Rounded crystals, minor undulose extinction, and ranges in size from .1-.5 mm.

Plagioclase - 5 % - Subrounded grains, moderate, polysynthetic twinning is present in most grains however all the plagioclase shows evidence of heavy alteration, average size is about .4.mm.

Calcite - 15% - elongate grains, high order birefringence pink colors, twinning. Sizes range from .3 - .7 mm.

Mica - 20% - elongate grains filling between spaces, clear in plain polarized light.

Alteration

The quartz is rounded to subround with minor amounts of undulose alteration. The calcite is crystalline with little deformation with some grains displaying twinning and striations. The plagioclase is the least abundant of the larger crystals and shows evidence of alteration while continuing to display polysynthetic twinning.

Figure A.15: Plain polarized view of plagioclase (lower right), calcite (upper left), and quartz crystals within the planar fabric of DC11-04 with shear stress indicators present on some grains. 40x magnification.

Figure A.16: Cross-polarized view of subrounded, twinned plagioclase (lower right), calcite (upper left), and subrounded quartz crystals within the planar fabric of DC11-04 with shear stress indicators present on some grains. 40x magnification.

APPENDIX B

Cathodoluminescence Images

VOLCANIC SANDSTONES

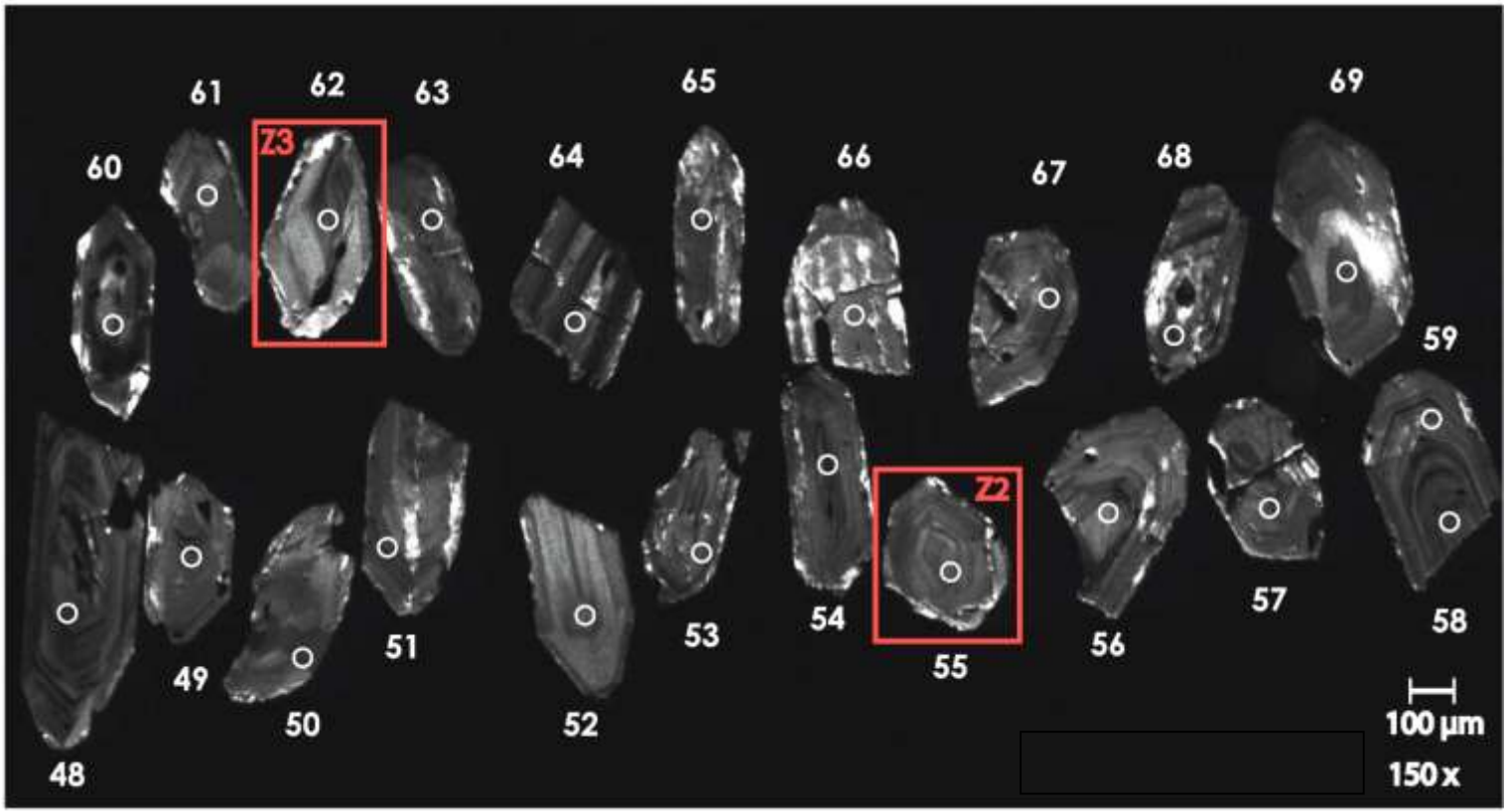

Figure B.1: CL images of sample LOM11-18. White circles represent 40-micrometer spot size locations. Numbers above or below grains is the LA-ICPMS analysis number. Red boxes and red number represent grains plucked for U-Pb geochronology using the CA-TIMS method.

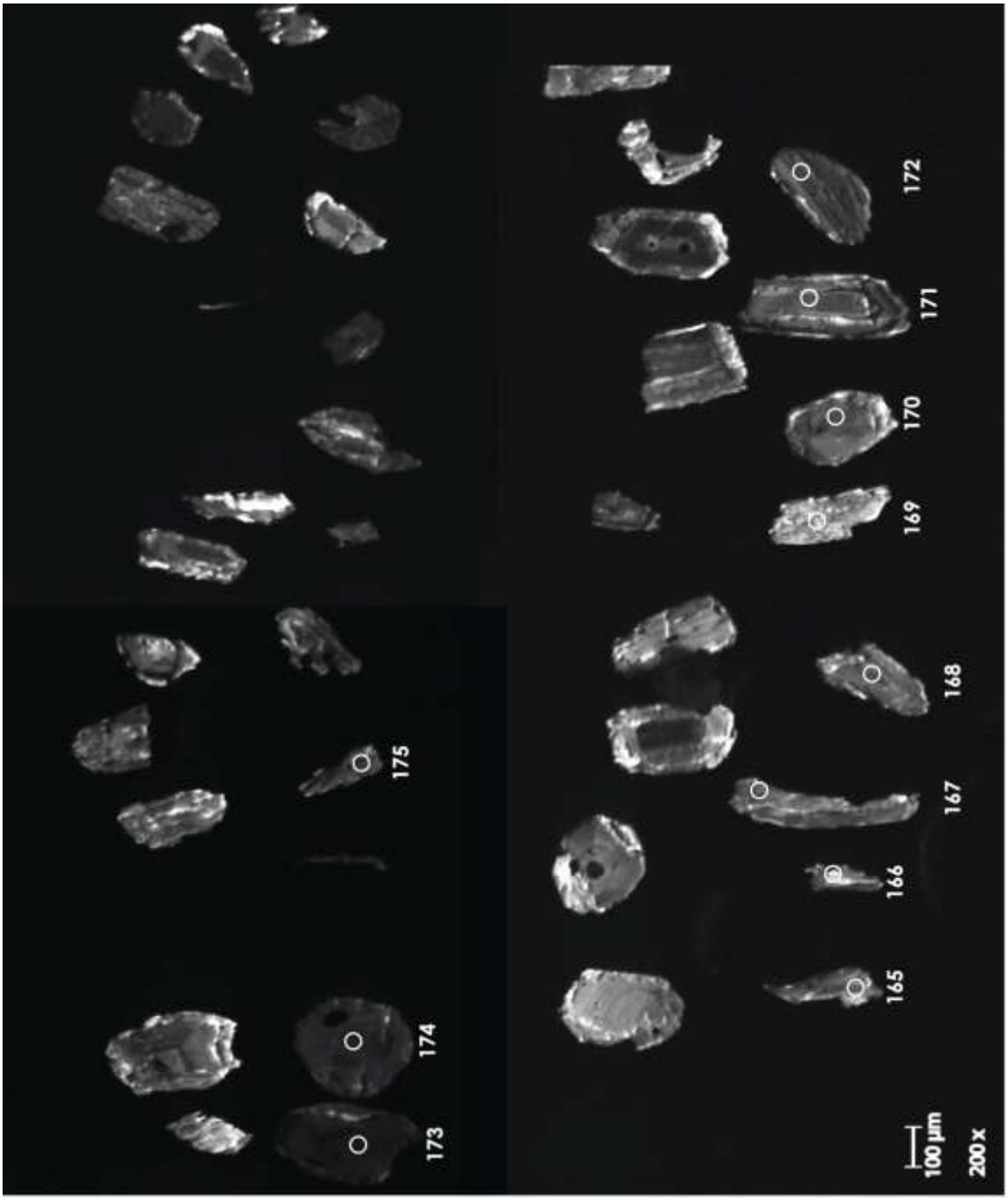
165
166
167
168
169
170
171
172
173
174
175
100 µm
200 x

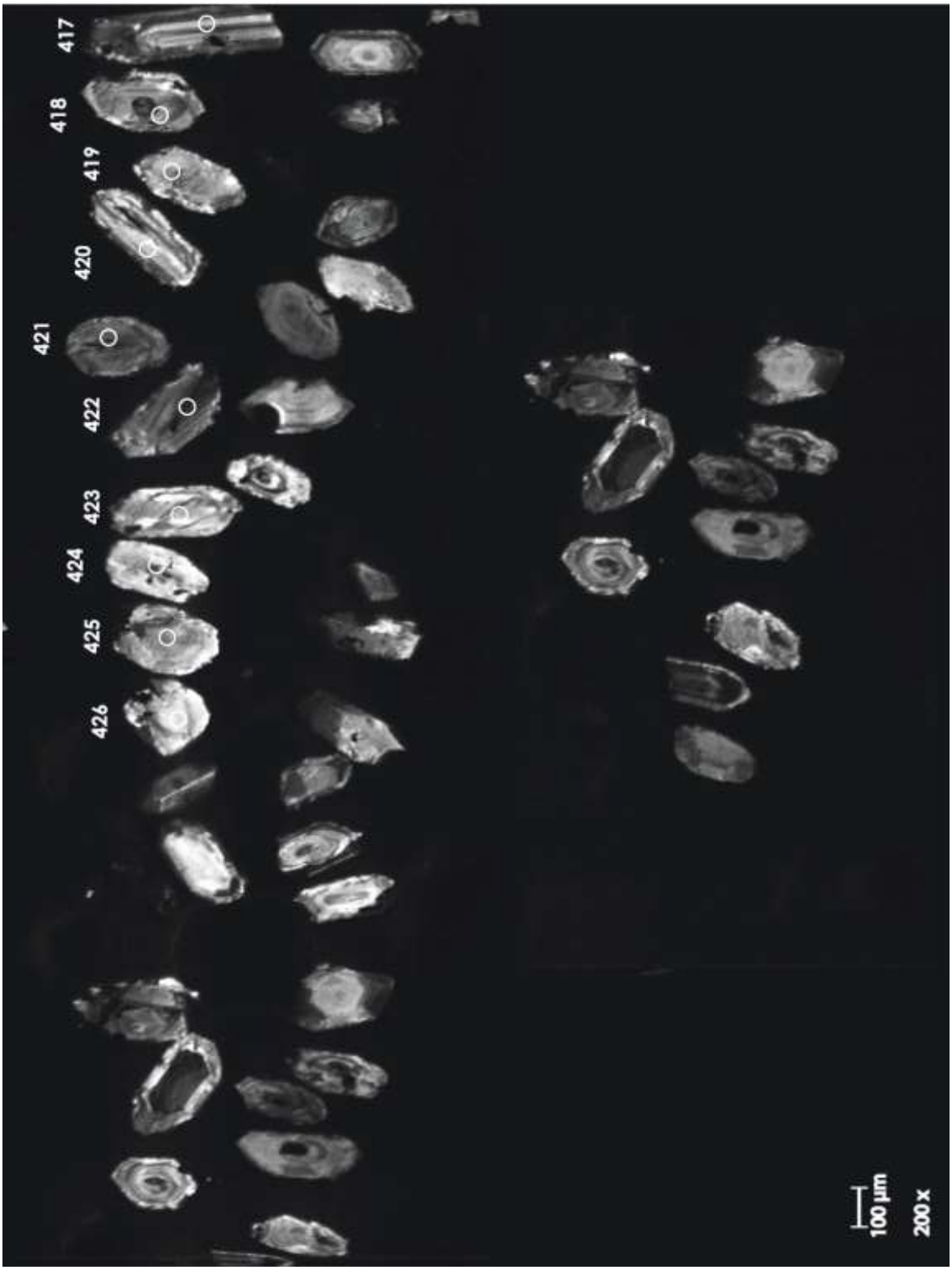
417
418
419
420
421
422
423
424
425
426
100 µm
200 x

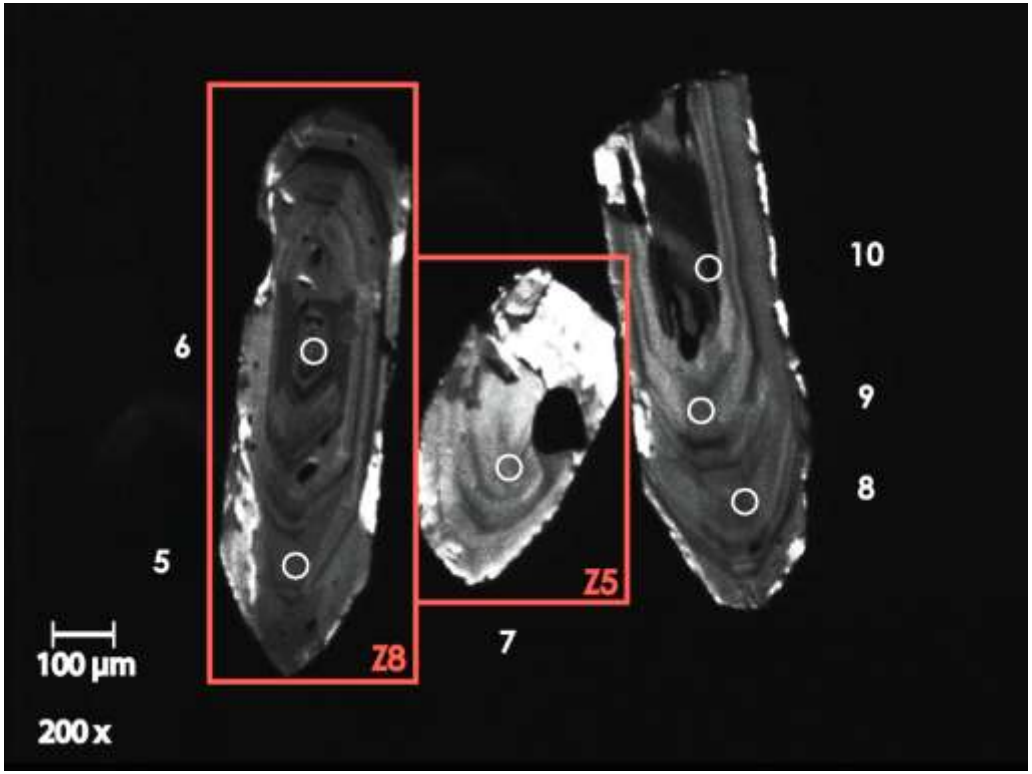

Figure B.2: CL images of sample LOM11-12. White circles represent 40-micrometer spot size locations. Numbers above, below, or beside grains is the LA-ICPMS analysis number. Red boxes and red numbers represent grains plucked for U-Pb geochronology using the CA-TIMS method.

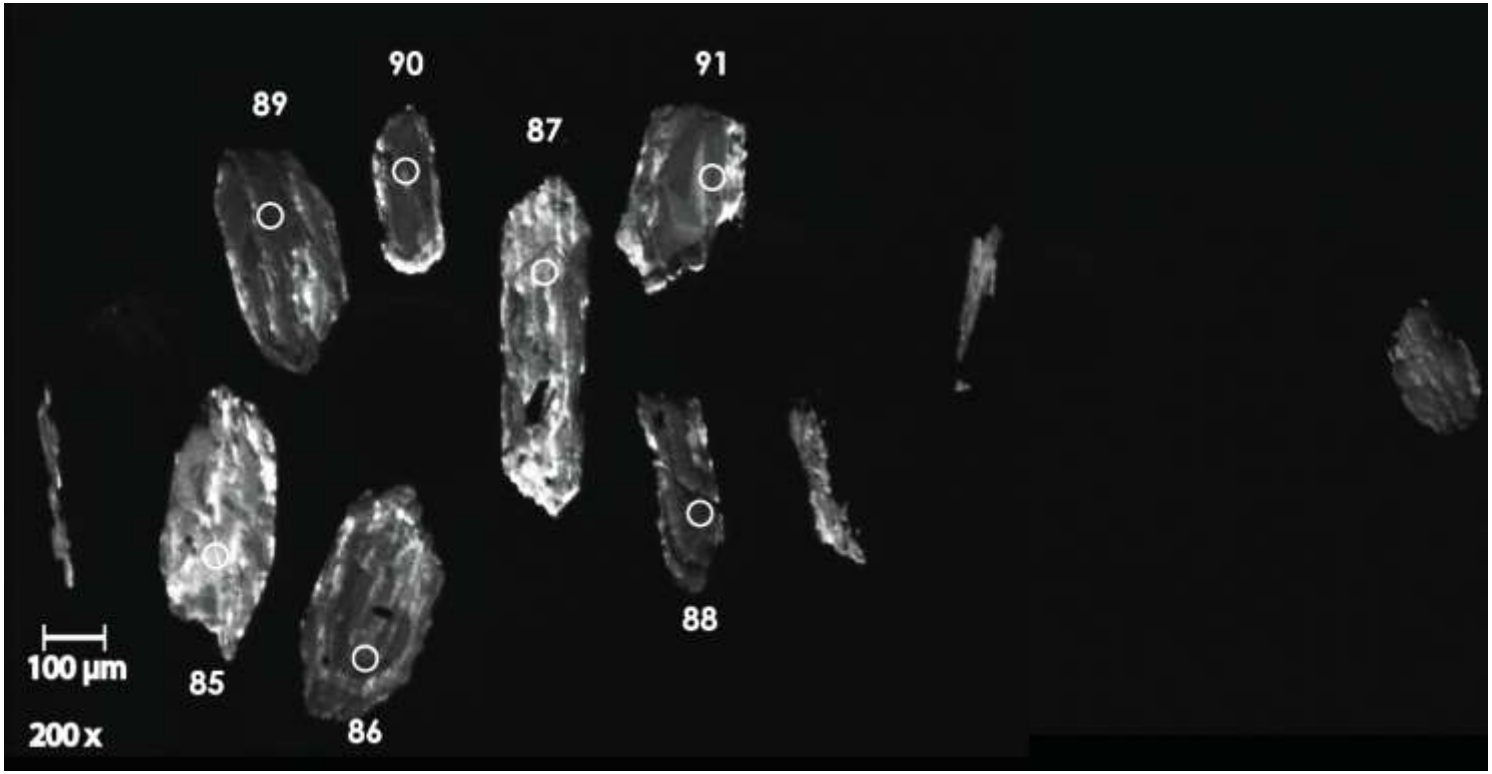
90
91
89
87
88
100 µm
85
200 x
86

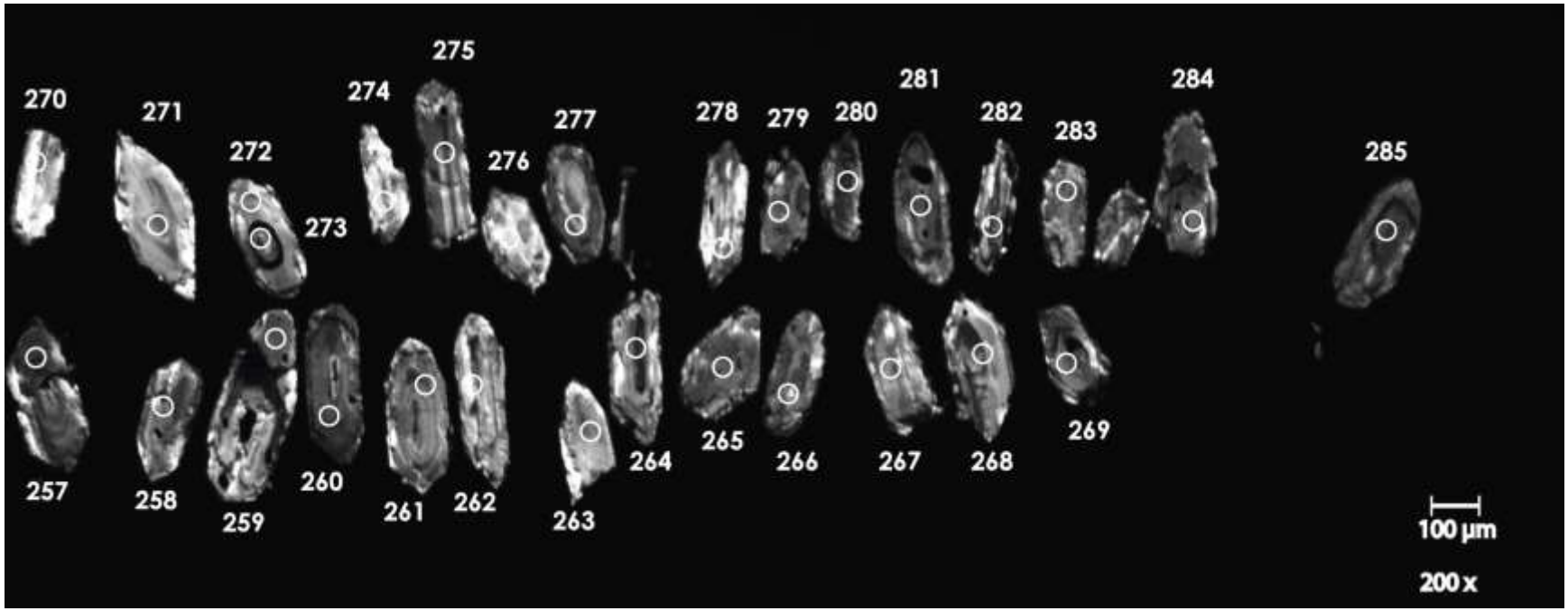
270
271
272
273
274
275
276
277
278
279
280
281
282
283
284
285
257
258
259
260
261
262
263
264
265
266
267
268
269
100 µm
200 x

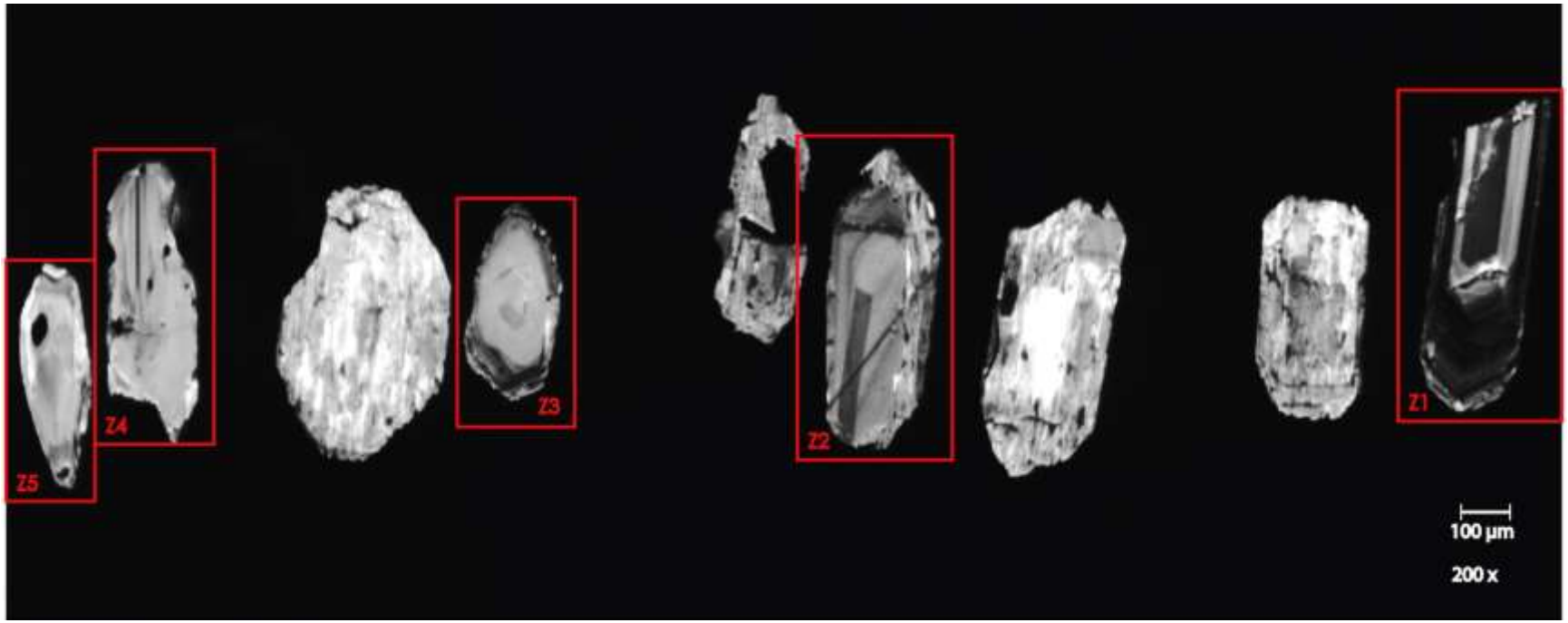

Figure B.3: CL images of sample LOM11-06a. White cycles represent 40-micrometer spot size locations. Numbers above or below grains is the LA-ICPMS analysis number. Red boxes and red numbers represent grains plucked for U-Pb geochronology using the CA-TIMS method. (Medium 1) represents initial grains chosen for U-Pb geochronology using the CA-TIMS method.

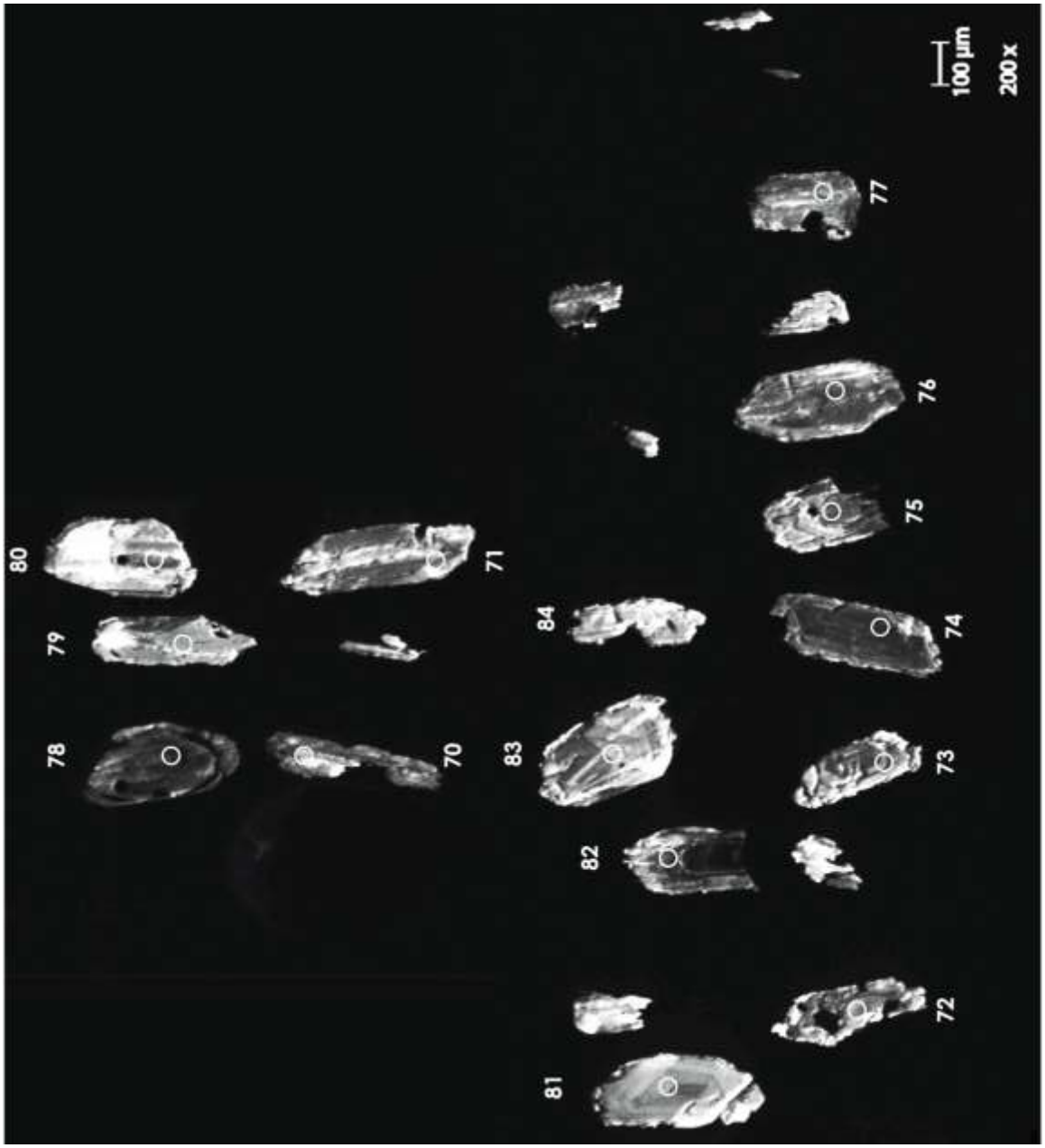
80
79
78
71
70
84
83
82
81
77
76
75
74
73
72
100 µm
200 x

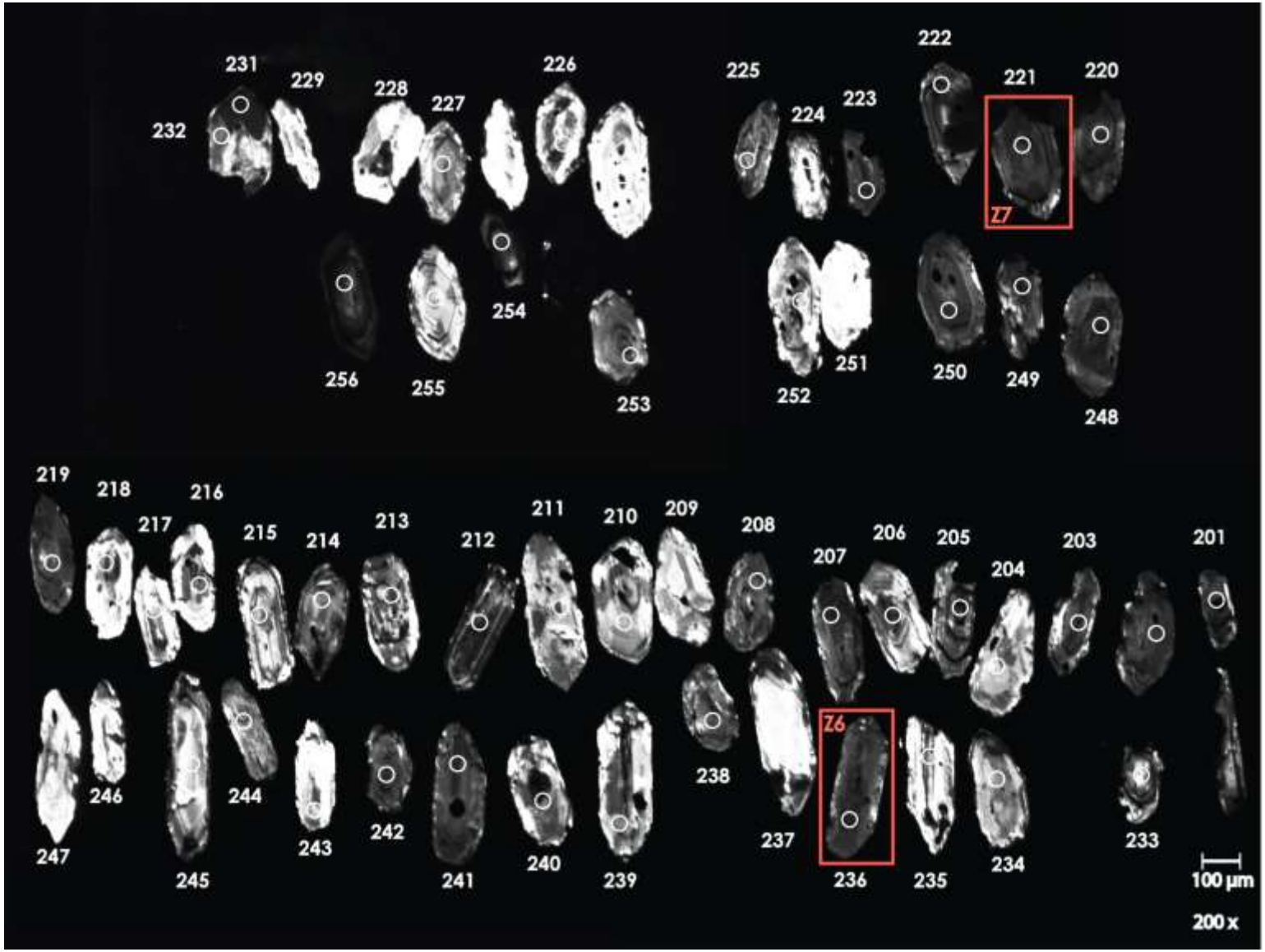
231
229
228
227
226
225
224
223
222
221
220
232
Z7
254
256
255
253
252
251
250
249
248
219
218
216
217
215
214
213
212
211
210
209
208
207
206
205
204
203
201
Z6
246
244
238
247
245
243
242
241
240
239
237
236
235
234
233
100 µm
200 x

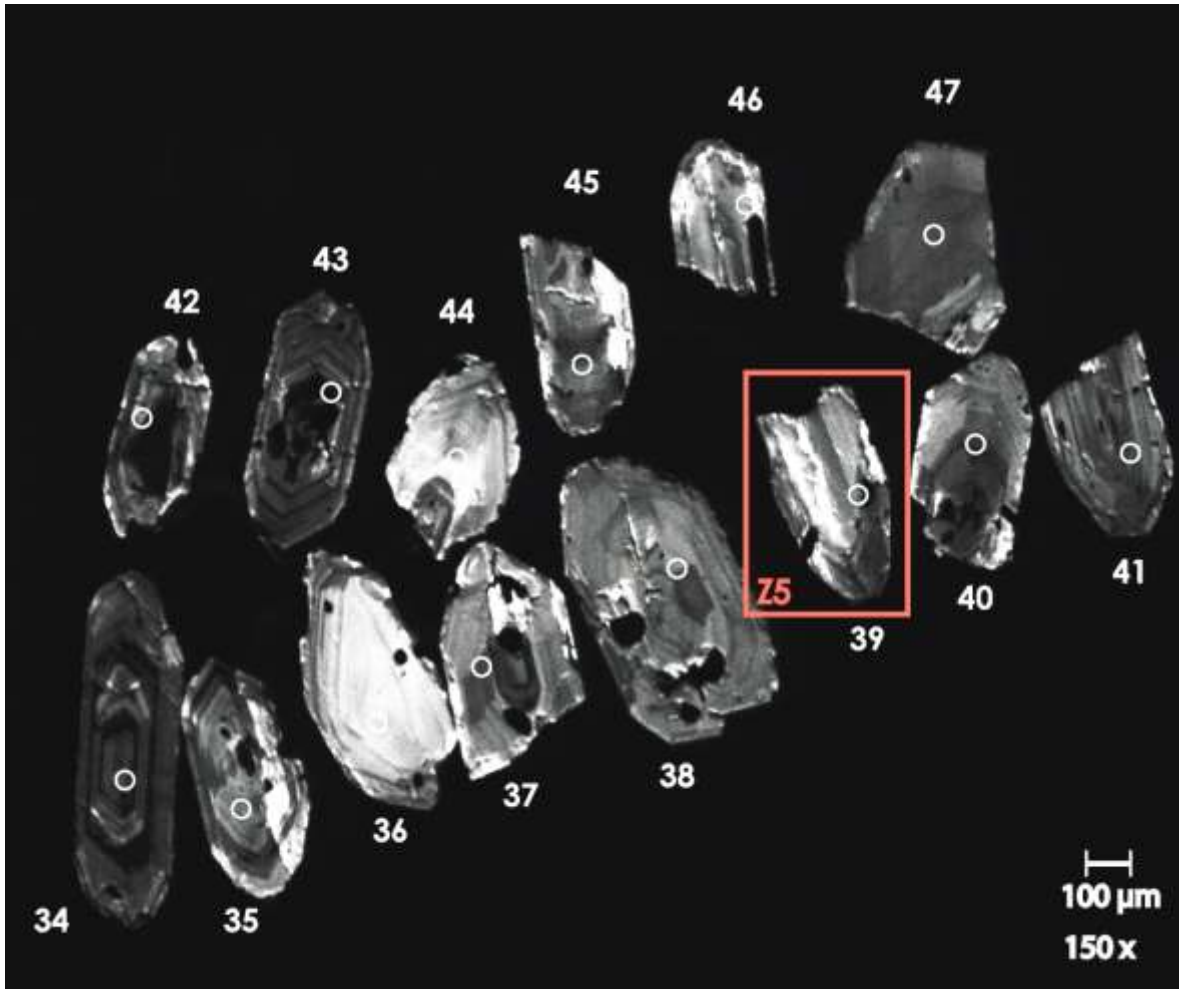

Figure B.4: CL images of sample LOM11-17. White cycles represent 40-micrometer spot size locations. Numbers above or below grains are the LA-ICPMS analysis number. Red boxes and red numbers represent grains plucked for U-Pb geochronology using the CA-TIMS method.

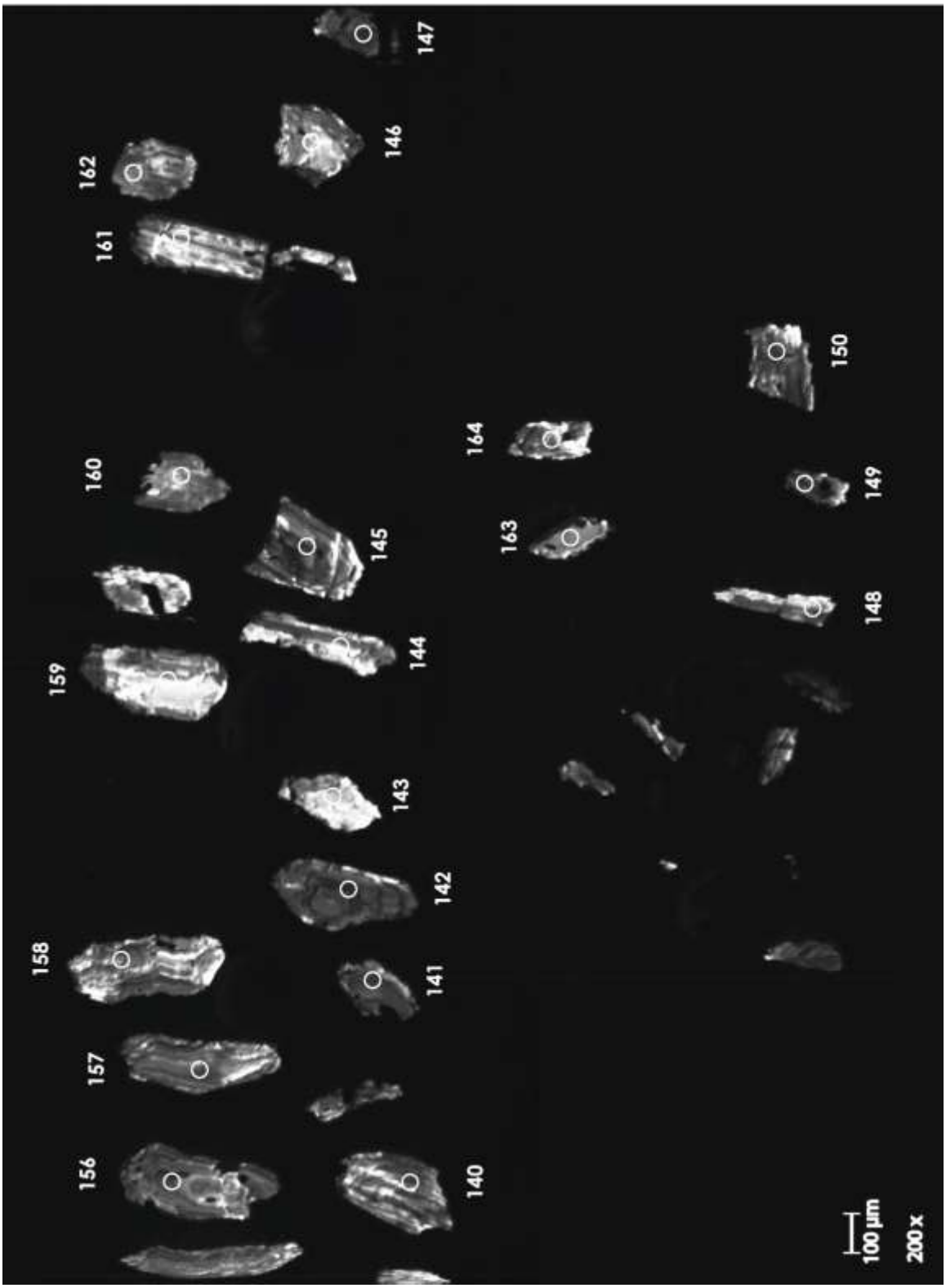
140
141
142
143
144
145
146
147
148
149
150
156
157
158
159
160
161
162
163
164
100 µm
200 x

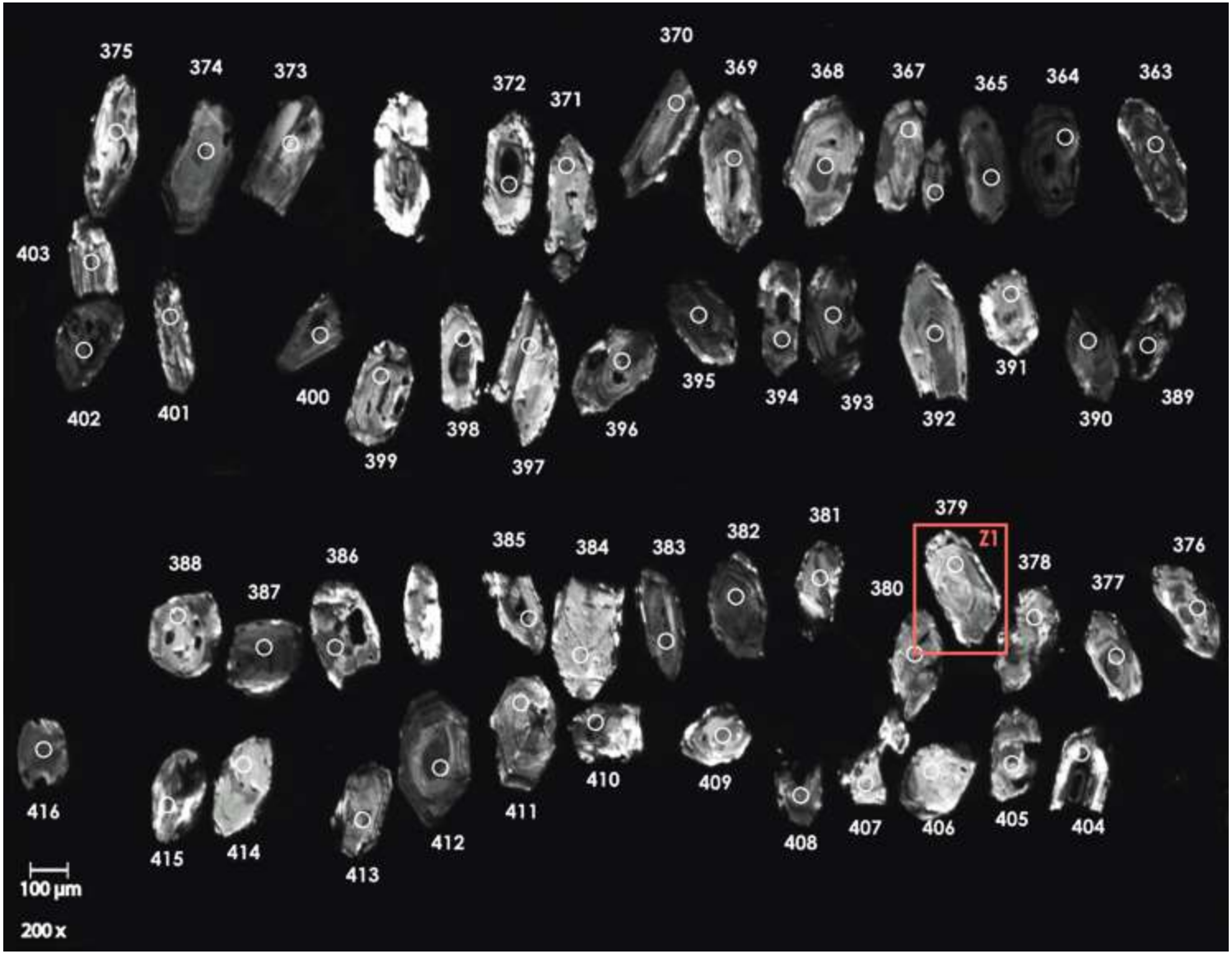
375
374
373
372
371
370
369
368
367
365
364
363
403
402
401
400
399
398
397
396
395
394
393
392
391
390
389
388
387
386
385
384
383
382
381
379
Z1
380
378
377
376
416
415
414
413
412
411
410
409
408
407
406
405
404
100 µm
200 x

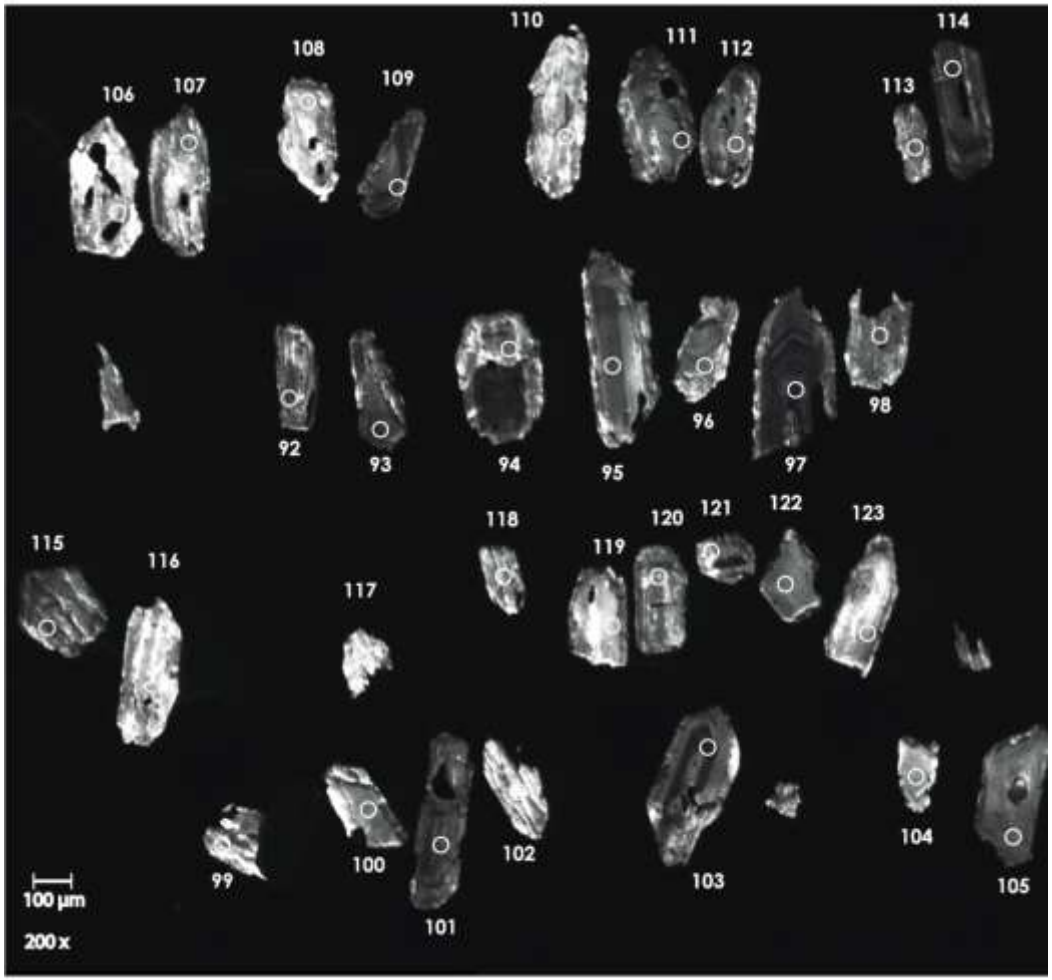

Figure B.5: CL images of sample DC11-05. White cycles represent 40-micrometer spot size locations. Numbers above or below grains are the LA-ICPMS analysis number. Red boxes and red numbers represent grains plucked for U-Pb geochronology using the CA-TIMS method.

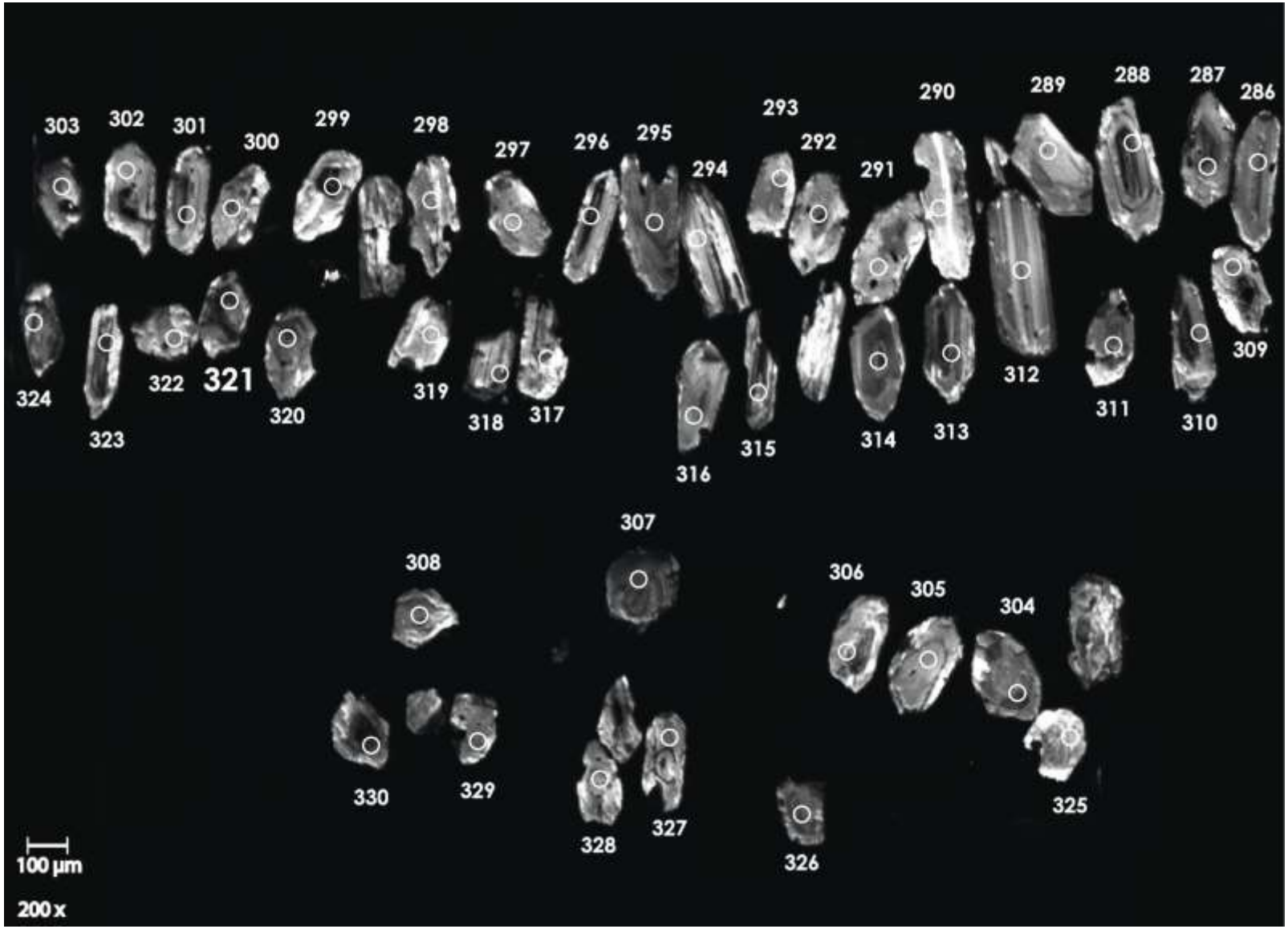
303
302
301
300
299
298
297
296
295
294
293
292
291
290
289
288
287
286
324
323
322
321
320
319
318
317
316
315
314
313
312
311
310
309
308
307
306
305
304
330
329
328
327
326
325
100 µm
200 x

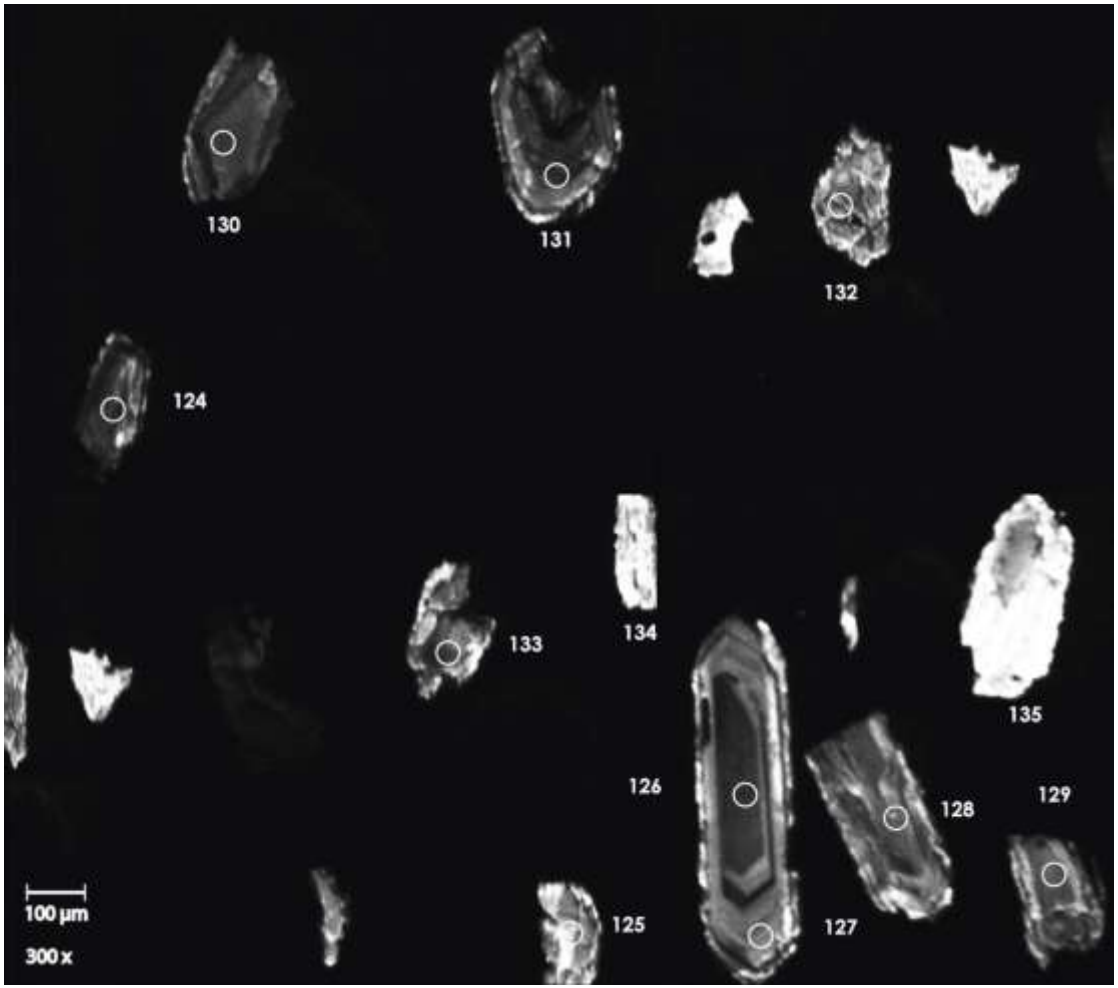

Figure B.6: CL images of sample DC11-04. White cycles represent 40-micrometer spot size locations. Numbers above, below, or beside grains are the LA-ICPMS analysis number. Red boxes and red numbers represent grains plucked for U-Pb geochronology using the CA-TIMS method.

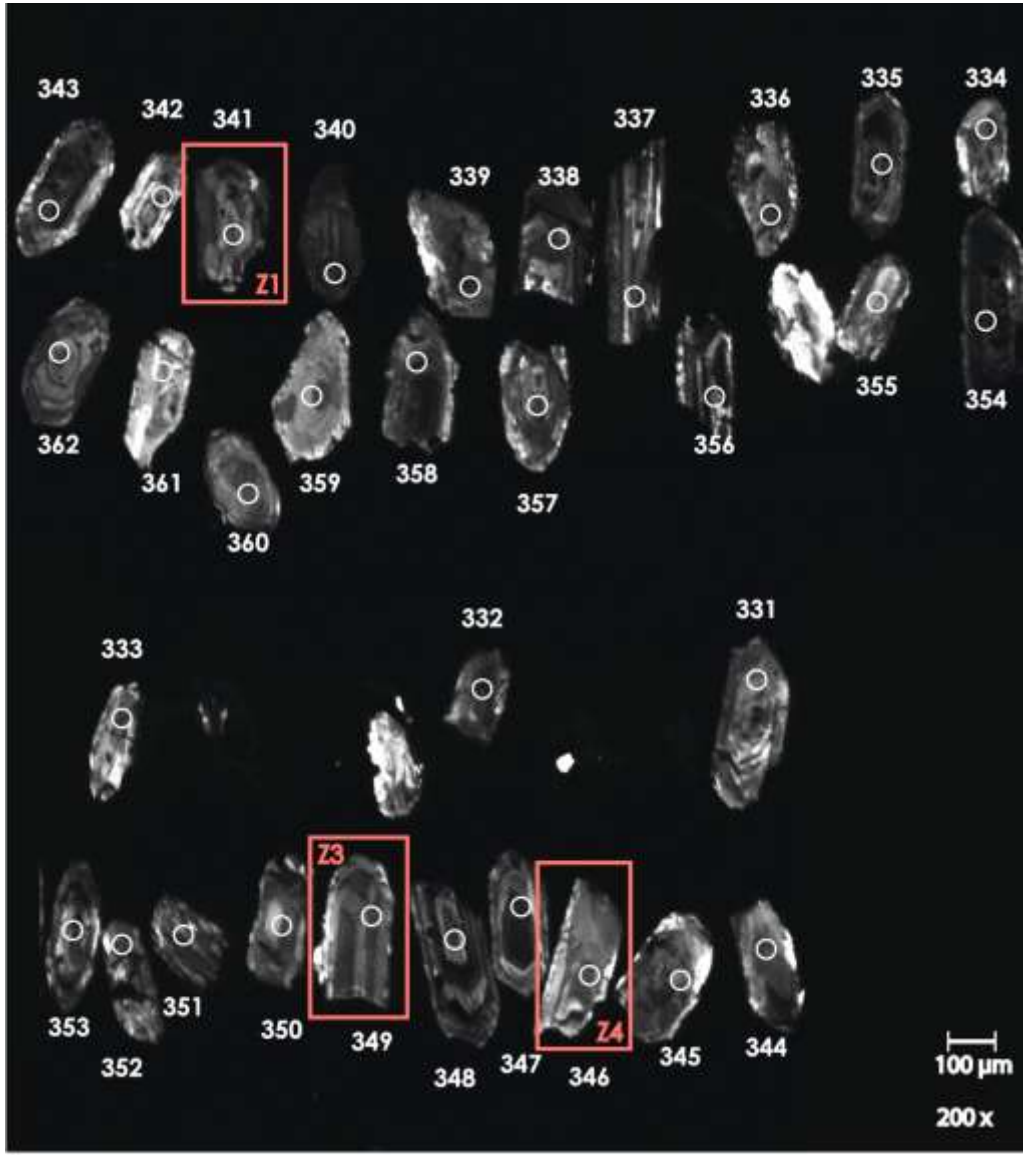
343
342
341
340
339
338
337
336
335
334
Z1
362
361
360
359
358
357
356
355
354
333
332
331
Z3
Z4
353
352
351
350
349
348
347
346
345
344
100 µm
200 x

PLUTONS

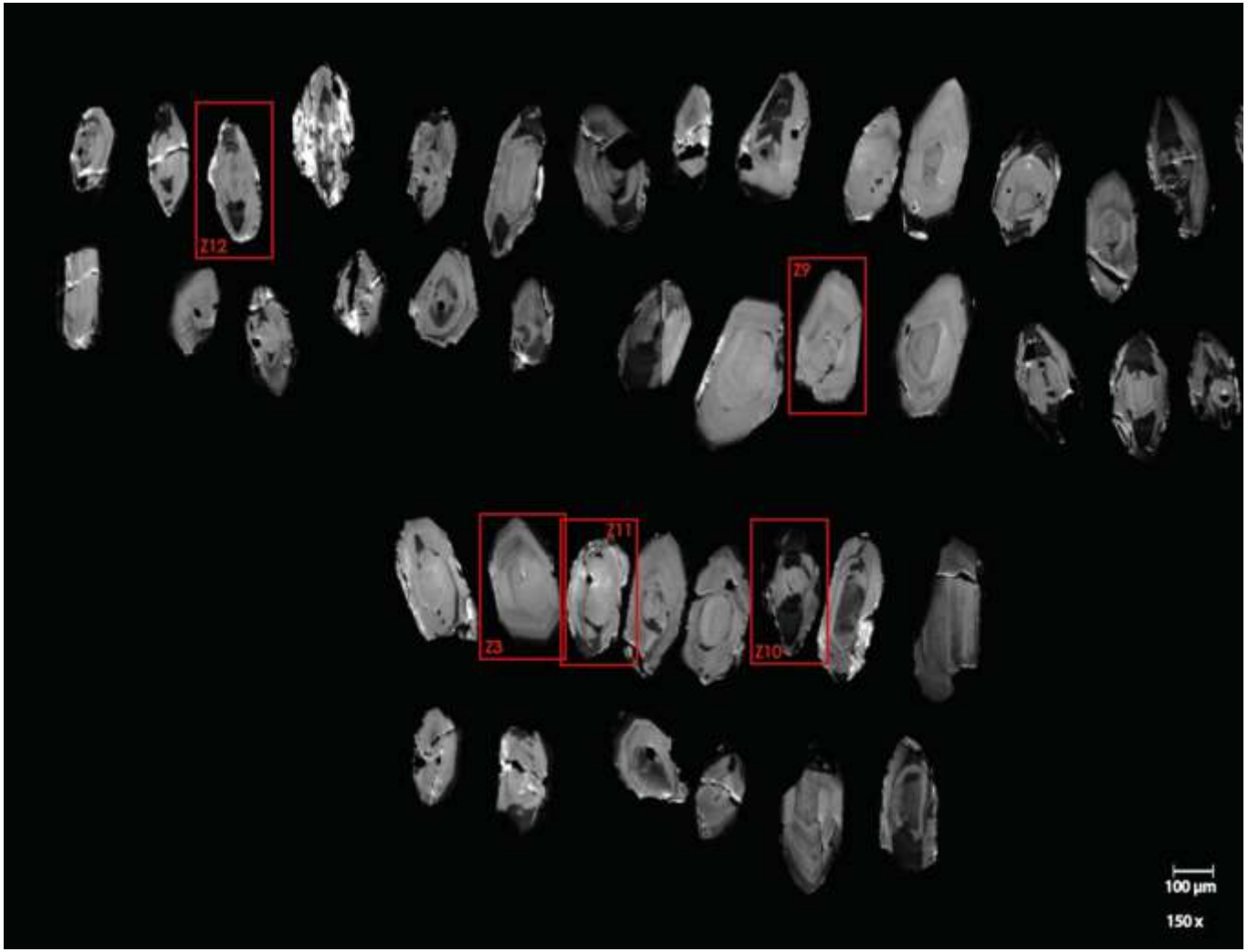

Figure B.7: CL image of zircons from Tureman Ranch pluton. Red boxes and red numbers represent grains plucked for CA-TIMS U-Pb geochronology.

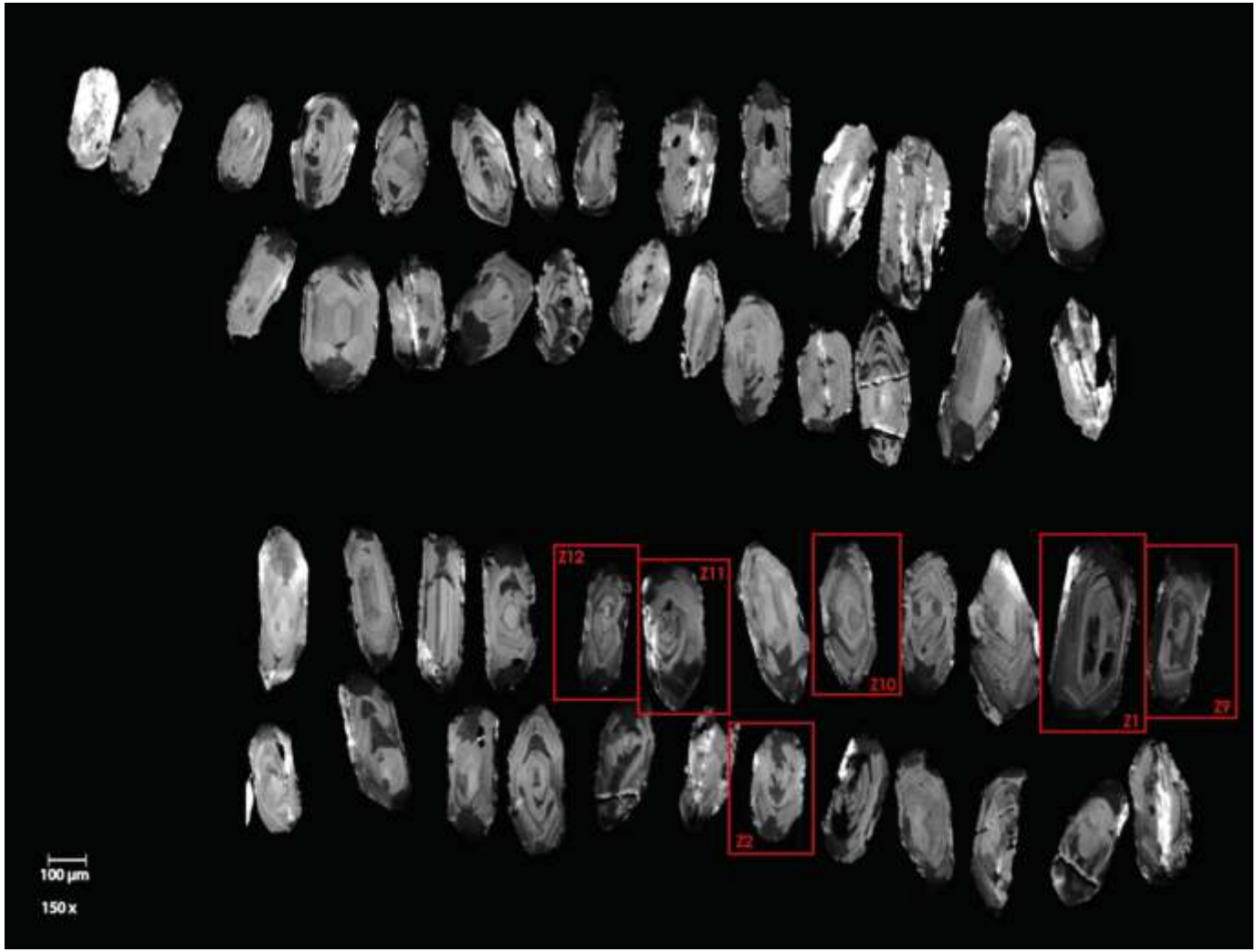

Figure B.8: CL image of zircons from Amelia pluton. Red boxes and red numbers represent grains plucked for CA-TIMS U-Pb geochronology.

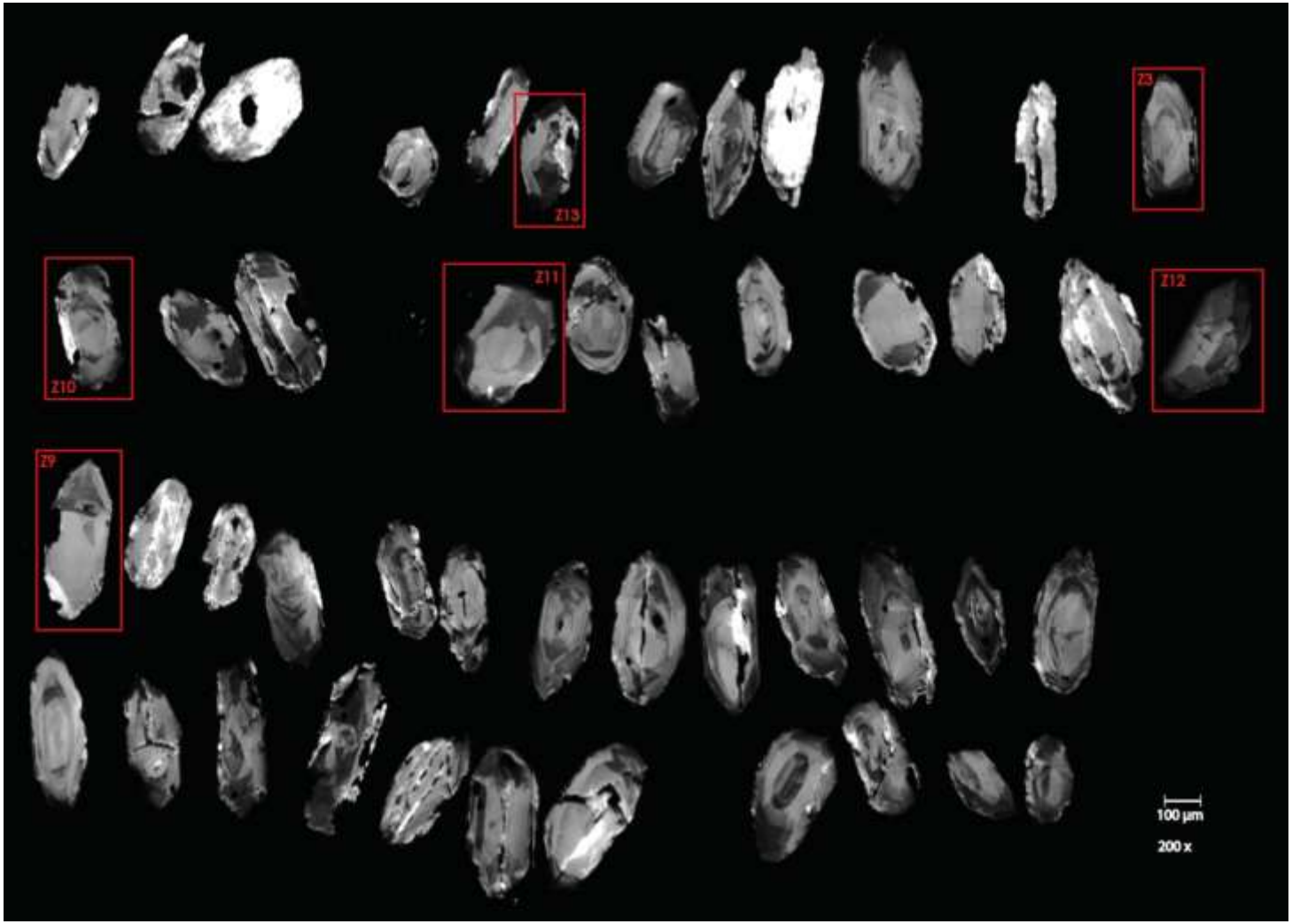

Figure B.9: CL image of zircons from Pedro Mountain pluton. Red boxes and red numbers represent grains plucked for CA-TIMS U-Pb geochronology.

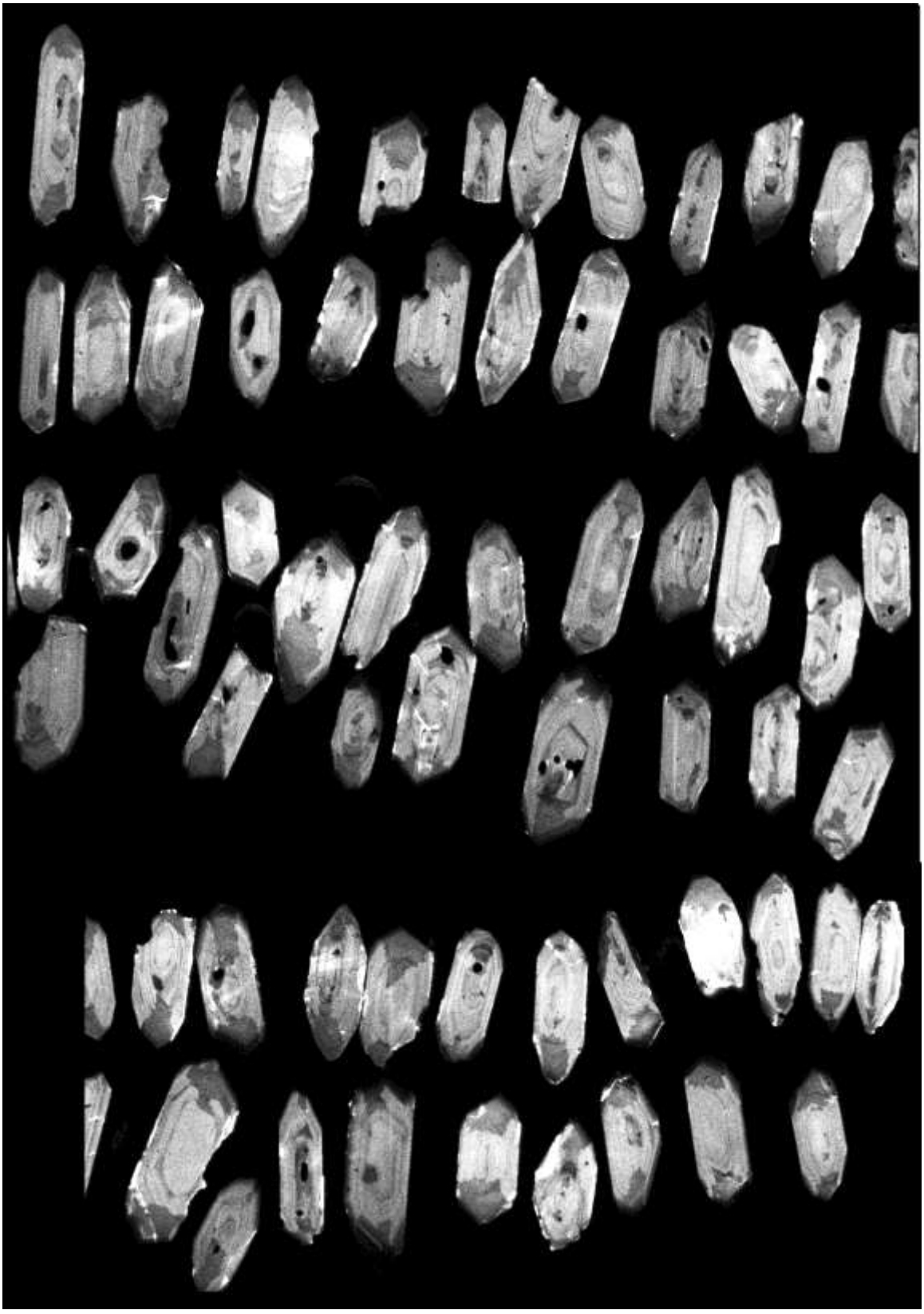

Figure B.10: CL image of zircons from Lookout Mountain pluton. Red boxes and red numbers represent grains plucked for CA-TIMS U-Pb geochronology.

APPENDIX C

U-Pb LA-ICPMS Results

Table C.1 DC11-04 U-Pb LA-ICPMS Results

			Corrected Isotope Ratios							Apparent Ages (Ma)						
Spot (a)	U ppm (b)	Th/U ppm (c)	$^{206}Pb/^{207}Pb$ (d)	±2σ (%) (e)	$^{207}Pb^*/^{235}U^*$	±2σ (%) (e)	$^{206}Pb^*/^{238}U$ (f)	±2σ (%) (f)	error corr. (g)	$^{207}Pb^*/^{206}Pb^*$ (h)	±2σ (Ma) (h)	$^{207}Pb^*/^{235}U$ (i)	±2σ (Ma) (i)	$^{206}Pb^*/^{238}U^*$ (j)	±2σ (Ma) (j)	% disc. (k)
DC11-04M_124	458	0.24	5.05	4.72	0.878	13.9	0.12	10.3	0.74	356	209	640	65.8	723	70.5	109
DC11-04M_126	135	0.26	19.0	7.88	3.46	15.8	0.11	11.8	0.75	3004	168	1518	124	686	77.1	81.1
DC11-04M_127	326	0.31	19.6	19.0	0.452	13.3	0.06	8.52	0.64	294	233	379	42.0	393	32.5	34.7
DC11-04M_128	184	0.21	17.0	6.55	1.47	28.5	0.21	21.3	0.75	248	437	917	172	1218	236	431
DC11-04M_129	305	0.48	19.8	6.89	1.09	15.6	0.15	12.3	0.79	309	219	747	82.6	901	103	206
DC11-04M_130	273	0.30	19.0	9.64	0.910	16.7	0.13	11.2	0.67	246	285	657	80.7	783	82.6	232
DC11-04M_131	394	0.32	17.6	9.64	0.215	13.3	0.03	9.48	0.71	277	213	198	23.8	191	17.8	31.6
DC11-04S_331	232	0.34	19.6	12.4	1.042	14.2	0.13	10.4	0.73	486	213	725	73.7	805	79.1	69.8
DC11-04S_332	738	1.17	18.6	9.27	0.200	9.73	0.03	7.62	0.78	317	138	185	16.5	175	13.2	45.4
DC11-04S_334	450	0.63	4.48	10.4	0.198	10.2	0.03	7.79	0.76	350	149	184	17.2	171	13.2	51.8
DC11-04S_335	370	0.26	19.2	10.2	0.195	10.6	0.03	7.64	0.72	126	172	181	17.5	185	13.9	47.2
DC11-04S_336	360	0.57	17.8	8.75	0.217	10.6	0.03	7.37	0.70	306	172	199	19.1	190	13.8	38.4
DC11-04S_337	561	0.52	20.4	6.57	1.12	11.7	0.16	9.44	0.81	216	160	764	62.8	965	84.5	374
DC11-04S_338	198	0.47	18.2	5.84	12.1	7.94	0.44	6.39	0.80	2810	77.2	2610	74.5	2361	126	19.0
DC11-04S_339	233	0.56	20.0	7.10	0.237	11.0	0.03	6.58	0.60	456	194	216	21.3	195	12.6	58.2
DC11-04S_340	438	0.28	26.1	20.0	1.49	10.2	0.18	7.76	0.76	563	143	925	61.7	1085	77.5	101
DC11-04S_341	447	1.10	19.3	9.30	0.197	9.40	0.03	7.07	0.75	312	141	182	15.7	172	12.0	45.4
DC11-04S_342	338	0.87	19.1	7.56	0.207	12.7	0.03	7.52	0.59	204	238	191	22.1	190	14.1	7.3
DC11-04S_343	780	0.37	19.9	10.3	1.60	12.0	0.22	9.05	0.75	316	179	972	75.0	1286	105	340
DC11-04S_344	42.0	0.23	19.9	6.12	0.160	21.6	0.03	7.99	0.37	-459	529	150	30.2	192	15.1	144
DC11-04S_345	394	0.39	19.7	6.49	0.207	9.43	0.03	6.85	0.73	225	150	191	16.4	188	12.7	16.6
DC11-04S_346	169	0.44	19.3	6.03	0.217	12.6	0.03	7.71	0.61	425	222	200	22.8	181	13.8	58.3
DC11-04S_347	895	0.44	20.6	7.30	0.231	11.2	0.03	9.60	0.85	411	131	211	21.4	193	18.3	53.7
DC11-04S_348	599	0.54	20.8	7.82	0.340	17.9	0.03	8.39	0.47	1392	304	297	46.1	177	14.7	88.4
DC11-04S_349	418	0.42	18.8	7.53	0.200	10.5	0.03	7.95	0.76	287	156	185	17.8	177	13.9	38.7
DC11-04S_350	367	0.79	20.3	9.31	0.194	11.6	0.03	7.69	0.66	228	200	180	19.1	176	13.4	23.2
DC11-04S_351	493	0.34	18.1	9.95	0.202	9.01	0.03	6.28	0.70	280	148	187	15.4	180	11.1	36.4
DC11-04S_352	620	0.51	19.3	6.46	0.205	9.44	0.03	7.19	0.76	202	142	189	16.3	188	13.3	6.9
DC11-04S_353	526	0.59	17.9	7.52	0.207	10.6	0.03	8.27	0.78	152	154	191	18.4	194	15.8	28.1
DC11-04S_354	687	0.33	19.5	6.29	0.209	11.1	0.03	8.49	0.77	194	165	193	19.4	192	16.1	1.0
DC11-04S_355	247	0.52	19.2	6.85	0.195	12.0	0.03	7.56	0.63	161	218	181	19.9	182	13.6	13.7
DC11-04S_356	351	0.39	11.3	15.8	0.209	8.85	0.03	6.48	0.73	282	138	193	15.6	186	11.9	34.6
DC11-04S_357	313	0.44	19.7	8.65	0.198	9.87	0.03	6.24	0.63	301	174	184	16.6	175	10.7	42.6
DC11-04S_358	656	0.61	19.0	6.05	0.198	8.97	0.03	6.39	0.71	248	145	183	15.0	178	11.2	28.6
DC11-04S_359	158	0.68	19.1	7.64	0.201	10.5	0.03	7.47	0.71	345	167	186	17.9	174	12.8	50.2
DC11-04S_360	261	0.79	18.7	7.40	0.211	11.4	0.03	8.50	0.75	337	171	194	20.1	183	15.3	46.4

Table C.1 DC11-04 U-Pb LA-ICPMS Results Cont.

			Corrected Isotope Ratios							Apparent Ages (Ma)						
Spot (a)	U ppm (b)	Th/U ppm (c)	$^{206}Pb/^{207}Pb$ (d)	±2σ (%) (e)	$^{207}Pb^*/^{235}U^*$	±2σ (%) (e)	$^{206}Pb^*/^{238}U$ (f)	±2σ (%) (f)	error corr. (g)	$^{207}Pb^*/^{206}Pb^*$ (h)	±2σ (Ma) (h)	$^{207}Pb^*/^{235}U$ (i)	±2σ (Ma) (i)	$^{206}Pb^*/^{238}U^*$ (j)	±2σ (Ma) (j)	% disc. (k)
DC11-04S_361	194	1.04	19.0	6.20	0.217	11.1	0.03	8.15	0.73	441	167	199	20.0	179	14.4	60.2
DC11-04S_362	506	0.50	18.7	6.61	0.192	10.6	0.03	7.14	0.67	101	185	178	17.3	184	13.0	83.6

Table C.2 DC11-05 U-Pb LA-ICPMS Results

			Corrected Isotope Ratios							Apparent Ages (Ma)						
Spot (a)	U ppm (b)	Th/U ppm (c)	$^{206}Pb/^{207}Pb$ (d)	±2σ (%) (e)	$^{207}Pb^*/^{235}U^*$	±2σ (%) (e)	$^{206}Pb^*/^{238}U$ (f)	±2σ (%) (f)	error corr. (g)	$^{207}Pb^*/^{206}Pb^*$ (h)	±2σ (Ma) (h)	$^{207}Pb^*/^{235}U$ (i)	±2σ (Ma) (i)	$^{206}Pb^*/^{238}U^*$ (j)	±2σ (Ma) (j)	% disc. (k)
DC11-05L_11	270	0.69	3.47	30.2	0.20	9.6	0.03	5.36	0.56	353	180	182	15.9	169	8.93	52.8
DC11-05L_12	182	0.49	12.6	42.3	0.19	11.5	0.03	5.75	0.50	310	228	175	18.6	165	9.39	47.2
DC11-05L_13	369	0.48	12.0	28.9	0.93	11.9	0.13	7.31	0.61	330	213	667	58.2	772	53.2	142
DC11-05L_14	305	0.56	15.9	31.9	0.19	9.3	0.03	5.67	0.61	185	171	177	15.1	176	9.86	4.92
DC11-05L_15	349	0.60	13.6	37.5	0.20	9.9	0.03	5.63	0.57	356	183	184	16.6	171	9.47	52.8
DC11-05L_16	515	0.66	18.5	22.9	0.18	8.3	0.03	5.07	0.61	173	154	170	13.0	170	8.49	1.83
DC11-05L_17	106	0.43	8.74	43.9	0.19	13.7	0.03	5.87	0.43	354	279	177	22.3	164	9.54	54.2
DC11-05L_18	254	0.56	9.80	26.5	0.24	9.9	0.03	5.77	0.58	755	171	219	19.6	173	9.83	78.1
DC11-05L_19	316	0.59	15.6	27.3	0.28	10.2	0.03	5.72	0.56	1,069	170	247	22.4	169	9.55	85.3
DC11-05L_20	231	0.46	4.79	29.9	0.17	10.5	0.03	5.99	0.57	119	203	162	15.6	164	9.72	38.7
DC11-05L_21	202	0.42	3.06	10.6	0.21	13.6	0.03	7.65	0.56	190	260	190	23.5	190	14.3	0.230
DC11-05L_22	87.8	0.46	11.5	20.4	0.19	13.3	0.03	5.83	0.44	243	276	177	21.6	172	9.90	29.7
DC11-05L_23	214	0.38	18.3	22.6	0.19	10.8	0.03	5.15	0.48	228	219	173	17.2	169	8.58	26.1
DC11-05L_24	198	0.65	7.87	19.8	0.35	17.5	0.03	7.44	0.43	1,260	309	304	45.9	195	14.3	85.8
DC11-05L_25	276	0.45	21.8	31.3	0.19	8.7	0.03	5.46	0.63	139	158	181	14.4	184	9.88	32.2
DC11-05L_26	385	0.24	15.9	21.0	0.18	9.3	0.03	5.74	0.62	159	170	171	14.5	171	9.72	8.22
DC11-05L_27	215	0.71	10.4	17.6	0.54	10.9	0.06	5.60	0.51	657	201	437	38.8	397	21.6	40.8
DC11-05L_28	185	0.42	18.9	9.39	0.17	10.1	0.03	5.84	0.58	-14.0	200	160	15.0	172	9.89	1,346
DC11-05L_29	60.8	0.59	16.7	19.3	0.26	17.8	0.03	6.50	0.37	985	336	236	37.4	168	10.8	84.0
DC11-05L_30	98.1	0.59	19.3	11.1	0.15	18.6	0.03	6.33	0.34	-178	436	145	25.0	165	10.3	195
DC11-05L_31	221	0.45	18.0	15.8	0.16	11.4	0.03	6.39	0.56	-51.7	231	153	16.2	166	10.5	427
DC11-05L_32	339	0.58	16.3	9.37	0.17	9.3	0.02	5.87	0.63	192	168	159	13.7	157	9.11	18.4
DC11-05L_33	140	0.39	18.5	12.6	0.18	10.9	0.03	6.66	0.61	197	201	168	16.9	166	10.9	16.0
DC11-05M_102	96.3	0.66	18.8	11.2	2.63	23.0	0.15	11.7	0.51	2,057	349	1,310	169	903	99.0	60.0
DC11-05M_103	391	0.72	6.34	25.7	0.20	11.8	0.03	8.18	0.69	64.1	203	186	20.1	196	15.8	208
DC11-05M_105	137	0.39	9.53	21.8	0.19	14.8	0.03	5.46	0.37	239	317	172	23.5	168	9.04	30.3
DC11-05M_106	104	0.68	22.5	10.7	0.28	22.5	0.03	15.7	0.70	613	347	251	50.0	214	33.1	66.1
DC11-05M_107	217	0.34	16.6	16.1	1.88	36.7	0.21	24.5	0.67	748	578	1,074	243	1,242	277	72.8
DC11-05M_109	320	0.31	20.0	9.60	1.16	28.2	0.15	16.8	0.60	398	507	783	154	925	145	142
DC11-05M_111	312	0.36	21.1	8.53	0.33	20.9	0.03	9.67	0.46	1,230	364	288	52.4	186	17.7	86.1
DC11-05M_112	315	0.47	12.1	15.8	0.26	12.5	0.03	7.56	0.60	797	209	237	26.5	185	13.8	77.9
DC11-05M_114	315	0.50	19.1	10.0	0.41	15.9	0.06	11.2	0.71	334	255	348	46.8	350	38.3	4.72
DC11-05M_115	247	0.41	20.0	11.2	0.22	12.6	0.03	7.64	0.61	303	227	199	22.7	190	14.3	37.8
DC11-05M_116	163	0.71	20.1	11.6	26.94	56.7	0.68	48.0	0.85	3,407	470	3,381	555	3,339	1,251	2.57
DC11-05M_118	204	0.46	12.3	18.5	1.90	24.2	0.16	13.1	0.54	1,366	393	1,082	161	947	115	33.0
DC11-05M_119	121	0.45	16.1	14.3	0.21	12.6	0.03	6.89	0.55	422	235	194	22.3	176	12.0	59.1

Table C.2 DC11-05 U-Pb LA-ICPMS Results Cont.

			Corrected Isotope Ratios							Apparent Ages (Ma)						
Spot (a)	U ppm (b)	Th/U ppm (c)	$^{206}Pb/^{207}Pb$ (d)	±2σ (%) (e)	$^{207}Pb^*/^{235}U^*$	±2σ (%) (e)	$^{206}Pb^*/^{238}U$ (f)	±2σ (%) (f)	error corr. (g)	$^{207}Pb^*/^{206}Pb^*$ (h)	±2σ (Ma) (h)	$^{207}Pb^*/^{235}U$ (i)	±2σ (Ma) (i)	$^{206}Pb^*/^{238}U^*$ (j)	±2σ (Ma) (j)	% disc. (k)
DC11-05M_120	499	0.67	19.5	10.9	2.51	46.7	0.25	28.0	0.60	1,036	757	1,274	339	1,419	356	41.2
DC11-05M_122	131	0.56	20.5	9.16	0.17	12.0	0.03	7.25	0.61	-69.3	233	160	17.7	176	12.6	359
DC11-05M_123	186	0.42	20.7	11.2	0.20	11.1	0.03	6.33	0.57	373	207	186	19.0	172	10.7	54.6
DC11-05M_92	200	0.37	15.2	10.0	4.20	64.0	0.38	48.1	0.75	1,181	836	1,674	525	2,095	860	91.0
DC11-05M_93	460	0.29	19.0	8.27	0.46	17.4	0.06	12.0	0.69	374	284	387	56.0	389	45.2	4.24
DC11-05M_94	140	0.33	20.2	4.97	1.74	22.5	0.13	14.1	0.63	1,546	330	1,024	145	798	106	51.4
DC11-05M_95	230	0.33	20.5	6.75	0.21	14.1	0.03	8.92	0.63	253	251	191	24.5	186	16.3	27.1
DC11-05M_96	202	0.28	19.5	8.56	0.63	14.3	0.09	8.98	0.63	275	254	495	55.8	543	46.8	102
DC11-05M_97	496	0.29	19.4	7.26	0.22	12.6	0.03	8.18	0.65	191	223	199	22.7	199	16.0	4.44
DC11-05S_286	382	1.05	21.4	12.2	3.38	45.5	0.21	11.9	0.26	1,870	791	1,500	356	1,252	136	36.3
DC11-05S_286	181	0.90	20.3	7.72	7.64	14.0	0.17	9.15	0.65	3,602	163	2,190	126	1,010	85.6	77.3
DC11-05S_287	319	0.70	21.2	10.3	0.18	9.6	0.03	6.83	0.71	149	157	169	14.9	170	11.5	14.3
DC11-05S_288	193	0.61	20.4	7.47	0.21	13.9	0.03	8.98	0.64	-89.9	261	197	24.9	221	19.5	352
DC11-05S_289	177	0.46	18.0	10.2	0.19	11.8	0.03	7.05	0.60	183	221	175	19.0	175	12.2	4.42
DC11-05S_290	252	0.85	18.1	10.5	0.25	15.1	0.03	8.23	0.55	791	265	223	30.2	173	14.0	79.2
DC11-05S_291	95.2	0.55	20.1	7.34	0.94	32.1	0.15	7.27	0.23	-7.26	756	674	158	894	60.7	13,321
DC11-05S_292	190	0.63	22.3	9.52	0.21	12.3	0.03	9.10	0.74	310	188	194	21.7	185	16.6	41.0
DC11-05S_293	389	1.18	20.2	6.99	0.18	9.5	0.03	7.06	0.74	335	144	171	15.0	160	11.2	52.9
DC11-05S_294	157	0.57	20.1	9.50	0.19	11.9	0.03	7.63	0.64	178	212	174	19.0	174	13.1	2.11
DC11-05S_295	353	0.68	19.8	7.05	0.19	10.1	0.03	6.80	0.67	231	173	174	16.2	170	11.4	26.7
DC11-05S_296	225	0.81	20.1	9.11	3.01	31.4	0.21	16.8	0.54	1,661	490	1,410	239	1,251	191	27.2
DC11-05S_297	152	0.77	15.3	12.63	0.18	14.0	0.03	7.04	0.50	163	284	165	21.4	165	11.5	1.18
DC11-05S_298	216	1.15	21.0	7.96	0.18	10.5	0.03	6.85	0.65	77.1	189	166	16.1	173	11.7	126
DC11-05S_299	926	1.93	15.5	8.08	0.20	10.7	0.03	9.49	0.89	169	116	183	17.9	184	17.2	8.67
DC11-05S_300	229	0.94	18.5	9.17	0.19	10.3	0.03	6.84	0.66	155	181	175	16.6	177	11.9	14.5
DC11-05S_301	278	1.06	19.6	12.0	0.19	10.1	0.03	7.26	0.72	176	163	175	16.2	175	12.5	0.246
DC11-05S_302	110	0.63	21.8	8.28	0.19	12.1	0.03	7.03	0.58	295	224	178	19.7	169	11.7	43.2
DC11-05S_303	382	0.88	20.3	7.27	0.19	10.0	0.03	7.06	0.71	218	163	177	16.2	174	12.1	20.3
DC11-05S_304	247	1.08	20.1	6.98	0.18	13.5	0.03	8.72	0.65	60.9	246	169	21.1	177	15.2	193
DC11-05S_305	128	0.64	18.6	8.10	0.17	14.5	0.03	9.56	0.66	-28.0	264	156	21.0	169	15.9	712
DC11-05S_306	231	0.78	20.3	10.4	5.12	33.3	0.18	14.6	0.44	2,895	485	1,839	283	1,055	142	68.6
DC11-05S_307	194	0.52	19.7	7.48	0.20	11.6	0.03	7.08	0.61	136	215	182	19.3	186	12.9	37.3
DC11-05S_308	133	0.68	20.4	6.70	0.54	19.0	0.07	10.7	0.56	437	351	438	67.7	438	45.1	0.243
DC11-05S_309	123	0.49	20.2	6.58	0.19	13.7	0.03	7.87	0.57	120	264	180	22.6	185	14.4	55.2
DC11-05S_310	319	0.91	19.1	9.80	0.20	11.4	0.03	7.51	0.66	249	197	184	19.1	178	13.2	28.8
DC11-05S_311	301	0.62	13.3	8.48	0.20	10.3	0.03	7.27	0.71	263	167	184	17.3	178	12.8	33.0

Table C.2 DC11-05 U-Pb LA-ICPMS Results Cont.

	Corrected Isotope Ratios									Apparent Ages (Ma)						
Spot (a)	U ppm (b)	Th/U ppm (c)	$^{206}Pb/^{207}Pb$ (d)	±2σ (%) (e)	$^{207}Pb^*/^{235}U^*$	±2σ (%) (e)	$^{206}Pb^*/^{238}U$ (f)	±2σ (%) (f)	error corr. (g)	$^{207}Pb^*/^{206}Pb^*$ (h)	±2σ (Ma) (h)	$^{207}Pb^*/^{235}U$ (i)	±2σ (Ma) (i)	$^{206}Pb^*/^{238}U^*$ (j)	±2σ (Ma) (j)	% disc. (k)
DC11-05S_312	130	0.63	19.7	9.49	0.18	14.3	0.03	7.38	0.52	33.2	292	168	22.0	177	12.9	440
DC11-05S_313	159	0.77	19.1	6.15	0.73	26.6	0.09	18.3	0.69	600	418	559	114	549	96.2	8.85
DC11-05S_314	698	0.69	18.7	7.95	0.19	10.0	0.03	7.88	0.79	303	140	178	16.3	169	13.1	44.9
DC11-05S_315	313	1.10	22.0	10.9	1.21	23.8	0.14	11.2	0.47	699	448	805	132	844	88.5	22.1
DC11-05S_316	141	0.85	13.9	16.5	0.21	13.7	0.03	9.16	0.67	429	228	195	24.4	177	16.0	59.6
DC11-05S_317	376	0.83	19.6	13.8	3.16	58.0	0.27	50.3	0.87	1,283	563	1,448	447	1,562	697	24.5
DC11-05S_318	325	0.78	18.1	9.31	0.53	23.8	0.04	9.63	0.40	1,714	401	434	84.2	234	22.1	87.9
DC11-05S_320	291	1.14	22.2	9.48	0.19	10.1	0.03	6.78	0.67	153	175	175	16.2	177	11.8	15.7
DC11-05S_321	462	1.86	20.0	8.66	0.20	11.6	0.03	6.86	0.59	417	208	184	19.5	167	11.3	60.7
DC11-05S_322	111	0.68	19.0	10.0	0.18	12.7	0.03	7.19	0.57	166	244	170	19.8	170	12.1	2.69
DC11-05S_323	367	1.07	20.3	12.1	1.61	25.1	0.22	10.2	0.41	374	516	974	157	1,260	116	261
DC11-05S_324	302	0.63	19.1	8.77	0.18	9.8	0.03	6.90	0.70	184	162	172	15.5	171	11.6	7.24
DC11-05S_326	223	0.84	23.4	17.5	0.19	11.6	0.03	7.55	0.65	296	200	174	18.5	165	12.3	44.9
DC11-05S_327	204	0.97	18.7	12.4	0.25	16.3	0.03	7.92	0.49	684	305	227	33.3	186	14.5	73.9
DC11-05S_328	191	0.96	20.7	8.59	0.21	15.6	0.03	10.4	0.66	185	271	190	26.9	190	19.4	2.72
DC11-05S_329	71.3	0.55	18.8	6.37	0.80	29.0	0.04	13.5	0.46	2,431	436	599	131	234	30.9	91.9
DC11-05S_330	115	0.71	20.0	7.20	2.16	37.0	0.25	18.9	0.51	706	678	1,168	257	1,431	242	115

Table C.3 LOM11-18 U-Pb LA-ICPMS Results

			Corrected Isotope Ratios							Apparent Ages (Ma)						
Spot (a)	U ppm (b)	Th/U ppm (c)	$^{206}Pb/^{207}Pb$ (d)	±2σ (%) (e)	$^{207}Pb^*/^{235}U^*$	±2σ (%) (e)	$^{206}Pb^*/^{238}U$ (f)	±2σ (%) (f)	error corr. (g)	$^{207}Pb^*/^{206}Pb^*$ (h)	±2σ (Ma) (h)	$^{207}Pb^*/^{235}U$ (i)	±2σ (Ma) (i)	$^{206}Pb^*/^{238}U^*$ (j)	±2σ (Ma) (j)	% disc. (k)
LOM11-18L_48	468	0.286	19.6	29.2	1.10	10.8	0.158	6.57	0.607	208	199	751	57.4	946	57.8	381
LOM11-18L_49	238	0.376	19.0	12.8	0.189	10.1	0.0311	5.75	0.570	-106	204	176	16.3	198	11.2	291
LOM11-18L_50	285	0.496	19.9	8.60	0.201	8.85	0.0276	5.55	0.627	323	157	186	15.1	176	9.62	46.2
LOM11-18L_51	231	0.267	18.3	9.85	0.199	9.17	0.0284	5.33	0.581	238	172	185	15.5	181	9.49	24.4
LOM11-18L_52	144	0.665	18.5	15.8	0.228	13.1	0.0307	5.75	0.438	371	266	209	24.8	195	11.0	48.2
LOM11-18L_53	191	0.433	20.0	8.52	0.197	10.6	0.0278	6.03	0.569	256	200	182	17.7	177	10.5	31.5
LOM11-18L_54	211	0.343	17.9	12.1	0.308	12.3	0.0316	5.37	0.436	954	227	273	29.5	200	10.6	80.2
LOM11-18L_55	121	0.410	19.4	14.3	0.179	10.7	0.0286	6.24	0.581	-34.4	212	167	16.6	182	11.2	637
LOM11-18L_56	154	0.359	20.5	12.6	0.205	12.2	0.0274	5.92	0.485	389	240	190	21.1	174	10.2	55.9
LOM11-18L_57	150	0.296	19.5	8.13	0.195	9.54	0.0291	5.39	0.565	128	185	181	15.8	185	9.81	44.8
LOM11-18L_58	328	0.345	13.5	13.1	0.625	10.6	0.0907	6.37	0.599	196	198	493	41.6	559	34.2	194
LOM11-18L_59	208	0.510	18.7	10.5	1.15	13.5	0.152	9.26	0.685	398	221	777	73.4	915	79.0	139
LOM11-18L_60	339	0.313	14.1	11.1	0.208	8.58	0.0289	5.47	0.638	295	151	192	15.0	184	9.90	38.3
LOM11-18L_61	241	0.333	22.7	8.28	0.184	10.3	0.0281	5.45	0.532	79.9	206	172	16.2	178	9.59	125
LOM11-18L_62	230	0.651	19.3	6.93	0.191	8.75	0.0274	5.46	0.624	216	158	177	14.2	175	9.40	19.3
LOM11-18L_63	125	0.431	18.5	11.8	0.619	13.1	0.0804	5.00	0.383	446	268	490	50.7	499	24.0	12.2
LOM11-18L_64	440	0.253	19.9	7.67	0.184	7.43	0.0274	5.10	0.687	136	127	171	11.7	174	8.76	28.1
LOM11-18L_65	177	0.263	18.6	6.55	1.31	15.0	0.181	7.68	0.513	308	292	850	86.2	1073	75.9	270
LOM11-18L_66	66	0.446	19.6	8.23	0.181	15.7	0.0269	6.05	0.384	140	341	169	24.5	171	10.2	22.2
LOM11-18L_67	294	0.503	15.3	8.91	0.198	9.19	0.0278	6.13	0.667	275	157	184	15.4	176	10.7	36.4
LOM11-18L_68	324	0.556	21.1	10.3	0.222	8.87	0.0277	5.77	0.651	540	147	204	16.4	176	10.0	68.3
LOM11-18L_69	88	0.339	19.2	9.55	1.34	30.8	0.191	9.75	0.317	236	674	863	179	1127	101	412
LOM11-18M_168	200	0.340	20.6	7.87	0.910	22.8	0.122	16.4	0.721	372	355	657	110	743	115	106
LOM11-18M_170	112	0.345	19.2	6.61	0.384	17.0	0.0540	9.07	0.534	265	329	330	47.8	339	30.0	28.8
LOM11-18M_171	354	0.329	20.1	7.15	0.193	13.5	0.0296	8.78	0.650	66.6	244	179	22.2	188	16.3	185
LOM11-18M_172	634	0.891	19.0	5.64	0.211	11.6	0.0301	8.19	0.706	240	190	195	20.6	191	15.4	20.8
LOM11-18M_173	321	0.454	22.0	8.75	0.297	18.0	0.0443	12.8	0.711	132	297	264	41.8	280	34.9	114
LOM11-18M_174	184	0.365	19.6	7.46	0.252	16.0	0.0343	12.1	0.755	345	237	228	32.7	217	25.8	37.6
LOM11-18S_417	427	0.538	19.9	9.85	0.197	10.3	0.0288	7.44	0.721	181	167	183	17.3	183	13.4	0.90
LOM11-18S_418	677	0.647	21.0	8.68	0.208	8.52	0.0286	6.39	0.750	315	128	192	14.9	182	11.5	42.9
LOM11-18S_419	313	0.580	19.5	8.72	0.224	9.42	0.0301	6.76	0.718	365	148	205	17.5	191	12.8	48.2
LOM11-18S_420	237	0.753	19.3	6.85	0.268	12.8	0.0297	9.14	0.716	789	187	241	27.4	189	17.0	77.2
LOM11-18S_421	237	0.489	17.2	6.73	0.247	12.0	0.0348	8.78	0.734	259	187	224	24.0	221	19.0	15.0
LOM11-18S_422	733	0.789	18.9	6.89	0.221	10.3	0.0310	7.58	0.738	276	159	203	18.9	197	14.7	29.3
LOM11-18S_423	182	0.487	19.8	6.84	0.212	12.2	0.0295	7.65	0.625	292	218	195	21.7	187	14.1	36.3
LOM11-18S_424	170	0.588	18.4	10.7	0.352	15.9	0.0345	9.04	0.569	1,046	263	307	42.0	218	19.4	80.4

Table C.3 LOM11-18 U-Pb LA-ICPMS Results Cont.

			Corrected Isotope Ratios							Apparent Ages (Ma)						
Spot (a)	U ppm (b)	Th/U ppm (c)	$^{206}Pb/^{207}Pb$ (d)	±2σ (%) (e)	$^{207}Pb^*/^{235}U^*$	±2σ (%) (e)	$^{206}Pb^*/^{238}U$ (f)	±2σ (%) (f)	error corr. (g)	$^{207}Pb^*/^{206}Pb^*$ (h)	±2σ (Ma) (h)	$^{207}Pb^*/^{235}U$ (i)	±2σ (Ma) (i)	$^{206}Pb^*/^{238}U^*$ (j)	±2σ (Ma) (j)	% disc. (k)
LOM11-18S_425	297	0.365	20.5	5.40	0.211	11.0	0.0305	7.91	0.718	209	178	195	19.5	193	15.1	7.54
LOM11-18S_426	143	0.533	20.5	14.5	0.196	12.0	0.0284	6.93	0.576	207	228	182	20.1	180	12.3	13.0

Table C.4 LOM11-17 U-Pb LA-ICPMS Results

			Corrected Isotope Ratios							Apparent Ages (Ma)						
Spot (a)	U ppm (b)	Th/U ppm (c)	$^{206}Pb/^{207}Pb$ (d)	±2σ (%) (e)	$^{207}Pb^*/^{235}U^*$	±2σ (%) (e)	$^{206}Pb^*/^{238}U$ (f)	±2σ (%) (f)	error corr. (g)	$^{207}Pb^*/^{206}Pb^*$ (h)	±2σ (Ma) (h)	$^{207}Pb^*/^{235}U$ (i)	±2σ (Ma) (i)	$^{206}Pb^*/^{238}U^*$ (j)	±2σ (Ma) (j)	% disc. (k)
LOM11-17L_34	540	222	16.2	19.4	0.22	8.43	0.03	5.75	0.68	277	141	205	15.7	199	11.3	28.5
LOM11-17L_35	257	95.8	18.3	22.4	0.20	7.78	0.03	5.14	0.66	230	135	186	13.3	183	9.28	20.8
LOM11-17L_36	69.5	39.2	20.3	30.4	0.25	14.4	0.03	5.77	0.40	713	281	226	29.2	182	10.3	75.6
LOM11-17L_37	192	95.7	10.7	15.7	0.25	12.7	0.03	5.60	0.44	674	244	228	26.0	187	10.3	73.2
LOM11-17L_38	139	59.2	17.5	14.8	0.18	13.3	0.03	5.46	0.41	82.8	288	167	20.5	173	9.34	111
LOM11-17L_39	147	85.8	19.7	8.14	0.19	10.3	0.03	5.53	0.54	171	202	178	16.8	179	9.74	4.65
LOM11-17L_40	281	105	16.9	12.2	0.23	9.07	0.03	5.44	0.60	430	162	207	17.0	188	10.1	57.2
LOM11-17L_41	250	150	16.7	12.5	0.22	11.2	0.03	6.75	0.60	314	203	206	20.8	196	13.1	38.0
LOM11-17L_42	260	138	20.9	12.2	0.27	9.66	0.04	6.27	0.65	388	165	242	20.8	227	14.0	42.2
LOM11-17L_43	350	118	18.6	11.2	0.21	9.43	0.03	5.63	0.60	213	175	193	16.6	191	10.6	10.5
LOM11-17L_44	210	92.1	19.9	12.1	0.20	10.6	0.03	5.41	0.51	82.9	216	184	17.8	192	10.2	133
LOM11-17L_45	295	130	20.0	8.20	1.06	14.3	0.15	7.60	0.53	209	281	736	74.9	920	65.2	364
LOM11-17L_46	127	43.0	20.8	14.0	0.21	11.2	0.03	5.56	0.50	351	220	194	19.8	181	9.93	49.0
LOM11-17L_47	313	182	21.6	15.3	0.38	9.78	0.06	5.33	0.54	197	191	330	27.6	350	18.1	80.0
LOM11-17M_136	236	114	20.1	14.1	1.23	16.9	0.19	11.58	0.69	87.5	290	814	94.4	1103	117	1267
LOM11-17M_137	201	73.4	18.4	7.35	0.25	17.8	0.04	10.94	0.61	98.1	332	223	35.6	235	25.2	142.1
LOM11-17M_138	213	103	7.95	11.3	1.66	24.8	0.21	19.86	0.80	503	326	994	157	1231	223	159
LOM11-17M_140	157	53.1	18.9	11.3	0.23	14.4	0.03	9.59	0.67	366	242	213	27.6	199	18.8	46.3
LOM11-17M_141	348	96.1	16.0	6.30	1.78	32.6	0.24	23.72	0.73	397	502	1039	212	1370	293	273
LOM11-17M_142	208	86.1	20.1	7.51	0.23	19.6	0.04	12.35	0.63	10.4	367	214	37.9	233	28.3	2180
LOM11-17M_145	163	58.0	20.7	9.42	0.25	17.2	0.04	9.85	0.57	187	328	225	34.6	228	22.1	22.2
LOM11-17M_150	432	131	17.4	10.9	1.59	16.4	0.19	10.91	0.67	578	266	967	102	1146	115	107
LOM11-17M_151	180	48.9	19.9	7.92	0.25	15.9	0.03	11.25	0.71	320	256	227	32.4	218	24.1	32.3
LOM11-17M_152	191	85.2	19.6	11.0	0.21	15.7	0.03	10.88	0.69	159	263	190	27.1	192	20.6	21.4
LOM11-17M_153	428	98.4	20.1	7.83	0.23	18.1	0.03	14.31	0.79	239	254	209	34.1	207	29.1	13.6
LOM11-17M_154	201	81.9	20.9	9.14	0.21	15.6	0.03	10.49	0.67	212	269	196	27.9	195	20.2	7.9
LOM11-17M_155	243	123	16.4	8.05	1.55	18.1	0.19	13.07	0.72	596	272	949	112	1109	133	93.7
LOM11-17M_156	262	95.9	20.8	8.34	0.22	13.9	0.03	10.17	0.73	120	222	202	25.4	210	21.0	76.6
LOM11-17M_157	234	87.7	20.9	14.1	0.21	17.5	0.03	10.37	0.59	92.3	334	192	30.6	200	20.5	119
LOM11-17M_158	381	176	22.3	13.4	1.18	16.8	0.16	12.50	0.74	363	252	792	92.3	952	111	175
LOM11-17M_159	115	45.1	19.3	6.16	3.03	19.7	0.23	11.96	0.61	1506	297	1415	151	1355	146	11.1
LOM11-17M_161	377	200	18.6	10.7	1.61	35.7	0.24	18.57	0.52	165	711	974	223	1368	229	810
LOM11-17M_164	381	98.5	20.5	9.08	2.09	25.7	0.25	16.89	0.66	659	417	1147	177	1421	215	129
LOM11-17S_363	391	143	19.3	7.72	0.21	10.6	0.03	7.28	0.69	338	174	192	18.5	180	12.9	47.3
LOM11-17S_364	327	107	19.6	8.06	0.19	12.1	0.03	7.67	0.63	138	220	176	19.6	178	13.5	30.0
LOM11-17S_365	286	192	21.2	7.17	0.18	12.6	0.03	8.75	0.69	32.6	219	170	19.8	180	15.5	457.6

Table C.4 LOM11-17 U-Pb LA-ICPMS Results Cont.

	Corrected Isotope Ratios									Apparent Ages (Ma)						
Spot (a)	U ppm (b)	Th/U ppm (c)	$^{206}Pb/^{207}Pb$ (d)	±2σ (%) (e)	$^{207}Pb^*/^{235}U^*$	±2σ (%) (e)	$^{206}Pb^*/^{238}U$ (f)	±2σ (%) (f)	error corr. (g)	$^{207}Pb^*/^{206}Pb^*$ (h)	±2σ (Ma) (h)	$^{207}Pb^*/^{235}U$ (i)	±2σ (Ma) (i)	$^{206}Pb^*/^{238}U^*$ (j)	±2σ (Ma) (j)	% disc. (k)
LOM11-17S_367	340	142	19.0	8.90	0.20	10.1	0.03	6.66	0.66	302	174	185	17.1	176	11.6	42.3
LOM11-17S_368	225	99.3	19.9	11.6	0.20	11.2	0.03	6.91	0.62	178	205	182	18.7	183	12.4	2.80
LOM11-17S_369	241	173	18.2	7.56	0.27	10.6	0.03	6.84	0.65	643	173	243	22.8	204	13.7	69.4
LOM11-17S_370	382	376	20.2	8.06	0.22	16.6	0.03	11.55	0.70	456	265	198	29.9	177	20.2	62.0
LOM11-17S_371	113	46.7	20.9	7.06	0.28	15.7	0.03	9.40	0.60	1005	256	252	35.1	179	16.6	83.3
LOM11-17S_372	534	254	20.6	10.6	0.19	9.47	0.03	6.64	0.70	127	159	180	15.6	184	12.0	45.4
LOM11-17S_373	193	124	20.3	11.3	0.20	9.70	0.03	6.45	0.67	307	165	187	16.6	178	11.3	42.8
LOM11-17S_374	207	135	20.0	6.22	0.21	11.8	0.03	7.17	0.61	378	210	192	20.6	177	12.5	53.8
LOM11-17S_375	650	836	21.0	9.10	0.20	9.64	0.03	7.43	0.77	316	140	186	16.4	176	12.9	45.0
LOM11-17S_376	321	142	15.0	20.4	0.20	9.46	0.03	6.11	0.65	131	170	183	15.9	187	11.3	43.1
LOM11-17S_377	478	287	19.8	7.57	0.23	12.9	0.03	10.19	0.79	204	184	207	24.1	207	20.8	1.64
LOM11-17S_378	285	157	17.4	9.85	0.20	11.4	0.03	7.66	0.67	231	194	187	19.5	184	13.9	21.0
LOM11-17S_379	200	100	22.9	10.2	0.19	11.0	0.03	7.03	0.64	136	198	177	17.8	180	12.5	32.7
LOM11-17S_380	171	79.7	20.9	7.92	0.24	13.4	0.03	7.55	0.56	658	237	215	26.0	177	13.2	74.2
LOM11-17S_381	396	378	18.1	8.25	0.21	9.66	0.03	6.77	0.70	341	156	191	16.8	179	11.9	48.3
LOM11-17S_382	273	190	17.4	11.0	0.21	12.1	0.03	7.88	0.65	89.3	217	197	21.6	206	16.0	132.9
LOM11-17S_383	246	135	13.8	12.2	1.43	14.9	0.21	12.52	0.84	227	188	903	89.3	1203	137	472
LOM11-17S_384	222	114	18.0	7.26	0.26	16.9	0.03	12.87	0.76	515	239	235	35.4	208	26.4	60.5
LOM11-17S_385	778	1188	16.1	11.4	0.29	14.3	0.03	12.87	0.90	689	134	261	33.0	216	27.3	69.8
LOM11-17S_386	269	190	20.6	7.22	0.20	9.65	0.03	6.58	0.68	94.9	167	186	16.4	193	12.5	105
LOM11-17S_387	219	150	19.0	7.71	0.21	10.6	0.03	6.61	0.62	108	197	195	18.9	203	13.2	89.7
LOM11-17S_388	120	84.1	20.0	7.38	0.18	12.3	0.03	6.91	0.56	-125	252	168	19.1	190	12.9	256
LOM11-17S_389	376	128	21.5	10.1	0.24	12.1	0.03	7.11	0.59	504	217	216	23.7	191	13.4	63.0
LOM11-17S_390	325	221	20.6	6.76	0.23	10.8	0.03	7.73	0.72	178	175	208	20.3	211	16.0	18.4
LOM11-17S_391	190	106	19.7	8.42	0.19	12.3	0.03	7.01	0.57	29.3	241	174	19.6	184	12.7	537
LOM11-17S_392	296	115	19.7	5.84	0.21	11.1	0.03	7.58	0.68	177	188	192	19.4	194	14.5	9.90
LOM11-17S_393	497	348	19.8	6.44	0.21	9.17	0.03	6.74	0.73	199	144	192	16.1	192	12.7	3.45
LOM11-17S_394	353	124	20.1	8.80	0.21	11.2	0.03	8.19	0.73	312	175	196	20.1	187	15.1	40.8
LOM11-17S_395	505	291	21.1	9.44	0.20	10.6	0.03	8.38	0.79	214	149	185	17.9	183	15.1	14.6
LOM11-17S_396	469	268	15.8	13.2	0.18	10.2	0.03	7.71	0.76	41.3	160	167	15.7	176	13.4	330
LOM11-17S_397	369	317	18.7	9.72	0.20	11.3	0.03	8.72	0.77	58.1	171	186	19.2	197	16.9	242
LOM11-17S_398	138	51.0	18.8	7.68	0.62	14.4	0.04	8.81	0.61	2041	200	487	55.5	225	19.5	90.5
LOM11-17S_399	287	206	20.5	8.41	0.20	10.3	0.03	7.17	0.70	198	171	186	17.5	185	13.1	6.99
LOM11-17S_400	590	350	21.4	9.13	0.24	12.4	0.03	7.43	0.60	789	209	219	24.5	170	12.5	79.5
LOM11-17S_401	196	117	20.0	7.18	0.30	15.1	0.03	8.92	0.59	1006	247	265	35.1	189	16.6	82.4
LOM11-17S_402	689	1063	13.8	12.6	0.22	11.3	0.02	8.09	0.72	790	165	198	20.3	152	12.2	81.7

Table C.4 LOM11-17 U-Pb LA-ICPMS Results Cont.

			Corrected Isotope Ratios							Apparent Ages (Ma)						
Spot (a)	U ppm (b)	Th/U ppm (c)	$^{206}Pb/^{207}Pb$ (d)	±2σ (%) (e)	$^{207}Pb^*/^{235}U^*$	±2σ (%) (e)	$^{206}Pb^*/^{238}U$ (f)	±2σ (%) (f)	error corr. (g)	$^{207}Pb^*/^{206}Pb^*$ (h)	±2σ (Ma) (h)	$^{207}Pb^*/^{235}U$ (i)	±2σ (Ma) (i)	$^{206}Pb^*/^{238}U^*$ (j)	±2σ (Ma) (j)	% disc. (k)
LOM11-17S_403	277	192	18.8	6.88	0.22	10.6	0.03	7.20	0.68	280	177	204	19.5	198	14.0	30.0
LOM11-17S_404	223	112	20.2	8.66	0.21	12.0	0.03	7.78	0.65	142	213	194	21.2	199	15.2	40.3
LOM11-17S_405	253	130	20.5	9.39	0.20	10.7	0.03	7.26	0.68	90.4	188	182	17.9	189	13.5	111
LOM11-17S_406	119	79.9	19.0	7.24	0.23	11.4	0.03	7.86	0.69	427	184	208	21.4	189	14.6	56.5
LOM11-17S_407	232	123	19.9	8.33	0.19	11.0	0.03	7.23	0.66	212	193	180	18.2	177	12.6	16.6
LOM11-17S_408	268	114	18.5	9.36	0.22	13.2	0.03	10.63	0.81	179	182	204	24.4	206	21.6	15.5
LOM11-17S_409	131	80.1	17.8	11.9	0.20	15.1	0.03	10.68	0.71	127	250	188	25.9	193	20.3	52.2
LOM11-17S_410	507	404	16.3	11.1	0.22	14.8	0.03	12.42	0.84	237	186	200	26.9	197	24.1	17.0
LOM11-17S_411	143	60.1	21.3	6.70	0.20	15.3	0.03	7.48	0.49	-59.3	327	181	25.5	200	14.7	444
LOM11-17S_412	297	238	19.0	6.14	0.19	9.71	0.03	6.54	0.67	191	167	180	16.0	179	11.6	6.21
LOM11-17S_413	179	84.3	19.1	7.64	0.24	12.5	0.03	5.90	0.47	512	243	215	24.3	189	11.0	64.1
LOM11-17S_414	71.8	36.7	21.0	12.1	0.28	22.3	0.03	9.00	0.40	825	426	248	49.1	191	17.0	77.9
LOM11-17S_415	185	73.1	15.3	9.95	0.23	10.0	0.03	6.53	0.65	406	169	211	19.1	194	12.5	52.9
LOM11-17S_416	229	122	15.3	7.88	0.19	11.7	0.03	6.85	0.59	74.3	224	175	18.7	182	12.3	147

Table C.5 LOM11-12 U-Pb LA-ICPMS Results

			Corrected Isotope Ratios							Apparent Ages (Ma)						
Spot (a)	U ppm (b)	Th/U ppm (c)	$^{206}Pb/^{207}Pb$ (d)	±2σ (%) (e)	$^{207}Pb^*/^{235}U^*$	±2σ (%) (e)	$^{206}Pb^*/^{238}U$ (f)	±2σ (%) (f)	error corr. (g)	$^{207}Pb^*/^{206}Pb^*$ (h)	±2σ (Ma) (h)	$^{207}Pb^*/^{235}U$ (i)	±2σ (Ma) (i)	$^{206}Pb^*/^{238}U^*$ (j)	±2σ (Ma) (j)	% disc. (k)
LOM11-12L_5	189	71.5	22.4	27.6	0.190	10.0	0.028	5.88	0.587	196	189	177	16.3	175	10.2	10.7
LOM11-12L_6	344	174	13.0	27.4	0.218	8.52	0.028	5.28	0.619	461	148	201	15.5	179	9.32	62.0
LOM11-12L_7	164	67.1	20.7	15.9	0.183	11.6	0.027	5.92	0.510	169	233	170	18.2	170	10.0	0.991
LOM11-12L_8	206	78.9	16.1	20.6	0.199	10.5	0.028	5.82	0.555	236	201	184	17.6	180	10.3	24.0
LOM11-12L_9	153	59.7	15.2	8.45	0.189	12.9	0.029	5.27	0.407	79.4	280	176	20.8	183	9.49	132.2
LOM11-12L_10	632	352	19.4	8.96	0.182	7.23	0.026	5.29	0.732	191	115	170	11.3	168	8.78	12.3
LOM11-12M_85	48.7	17.6	18.6	12.2	1.67	31.8	0.270	15.9	0.499	-70.9	674	996	202	1543	218	2572
LOM11-12M_86	134	64.8	21.3	11.3	1.38	13.0	0.152	9.86	0.759	805	177	881	76.5	911	83.7	14.0
LOM11-12M_87	186	88.0	18.7	7.48	0.971	16.8	0.131	11.6	0.689	357	275	689	84.0	795	86.5	130.5
LOM11-12M_88	184	88.1	18.4	7.27	0.511	18.3	0.066	11.0	0.604	453	323	419	62.7	413	44.2	8.96
LOM11-12M_89	159	63.7	19.1	9.19	0.229	13.5	0.035	8.69	0.642	96.4	246	210	25.6	220	18.8	130
LOM11-12M_91	265	122	17.9	14.6	0.227	14.3	0.035	9.73	0.679	72.4	250	207	26.9	219	21.0	207
LOM11-12S_257	276	170	20.8	7.22	0.230	8.89	0.031	6.63	0.745	332	134	210	16.9	199	13.0	40.6
LOM11-12S_258	236	143	12.2	11.0	0.204	10.9	0.029	7.44	0.681	211	185	188	18.7	186	13.7	11.8
LOM11-12S_259	203	87.2	19.9	8.81	0.192	10.7	0.027	6.54	0.612	247	195	178	17.4	173	11.2	30.4
LOM11-12S_260	271	185	20.9	10.4	0.211	10.8	0.030	7.82	0.721	263	173	195	19.2	189	14.6	28.5
LOM11-12S_261	188	68.7	21.1	10.5	0.188	11.8	0.028	7.44	0.633	121	215	175	18.9	179	13.2	48.9
LOM11-12S_262	208	115	19.4	9.17	0.978	12.9	0.138	9.32	0.721	266	206	693	64.9	831	72.7	226
LOM11-12S_263	177	76.0	14.4	11.4	0.188	12.5	0.026	7.34	0.587	353	229	175	20.1	162	11.8	54.7
LOM11-12S_264	251	120	18.8	5.93	0.197	11.0	0.030	7.41	0.672	92.8	193	183	18.4	190	13.8	106
LOM11-12S_265	221	93.9	20.6	8.93	0.201	11.6	0.030	7.44	0.640	127	210	186	19.7	191	14.0	50.8
LOM11-12S_266	204	115	20.9	8.16	0.189	12.6	0.029	7.57	0.602	40.4	241	176	20.3	186	13.9	366
LOM11-12S_267	135	62.2	19.4	7.52	0.195	13.0	0.028	7.74	0.597	194	242	181	21.5	180	13.7	7.02
LOM11-12S_268	572	839	19.9	7.99	0.194	9.21	0.027	7.19	0.780	246	133	180	15.2	175	12.4	29.5
LOM11-12S_269	243	195	21.4	10.1	0.241	11.4	0.035	7.20	0.633	209	204	219	22.4	220	15.6	5.18
LOM11-12S_270	92.4	58.2	20.0	10.5	0.533	13.5	0.047	7.82	0.578	1250	216	434	47.7	296	22.6	78.0
LOM11-12S_271	124	60.6	20.7	7.75	0.790	14.1	0.122	8.45	0.598	41.9	271	591	63.3	744	59.4	1774
LOM11-12S_272	616	454	21.0	11.8	0.302	14.2	0.032	8.48	0.597	916	235	268	33.5	200	16.7	79.4
LOM11-12S_273	196	74.3	18.7	8.75	0.675	12.1	0.094	7.85	0.650	301	209	524	49.5	576	43.3	95.5
LOM11-12S_275	238	127	20.0	10.4	0.202	12.9	0.029	7.55	0.584	200	243	186	22.0	185	13.8	7.66
LOM11-12S_276	280	204	19.7	8.72	0.725	10.4	0.097	7.40	0.713	389	163	553	44.3	594	42.0	55.5
LOM11-12S_277	290	224	22.0	6.65	0.195	10.7	0.029	7.40	0.690	119	183	180	17.7	185	13.5	56.5
LOM11-12S_278	167	65.8	20.6	9.11	0.409	10.8	0.062	8.05	0.745	108	170	348	31.9	385	30.1	266
LOM11-12S_279	207	101	17.8	6.69	0.212	12.1	0.029	8.35	0.691	344	198	195	21.5	183	15.1	47.6
LOM11-12S_280	281	219	20.0	8.12	1.66	23.3	0.194	10.9	0.465	683	441	995	148	1142	114	73.4
LOM11-12S_281	311	217	19.6	5.76	1.30	19.9	0.196	11.9	0.601	118	374	848	114	1151	126	955

Table C.5 LOM11-12 U-Pb LA-ICPMS Results Cont.

	Corrected Isotope Ratios									Apparent Ages (Ma)						
Spot (a)	U ppm (b)	Th/U ppm (c)	$^{206}Pb/^{207}Pb$ (d)	±2σ (%) (e)	$^{207}Pb^*/^{235}U^*$	±2σ (%) (e)	$^{206}Pb^*/^{238}U$	±2σ (%) (f)	error corr. (g)	$^{207}Pb^*/^{206}Pb^*$ (h)	±2σ (Ma) (h)	$^{207}Pb^*/^{235}U$ (i)	±2σ (Ma) (i)	$^{206}Pb^*/^{238}U^*$ (j)	±2σ (Ma) (j)	% disc. (k)
LOM11-12S_282	118	65.9	19.6	8.45	2.71	31.3	0.255	15.0	0.481	1122	546	1332	232	1467	197	34.3
LOM11-12S_283	211	117	20.2	10.0	0.178	9.27	0.028	6.46	0.697	-26.0	161	166	14.2	180	11.5	802
LOM11-12S_284	199	133	20.0	4.92	0.828	10.3	0.112	7.09	0.688	346	169	613	47.4	687	46.2	104
LOM11-12S_285	203	151	18.7	10.1	0.225	11.7	0.032	7.31	0.623	263	211	206	21.8	201	14.4	24.1

Table C.6 LOM11-06a U-Pb LA-ICPMS Results

			Corrected Isotope Ratios							Apparent Ages (Ma)						
Spot (a)	U ppm (b)	Th/U ppm (c)	$^{206}Pb/^{207}Pb$ (d)	±2σ (%) (e)	$^{207}Pb^*/^{235}U^*$	±2σ (%) (e)	$^{206}Pb^*/^{238}U$ (f)	±2σ (%) (f)	error corr. (g)	$^{207}Pb^*/^{206}Pb^*$ (h)	±2σ (Ma) (h)	$^{207}Pb^*/^{235}U$ (i)	±2σ (Ma) (i)	$^{206}Pb^*/^{238}U^*$ (j)	±2σ (Ma) (j)	% disc. (k)
LOM11-06aL_1	229	0.56	18.5	11.1	0.204	8.74	0.028	5.51	0.630	297	155	188	15.0	180	9.77	39.9
LOM11-06aL_2	134	0.38	17.8	18.0	0.216	11.7	0.029	5.76	0.494	415	226	199	21.1	181	10.3	57.1
LOM11-06aL_3	94.0	0.33	15.9	18.6	0.193	19.0	0.028	6.58	0.346	175	416	179	31.2	180	11.7	2.8
LOM11-06aL_4	388	0.60	15.6	13.1	0.180	9.22	0.026	5.47	0.593	236	171	168	14.3	163	8.81	31.3
LOM11-06aM_71	260	0.50	15.8	16.5	0.757	14.0	0.102	11.4	0.812	373	185	572	61.4	624	67.8	70.8
LOM11-06aM_75	240	0.28	16.0	13.0	1.55	26.5	0.177	20.7	0.783	724	350	949	163	1048	201	48.6
LOM11-06aM_76	86.5	0.36	19.3	7.50	0.298	15.5	0.033	7.99	0.515	783	280	265	36.2	210	16.5	74.3
LOM11-06aM_78	544	0.64	18.5	8.20	0.385	17.4	0.043	13.6	0.782	765	228	331	49.1	272	36.3	65.7
LOM11-06aM_79	159	0.32	18.0	10.6	0.629	16.2	0.087	13.1	0.808	297	218	495	63.6	539	67.9	84.9
LOM11-06aM_80	183	0.49	19.1	9.56	1.02	16.2	0.118	9.69	0.599	696	276	712	82.8	717	65.7	3.13
LOM11-06aM_81	132	0.32	19.8	10.1	0.222	13.1	0.030	10.2	0.779	384	185	203	24.2	188	18.9	51.8
LOM11-06aM_82	234	0.25	19.5	7.89	0.499	15.3	0.072	11.5	0.752	214	234	411	51.7	447	49.6	113
LOM11-06aM_83	245	0.45	15.5	10.8	0.225	9.94	0.028	6.82	0.686	548	158	206	18.5	177	11.9	68.6
LOM11-06aS_201	462	0.37	19.9	5.53	0.422	11.6	0.060	8.54	0.735	253	181	357	35.0	374	31.0	49.1
LOM11-06aS_202	177	0.52	15.3	13.3	0.205	14.2	0.030	9.53	0.671	179	245	190	24.5	190	17.9	6.52
LOM11-06aS_203	186	0.61	12.1	16.7	0.224	10.6	0.030	7.54	0.711	413	167	205	19.7	187	13.9	55.5
LOM11-06aS_204	251	0.39	18.8	7.61	0.194	11.6	0.027	8.03	0.693	281	191	180	19.1	172	13.6	39.2
LOM11-06aS_205	406	0.66	19.8	7.65	0.231	9.66	0.033	7.92	0.820	212	128	211	18.4	211	16.4	0.45
LOM11-06aS_206	380	0.58	19.3	8.77	0.360	18.4	0.032	7.77	0.423	1256	326	312	49.4	201	15.4	85.3
LOM11-06aS_207	446	0.41	19.9	10.2	0.192	9.74	0.027	7.12	0.731	302	152	178	15.9	169	11.9	44.7
LOM11-06aS_208	321	0.53	19.5	5.79	0.215	10.5	0.029	7.47	0.712	378	166	198	18.9	183	13.5	52.2
LOM11-06aS_209	365	0.64	19.7	7.66	0.186	9.79	0.028	7.00	0.715	125	161	174	15.6	177	12.2	42.6
LOM11-06aS_210	115	0.36	20.4	6.68	0.174	15.0	0.028	8.14	0.544	-35.7	305	163	22.6	177	14.2	604
LOM11-06aS_211	154	0.45	20.1	8.30	0.202	11.2	0.028	7.48	0.669	300	190	187	19.1	178	13.1	41.4
LOM11-06aS_212	388	0.53	20.5	6.43	0.191	10.3	0.028	7.74	0.753	160	158	178	16.7	179	13.6	11.8
LOM11-06aS_213	325	0.62	19.5	7.85	0.186	11.8	0.028	7.78	0.659	133	209	173	18.8	176	13.5	33.5
LOM11-06aS_214	175	0.61	17.8	8.91	0.200	11.9	0.030	7.74	0.651	155	211	186	20.1	188	14.3	21.7
LOM11-06aS_215	247	0.65	20.1	10.5	0.193	10.3	0.027	7.31	0.710	236	167	179	16.9	175	12.6	26.2
LOM11-06aS_216	644	0.84	13.4	9.19	0.190	10.2	0.028	7.61	0.744	156	160	177	16.6	179	13.4	14.7
LOM11-06aS_217	428	0.80	18.4	8.23	0.798	10.5	0.112	7.34	0.699	275	172	596	47.3	684	47.6	157
LOM11-06aS_218	482	0.63	20.2	8.05	0.178	11.2	0.027	7.98	0.710	77.9	188	166	17.2	172	13.6	123
LOM11-06aS_219	204	0.69	20.3	9.01	0.261	11.9	0.028	7.69	0.649	857	187	236	24.9	178	13.5	80.3
LOM11-06aS_220	288	0.76	18.2	7.47	0.203	10.1	0.027	7.89	0.781	362	142	188	17.3	174	13.6	52.6
LOM11-06aS_221	377	0.77	18.7	8.79	0.198	9.18	0.027	6.98	0.760	318	136	183	15.4	173	11.9	46.2
LOM11-06aS_222	562	0.75	19.4	7.81	0.202	8.20	0.029	6.22	0.758	251	123	187	14.0	182	11.1	27.9
LOM11-06aS_223	224	0.54	18.7	8.52	0.214	11.6	0.030	8.65	0.749	236	177	197	20.7	194	16.5	18.1

Table C.6 LOM11-06a U-Pb LA-ICPMS Results Cont.

			Corrected Isotope Ratios							Apparent Ages (Ma)						
Spot (a)	U ppm (b)	Th/U ppm (c)	$^{206}Pb/^{207}Pb$ (d)	±2σ (%) (e)	$^{207}Pb^*/^{235}U^*$	±2σ (%) (e)	$^{206}Pb^*/^{238}U$ (f)	±2σ (%) (f)	error corr. (g)	$^{207}Pb^*/^{206}Pb^*$ (h)	±2σ (Ma) (h)	$^{207}Pb^*/^{235}U$ (i)	±2σ (Ma) (i)	$^{206}Pb^*/^{238}U^*$ (j)	±2σ (Ma) (j)	% disc. (k)
LOM11-06aS_224	251	0.70	19.7	6.54	1.78	20.0	0.230	8.58	0.430	454	400	1038	130	1337	104	216
LOM11-06aS_225	220	0.84	20.1	8.48	1.97	20.9	0.227	9.37	0.449	708	397	1107	141	1321	112	95.7
LOM11-06aS_226	241	0.95	19.6	8.20	0.237	10.5	0.029	7.60	0.722	607	158	216	20.5	182	13.6	71.0
LOM11-06aS_227	281	0.55	18.5	7.37	0.202	11.5	0.030	8.25	0.716	174	188	187	19.7	188	15.3	8.25
LOM11-06aS_228	261	0.76	16.6	7.29	0.232	12.9	0.032	10.4	0.807	337	172	212	24.6	201	20.5	41.1
LOM11-06aS_229	203	0.78	19.5	5.34	0.217	12.0	0.029	8.14	0.679	348	199	199	21.7	187	15.0	47.0
LOM11-06aS_231	732	1.38	20.9	11.0	0.205	10.6	0.029	8.39	0.789	229	151	189	18.3	186	15.4	19.1
LOM11-06aS_232	526	0.97	20.4	10.2	0.199	9.60	0.028	7.04	0.733	259	150	185	16.2	179	12.4	31.5
LOM11-06aS_234	195	0.40	18.2	10.1	0.188	13.3	0.029	7.39	0.557	90.8	261	175	21.4	181	13.2	101
LOM11-06aS_235	153	0.57	19.1	6.79	0.308	13.0	0.030	9.14	0.705	1060	185	272	31.0	190	17.1	83.3
LOM11-06aS_236	198	0.45	20.2	17.8	0.208	10.8	0.029	7.41	0.688	265	179	192	18.9	186	13.6	30.2
LOM11-06aS_237	249	0.50	17.9	12.2	0.207	10.0	0.028	6.51	0.649	369	172	191	17.5	177	11.4	52.7
LOM11-06aS_238	182	0.48	20.3	6.77	0.208	11.1	0.030	7.43	0.667	179	193	192	19.5	193	14.2	8.4
LOM11-06aS_239	475	0.76	19.5	6.53	0.206	10.5	0.030	8.09	0.771	152	157	190	18.2	194	15.4	27.8
LOM11-06aS_240	365	0.51	20.3	6.82	0.203	11.8	0.029	8.51	0.720	244	189	188	20.3	183	15.4	25.2
LOM11-06aS_241	387	0.88	14.8	9.01	0.205	10.2	0.030	7.98	0.779	141	151	189	17.7	193	15.2	37.6
LOM11-06aS_242	251	0.63	19.1	8.32	0.214	10.9	0.030	7.59	0.695	248	181	197	19.5	193	14.4	22.6
LOM11-06aS_243	172	0.46	18.5	7.62	1.59	15.8	0.180	8.78	0.556	748	277	966	98.3	1065	86.2	46.0
LOM11-06aS_244	240	0.55	17.1	7.23	1.85	16.8	0.248	12.7	0.754	378	249	1064	111	1427	163	311
LOM11-06aS_245	147	0.82	20.6	6.84	0.222	10.9	0.031	6.41	0.590	279	201	203	20.0	197	12.4	29.9
LOM11-06aS_246	178	0.48	22.0	12.6	0.672	13.6	0.088	8.56	0.627	430	237	522	55.7	543	44.6	27.5
LOM11-06aS_247	296	0.82	21.5	7.44	0.179	9.83	0.028	6.42	0.653	28	178	167	15.1	177	11.2	542.3
LOM11-06aS_248	314	0.71	20.5	8.88	0.220	10.2	0.032	6.70	0.659	224	177	202	18.7	200	13.2	10.6
LOM11-06aS_249	333	0.85	19.7	7.25	0.200	11.8	0.029	8.18	0.694	189	197	185	20.0	185	14.9	1.99
LOM11-06aS_250	159	0.57	18.6	6.31	0.214	13.1	0.031	8.09	0.620	211	237	197	23.4	196	15.6	7.39
LOM11-06aS_251	117	1.29	19.0	5.97	0.218	15.1	0.028	8.82	0.585	451	271	200	27.4	180	15.6	61.0
LOM11-06aS_252	241	0.56	21.0	7.92	0.233	12.5	0.030	8.73	0.700	458	198	213	23.9	191	16.4	59.2
LOM11-06aS_253	337	0.69	19.3	8.34	0.217	10.1	0.031	8.23	0.818	250	133	200	18.2	195	15.8	22.1
LOM11-06aS_255	267	0.60	19.1	6.65	0.216	12.7	0.029	9.39	0.741	352	192	199	22.9	186	17.2	47.8
LOM11-06aS_256	247	0.33	19.6	7.42	0.193	13.1	0.029	8.30	0.633	152	238	179	21.6	181	14.9	19.4